SANDIA REPORT
SAND2018-9884
Unlimited Release
Printed September 2018

An Assessment of MELCOR 2.1: Containment Thermal-Hydraulic Tests in the Heissdampfreaktor (HDR) Facility

J.Tills, J.Phillips, A.Notafrancesco

Prepared by
Sandia National Laboratories
Albuquerque, New Mexico 87185 and Livermore, California 94550

Sandia National Laboratories is a multimission laboratory managed and operated by National Technology and Engineering Solutions of Sandia, LLC, a wholly owned subsidiary of Honeywell International, Inc., for the U.S. Department of Energy's National Nuclear Security Administration under contract DE-NA0003525.

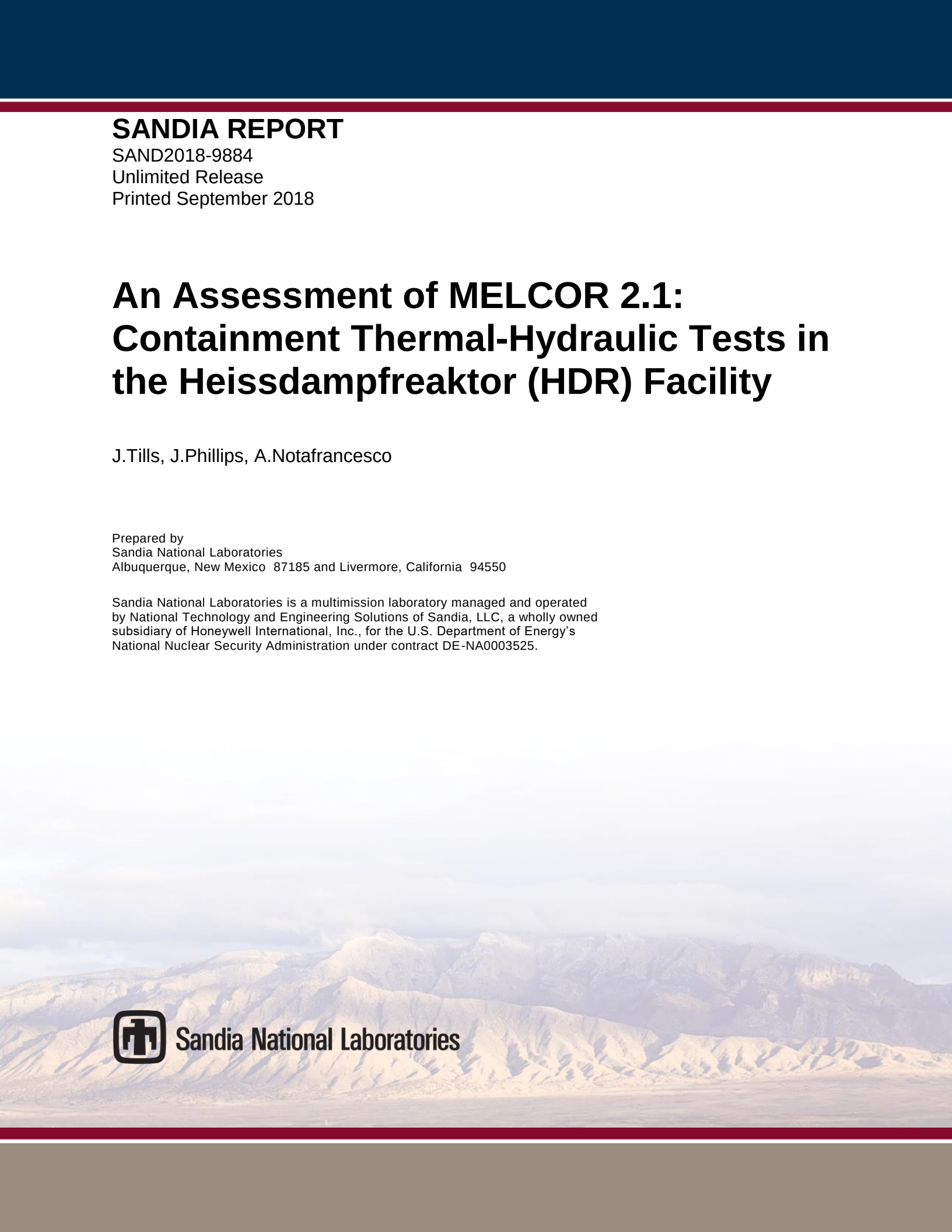

Issued by Sandia National Laboratories, operated for the United States Department of Energy by National Technology and Engineering Solutions of Sandia, LLC.

Available to DOE and DOE contractors from
U.S. Department of Energy
Office of Scientific and Technical Information
P.O. Box 62
Oak Ridge, TN 37831

Telephone: (865) 576-8401
Facsimile: (865) 576-5728
E-Mail: reports@osti.gov
Online ordering: http://www.osti.gov/scitech

Available to the public from
U.S. Department of Commerce
National Technical Information Service
5301 Shawnee Rd
Alexandria, VA 22312

Telephone: (800) 553-6847
Facsimile: (703) 605-6900
E-Mail: orders@ntis.gov
Online order: https://classic.ntis.gov/help/order-methods/

SAND2018-9884
Unlimited Release
Printed September 2018

An Assessment of MELCOR 2.1: Containment Thermal-Hydraulic Tests in the Heissdampfreaktor (HDR) Facility

Jack Tills
Jack Tills & Associates, Inc.
Sandia Park, New Mexico 87047-0549
Sandia Contract No. 176741

Jesse Phillips
Severe Accident Analysis
Sandia National Laboratories
P.O. Box 5800
Albuquerque, New Mexico 87185-0748

Allen Notafrancesco
Office of Nuclear Regulatory Research
U.S. Nuclear Regulatory Commission
Washington, DC 20555-0001

Abstract

MELCOR is being developed at Sandia National Laboratories for the U.S. Nuclear Regulatory Commission. MELCOR is a fully integrated code (encompassing the reactor coolant system and the containment building) that models the progression of postulated accidents in light water reactor power plants. It provides a capability for independently auditing analyses submitted by reactor manufacturers and utilities. In order to assess the adequacy of containment thermal-hydraulic modeling incorporated in the MELCOR code, a key containment test facility was analyzed. This report documents MELCOR code calculations for simulating steam-water blowdown tests performed in the Heissdampfreaktor (HDR) de-commissioned containment facility located near Frankfurt, Germany. These tests are a series of blowdown experiments in a large scaled test facility; including some tests with the addition of hydrogen release which are intended to simulate a variety of postulated breaks inside large containment buildings. The key objectives of this MELCOR assessment are to study: (1) the expansion and transport of high energy steam-water releases, (2) heat and mass transfer to structural passive heat sinks, and (3) containment gas mixing and stratification. Moreover, MELCOR results are compared to the CONTAIN code for the same tests.

ACKNOWLEDGMENTS

The authors would like to acknowledge the U.S. Nuclear Regulatory Commission for supporting this work. In particular, we would like to express our thanks to our principle manager and co-author Allen Notafrancesco, who has supported the development, validation, and application of the CONTAIN code since the 1980s. As the MELCOR code validation has been extended to support similar applications, his guidance, knowledge, and expertise have been a tremendous value.

CONTENTS

FIGURES

TABLES

NOMENCLATURE

AP1000	AP1000 Pressurized Water Reactor Design
ASM	Analytical Simulation Model
C	Corrective
CV	Control Volume
CVH	Control Volume Hydrodynamics Package in MELCOR
CVTR	Carolinas-Virginia Tube Reactor
DBA	Design Basis Accident
ECCS	Emergency Core Cooling System
EOS	Equation of State
EPR	Evolutionary (or European) Pressurized Water Reactor Design
FL	Flow Path Package in MELCOR
FOG	MELCOR Input Card Allowing Fog Formation
H	High PIRT Ranking
HDR	Heissdampfreaktor
HECTR	Hydrogen Event: Containment Transient Response, USNRC Computational Code
HEM	Homogeneous Equilibrium Model
HFM	Homogeneous Frozen Model
HMS	Hydrogen Mixing Studies, USNRC Computational Code
HMTA	Heat and Mass Transfer Analogy
HS	Heat Structure Package in MELCOR
ISP	International Standard Problem
LOCA	Loss of Coolant Accident
M-H	Medium-to-High PIRT Ranking
MSLB	Main Steam Line Break
NOFOG	MELCOR Input Card Disallowing Suspended Liquid Water in the Atmosphere
NTU	Number of Transfer Units
NUPEC	Nuclear Power Engineering Corporation
OECD	Organization for Economic Cooperation and Development
P	Parity
PF	Pressure Flash
PHDR	Project Heissdampfreaktor
PIRT	Phenomena Information and Ranking Table
PWR	Pressurized Water Reactor
RCS	Reactor Coolant System
RN	RadioNuclide Package in MELCOR
SA	Severe Accident
SNL	Sandia National Laboratories
TF	Temperature Flash
USNRC	United States Nuclear Regulatory Commission (or simply NRC)
wRN	RN Package Enabled for Aerosol Physics
C_F	Irreversible Loss Coefficient in CONTAIN
cf_n	Cooling Fraction in Cell n
δ	Film Thickness

f_n	Fraction of Heat Removal in Cell n
Fr	Friction Loss Coefficient in MELCOR
$h_{blowdown}$	Blowdown Specific Enthalpy
h_g	Gas Specific Enthalpy
h_f	Fluid Specific Enthalpy
K_F	Form Loss Coefficient in MELCOR
k_{film}	Film Thermal Conductivity
K_F'	Irreversible Loss Coefficient in MELCOR
Nu	Nusselt Number
Nu_{forced}	Forced Convection Nusselt Number
Nu_{nat}	Natural Convection Nusselt Number
Pr	Prandtl Number
$P_{v,n}$	Steam Partial Pressure in Cell n
q_{conv}	Sensible Heat Flux
q_{cond}	Latent Heat Flux
q_{film}	Energy Transfer Flux Due to Film Drainage
q_{wall}	Energy Flux to the Wall Surface
Ra	Rayleigh Number
Re	Reynolds Number
R_{film}	Thermal Resistance of the Film
R_{gas}	Thermal Resistance of the Gas
T_b	Bulk Temperature
T_{if}	Interface Temperature
T_s	Surface Temperature
T_{sat}	Saturation Temperature
T_{mix}	Well-Mixed Atmospheric Temperature
T_w	Wall Temperature
ΔP_{cal}	Calculated Pressure – Initial Pressure
ΔP_{data}	Instrument Pressure – Initial Pressure

1. INTRODUCTION

This report documents a containment validation exercise for the MELCOR code, using data obtained from four large-scale integral tests performed in the Heissdampfreaktor (HDR) de-commissioned containment facility near Frankfurt Germany, which has now been disassembled. This exercise is part of a larger on-going effort to validate the MELCOR code for applications that include simulations of design basis accidents (DBAs) and severe accidents (SAs) in pressurized water reactor (PWR) type plants of current and advanced design [Hum15c]. Other containment related validation exercises performed for the MELCOR code [Til08], as well as the CONTAIN code [Til02a], have been used to develop the outline for this report.

The MELCOR computer code [Hum15a, Hum15b] has been developed by Sandia National Laboratories (SNL) under United States Nuclear Regulatory Commission (USNRC) sponsorship to provide, in part, the calculation capability for independently auditing containment performance analyses submitted by reactor manufactures and utilities. MELCOR is a fully integrated code (encompassing the reactor coolant system (RCS) and the containment building) that models the progression of postulated accidents in light water reactor power plants. Characteristics of accident progression that can be treated with MELCOR include the thermal-hydraulic response in the RCS, reactor cavity, containment and confinement buildings. The emphasis in this report is with the modeling and validating effort associated with containment accident events, and mainly those events considered in design basis accidents assessment.

The CONTAIN computer code [Mur97] was also developed at SNL under the USNRC and is a specialized computer code used to perform thermal-hydraulic calculations inside containment following a variety of postulated high energy breaks. CONTAIN serves as a repository of accumulated knowledge in the area of containment analysis technology. CONTAIN incorporates the best current understanding of all relevant phenomena, and has an extensive validation base. The code has been the principal containment analysis tool used to audit industry's safety analysis calculations by the USNRC. CONTAIN achieved sufficient maturity to support regulatory analyses; therefore, continual code development was no longer necessary.

CONTAIN was developed to perform containment audit analyses for reactor systems which applied active safety systems, where dependencies between the RCS and containment can be adequately characterized by the break source into the containment. CONTAIN, therefore, was developed to model the thermal-hydraulics of the containment explicitly decoupled from the RCS. Assessing advance reactor designs with passive systems, which by design couple the thermal-hydraulics of the RCS and containment, requires a code developed with the intent of performing integral-system analyses. MELCOR meets this requisite as well as adding additional flexibility for incorporating new capabilities and features to support the modeling of advancing technology.

In order to assess the adequacy of containment thermal-hydraulic modeling incorporated in the MELCOR code, both rapid and long-term pressurization/depressurization tests performed in the HDR facility are analyzed. These tests are documented as a series of pressurization events resulting from various sized and positioned water pipe ruptures in a large scaled test facility. Additionally, some of the tests also included light gas (hydrogen/helium mixture) releases at various elevations. The purpose for gas releases was to simulate hydrogen/air/steam mixing that

may occur during a beyond DBA or SA when a portion of the reactor core is oxidized. The key objectives of this MELCOR containment modeling assessment are therefore to study: (1) the expansion and transport of high energy steam-water releases, (2) the effects of atmosphere-to-structure heat and mass transfer on predicted containment loads (pressure and gas temperature), and (3) the containment gas mixing and stratification processes under a variety of simulated accident scenarios.

The four selected HDR experiments presented here are part of the overall traditional suite of integral containment tests used for assessing the adequacy of containment modeling. Previously, MELCOR was assessed against experiments conducted in the Carolinas Virginia Tube Reactor (CVTR) test facility which were also large scaled integral tests, however, these tests focused only on steam blowdowns [Til08] and the late response of the containment atmosphere to spray activation. The HDR tests, without engineered safety features (fan coolers or sprays) activated are more appropriately discussed in the context of recently studied advanced plants that do not include either fan coolers or spray activations during DBA events. In addition, the CONTAIN code was also assessed against the HDR and CVTR test data and selected separate effects testing, and this assessment was documented in Til02a. That reporting and other CONTAIN validation efforts serve therefore as benchmarks for the MELCOR assessments discussed in this report.

Section 2 of this report provides a description of the HDR facility, test procedures, instrumentation, and relevant scaling. The section provides a discussion of the similitude of the HDR tests and facility to current and advanced PWR containments recently analyzed with the MELCOR code [Til09]. Section 3 addresses the containment thermal-hydraulic phenomena investigated and associated with the MELCOR HDR model, including relevant input examples of selected code "packages." A review of the HDR test data and analysis is presented in Section 4. Here the processes or events previously discussed in Section 3 are linked to the HDR test measurements and code calculations. Since the CONTAIN code was also assessed against the HDR tests [Til02a], a code-to-code benchmarking exercise is included in this section. In some instances, the calculations differ and the causes for some of these differences are explained. Section 5 presents a summarization of the findings and conclusions for this validation exercise, and provides a few recommendations when using the MELCOR code for performing containment analysis.

Finally, three appendices are included in the report. Appendix A provides a detailed description of various phenomena identified as occurring in containments during postulated accident events. Appendix B presents MELCOR subcompartment analyses of the HDR rapid pressurization tests focusing the discussion on measured and calculated compartment pressure differentials. The MELCOR input decks for the reference cases discussed in this report are provided in a supplement report [Til18].

2. FACILITY AND TEST DESCRIPTION

2.1 Facility

HDR is a de-commissioned reactor facility located near Frankfurt Germany. The selected series of experiments presented here were performed in the 1980's and early 90's. The HDR containment, shown in Figure 2-1 and Figure 2-2, is a reinforced concrete, right vertical cylindrical structure (diameter 20 m) with a flat base and hemispherical dome. Surrounding a primary containment boundary is a secondary containment that vents to the environment. The height of the primary containment building is ~ 60 m with a total volume of ~11300 m^3 in which the open volume above the operating deck (room 11004) accounts for about one-third of the total volume. Below the operation deck at 30.8 meters there are 70 subcompartments or rooms. The rooms are numbered according to associated elevation levels, ranging from 1200 to 1900. Figure 2-3 shows rooms grouped into six combined levels (including the dome region above the operation floor at 30.8 meters). Free volume, metal mass, and concrete surface areas are listed in Table 2-1 according to these combined levels. Two features of the facility that become important in the tests, especially for long-term tests, are the vertical pathways that allow steam/gas to flow from break locations below the operating deck to the dome region. There are essentially two major vertical pathways along the 270 – 90 degree sectional, Figure 2-4. On the 270 degree side is a spiral staircase and equipment shaft. On the opposite side (at the 90 degree location) is the vertical stairs and second equipment shaft. From the operation deck to the bottom of the reactor vessel there are no major pathways connecting either side of the facility, as a result there is a large circulation loop that effectively connects the dome region to lower compartments below the reactor vessel especially noticeable during the long-term tests such as test E11.2.

The HDR facility was a multiple use test facility used for shake, fire, and numerous high energy line break tests. Consequently, the materials within the facility were not in "as-built" condition for the tests described here. As a participant in most of the HDR International Standard Problems (ISPs) tests, SNL representatives performed numerous walk-downs through the facility prior to tests. These walk-downs confirmed that paint on steel and many concrete surfaces was largely absent or severely degraded. Additionally, in some regions exposed repeatedly to high temperature steam, the concrete structures with missing paint appeared to have a porous surface that could absorb condensate over a prolonged exposure period. These observations have been factored into the preparation of sensitivity calculations especially for the long-term tests and for those tests these sensitivity tests may be more reflective of the facility condition at the time of testing. For example, prolonged exposure tests (E11.2 and E11.4) are calculated with both low and high concreate thermal conductivities to simulate extreme effects of water migration into concrete. And for all calculations, paint is not included in the structure modeling.

2.2 Tests

The four selected HDR experiments analyzed in the report are characterized as either rapid or slow pressurization/depressurization containment tests driven by steam-water and/or steam injections. The injections, which are located at various elevations within the facility, are further characterized according to the type of accident being simulated: design basis loss-of-coolant accidents (LOCAs) are simulated as resulting from a large pipe rupture (with the associated rapid steam-water

blowdown), and long-term SAs are simulated with smaller prolonged steam injections (small break LOCA). Both SA tests (E11.2 and E11.4) included a late-time light gas release, and one of the large pipe rupture tests (T31.5) also had a light gas release included shortly after the blowdown terminated, thereby simulating in its extended time period a beyond design basis accident. Three of the four experiments were selected as ISPs, and therefore are tests having a substantial amount of documentation pertaining to the facility and test description (layout, instrumentation and procedure), measurements, reporting (blind and post-blind), and review. This report focuses mainly on the calculations and data comparisons associated with those ISPs (ISP-16, ISP-23, and ISP-29). The one test not reported as an ISP test, E11.4, is included in this report since the test compliments one of the ISP tests (ISP-29) by providing an alternate choice of steam and light gas injection location, creating a different gas mixing profile. Table 2-2 summarizes the tests that were analyzed, and provides a list of reference documentation for each of the tests. An overview of the type of tests discussed here can be found in an Organization for Economic Cooperation and Development (OECD) state-of-the art report on containment thermal hydraulics and hydrogen distributions [OECD99].

2.3 Instrumentation

Various types of sensor instrumentation were incorporated into the HDR facility. The main thermal-hydraulic data gathered were from pressure, pressure differential, and gas temperature sensors. For example, Figure 2-2 shows a few locations of a pressure and pressure differential sensors for the T31.5 test. A large number of temperature and light gas sensors were located throughout the facility Figure 2-5 and Figure 2-6 show these locations. Key locations for the temperature and gas sensors were along the spiral stair (280°), staircase (80º), and dome (above 30.85 meters).

Table 2-3 shows the uncertainties associated with the thermal-hydraulic sensors, as reported for test V44 (ISP-16). Typical uncertainties are overlaid onto measurements in one of large pipe rupture tests in Figure 2-7 and Figure 2-8 for illustration purposes. In the analysis these relatively small measurement uncertainties are not included in plots; rather, as provided in the ISP final reports, only direct measurements (without uncertainty bands) are plotted for comparison purposes. Instruments to measure liquid water carry-over from break to surrounding compartments unfortunately did not give reliable data, and therefore these measurements are not reported or available for analysis. Pressure differential measurements during the first 5 seconds of the large pipe rupture tests were considered reliable and are used to investigate important phenomena occurring during the early pipe rupture time period; these investigations are discussed in Appendix B. In general, steam and light gas concentration measurements provided very accurate representation of gas mixing profiles although specific uncertainties were not reported in the ISP documentation. When available, gas and steam concentration measurements are a preferred data for determining gas mixing behavior. These data are only available for T31.5, E11.2, and test E11.4. Local temperature measurements are available for all tests, but these measurements are not as useful for determining mixing behavior due to the sometimes conflicting effects that energy transfers within (to suspended liquid) the atmosphere and to surrounding heat sinks has on local temperatures.

2.4 Scaling

When comparing the HDR facility and tests against a typical PWR large dry containment (see Figure 2-9) and a representative DBA event, the following scaling aspects are highlighted:

a. The HDR total free volume is about one-fifth of a "generic" PWR large dry containment;
b. The HDR heat sink surface (area or mass) to volume ratio is about four times larger and the aspect ratio (height/diameter) is about three times larger than that of a "generic" PWR large dry containment;
c. The lower two-thirds of the HDR containment volume includes a complicated network of rooms;
d. The HDR blowdown releases are more representative of an intermediate size LOCA (break area) resulting in a longer steam-water release duration than a postulated design basis LOCA in a PWR large dry containment which are characterized by higher release rates in about one-half the transient time.
e. The HDR facility has only a third of the total facility volume in the region above the operating floor, whereas typical PWR large dry containments in the current U. S. plant fleet has above 70 to 80% of free volume above the operating floor.

Therefore, considering these key scaling attributes, the HDR pressure responses are more sensitive to the heat and mass transfer processes (i.e., overall heat transfer to the containment structure and components is above the nominal PWR DBA event) than in the full-scale plant configuration. Also, possible distortions in bulk containment circulation due to the facility design versus more open large dry containments should be recognized.

Table 2-1 HDR facility free volume, steel mass, and concrete surface area tabulated by elevation levels.

Level	Free Volume [m^3]	Steel Mass [kg * 10^6]	Concrete Surface Area [m^2]	Steel Mass/Free Volume [kg/m^3]	Concrete Surface Area/Free Volume [m^{-1}]
1200-1400	1928	0.124	3139	64.2	1.63
1500	1011	0.056	1398	55.7	1.38
1600	1005	0.096	1335	95.7	1.33
1700	1349	0.159	1781	118.1	1.32
1800-1900	1106	0.252	1252	228.0	1.13
Dome	4800	0.449	624	93.5	0.13

Table 2-2 HDR Experiments on Containment Thermal Hydraulics & Gas Distribution

Experiment	Type	Test Conditions	General Observations	References
HDR V44 (ISP-16)	LOCA	55 sec 2-phase steam blowdown in a small (280 m^3) mid-elevation room.	Test provides an indication of the effect of force convective condensation during a blowdown event. Pressure differentials between blowdown and adjacent compartments are recorded.	Fir85, Val83, Wol83, Til02a
HDR T31.5 (ISP-23, Project HDR benchmark)	LOCA	55 sec 2-phase steam blowdown in a large (793 m^3) mid-elevation room. ISP-23 exercise extends to 20 minutes. Hydrogen/helium injection began at 20 minutes after blowdown and lasted for 15 minutes with the test continuing out to 1 hour.	Pressure response similar to V44. Hydrogen tracing in the containment 20 minutes to 1hour provide a database for gas distribution modeling.	Kar89, Wen87, Til02a, OECD99
HDR E11.2 (ISP-29)	SBLOCA	12 hr steam injection for pre-heating prior to 20 min hydrogen/helium injection (injections at mid-elevation). Followed by 3 hr steam injection in lower containment and 3 hr 45 min. outer vessel spray cooling.	Stable temperature and steam stratification developed near the injection location. Hydrogen stratification observed with enhancement in the upper containment due to low steam injection and later outer spray cooling.	Kar92, Til92, Mur96, Til02a, OECD99
HDR E11.4 (Project HDR benchmark)	SBLOCA	Similar to E11.2 but with 34 hr pre-heat. Steam and hydrogen/helium release into lower containment. Simulation of core degradation effects on containment response using dry heat addition to lower containment atmos. And steam injection into sump.	Uniform mixing (no stratification) due to low injections. Alpha block heat transfer data provides assessment of long-term natural convection condensation.	Val92, Gre92, OECD99

Table 2-3 Sensor uncertainties tabulated for HDR test V44.

Measure-ment position	Variable	Maximum reading	Relative error maximum	Relative error average	Absolute error maximum	Absolute error average
CP 3501	Absolute pressure	2.45 bar	2.3 %	1.3 %	0.06 bar	0.03 bar
CP 6311	Absolute pressure	2.45 bar	2.0 %	1.1 %	0.05 bar	0.03 bar
CP 6301	Diff. pressure	0.8 bar	21.0 %	7.1 %	0.17 bar	0.06 bar
CP 6303	Diff. pressure	0.8 bar	8.0 %	2.6 %	0.06 bar	0.02 bar
CT 6303	Temperature	130 °C	2.4 %	1.3 %	3.1 °C	1.7 °C
CT 402	Temperature	100 °C	3.6 %	1.6 %	3.6 °C	1.6 °C

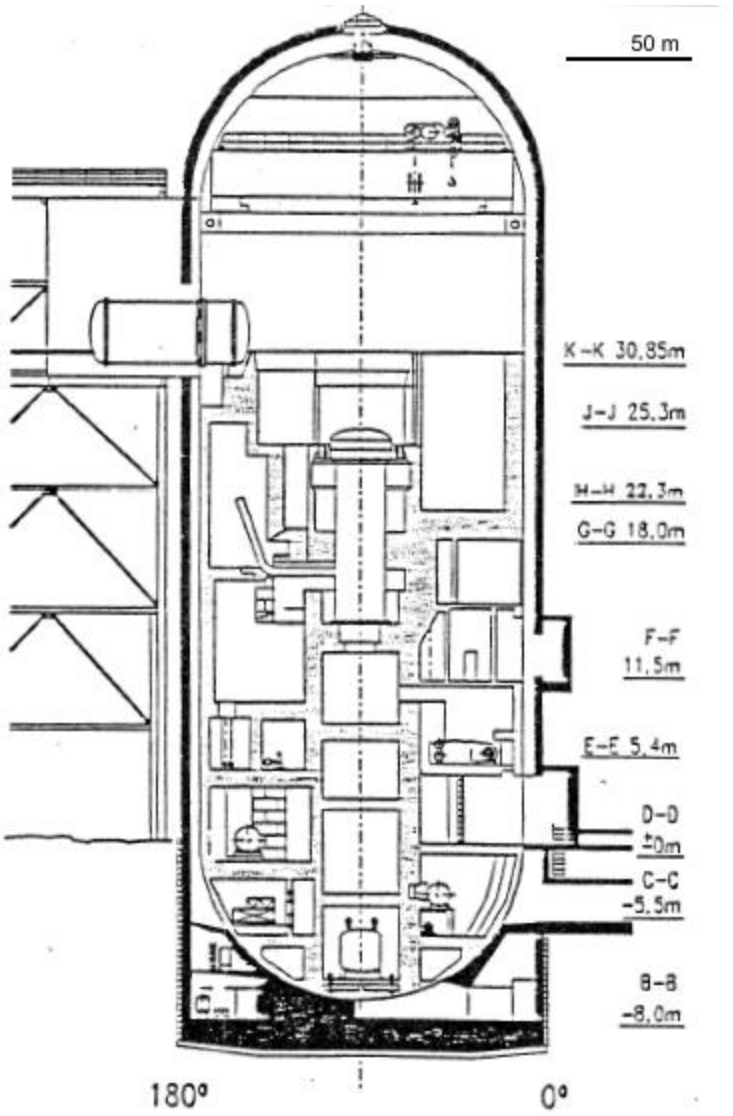

Figure 2-1 HDR Test Facility (break room 1704 is for Test T31.5) 180—0 deg. section.

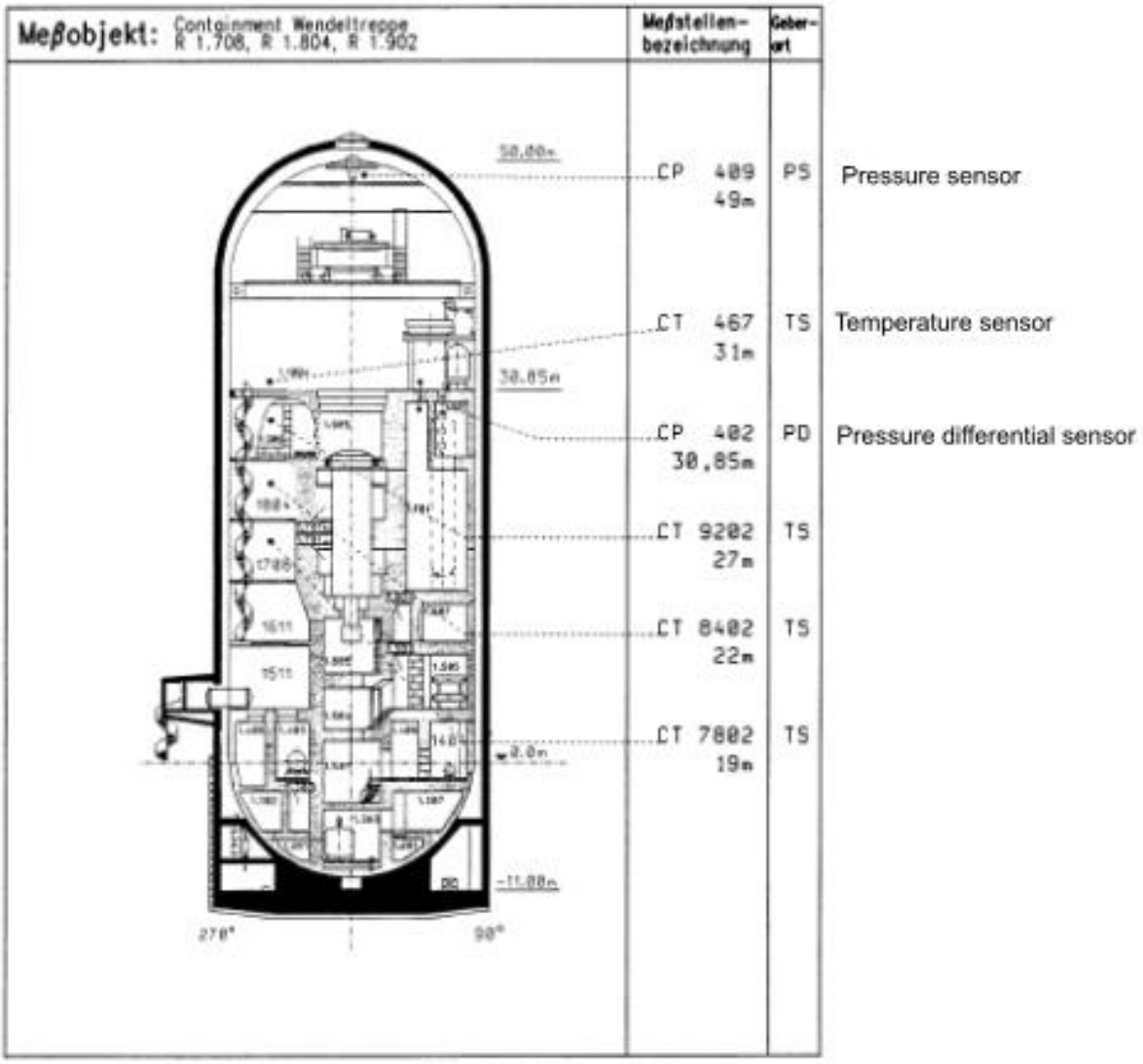

Figure 2-2 HDR Test Facility (showing spiral staircase) 270—90 deg. section.

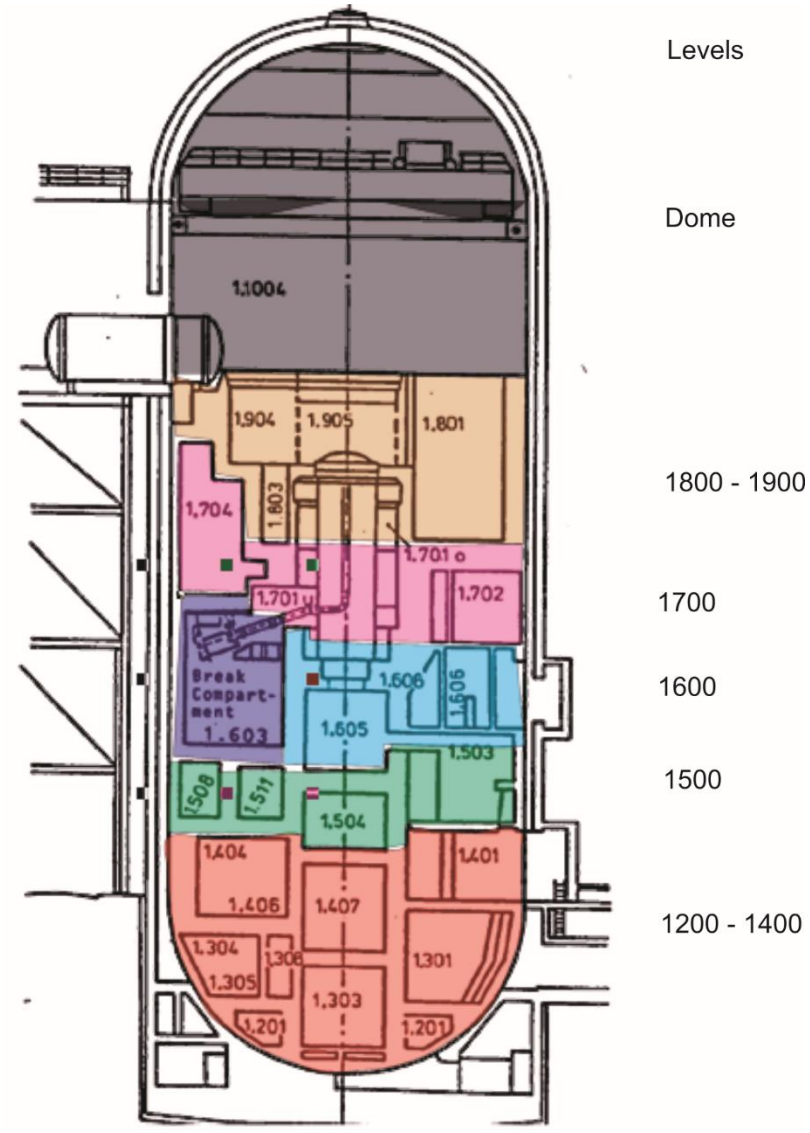

Figure 2-3 HDR Test Facility levels (break room 1603 is for Test V44).

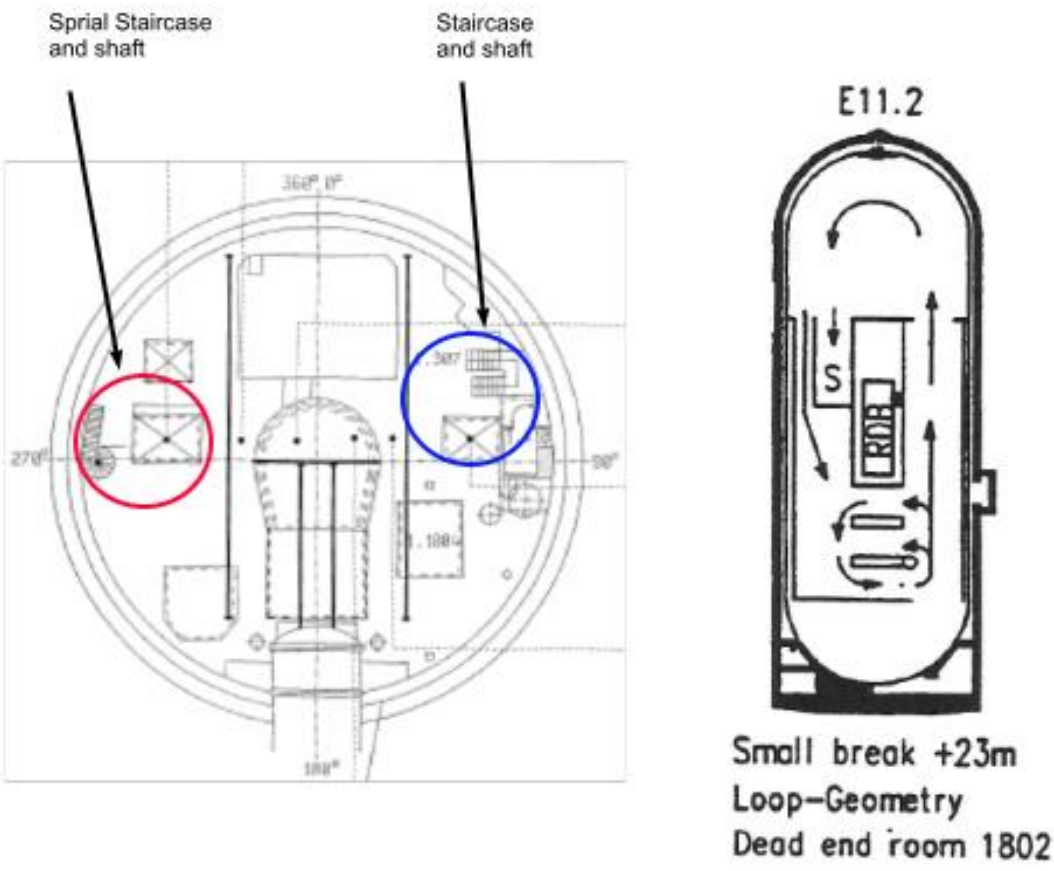

Figure 2-4 **Dome to lower compartment pathways, and sketch of circulation loops for long-term injection tests in the HDR facility**

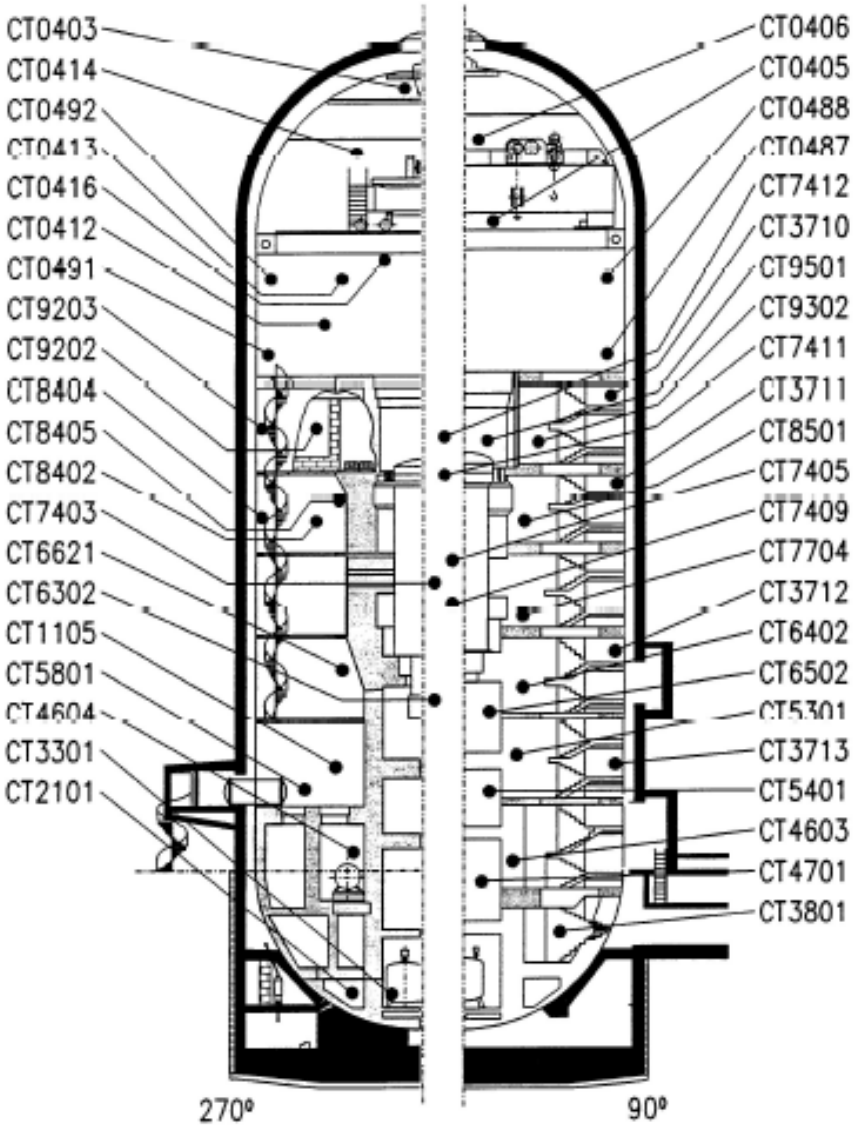

Figure 2-5 HDR temperature sensors.

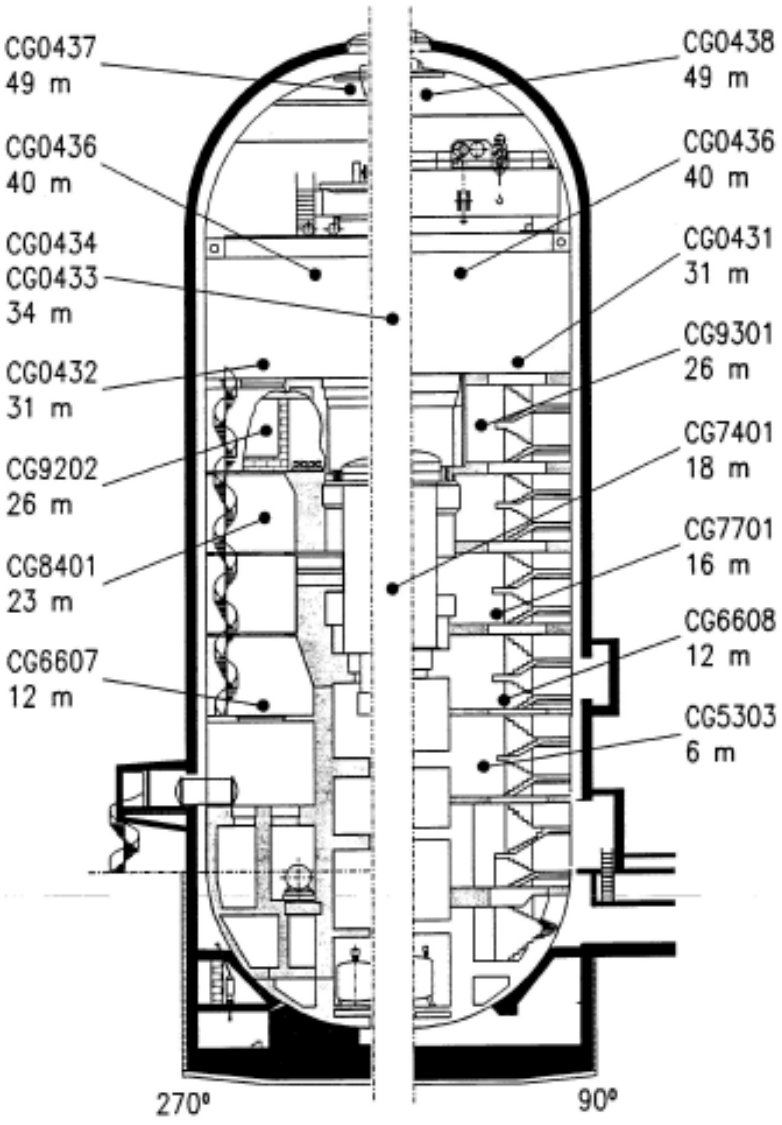

Figure 2-6 HDR light gas sensors.

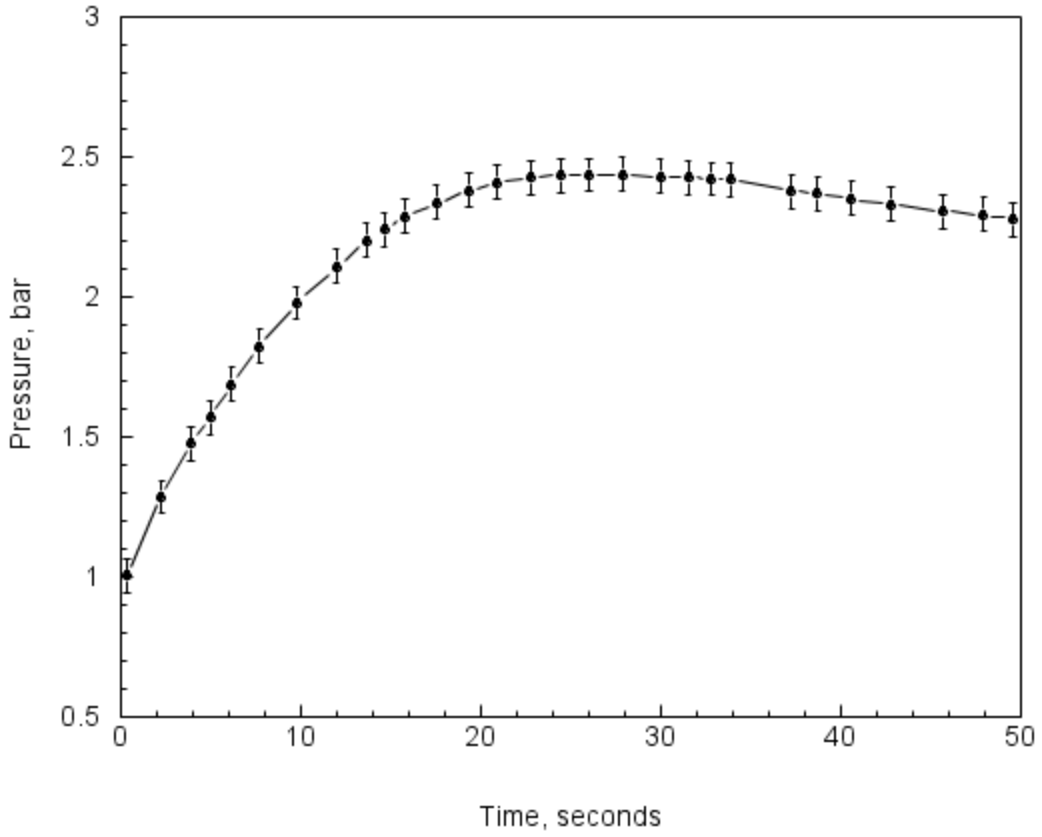

Figure 2-7 Measured containment pressure for HDR test V44, showing maximum error of sensor.

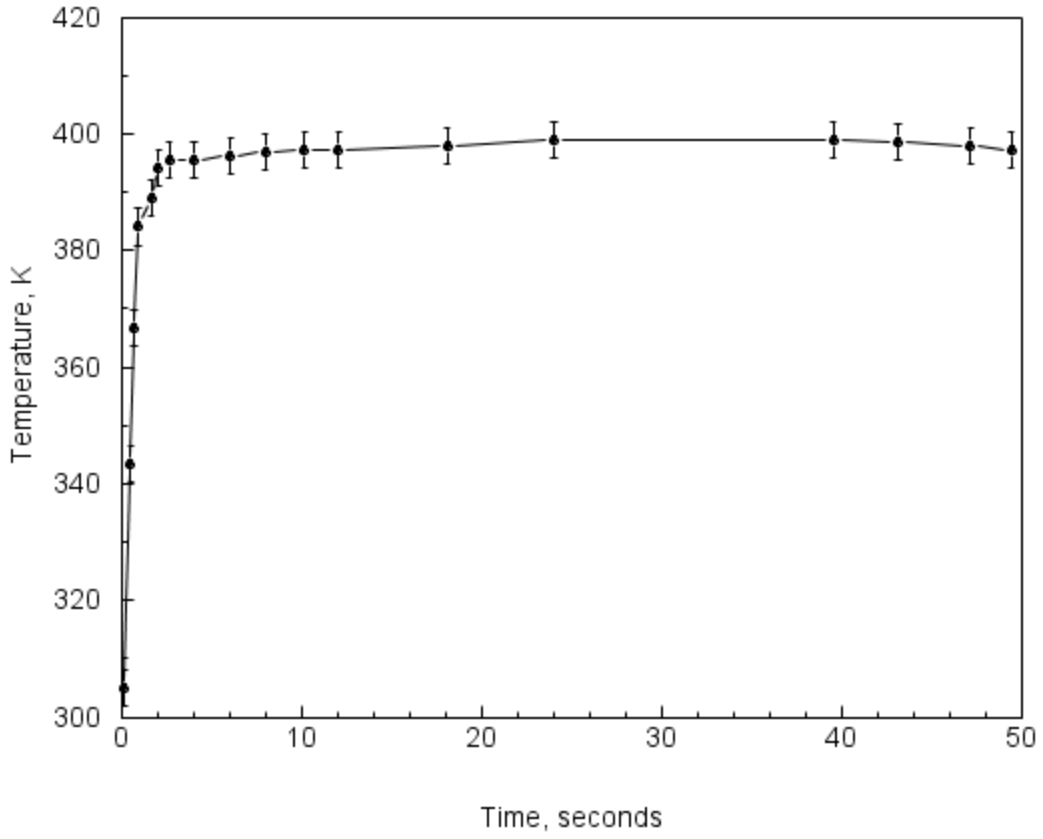

Figure 2-8 Measured containment breakroom temperature for HDR test V44, showing maximum error of sensor.

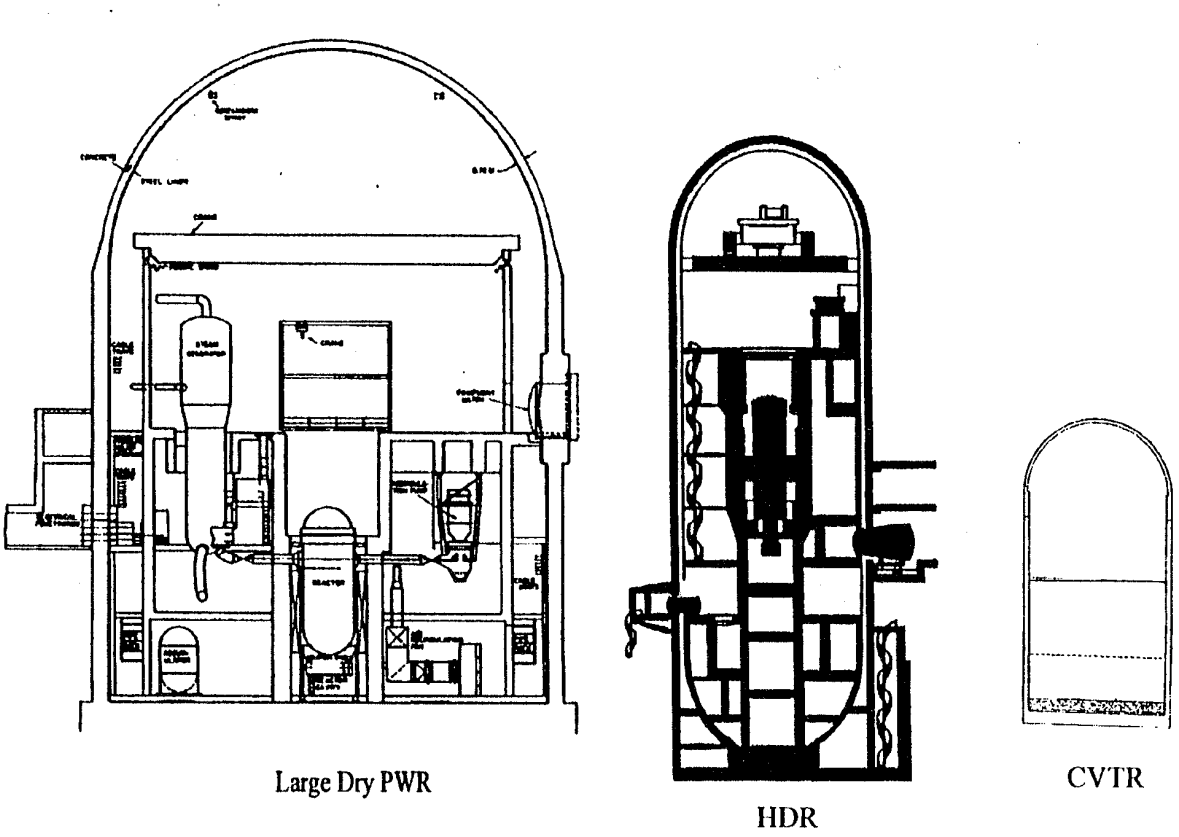

Figure 2-9 **Approximate scales of integral test facilities compared to a large dry PWR containment.**

3. MELCOR MODEL DESCRIPTION

3.1 Containment Phenomena Identification and Validation Focus

To establish a connection between an experimental program, code validation and containment accident analysis, it is helpful to systematically identify and assign importance to various phenomena occurring within the containment, and then establish the corresponding connection with code models and experiments selected to validate those models. This effort has been performed in previous studies [Til02a, Til02b] where Phenomena Identification and Ranking Tables (PIRTs) have been developed for both rapid and slow pressurization accidents in large dry PWR type containments. Table 3-1 and Table 3-2 are extracted from Til02a (with minor changes). For completion, phenomena descriptions are provided in Appendix A.

With respect to the Project HDR program, the test program reports data (measured) for a reduced grouping of process/phenomena. In some cases, for example phenomena associated with engineering safety features (sprays and fan coolers) are simply not present in the tests, or in other cases the phenomena may be present but not directly measured, water ingress into concrete. Additionally, for practical reasons we focus our validation efforts on phenomenon that ranks medium to high (M-H) or high (H) in the PIRT, eliminating further consideration of lower ranking phenomena. With these caveats concerning key phenomena, the corresponding process/phenomena that is either present and/or present and measured in the HDR tests is listed in Table 3-3 along with other integral and separate effects tests that are used to validate phenomenological models. The validation efforts associated with the separate effects and other integral tests (besides the HDR tests) are described for the CONTAIN code in reference Til02a and the MELCOR code in references Til08 and Hum15c.

The key figures-of-merit in comparing code results to test data are containment pressures, local gas temperatures and gas concentrations (or composition), along with condensation coefficients for structural heat sinks added as a key model indicator. Typically for containment testing and design basis transient analyses, containment pressure is appropriately treated as a global parameter and therefore the use of a simpler calculation methodology (e.g., modeling with fewer control volumes) may be possible to predict this parameter. Whereas, when attempting to calculate *regional* containment gas temperatures resulting from steam transport and potential stable steam/gas stratification, a more complicated model is warranted. These aspects are pursued in this report and key insights are discussed later in Section 4.

With reference to the MELCOR code, it is noted that each of the important phenomena listed in Table 3-3 has corresponding models included and discussed in the MELCOR reference manual [Hum15b], shown here in Table 3-4. The exception concerns phenomena associated with jet-plume gas interaction and entrainment processes. For these processes, neglect of momentum transport within a control-volume along with the absence of concentration front tracking precludes the ability to predict or distinguish jet-plume behavior arising from injections of high energy line breaks.[1] In most cases associated with large pipe rupture events the jet-plume importance is limited

[1] The MELCOR code does allow the user the flexibility to include (by input) volumetric flow from jets into a volume, with a control volume calculated velocity that is specified by the user through the use of an effective control volume hydraulic flow area. Usage of this type of input specification is intended mainly for sensitivity analysis, and is

to short periods (blowdown), and neglect of the exceedingly complex phenomenon (linked to geometry, etc.) typically results in a conservative (*over*) estimate of peak containment pressure due to the blowdown. Local temperatures may, however, be under predicted within the jet or plume; yet, because the period of interest is relatively short, the error is limited to localities near the break. Consequently, neglect of jet-plume phenomenon modeling is often considered an acceptable short-coming for the control-volume approach to accident analysis, with the possible exception dealing with hydrogen distribution predictions required for initiating events such as deflagrations. The HDR tests provide important data on steam-water blowdown tests with the addition of hydrogen releases which are intended to simulate a variety of postulated breaks inside large containment buildings. These tests investigate both the global and regional effects. The process modeling for pressurization, mixing, transport, heat and mass transfer are all addressed in the HDR tests to some extent, and MELCOR modeling is assessed for each of these processes in Section 4. Specific comments related to phenomenon and process modeling for the MELCOR code with relevant comparison to the CONTAIN code are presented in Table 3-5.

3.2 Nodalization Model

A reference nodalization scheme is used in this report to model the HDR tests. The model is derived directly from a previous model documented in SNL submittals to ISP exercises using the CONTAIN code. For the two large pipe rupture tests (V44 and T31.5) involving a rapid containment pressurization (both DBA and beyond DBA type events) a 33 control volume (33-CV) model is used. The nodalization model is sketched in a block layout in Figure 3-1 and Figure 3-2, and further described in tabular format according to HDR compartment and CV correspondence in Table 3-6. In the case of severe accident test simulations (E11.2 and E11.4) that run for many hours, two separate nodalizations are used to include modeling of the secondary annular space between the HDR shell and outer containment building. These nodalizations (15-CV and 48-CV) are used only for the E-series tests and have been derived also from documented CONTAIN submittals for E11.2 (15-CV) and E11.4 (48-CV) test simulations. These nodalizations are further described in Section 4.

Various sensitivity cases are included in this report to examine model and specification uncertainties. One class of sensitivity cases focuses on the nodalization scheme, where the 33-CV model is simplified to a single control volume (1-CV). The single control volume modeling approach has been used before for DBA containment analysis for large dry containments where the blowdown injections are at low elevations and enter into a relatively large open space region (above the operation deck). The injection scenario and geometry of the large dry containments favor a well-mixed atmosphere, and well-mixing is further aided by early activation of fan coolers that help to mitigate DBA containment loads (peak pressure and temperature). In the case the HDR facility with the extreme high aspect ratio (height/diameter), compartmentalization, lack of active mixing forces, and mid-level injection (V44 and T31.5), the 1-CV model is not an appropriate model. This conclusion is demonstrated in the nodalization sensitivity cases presented throughout Section 4. In more recent DBA analysis of PWR advanced large dry containments (such as the AP1000 and EPR containments), especially without active mixing forces such as fan coolers, multi-volume nodalization schemes are required for a more accurate representation of

demonstrated in the multi-cell HDR calculations to investigate the importance of forced convective condensation on predicted peak pressure during the blowdown period.

regional mixing. Consequently, the HDR test with the 33-CV model is more reflective of the current nodalization methodology for PWR containment modeling.

It is also noted that the reference nodalization model utilized in this report uses the same model adopted in previous SNL CONTAIN analyses for the T31.5 (ISP-23) international standard problem and the longer-term Project HDR submittal with hydrogen injection. The MELCOR representation of prior CONTAIN modeling therefore promotes similitude for CONTAIN/MELCOR benchmarking, which is discussed in detail in code benchmark subsection of Section 4.

Adjustment for MELCOR HDR Model. Liquid water mass suspended in the atmosphere, referred to as fog in MELCOR, is treated as aerosol when the RadioNuclide (RN) package is enabled, i.e., aerosol physics models are applied. Unlike CONTAIN, conservation of aerosol mass is imposed through additional input requirements in MELCOR. Aerosol deposition due to gravitational settling requires a prescriptive host, either a receptive control volume or heat structure, to receive settling aerosols. If the RN package is enabled, either the definition of a heat structure or flow through area to another control be present for settling aerosols to be transported. If a flow-through area is defined, the donor and receiver control volumes must share some physical altitude. Given the CONTAIN 33 node input file did not directly meet these requirements; modifications were made to the physical layout in the final MELCOR deck. The additions of flow-through areas, floor heat structures, and control volume overlap are presented in Table 3-7. The increase in control volume altitudes adds a small amount of mass to atmosphere as well as a negligible change to the gravitational head.

3.3 MELCOR Models and User Input

There are four modeling categories that define the thermal-hydraulic phenomena that users must prepare code input for in order to arrive at an integrated analytical simulation model (ASM) for a specific scenario. The categories of inputs are associated with a specific accident scenario occurring within a facility described by a nodalization scheme. These modeling inputs are grouped accordingly as 1) flash and liquid water suspension input, 2) mass and energy transfer to structures input, 3) local/regional mixing via intra-compartment flow pathways inputs and, when present, 4) engineering safety features input. In the case of the MELCOR code both the flash/suspension and local/regional mixing models are included in the Control Volume Hydrodynamic/Flowpath (CVH/FL) package described in the MELCOR reference manual and users' guide [Hum15a, Hum15b]. The mass and energy transfer modeling input is defined in the HeatStructure (HS) package, and the engineering safety features input are described in their separate packages for either spray or fan cooler. Since the HDR tests do not included the sprays or fan coolers, the only packages that require some discussion in terms of impact on the HDR analytical simulation model are the CVH/FL and HS packages. The one exception to the HDR packaging described here is the RN package that includes aerosol modeling and this package is relevant only when water aerosols are modeled in order to provide a more detailed representation of suspended liquid water in the atmosphere. Discussion of this phenomenon and input are addressed later in Section 4. In this section only the more simplified approach to liquid water suspension is considered according to input in the CVH package.

A representation of the HDR ASM is shown in Figure 3-3. Phenomena associated with high energy water injections into the lower pressure containment includes the process of flashing a two-phase water injection along with the subsequent suspension and/or removal of liquid water within the containment atmosphere. Modeling mass and energy transfer from the containment atmosphere to exposed structures is treated through a mechanistic modeling method relying on a known similarity between mass diffusion and boundary layer heat transfer. Since the containment atmosphere can include mixtures of air, hydrogen, and steam, the modeling must include the process of condensation in the presents of non-condensable gases. And because the atmosphere may be flowing in a turbulent fashion from high to lower pressure regions, the process will allow for both natural and force convective regimes. Finally, for analysis of steam and hydrogen mixing, a regional stratification modeling capability must be included to handling regional mixing driven by pressure and buoyancy forces.

3.3.1 Flashing and Liquid Water Suspension

In the early 80's, development of containment analysis type codes focused on both experimental studies and plant accident applications. For the experimental studies, codes such as HMS and HECTR were developed primarily to address hydrogen mixing and deflagration in experimental programs. These codes modeled the containment atmosphere as a single phase gas mixture (H_2/Air/Steam). Parallel development of the codes MELCOR and CONTAIN emphasized modeling of plant accidents (design basis and severe accidents) with a capability to treat two-phase atmospheric processes (H_2/Air/Steam/Liquid water); an important process for the plant accident codes was the treatment of two-phase thermodynamics especially as related to the source or blowdown injection. Single phase (steam) injections also occur in plant accidents, typically characterize as main steam line break (MSLB) accidents. Two-phase injections occur mainly during LOCA. The injection mass and energy source to the atmosphere is input using tabular mass rate and specific enthalpy values. Since water quality at the break is typically not measured, phenomena involved during the two-phase water injection into the facility atmosphere must be simulated. Shown in Figure 3-4 and Figure 3-5 are single- and two-phase water injections for a representative PWR plant. A simulated MSLB accident has previously been analyzed in an integral test performed in the CVTR facility, reported in references Til02a and Til08. Here the HDR containment response for a two-phase injection as a result of a large pipe rupture in tests V44 and T31.5 is analyzed. The similarity between the plant injection for a LOCA and these tests are shown by comparing the plant (Figure 3-5) LOCA source with the injection from a depressurizing vessel in the HDR containment that is used to generated the HDR V44 and T31.5 pipe rupture break, Figure 3-6.

To determine phase separation based on the specific enthalpy of the source, a flashing model is formulated based on an assumption regarding the two-phase expansion process occurring within the containment. For both the MELCOR and CONTAIN codes the expansion process is assumed to be an isenthalpic expansion either with or without mixing of the phase components (steam and liquid) within the containment atmosphere

$$Flash\% = \frac{h_{blowdown} - h_f(x)}{h_g(x) - h_f(x)} * 100 \qquad (3\text{-}1)$$

where

$h_{blowdown}$ = specific enthalpy of water entering containment
$h_f(x)$ = saturation enthalpy of liquid water
$h_g(x)$ = saturation enthalpy of steam

The most common method for treating a flashing process in each code is the thermal equilibrium method where the injection mass and atmosphere gases and suspended liquid are fully mixed with equilibrium assumed such that $x \stackrel{\text{def}}{=} T_{sat} = T_{mix}$; that is, this model assumes perfect contact between all atmospheric components. In the accident analysis realm this modeling method is referred to as the temperature flash (TF) model. The modeling is specified in MELCOR using the CVH/FL package with input stream,

```
CV_SOU 2   ! number of mass or energy sources
!      index  ctyp  interp  iessrc       edfnam  numchn idmat esscal
       1      MASS    rate     EDF  'v44source'       1     3    1.0
!      index ctyp   interp  iessrc       edfnam  numchn esscal
       2       AE     rate     EDF  'v44source'       2    1.0
```

where the external atmosphere source file "v44source" is defined with the mass rate (kg/s) and the enthalpy rate (kJ/sec). The input "AE" input indicates that the enthalpy is added directly to the atmosphere for a thermal equilibrium calculation. By default the MELCOR code also assumes that the fraction of unflashed liquid water is retained in the atmosphere as "fog" (water aerosol) and removed by aerosol deposition and settling processes. The treatment of unflashed water is specified using the CV_THR input stream as

```
!         icvthr  ipfsw  icvact
CV_THR  NONEQUIL    FOG  ACTIVE
```

where FOG is the default setting.

In the case where it may be assumed that liquid water in the atmosphere drops out at the end of a time step, a specification for "no fog" is activated with the input

```
!         icvthr  ipfsw  icvact
CV_THR  NONEQUIL  NOFOG  ACTIVE
```

In most plant calculations a temperature flash model along with a NOFOG setting results in the maximum containment pressure response, and therefore represents a conservative approach used for licensing when the containment can be modeled also as a single well-mixed volume. Another model, typically used for containment analyses where a minimum pressure is desired, is the "pressure flash" model that finds utility for conservative emergency core cooling system (ECCS) backpressure predictions. This model replaces the independent variable x in the enthalpy function by the saturation pressure which is taken as the total containment pressure, that is, $x \stackrel{\text{def}}{=} P_{total}$. Similar input for mass and energy sources are used for a pressure flash,

```
CV_SOU 2
!       index  ctyp  interp  iesscrc       edfnam  numchn  esscal
        1        WM    rate      EDF  'v44source'       1     1.0
!       index  ctyp  interp  iesscrc       edfnam  numchn  elev  isautopt
        2        WE    rate      EDF  'v44source'       2  14.0     SC 0
```

Flashing Model. Shown in Figure 3-7 and Figure 3-8 are the calculated flashing percentages for various energy sources based on a temperature and pressure flash model, respectively. For a comparative illustration, the V44 injection and measured breakroom temperature and pressure shown in Figure 3-9 is used to estimate the amount of flashed steam at 20 seconds into the test using each flashing model for a range of injection enthalpies. For enthalpy injections ranging from 1500 to 2000 kJ/kg, the flashing percentages are between 45 and 67% for a temperature flash in the breakroom, and because the breakroom atmosphere rapidly transitions to a pure steam environment the pressure flash model predicts the same flashing percentages. Had the injection location been chosen to occur in a large volume region that does not transition to pure steam the percentages calculated with each model would differ by a small amount. Continuing with this illustration, we chose the dome region with the same range in injection enthalpy and find that the temperature flash model estimates the flashing percentage range at 50 to 70%, while the pressure flash model predicts a percentage range of 43 to 67%. Therefore, as we move from a pure steam region to a region with a steam/air environment at lower mixture temperatures but same total pressure, a slight reduction in flashing percentage occurs with the pressure flash model with more liquid water available for suspension.

Liquid Suspension. One significant effect on calculated containment temperature and pressure is the assumption regarding liquid water suspension and removal from the containment atmosphere. For MELCOR, both the temperature and pressure flash modeling assumes complete mixing of the injection water and atmosphere during the flashing period. What this means is that for flashed percentage less than 100% the atmosphere will be saturated at end of a calculation time step whether the suspension model is characterized with a keyword FOG or NOFOG. To demonstrate suspension effects, the HDR facility Figure 3-10a) is modeled first as a single cell containment (Figure 3-10b) and then as a two cell volume (Figure 3-10c) with the breakroom separated from the large volume containment. Each calculation case focuses on flashing model and method used for suspension of water. Each case assumes adiabatic boundary conditions (no structures). Figure 3-11 and Figure 3-12 show the results for the single cell containment with a NOFOG setting. In each case, the pressure response is similar with the pressure flash model resulting in a slightly lower pressure. Temperatures calculated for the containment show identical results for the FOG setting case, and a small amount of superheating when the setting is changed to NOFOG. A larger variation in containment response is shown for a two cell containment model, Figure 3-13 and Figure 3-14. For the two cell model, with the FOG setting, the containment response in Figure 3-13 is similar to the single cell case with FOG, indicating no variation between a choice of temperature or pressure flash modeling. The reason for this behavior is due to the small breakroom that rapidly becomes pure steam and therefore both the flashing models result in identical flash percentages. When the two cell model has the fog setting changed from FOG to NOFOG the containment for each flashing model is significantly superheated since essentially all liquid water suspended in the breakroom is removed prior to water being driven into the downstream containment volume. The significant amount of superheating in the containment results in an elevated pressure response. Since HDR reference calculation are multi-cell models, there will also

be a tendency to superheat; however, the superheating represents a small incremental energy increase in the atmosphere and energy transfer to structures can mitigate the effect of superheating on pressure. Selecting a NOFOG treatment of suspended liquid water will be a conservative choice from a containment loads (temperature and pressure) perspective. These atmospheric responses to various flashing models (temperature or pressure), liquid suspension, and nodalization can be important to the analysis of the HDR pipe rupture tests and therefore are addressed below in Section 4.

3.3.2 Mass and Energy Transfer from Atmosphere to Structures

The MELCOR modeling for heat and mass transfer from containment atmosphere to passive structures and components is based on a heat and mass transfer analogy (HMTA) where common heat transfer correlations (natural, mixed and forced circulation) are used to determine sensible (q_{conv}) and latent (q_{cond}) energy transfers through temperature and concentration boundary layers, respectively. A sketch of the energy transfer modeling used both in MELCOR and CONTAIN is shown in Figure 3-15. Table 3-9 lists sketched parameter labels with corresponding MELCOR plot quantities. The importance of energy transfer to containment response will become evident in the discussion in Section 4. Here we focus on the separate effect of energy transfer to demonstrate some important features of the HMTA model.

In most containment analysis scenarios, the dominant transfer process in the containment affecting figures-of-merit such as pressure or gas temperature is process of latent or condensation energy (i.e., via mass transfer) transfer in the presence of noncondensible gases. In this situation the main resistance to condensation is the build-up of noncondensible gases near the surface of the structure, i.e., within the gas boundary layer. The built-up noncondensibles in this diffusion layer effectively depresses the partial pressure of vapor and degrades the condensation process. Consequently, condensation heat transfer coefficients are known to be sensitive to small amounts of bulk air concentrations (i.e., air/steam mass ratios), especially for natural convective conditions (low atmospheric velocities). This behavior and MELCOR's modeling ability to simulate the process is discussed in detail for the Dehbi natural convection separate-effects test in Appendix B of reference Til08. Below, various features of the HMTA model are addressed using the Dehbi test geometry to illustrate energy transfer sensitivity to boundary layer convection and condensate film thickness modeling.

Energy Transfer Models. A widely used heat transfer correlation for Nusselt number, *Nu*, developed for turbulent, vertical wall heat transfer under natural convection conditions, is modeled in MELCOR as $Nu_{nat} = CRa^m + D$, where *C*, *m*, and *D* are constants set by the user (or remain as defaults); and, *Ra* is the Rayleigh number. For turbulent, forced flow the Nusselt equation is $Nu_{forced} = C\,\mathrm{Re}^m\,\mathrm{Pr}^n + D$, where again the constants *C*, *m*, *n*, and *D* are set by the user; *Re* and *Pr* are the Reynolds and Prandtl numbers, respectively. In order to conform to the heat transfer equations for Nusselt number used in the CONTAIN assessment report [Til02a], the value of C in the free convection equation is set (sensitivity coefficient 4110(1)) to 0.14; *m* remains set to the default setting of 1/3, and D is zero, by default. As with the CONTAIN equations for forced flow, the default MELCOR settings *C* = 0.037, *m*=0.8, and *n*=1/3 are used. Although equations for laminar flow are also included in the MELCOR modeling for convection, turbulent conditions are most often used based on the expected flow conditions inside containments and the default laminar

to turbulent range settings. Transition from natural to forced convection is, as in CONTAIN, set to the maximum of either the free or forced Nusselt number, $Nu = \max\left[Nu_{nat}, Nu_{forced}\right]$. In MELCOR, this setting is invoked by setting the sensitivity coefficient 4060 (1) equal to -1. For both single- and multi-cell calculations, the calculated lumped cell flow velocity (forced) along structure surfaces is too small to force $Nu_{forced} > Nu_{nat}$, that is, unless flows within a control volume are specified by input for the blowdown period, either directly or by setting the hydraulic area of the control volumes to a value that causes $Nu_{forced} > Nu_{nat}$ in the region of the break. Specification of flows in such cases is not a normal feature for design basis analyses since estimation of blowdown driven air/steam flows is outside the scope of analytical modeling, whether by finite-difference or control volume methods, and for these reasons a conservative assumption that neglects the enhancement effect of atmospheric velocity on energy transfer in the containment is adopted. However, the use of flow or velocity specification for structure condensation heat transfer is useful for other purposes, e.g., for minimum backpressure calculations, sensitivity investigations, or for indirect confirmation of measured velocities via structure heat flux measurements.

In the HDR breakrooms (Rooms 1608 and 1704) and surrounding regions there is a large amount of exposed metal structures, making the facility somewhat non-prototypical compared to a commercial plant design. During the early portion of the HDR blowdowns, when these regions are exposed to high steam concentrations and the attending high velocities, the noncondensible boundary layer resistance is relatively small and consequently importance of condensate film resistance becomes an important feature of the energy and mass transfer process affecting atmospheric pressure and temperature. Using the Dehbi test validation as a basis for exploring these sensitivities that involve flow velocity and condensate resistance these trends are demonstrated. In Figure 3-16 the Dehbi calculated heat transfer coefficient for a 1.5 bar saturated atmospheric test is shown for a structure where the atmospheric or bulk temperature (T_b) to surface temperature (T_s) drop is fixed at 30 degrees. The first calculation assumes near quiescent conditions along the structure surface (natural convection), Figure 3-16. For air mass fractions ranging from 0.3 to 0.9 the MELCOR HMTA model has been shown to be validated [Til08] for natural convection conditions. For the case shown, the air mass fraction are reduced to very small values that are typical of breakroom conditions during pipe ruptures. Shown in the figure are the condensate film resistance percentages ($R_{film}/(R_{film}+R_{gas})$)*100) as a function of air mass fraction. As indicated, for air mass fractions of ~ 0.4, typical of single volume containment modeling, the film resistance is of minor importance. However, if the containment is modeled to include the breakroom and surrounding regions, these regions will be characterized as low air mass fraction regions and the importance of condensate film resistance is magnified. In early versions of the MELCOR code (1.8.6 and 2.X) the default dynamic film flow model (i.e., with Nusselt laminar film flow) was the only functioning model for addressing condensate film resistance. Codes such as CONTAIN however included both film dynamic flow and a maximum film thickness model to offer additional control over how condensate resistance prediction might be treated. Recently, during the fall of 2015, a new maximum film thickness model (Enforcemax) was incorporated into the MELCOR code similar to the default fixed film thickness method used in the CONTAIN code. In this model the film is allowed to build up to a set maximum thickness before overflowing to a pool region. Addition of this model allows for a more complete direct comparison to the CONTAIN code input used in HDR calculations, and allows the user to impose a conservative modeling methodology on estimated condensate film resistance. This optional treatment by the

"Enforcemax" keyword in MELCOR HS package adds a capability that reflects better on an approach most often associated with a conservative DBA analysis. In the reference HDR calculations, however, the default dynamic film model is used, but for code benchmarking and sensitivity cases the maximum film thickness model is added, where noted, to make appropriate comparisons to CONTAIN code results as well as to assess the degree of conservatism that may be invoked by using a varying film resistance model.

In the immediate vicinity of the pipe rupture and surrounding area the high concentration steam is also attended by relatively high atmospheric velocities. As the heat transfer regime transitions from natural or mixed to forced convective flow the heat transfer coefficients also increase as shown in Figure 3-17. However, there is a threshold velocity below which heat transfer is predicted to be defined as natural convection and an upper bound where further velocity increases have only a marginal increase in heat transfer, especially for high steam concentrations. For the conditions indicated in this illustrative calculation, the first threshold is approximately 3 m/s for natural convection and approximately 10 m/s for the forced convection limiting region. These regime boundaries are a useful guide in establishing conservative model settings for various containment applications.

Other Resistances to Structure Energy Transfer. In most "as-built" containments, major structural walls and equipment have a layer of paint which also represents a resistance to condensation heat transfer. In the CONTAIN code, for example, paint resistance is explicitly modeled with a series conductance added to the film layer and surface node resistance. For MELCOR, there is no explicit modeling of paint resistance, and therefore in essentially all containment analyses to date, paint resistance has been neglected. Two options for including paint resistance are available however. In the first option, the paint layer is modeled as a separate material layer for representing a composite structure (e.g., paint over concrete or steel). The disadvantage of this approach is that the thin paint layer with its small thermal capacitance can require small timesteps for adequate convergence of the heat conduction solution. Another approach is equivalent to the method implemented in the CONTAIN modeling where the heat capacity of the paint is neglected compared to the surface node of the structure, with only the resistance (or conductance) of the paint accounted for in the conduction model. The CONTAIN method for treating paint layers can be simulated in MELCOR by adjusting the thermal conductivity of the surface node; that is, by modifying the effective conductivity to include the added resistance of the paint layer. This method has been used in previous integral test cases like the CVTR tests; however, since the HDR facility had noticeable deterioration of surface paint, the paint resistance modeling is neglected in the reference cases.

While thermal radiation heat transfer between the containment atmosphere and structures is a small contributor to the total heat transfer for containment analysis, it is nevertheless, treated in the MELCOR modeling and its inclusion may be of some importance in correctly modeling conditions where the containment gas has significant superheat; for example, in cases involving deflagrations or fires. Due to the small degree of superheating observed in the HDR tests, this feature of MELCOR modeling is not included in the HDR calculations.

3.3.3 Local and Regional Mixing

Flow Pathways. The irreversible loss coefficients presented in the original CONTAIN input files, C_F, were implemented in the MELCOR deck using the relationship $2*C_F=K_F'$. The K_F' in this relationship is the irreversible loss coefficient for MELCOR; however, the irreversible loss coefficient is the combination of a friction loss coefficient, Fr, and form loss coefficients, K_F, i.e., $K_F'=K_F+Fr$. Since CONTAIN takes the irreversible loss coefficient, C_F, directly as user input, MELCOR input was specified to minimize Fr such that the irreversible loss could be defined using only the form loss coefficient. This was performed by setting SLEN, the length used to determine the friction factor for a flowpath, to 0.001 and SHYD, the hydraulic diameter, to 10.0. The form loss coefficients are specified for forward and reverse flow on FL_USL in MELCOR using the relationship of $2*C_F$.

Stratification. Lumped parameter codes like MELCOR and CONTAIN tend to overmix regions that would normally be stratified under conditions that are primarily buoyancy driven. Due to slight differences in the methods for defining gravity heads between connected control volumes, the MELCOR and CONTAIN codes predict stratification profiles somewhat differently and therefore agreement in the buoyancy driven stratification prediction is not expected. Additionally, for CONTAIN, a hybrid flow solver has been incorporated to improve on the overmixing tendencies and therefore especially for longer-term tests such as Project T31.5 and the E-series (E11.2 and E11.4), the MELCOR code will tend to show a more well-mixed atmosphere during and after light gas injections than the CONTAIN code. In situations that favor well-mixing (low elevation injections), the mixing issue is often overstated, but for mid-level injections and dome cooling as modeled in the E11.2 test, for example, regional mixing becomes an important feature of the containment model.

To demonstrate the over-mixing problem, a plume simulation is modeled with connected lumped parameter control volumes, Figure 3-18. With a lighter gas (nitrogen) injected into volume #12, the analytical solution to this problem shows that the nitrogen accumulates in the region above the source injection. Modeling the plume geometry as indicated in Figure 3-18 with CONTAIN and MELCOR show the over-mixing tendency, except for the density formulation using the hybrid flow solver in CONTAIN. Both codes show over-mixing by calculating flows below the injection location. While over-mixing is generally not an issue for global atmospheric response (pressure, for example), mixing is often more critical for predicting regional temperature profiles, and even more critical in modeling regional light gas concentrations with elevated injections. These concerns regarding stratification are noted in the discussion of temperature and light gas concentration profiles for both the Project T31.5 and E-series tests where light gas injections are simulated for beyond DBA and SA long-term scenarios.

3.4 Sensitivity Calculations

Sensitivity studies are required to investigate uncertainties in any analytical simulation modeling of an experiment, or postulated plant accident. Three major modeling components are the code user, the code itself, and the accident (experiment) scenario. Uncertainties can be found in each component and these uncertainties should be identified, as much as practical. The results of sensitivity studies provide important feedback for the ranking of phenomena, which in turn helps

to focus these types of investigations. In most experiments, sensitivities studies are paramount to an understanding of the physics occurring in the experiments. Many of these types of sensitivities are explored here to better understand controlling processes in each HDR test assessment. Clearly, a good series of sensitivity studies depends on how well certain basic phenomena are simulated by the code; therefore, feedback from sensitivity studies is used to improve physical modeling, which in turn benefits user guidance in selecting model inputs for various applications requiring either conservative or best-estimate results. Shown in Table 3-10 are some of the sensitivity cases explored for the HDR series of tests.

Table 3-1 Illustrative Phenomena Identification and Ranking Table for during the Rapid Pressurization Phase of a DBA in a Large Dry PWR Containment

Component	Process	Phenomena	Rank	
			Pressure	Temperature
Atmosphere:				
	Pressurization/ depressurization	Multi-component gas compression/ expansion	H	H
		Aerosol mass and energy exchange	L	L
		Spray mass and energy exchange	M	M
		Volume displacement/pool filling or draining	L	L
		Atmosphere cooling by fan cooler	L-M	L-M
	Mixing	Jet-plume gas interaction/entrainment (localized)	L-M	M-H*
		Buoyancy/stratification (regional)	L-M	L-M
		Buoyancy/wall interaction (regional)	L-M	L-M
		Diffusion (turbulent)	L	L
		Spray dynamics	L-M	M
		Fan dynamics	L	L-M
	Transport (inter-compartment)	Buoyancy	M	M-H
		Form and friction losses	L	M-H
		Aerosol coupling	L	L
		Liquid water carry over	L-M	M
Structure:				
interior	Heat transfer	1-D transient conduction	M	M
		2- or 3-D transient conduction	L	L
	Mass transfer	Outgassing (concrete)	L	L
surface (solid and film)	Sensible heat transfer	Spray/aerosol deposition or impingement	L	L-M
		Free convection	L	L
		Forced/mixed convection	L	L-M
		Radiation (structure to atmosphere)	L	L-M
		Radiation (structure to structure)	L	L-M
		Liquid film resistence	L	L
		Liquid film advection	L	L
	Latent heat and mass transfer (condensation/ evaporation)	Free convection	M	M
		Forced/mixed convection	M	M
	Transport (film flow)	Liquid film advection	L-M	L-M
		Interfacial shear (film/gas interaction)	L	L

Table 3-1 (cont.)

Component	Process	Phenomena	Rank	
			Pressure	Temperature
Pool:				
	Mixing	Buoyancy/stratification	L	L
		Bubble dynamics	L	L
	Transport	Filling	L	L
		Displacement	L	L
Interior	Heat transfer	Convection (flooded structures)	L	L
		Boiling	L	L
		Steam condensation(bubbles)	**	**
Surface	Sensible heat transfer	Free convection	L	L
		Forced/mixed convection	L	L
		Aerosol/spray deposition	L	L
	Latent heat and mass transfer	Free convection	L	L-M
		Forced/mixed convection	L	L

*The high ranking of this phenomenon is conditional, depending on the characterization of the injection (break size, location, and orientation).

**Not applicable for this accident phase or reactor type (may apply for BWR type).

Table 3-2 Illustrative Phenomena Identification and Ranking Table for the Slow Pressurization/Depressurization and Core Damage Phase of a DBA or Beyond DBA in a Large Dry PWR Containment

Component	Process	Phenomena	Rank		
			Pressure	Temp	Composition
Atmosphere:					
	Pressurization/ depressurization	Multi-component gas compression/ expansion	M	M-H	M
		Aerosol mass and energy exchange	L	L	L-M
		Spray mass and energy exchange	M-H	M-H	M-H
		Volume displacement/pool filling or draining	L	L	L
		Atmosphere cooling by fan cooler	M-H	M-H	H
	Mixing	Jet-plume gas interaction/entrainment (localized)	L	L(H)*	L(H)*
		Buoyancy/stratification (regional)	L-M	M	M
		Buoyancy/wall interaction (regional)	L	M	M
		Diffusion (turbulent)	L	L	L
		Spray dynamics	L-M	M	H
		Fan dynamics	L	M	H
	Transport (inter-compartment)	Buoyancy	M	M-H	H
		Form and friction losses	L	L-M	L-M
		Aerosol coupling	L	L	L
		Liquid water carry over	L	L	L
Structure:					
interior	Heat transfer	1-D transient conduction	M-H	M-H	M-H
		2- or 3-D transient conduction	L	L	L
	Mass transfer	Outgassing (concrete)	L	L	L
surface (solid and film)	Sensible heat transfer	Spray/aerosol deposition or impingement	L	L-M	L-M
		Free convection	L	L	L
		Forced/mixed convection	L	L-M	L
		Radiation (structure to atmosphere)	L	L-M	L
		Radiation (structure to structure)	L	L-M	L
		Liquid film resistance	L	L	L
		Liquid film advection	L	L	L
	Latent heat and mass transfer (condensation/ evaporation)	Free convection	H	H	H
		Forced/mixed convection	L-M	L-M	L-M

Table 3-2 (cont.)

Component	Process	Phenomena	Rank		
			Pressure	Temp	Composition
surface (solid and film)	Transport (film flow)	Liquid film advection	L-M	L-M	L-M
		Interfacial shear (film/gas interaction)	L	L	L
Pool:					
	mixing	Buoyancy/stratification	L	L-M	L
		Bubble dynamics	L	L	L
	transport	Filling	L	L-M	L-M
		displacement	L	L	L
interior	Heat transfer	Convection (flooded structures)	L	L-M	L
		Boiling	L	L	L
		Steam condensation(bubbles)	**	**	**
surface	Sensible heat transfer	Free convection	L	L	L
		Forced/mixed convection	L	L	L
		Aerosol/spray deposition	L	L	L
	Latent heat and mass transfer	Free convection	L	L-M	L-M
		Forced/mixed convection	L	L	L

*The high ranking of this phenomenon is conditional, depending on the characterization of the injection (break size, location, and orientation).

**Not applicable for this accident phase or reactor type (may apply for BWR type).

Table 3-3 Important containment phenomena addressed in experiments based on design and beyond design basis ranking criteria (containment pressure and temperature).

		Experiment												
		Separate			Integral									
Component/ Process	Phenomena	Wisc. Flat plate	Phebus FPTO	JAERI spray tests	HDR V44	HDR T31.5	HDR E11.2	HDR E11.4	CVTR Test #3	CVTR Test #4-5	NUPEC M-7-1	NUPEC M-8-2	NUPEC M-8-1	NUPEC M-4-3
Atmosphere:														
Pressurization	Multi-component gas compr/exp		3	3	3	3	3	3	3	3	3	3	3	3
	Spray mass and energy exchange			3						3	2	2		
	Cooling by fan cooler													
Mixing	Jet-plume gas interaction/entrain				1	1	2	1	1	1	1	1	1	1
	Buoyancy/stratification (regional)			3	3	3	3		3	3	3	3	3	3
	Buoyancy/wall interaction (regional)				1	1	1	1						
	Spray dynamics			2						2	2	2		
	Fan dynamics													
Transport	Buoyancy				1	3	3	3	3	3	3	3	3	3
	Form and friction losses				3	3	1	1	1	1	1	1	1	1
	Liquid water carry over				2	2	1	1						
Structure Interior:														
Heat transfer	1-D transient conduction				3	3	3	3	3	3	3	3	3	3
Structure Surface:														
Mass transfer (cond/evap)	Free convection	3	3	1	3	3	3	3	3	3	1	1	1	1
	Forced/mixed convection	3			1	1	1	1	3	3				

[ ] not present, 1- present, 2- present and significant, 3- measured

Table 3-4 MELCOR modeling of phenomena occurring during accidents within large dry containments.

Component: Process	Phenomena	Model Comments with Comparison to CONTAIN Code
Atmosphere:		
Pressurization	Multi-component gas compression/expansion	Equivalent atmospheric equilibrium approach with slight difference due to variation in gas property relationships and treatment of two-phase (atmosphere/pool) interaction via voiding/energy exchange
	Spray mass and energy exchange	Equivalent approach with MELCOR has added capability in treating droplet size distributions and control volume fall though, in addition to rainout from structures
	Atmospheric cooling by fan cooler	Limited modeling capability for MELCOR; mechanistic treatment of fan cooler condensation field in development
Mixing	Jet-plume gas Interaction/entrainment	Both codes allow similar specification of flow velocity via volume velocity calculation based on effective volume flow area (useful for sensitivity analysis only)
	Buoyancy/stratification (regional)	CONTAIN uses a hybrid flow solver to prevent nonphysical circulation flows between control-volumes that is unique to code.
	Spray dynamics	Neither code allows spray induced mixing via droplet/gas drag.
	Fan dynamics	Both codes allow intra-compartment fan flow w/o momentum transport.
Transport	Buoyancy	Equivalent approach with variable static head calculated as function of elevation
	Form and friction losses	MELCOR pipe friction modeled separately with forward/reverse form factors
Structure Interior:		
Heat transfer	1-D transient conduction	CONTAIN uses Crank-Nicholson scheme (cell-centered difference) with explicit paint conductance; MELCOR fully implicit scheme (cell boundary difference) – no explicit paint conductance
Structure Surface:		
Heat and Mass Transfer (evap/cond)	Free convection	Heat and Mass Transfer Analogy (HMTA): Default convection correlation is a factor 0.1/0.14 lower; dynamic condensate film flow is by default using a Nusselt film theory approach (laminar flow range applicability equivalent to CONTAIN optional modeling approach)
	Forced convection	Equivalent HMTA approach: MELCOR/CONTAIN velocity calculated at cell level using input hydraulic areas.

Table 3-5 MELCOR/CONTAIN code model comparison for specific phenomena/processes

Phenomena/Process	Code Model / Parameter defaults	
	MELCOR	**CONTAIN**
Two-phase separation	Temperature flashing Pressure flashing (saturation constraint) Water aerosol distribution profile with pressure flash model	Temperature flashing Pressure flashing (not constrained to saturation curve since the flashing is performed without mixing)
Water aerosol deposition	MAEROS aerosol physics model	MAEROS aerosol physics model
Water aerosol/gas interaction (thermodynamics)	Specific heat and mass accounting / include aerosol/gas mass transfer by analogy to heat transfer (HMTA)	Neglect specific heat and mass accounting / include aerosol/gas mass transfer by analogy to heat transfer (HMTA)
Water aerosol/gas interaction (thermal hydraulics)	Aerosol density included in flow equations	Aerosol density neglected in flow equations; suspended liquid density included if aerosol input omitted
Suspended liquid water (fog) without aerosol physics (thermodynamics)	Specific heat and mass accounting	Specific heat and mass accounting
Suspended liquid water (fog) Without aerosol physics (thermal hydraulics)	Liquid density included in flow equations	Liquid density included in flow equations
Pool transfers	Mechanistic liquid flows between compartments	Parametric compartment overflows
Structure heat and mass transfer	Heat and mass transfer analogy (HMTA), with equations for orientation and surface convective boundary conditions	Heat and mass transfer analogy (HMTA), with equations for orientation and surface convective boundary conditions
Wall condensate tracking	Default film tracking; with optional film thickness set by structure	Default film thickness limit with overflow; film tracking by optional setting
Gas mixing and stratification	Lumped parameter flow equations with some over-mixing tendency	Hybrid flow solver to partly correct lumped parameter over-mixing tendency

Table 3-6 HDR Facility Nodalization

Cell	Volume, m^3	Bottom Elevation, m	Rooms
1	1893	-3.435	1201, 1202, 1203, 1301, 1302, 1303, 1304, 1305, 1307, 1308, 1311, 1317, 1401, 1403, 1404, 1405, 1406, 1408, 1409, 1410, 1420, 1421
2	655	4.8435	1501, 1502, 1503, 1504, 1505, 1506, 1507, 1512, 1513
3	295	5.285	1508, 1511, 1514
4	280	11.9	1603 (breakroom – V44)
5	192	10.005	1611
6	303	10.0045	1602, 1609, 1606
7	190	8.938	1604, 1607, 1608, 1605
8	44	13.85	1701u
9	64	20.6	1701o
10	793	14.255	1704 (breakroom – T31.5)
11	90	15	1708
12	119	15	1707
13	156	15	1702, 1703, 1706
14	164	25.1015	1803, 1904, 1905
15	343	21.05	1801
16	58	20.6	1805
17	125	20.6	1802
18	79	20.6	1804
19	38	25.3	1902
20	78	25.3	1901, 1911
21	71	25.3	1903
22	61	5.4	1327
23	40	10	1337
24	83	15	1347
25	68	20.6	1357
26	82	25.3	1367
27	947.98	30.85	11004*
28	947.98	30.85	11004*
29	216.3	30.85	11004*
30	216.3	37.85	11004*
31	890.62	37.85	11004*
32	890.62	37.85	11004*
33	690.19	44.275	11004*

Table 3-7 33-CV MELCOR Modifications

Location	Modification 1	Modification 2
Cell#14	Flow-Through Area (FTA) to Cell#15.	-
Cell#15	Floor heat structure added (15subflor)	-
Cell#16	FTA to Cell#25	-
Cell#18	FTA to Cell#10	-
Cell#20	FTA to Cell#19	-
Cell#22	FTA to Cell#2	Adjust cell height by +0.1 m
Cell#23	FTA to Cell#22	Adjust cell height by +1.0 m
Cell#24	FTA to Cell#23	Adjust cell height by +1.5 m
Cell#25	FTA to Cell#24	Adjust cell height by +0.2 m
Cell#26	FTA to Cell#25	-
Cell#30	FTA to Cell#29	-
Cell#31	FTA to Cell#27	-
Cell#32	FTA to Cell#28	-
Cell#33	FTA to Cell#30	-

Table 3-8 Key modeling/input options used in MELCOR HDR reference calculations

Test (ISP/HDR Proj)	Model/Input Option
V44 (ISP-16)	• 33 cell nodalization (33-CV) • HDR thermal properties for steel and concrete • No convective velocities • Default film thickness (film tracking) • No thermal radiation • Condensate drained to pools • Flow loss coefficients set to unity • Temperature flashing (default) • No fog
T31.5 (ISP-23)	• Same as V44 (ISP-16)
T31.5 (Project HDR)	• Same as T31.5 (ISP-23) • Includes late-time He/H2 injection (start at 20 minutes)
E11.2 (ISP-29)	• 15 cell nodalization (15-CV) includes secondary containment space • CONTAIN thermal properties for steel and concrete • No convective velocities • Default film thickness (dynamic film flow) • No thermal radiation • Blowdown & late-time external steam injection for pre-conditioning • Coolant energy extraction (Hydrogen sensors) • Condensate drained to pools • Overflow of pools to sump • Flow loss coefficient set to unity • Temperature flashing (default) • Fog model using aerosol physics • Exterior shell water flooding of dome • Secondary containment space modeled
E11.4 (Project HDR)	• Same as E11.2 • 48 cell nodalization (48-CV) includes secondary containment space

Table 3-9 Structure energy transfer parameters used to determine heat transfer coefficient

Parameter	Description	MELCOR variable	Comment
T_b	Bulk atmosphere gas temperature (K)	CVH-TVAP	Gas temperature may be superheated or saturated
T_{if}	Temperature of film/atmosphere interface	HS-FILM-TEMP	Dehbi illustrative calculation run with (T_b-T_{if}) = 30 degrees
q_{conv}	Sensible heat flux	HS-QFLUX-ATMS	Heat flux to the film/atmosphere interface at temperature T_{if}
q_{cond}	Latent heat flux	HS-ENERGY-FLUX	Energy flux associated with condensation/evaporation
q_{film}	Energy transfer flux due to film drainage	No variable defined for printing or plotting	At steady state the film drainage energy flux is the condensate mass flux (HS-MASS-FLUX) times the film enthalpy (HS-FILM-ENTH)
δ	Average film thickness	HS-FILM-THICK	Film dynamic flow thickness determined by film flow correlation (most cases the equation for flow is the Nusselt laminar film flow equation)
T_s	Structure surface temperature	HS-TEMP	First node of the structure temperature profile
q_{wall}	Energy transfer flux to the structure wall surface	No variable defined, must be calculated separately from available HS variables	$q_{wall} = k_{film}*(T_{if}-T_s)/\delta$

* $h = q_{wall}/(T_b-T_s)$

Table 3-10 Sensitivities investigated for the HDR facility tests

Sensitivity	Variations	Test				
		V44 (ISP-16)	**T31.5 (ISP-23)**	**T31-5 Project HDR Benchmark**	**E11.2 (ISP-29)**	**E11.4 Project HDR Benchmark**
Flashing	*TF*	R	R	R	R	R
	PF	X				
Aerosol Physics	*NOFOG*	R	R	R		
	FOG	X				
	FOG wRN	X	X		R	R
Natural** **Convection**	*Regime Determined*	R	R	R	R	R
Forced Convection (20 m/s) in Rooms	*1600s*	X				
	1600s, 1700s	X				
	1500s – 1700s	X	X			
Nodalization	*1-CV*	X	X	X		
	33-CV	R	R	R		
	15-CV				R	R
	48-CV				X	X
Dynamic Film Thickness		R	R	R	R	R
Maximum Film Thickness, m	*0.0005*	X	X	X	X	X
	0.0001	X				
	0.00005	X	X			
Concrete Material Properties	CONTAIN*				R	R
	HDR**				X	X
	HDR Enh.***				X	
Sensor Cooling Lines	Included				R	R
	Ignore Energy Removal				X	

R – Represents the reference analysis

X – Represents the sensitivities performed

X – Indicates that an additional analysis combining these sensitivities was performed

* Default CONTAIN concrete properties

** HDR specified concrete properties

*** Enhanced density, conductivity, and specific heat

**** The regime is internally determined by the code, resulting in natural convection being dominantly determined.

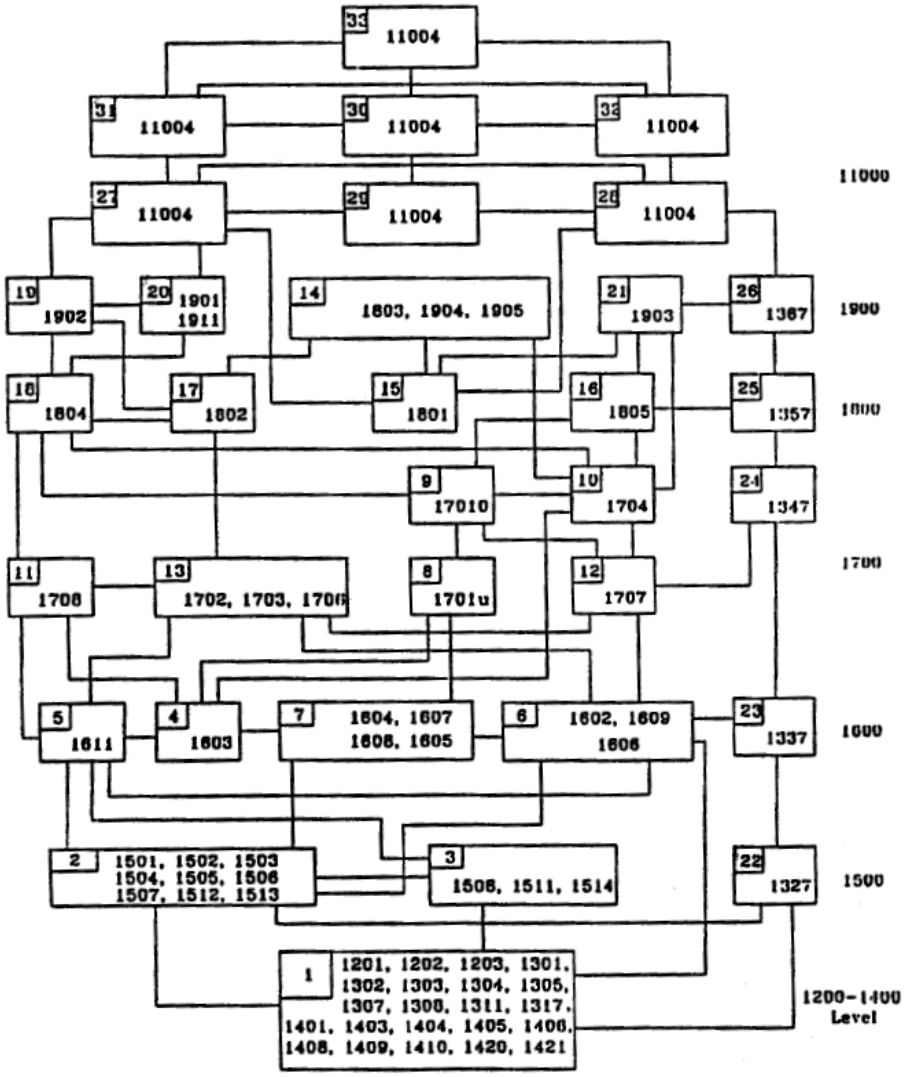

Figure 3-1 Depiction of the rooms incorporated in the 33-CV nodalization. [Til02a]

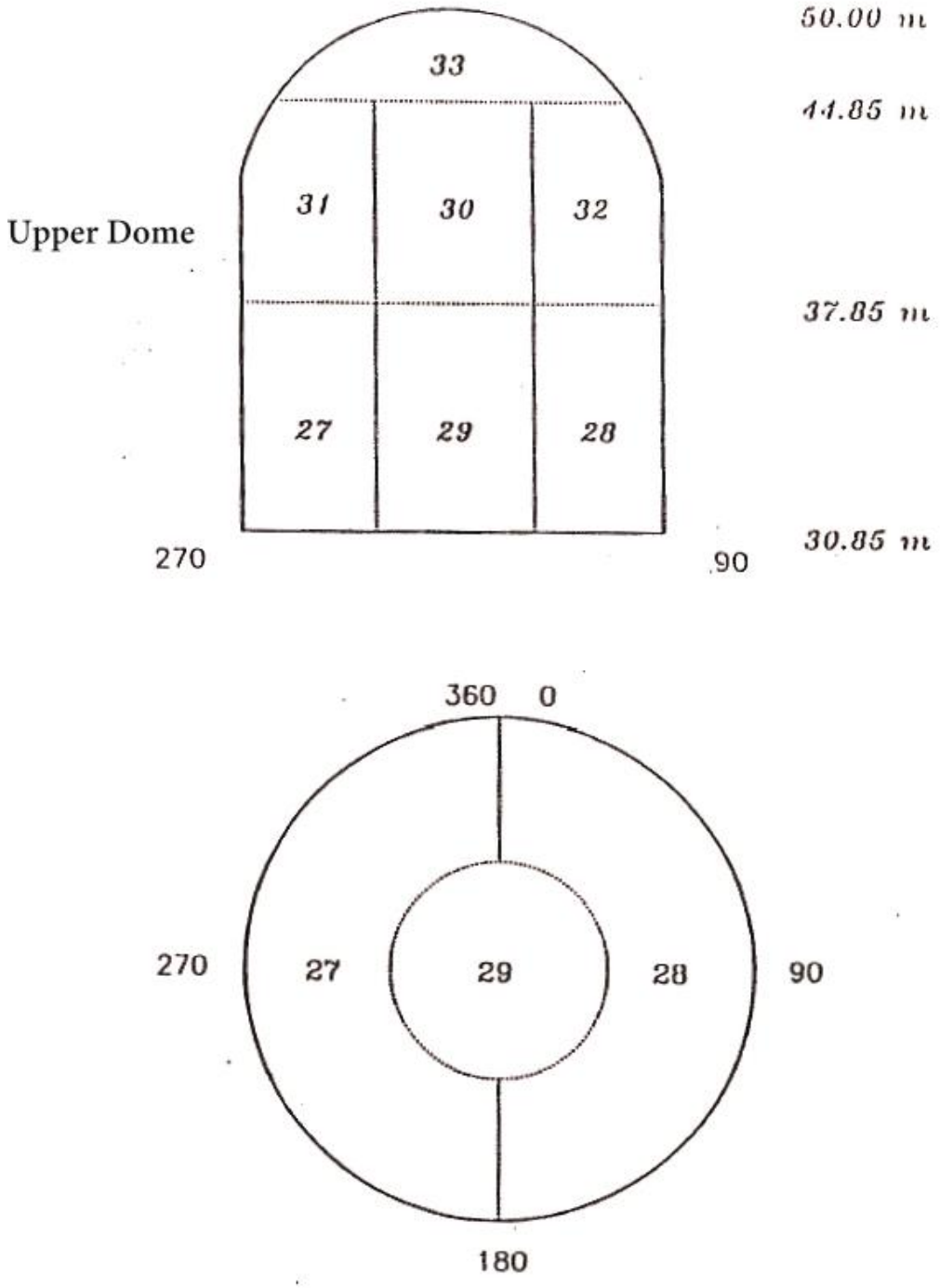

Figure 3-2 Upper dome nodalization for the 33-CV HDR model.

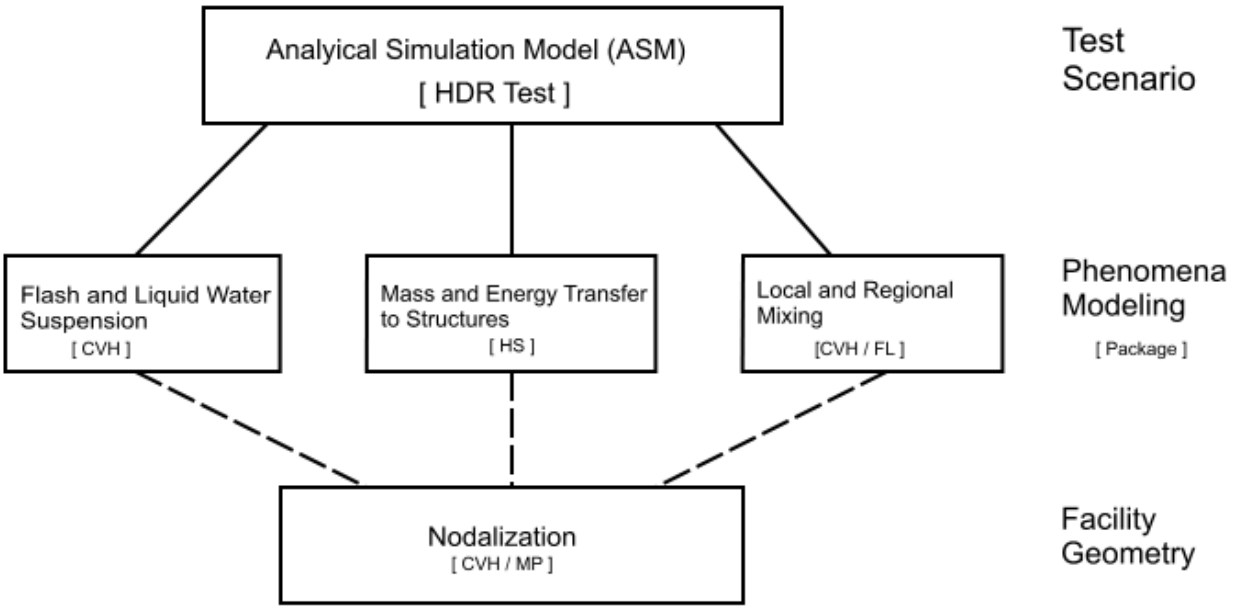

Figure 3-3 User inputs for the HDR ASM.

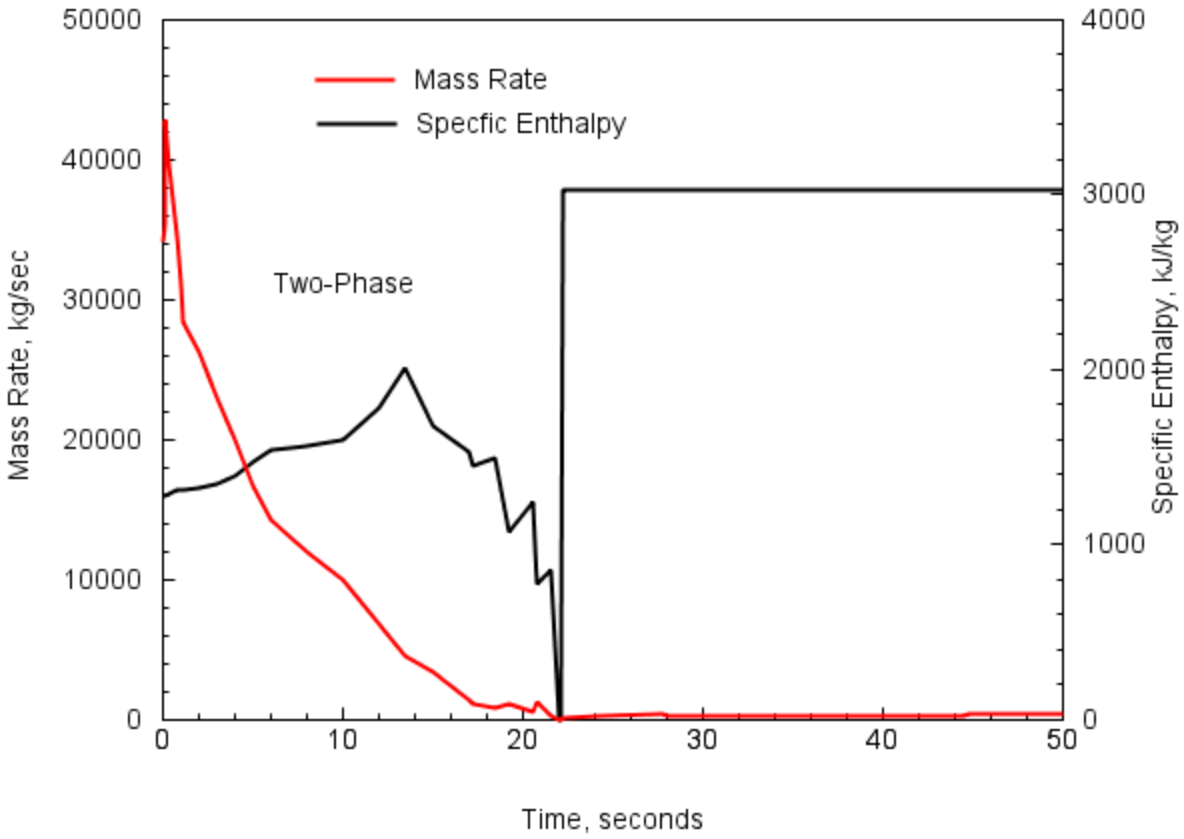

Figure 3-4 Typical PWR plant LOCA injection source.

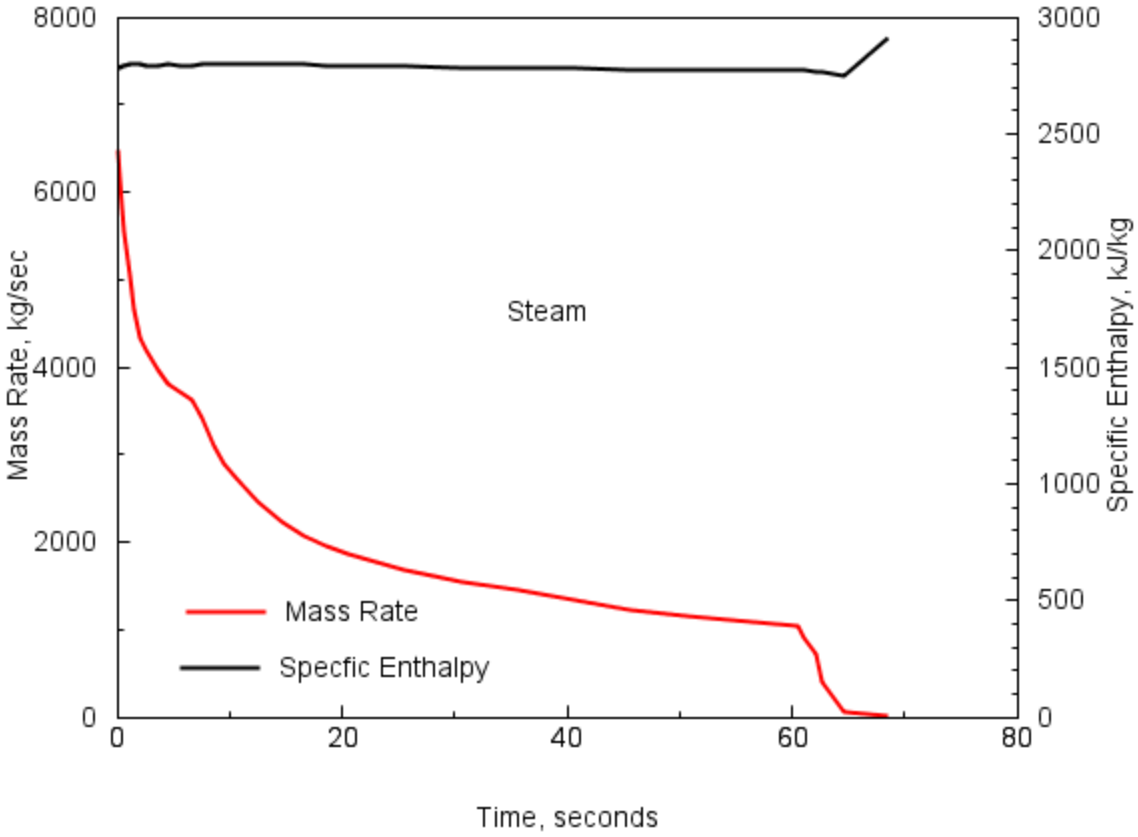

Figure 3-5 Typical PWR plant MSLB injection source.

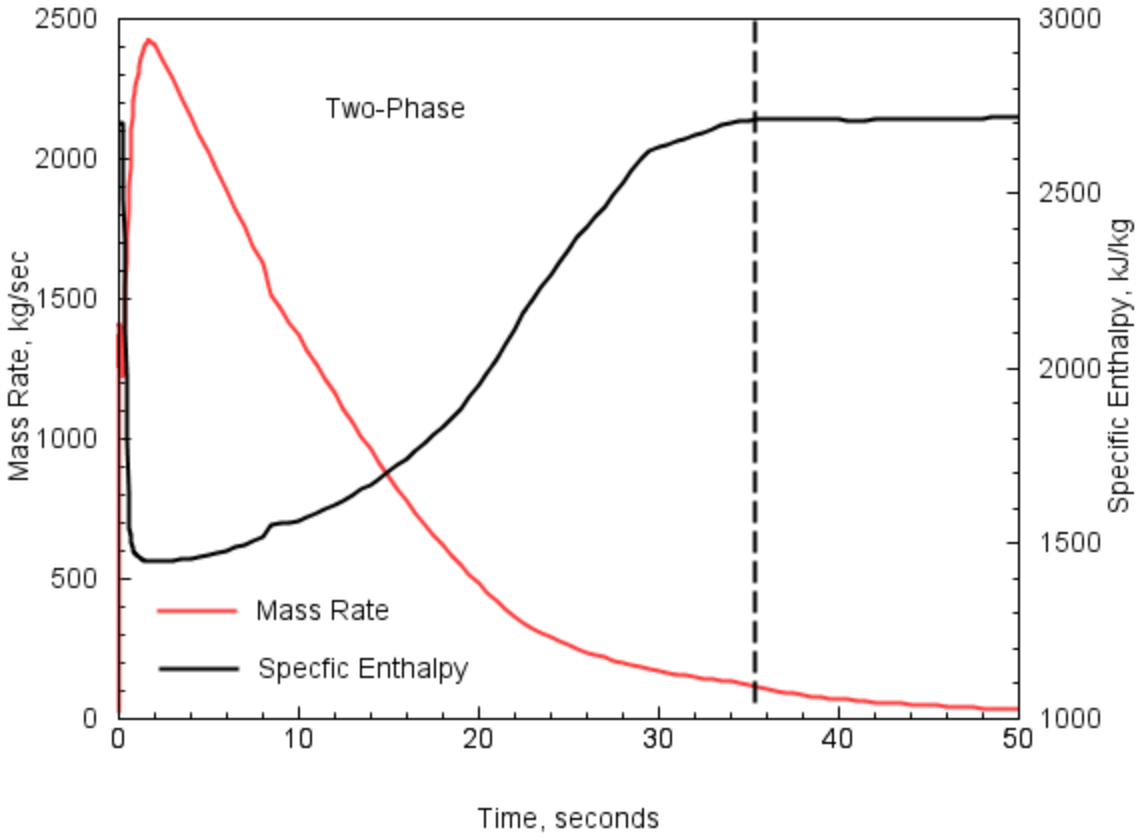

Figure 3-6 **HDR pipe rupture break injection for test V44 (similar for test T31.5).**

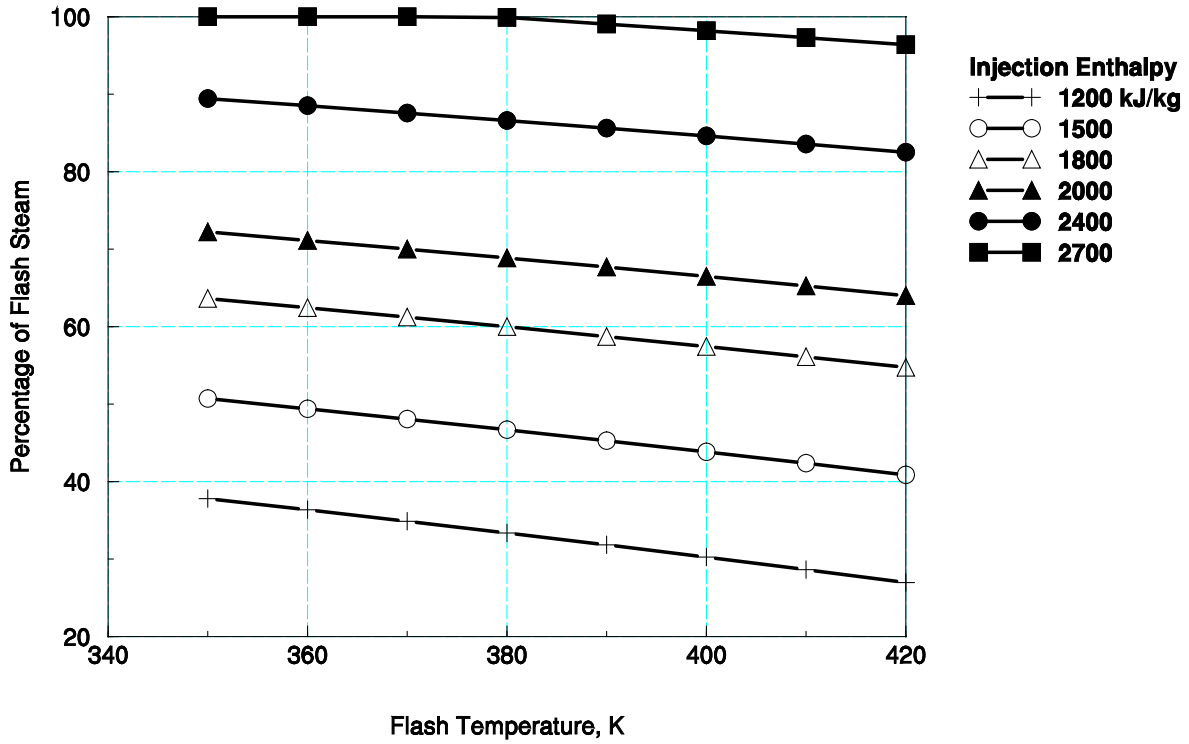

Figure 3-7 **Temperature flash model for determining percentage of flashed water for various injection enthalpies.**

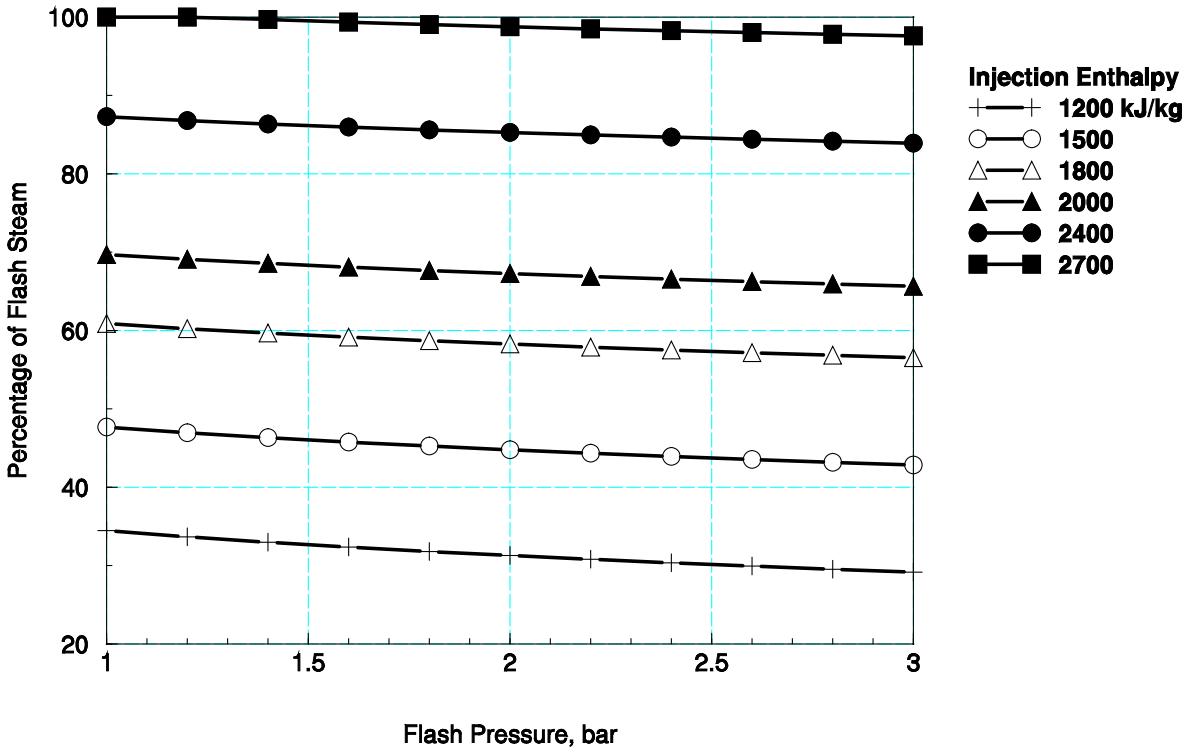

Figure 3-8 **Pressure flash model for determining percentage of flashed water for various injection enthalpies.**

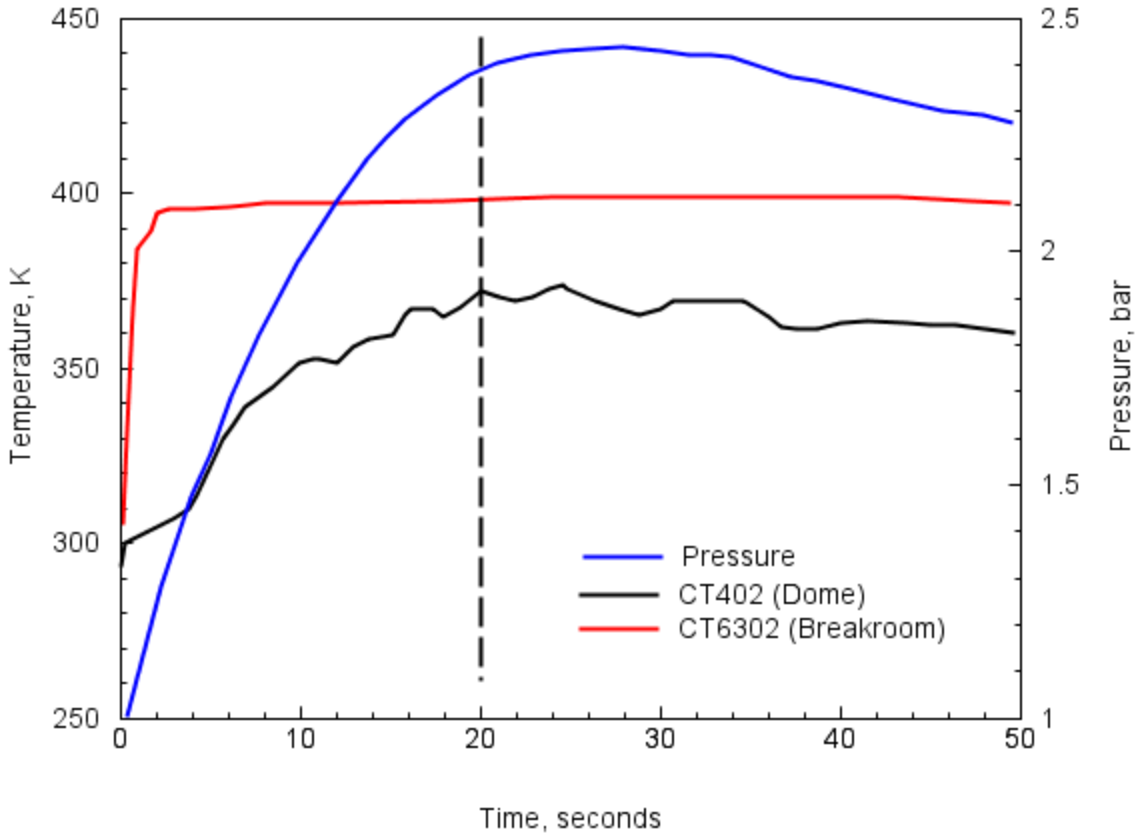

Figure 3-9 Measured temperatures and pressure in HDR containment for test V44.

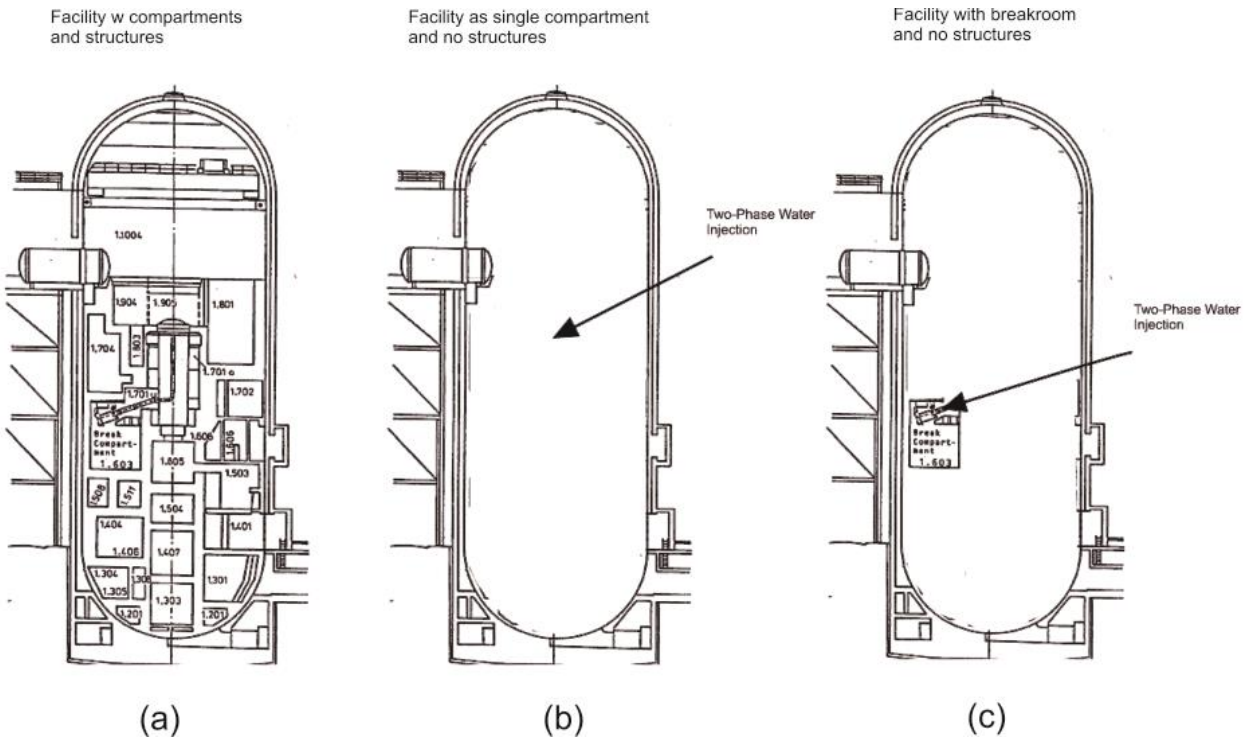

Figure 3-10 Illustrative flashing geometries for the HDR facility and HDR test V44.

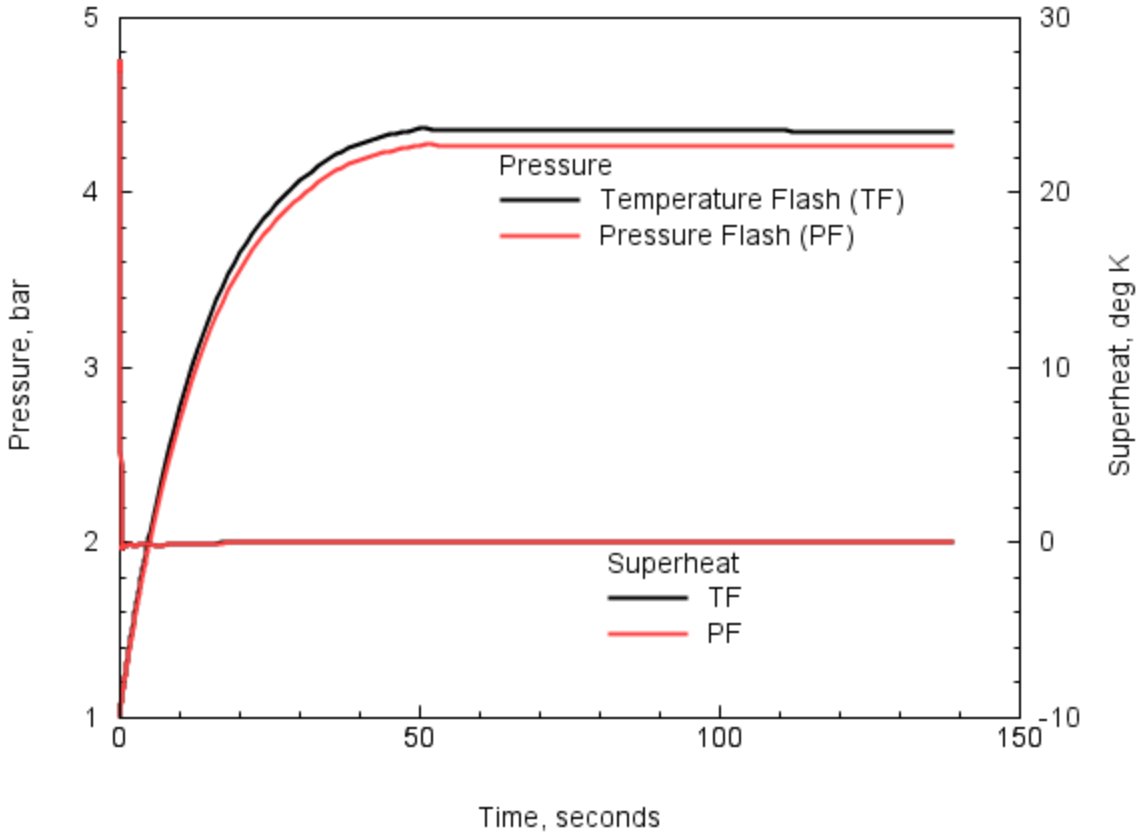

Figure 3-11 HDR V44 containment flashing response for single cell adiabatic facility with FOG setting.

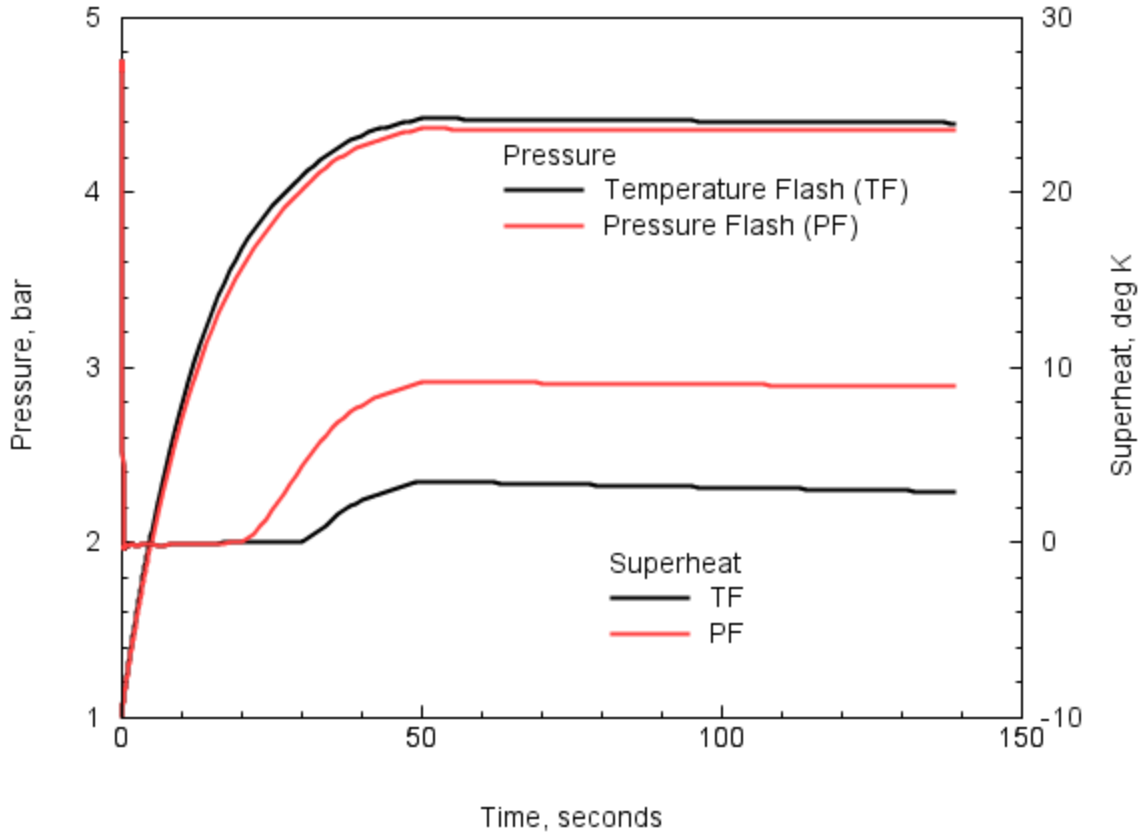

Figure 3-12 HDR V44 containment flashing response for single cell adiabatic facility with NOFOG setting.

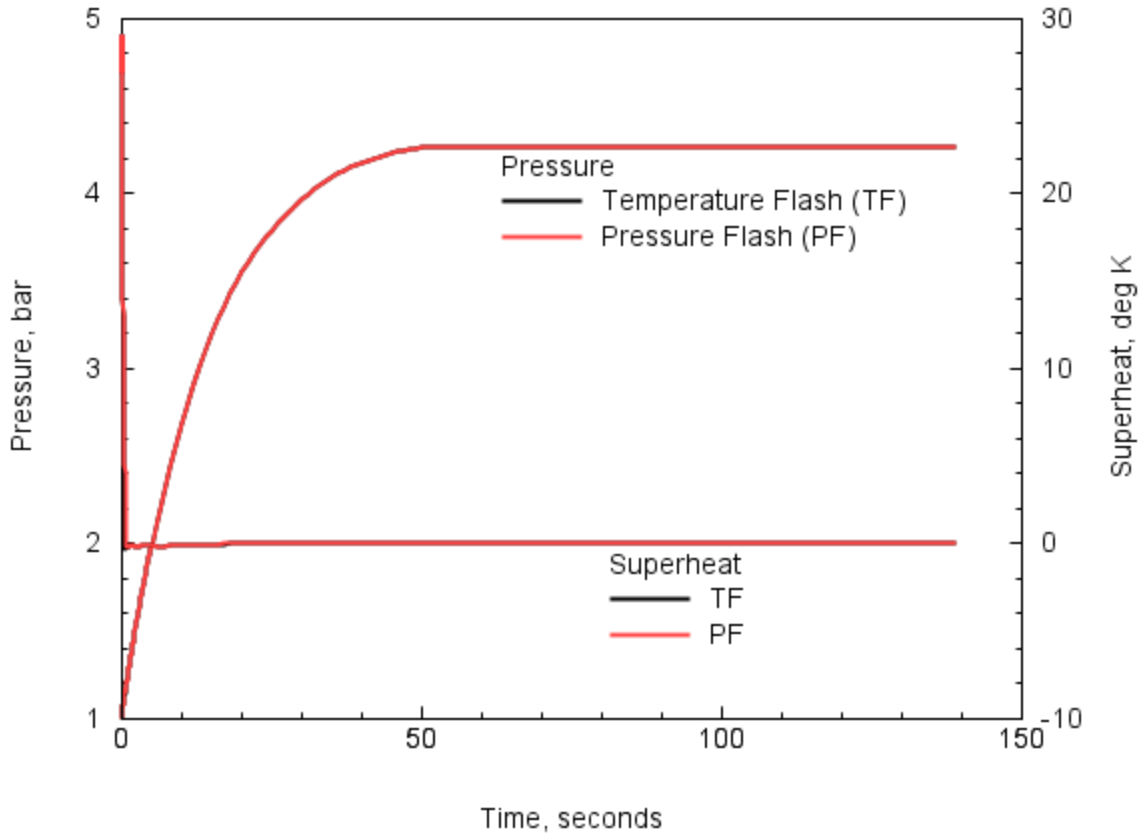

Figure 3-13 HDR V44 containment flashing response for the two-cell adiabatic facility with a FOG setting.

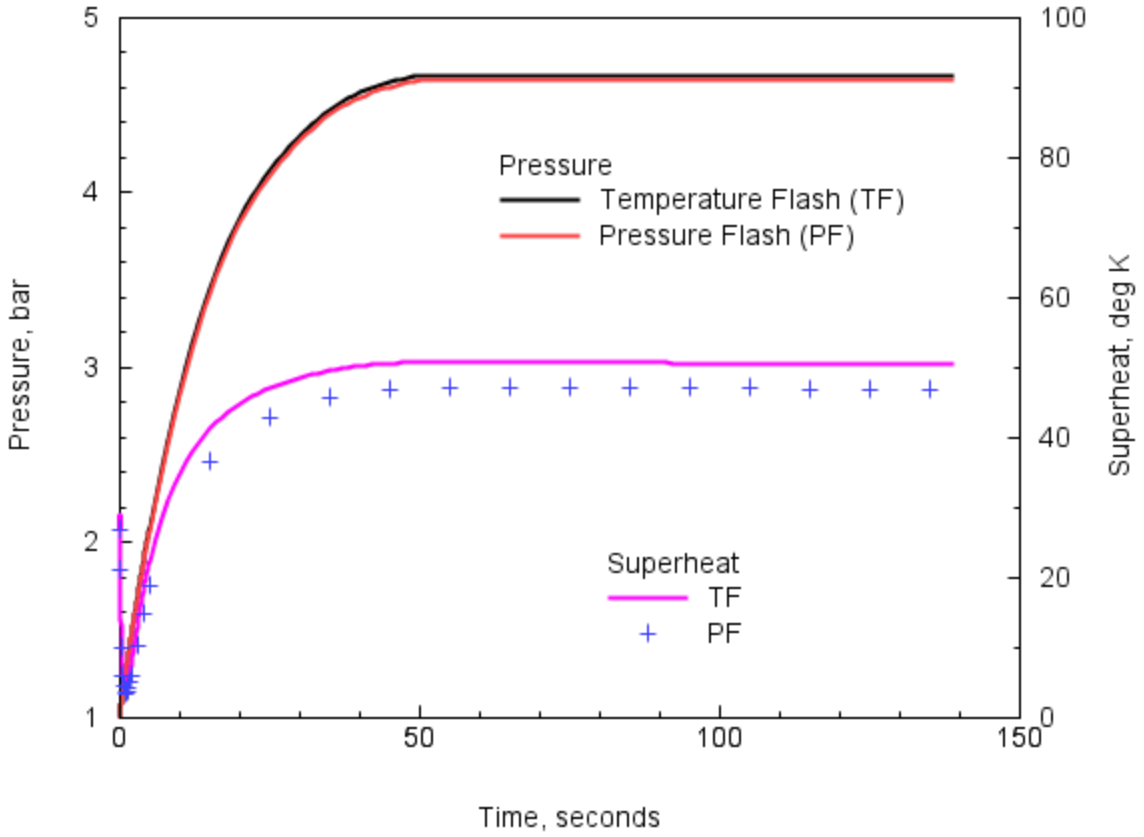

Figure 3-14 **HDR V44 containment flashing response for the two-cell adiabatic facility with a NOFOG setting.**

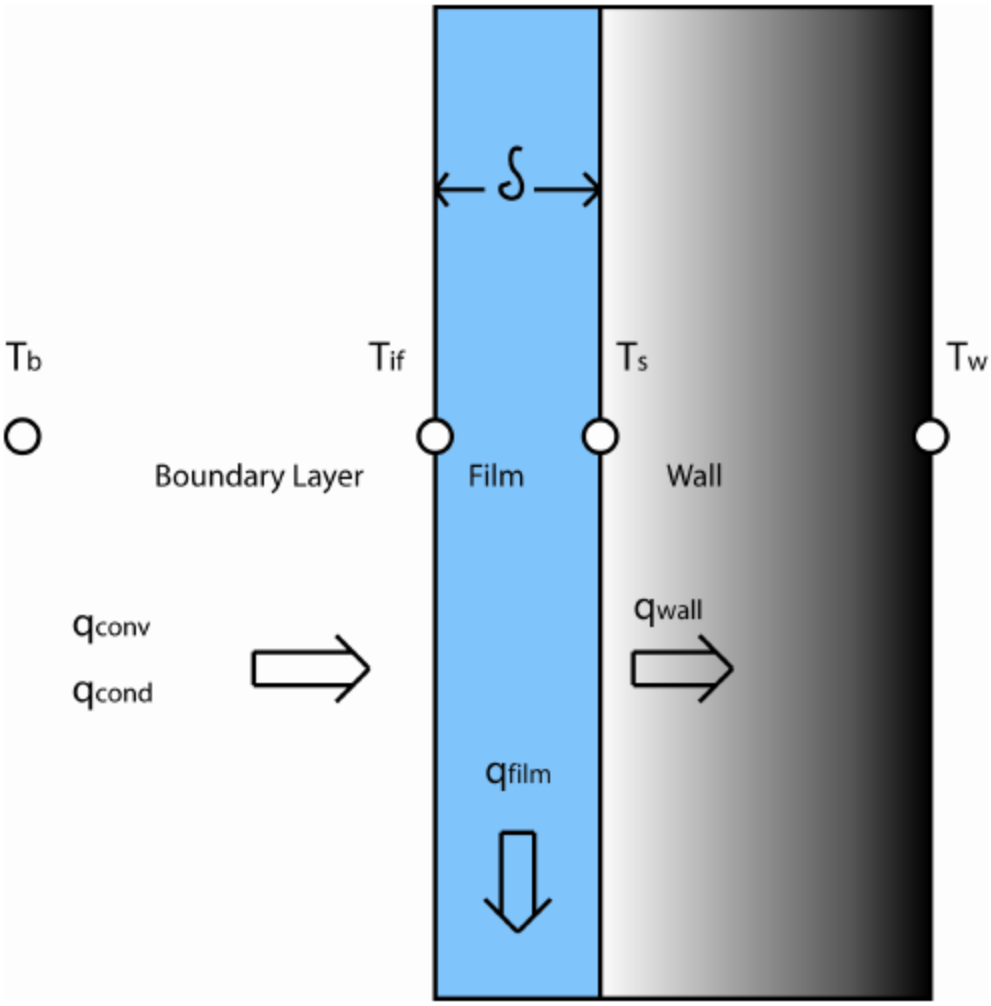

Figure 3-15 Sketch of the structure energy transfer modeling used in the MELCOR/CONTAIN codes.

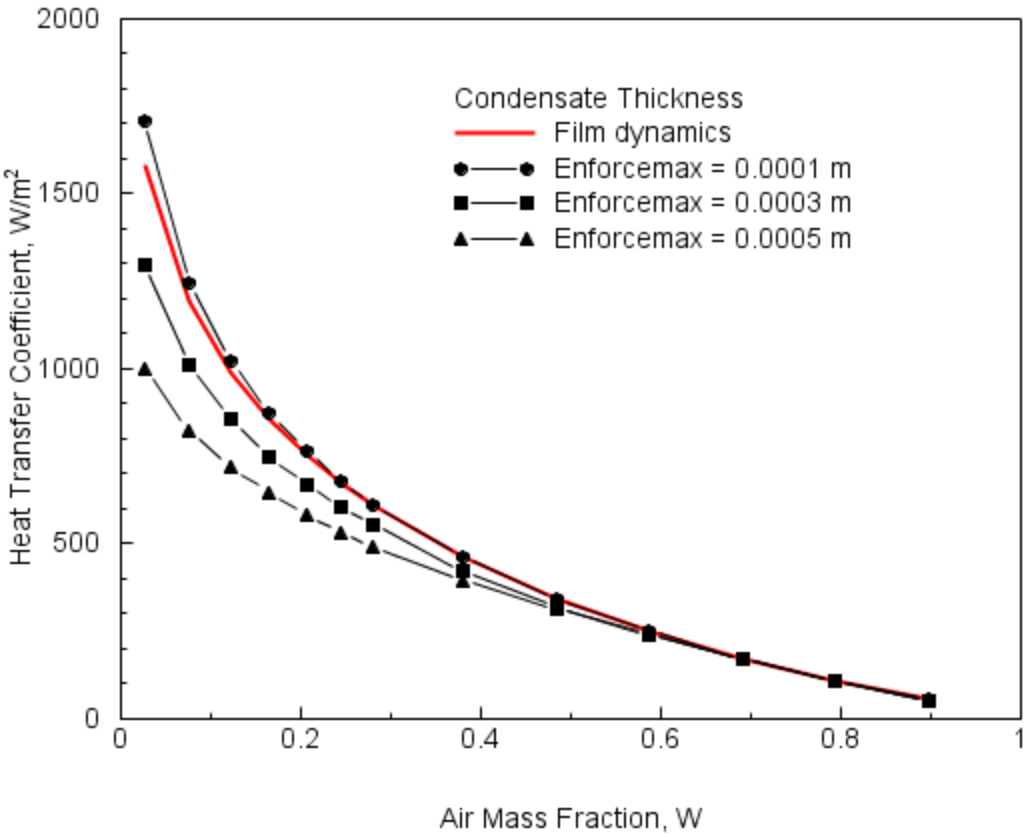

Figure 3-16 **MELCOR calculated heat transfer coefficient for various condensate film flow models using the Dehbi test geometry for structure and conditions: 1.5 bar saturated atmosphere, with a 30 degree temperature drop from bulk atmosphere to structure surface temperature.**

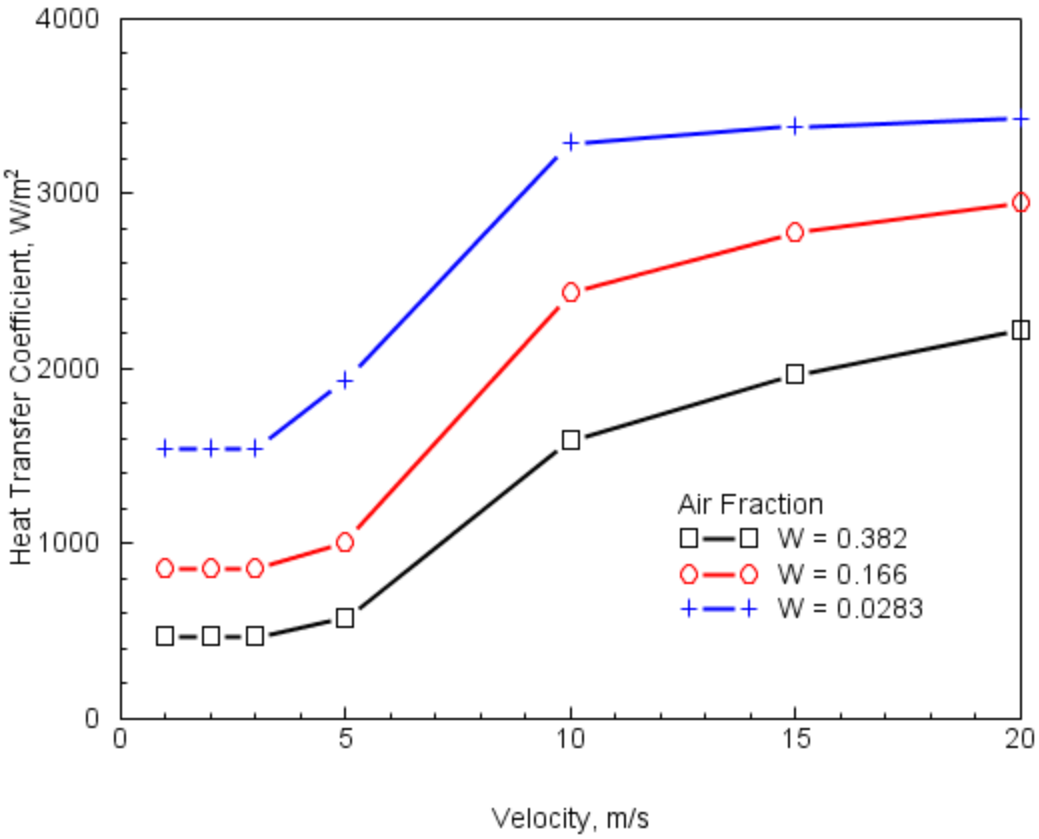

Figure 3-17 **MELCOR calculated heat transfer coefficient for forced velocity profiles directed parallel to structures surface using the Dehbi structure geometry and atmospheric condition of 1.5 bar saturated air and a 30 degree temperature drop from bulk to structure surface temperature.**

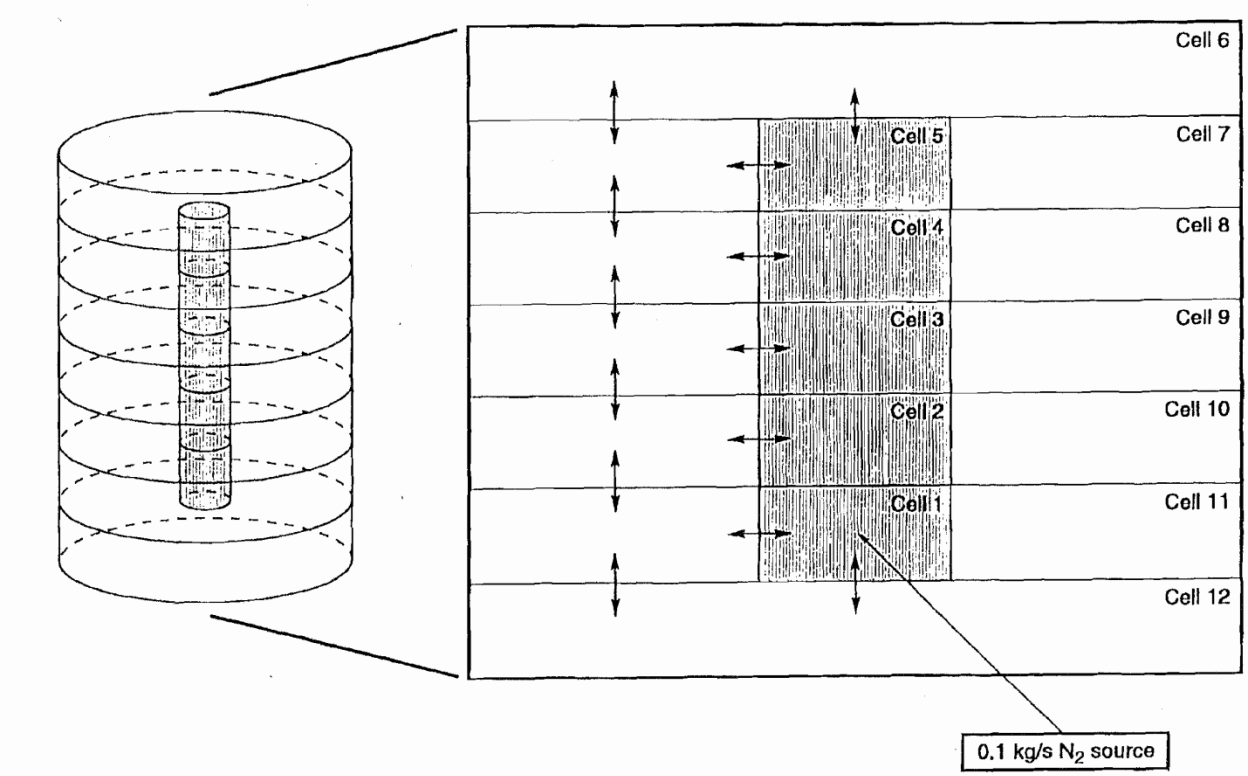

Figure 3-18 Plume illustration problem to demonstrate over-mixing for lumped parameter codes using an average density formulation to determine gravity heads in the momentum equation.

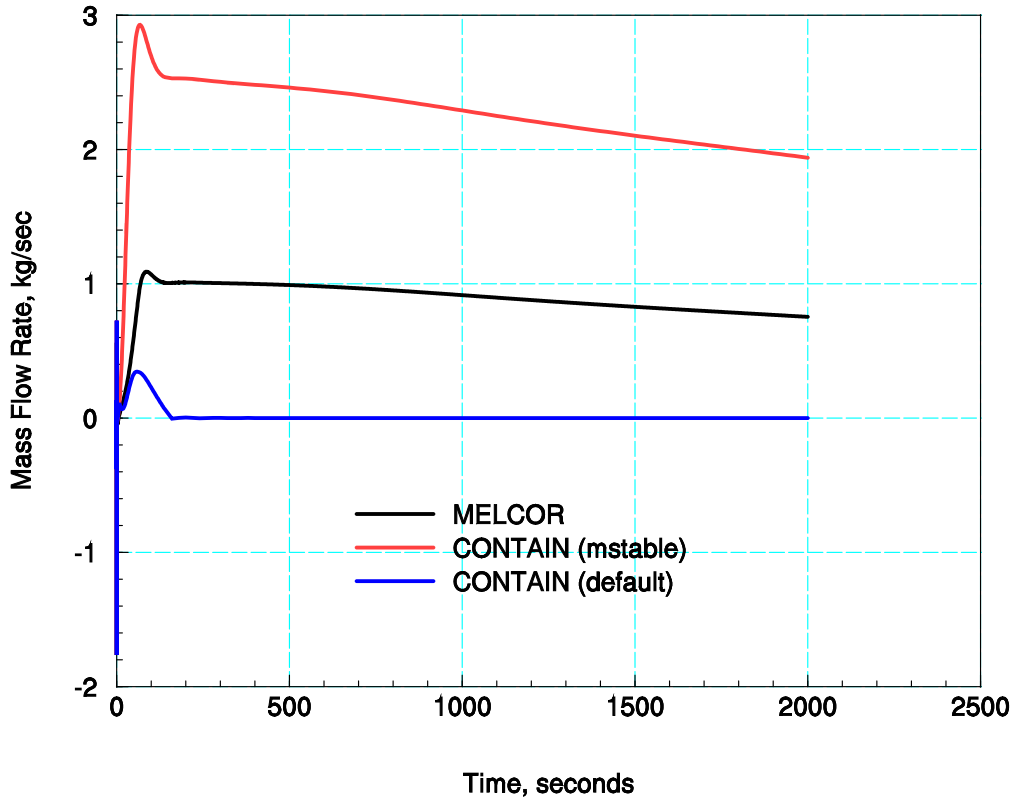

Figure 3-19 **Calculated mass flow from below source (cell #12) to source cell (cell #1). Analytic solution corresponds to the CONTAIN (default) or hybrid flow solver. Over mixing predicted with MELCOR, but noticeably less severe than the older implementation of flow solver in CONTAIN (mstable).**

4. MELCOR HDR ASSESSMENTS

4.1 Test V44 [ISP-16]

The HDR test V44 was chosen for ISP-16 to compare experimental results and computer code simulations demonstrating the efficacy of modeling practices and the computer codes, commonly used for licensing and regulatory activities. ISP-16 represents a large break LOCA for the purpose of evaluating containment response, primarily containment pressurization, peak pressure, differential pressure and temperature distributions. The mass and specific enthalpy of the LOCA source to the break room are shown in Figure 4-1.

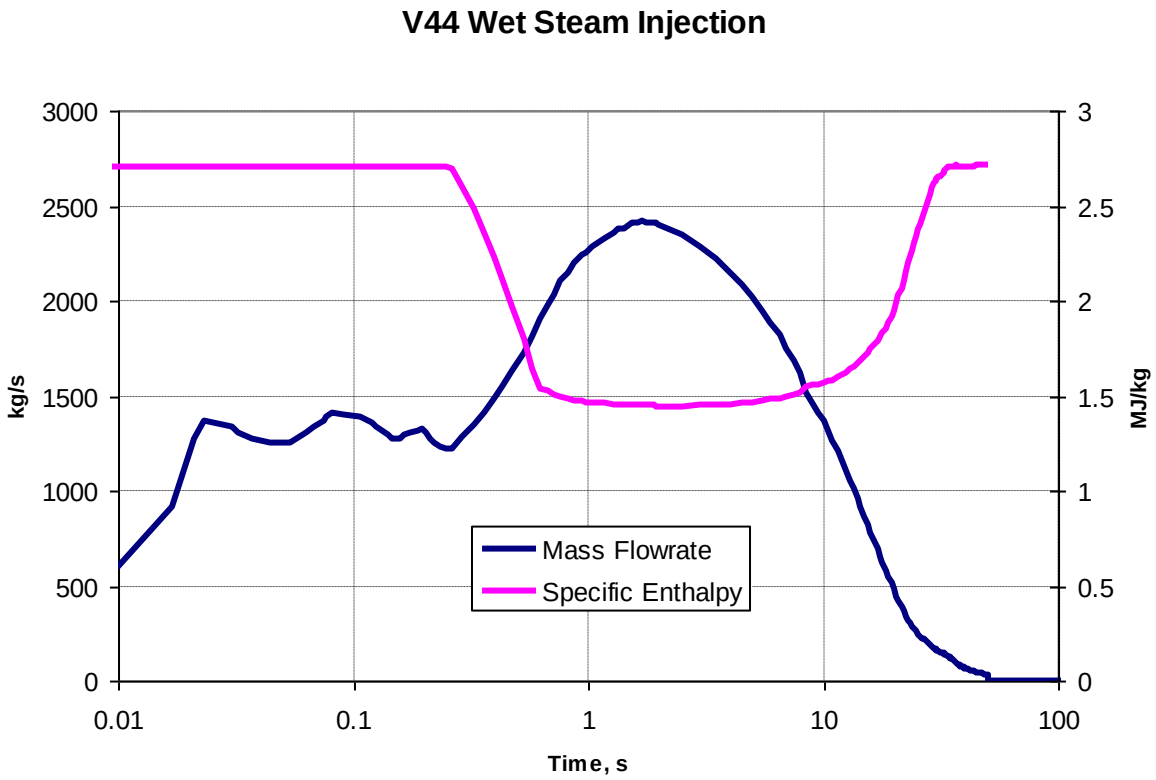

Figure 4-1 The mass flowrate (kg/s) and specific enthalpy (MJ/kg) of the entering water are presented for the wet steam injection during the V44 test.

4.1.1 Reference Case

In the reference calculation the 33 CV nodal model is used, with unflashed liquid water formed in the atmosphere by temperature flashing and dropped out within the breakroom (NOFOG). Condensate on structures is modeled with flow according to the dynamic film flow model. Figure 4-2 shows the predicted pressure for the reference calculation compared to the measured pressure. Comparisons of calculated and measured temperatures in the upper containment, breakroom, and basement are shown in Figure 4-3 through Figure 4-5. The locations for these temperatures are

shown approximately in the facility sketch for HDR test V44, Figure 4-6. Peak pressure is over-predicted by about 0.3 bar, which in terms of overpressure of ~ 20% with respect to the data.[2] The local temperature prediction in the upper containment shows a significant amount of superheating which appears not to be evident in the measurements. The superheating is believed to be due to removal of suspended unflashed water in the breakroom through the use of the keyword NOFOG in the CVH input. The local temperature response is similar to the illustrative modeling of suspended liquid water discussed in Section 3.3 for multi-cell models, which could be improved when suspended liquid is modeled with an aerosol physics model, either specifying FOG with/without RN active. Within the breakroom, the local temperature is well modeled and is shown to be calculated as the saturation temperature. For the basement region, the early response is also well modeled with the calculation indicating early superheating which is an anticipated response as lower compartment air is compressed during the initial blowdown.

Forced-convective velocities are not specified in the reference calculation; rather, the default treatment of forced convective velocities for heat and mass transfer along structure surfaces is used. The default convection option uses flow path velocities and a cell hydraulic area to represent surface velocities. If the hydraulic area is undefined, the area is assumed be the volume divided by the height of the control volume. The large hydraulic areas specified in the reference case result in small convective velocities. The velocities are small enough that natural convective process dominates heat and mass transfer. Forced convection velocities for heat sinks during a blowdown are very difficult, if not impossible, to estimate (even for fluid dynamic codes); therefore, there is considerable uncertainty associated with making such estimates. Sensitivity calculations used to explore the impact of modeling forced convection in the location of the blowdown are discussed in the next subsection along with flashing and liquid water suspension modeling.

[2] $(\Delta P_{cal} - \Delta P_{data})/\Delta P_{data}))*100$

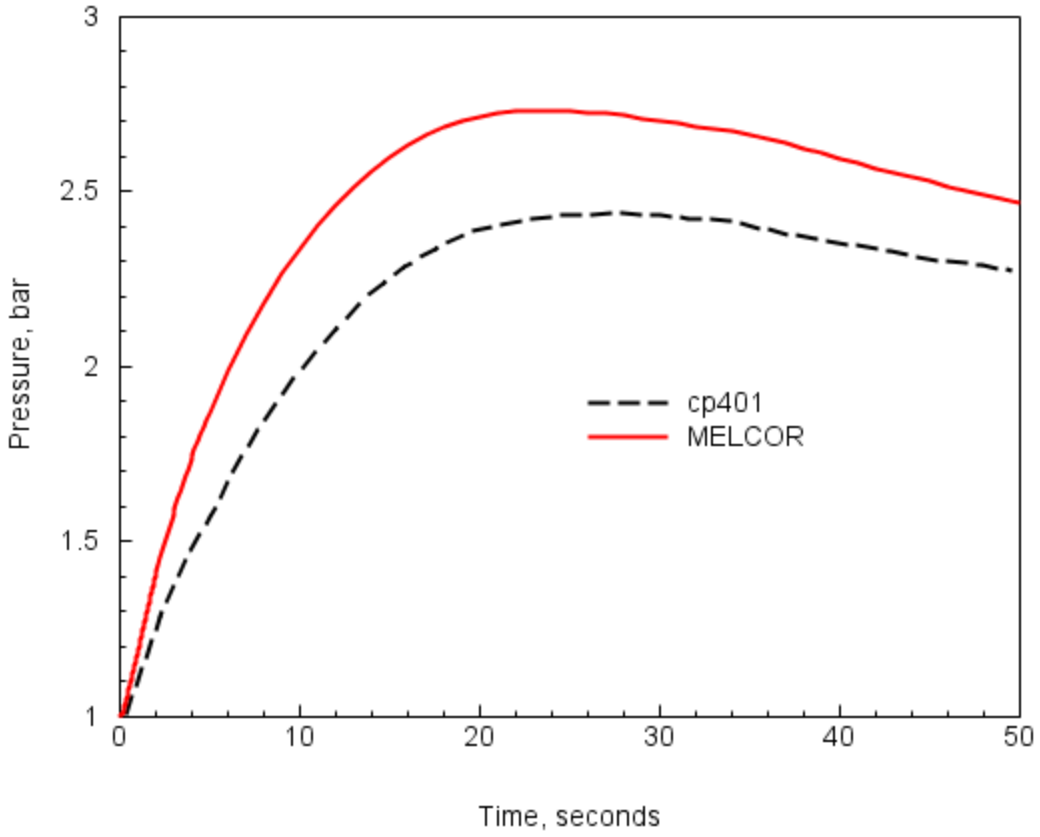

Figure 4-2 **Comparison of MELCOR calculated and measured HDR containment pressure for test V44 using the reference case input.**

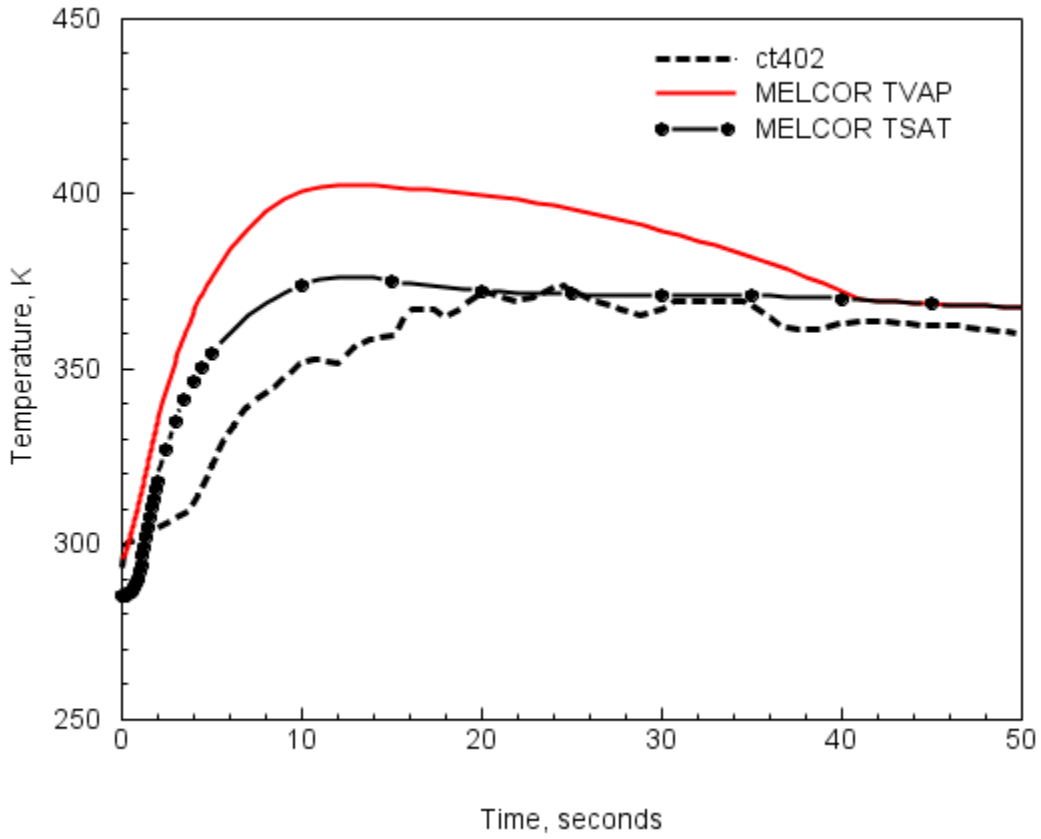

Figure 4-3 **Comparison of MELCOR calculated and measured local gas temperature for the HDR V44 test at the upper containment location, using the reference case input.**

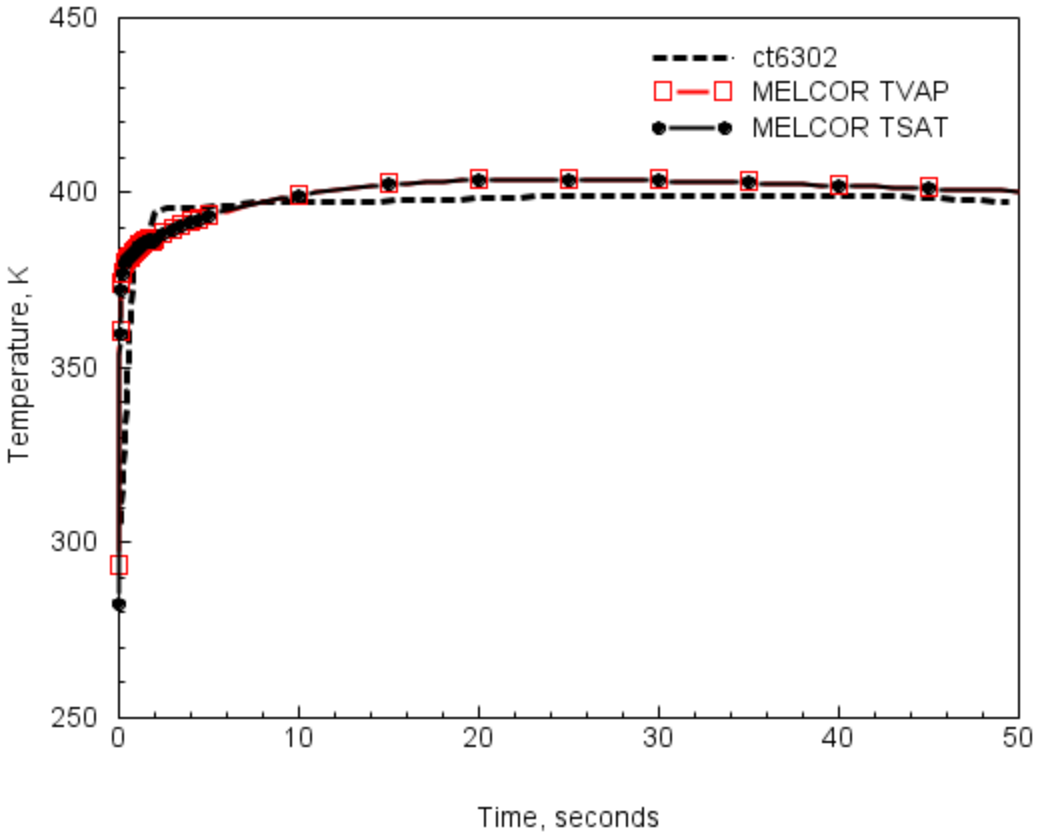

Figure 4-4 **Comparison of MELCOR calculated and measured local gas temperature for the HDR V44 test in the breakroom (1603) location, using the reference case input.**

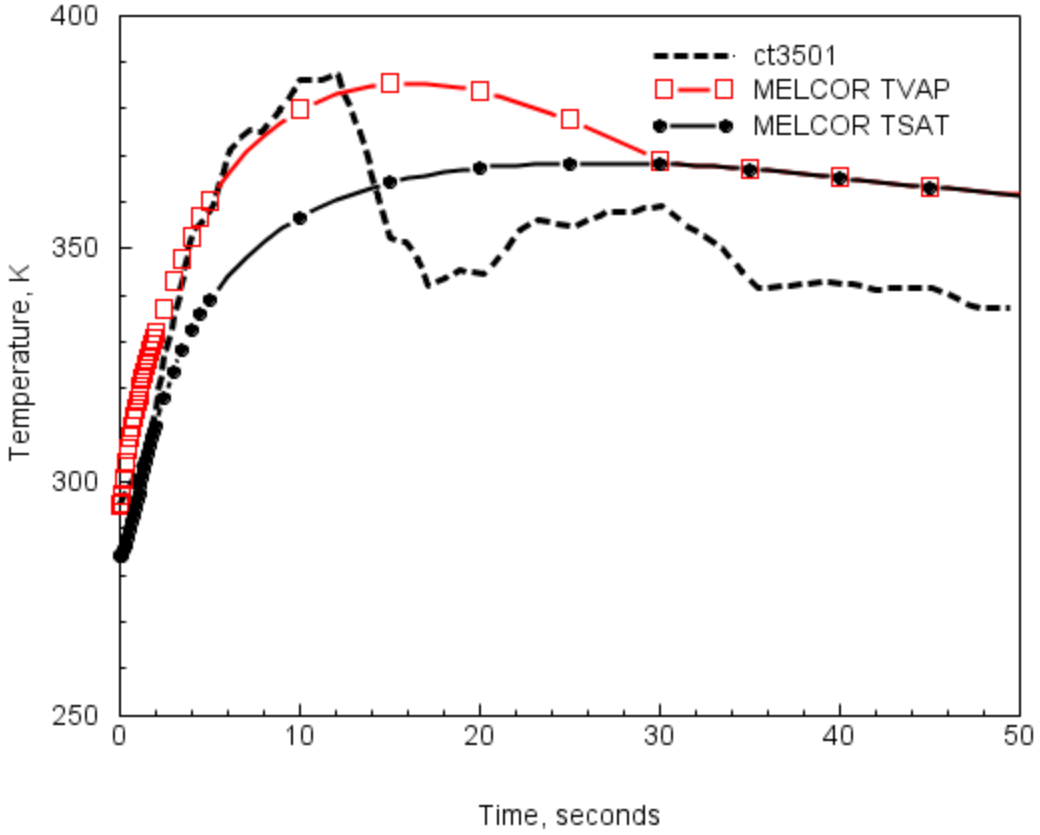

Figure 4-5 **Comparison of MELCOR calculated and measured local gas temperature for the HDR V44 test at the basement location, using the reference case input.**

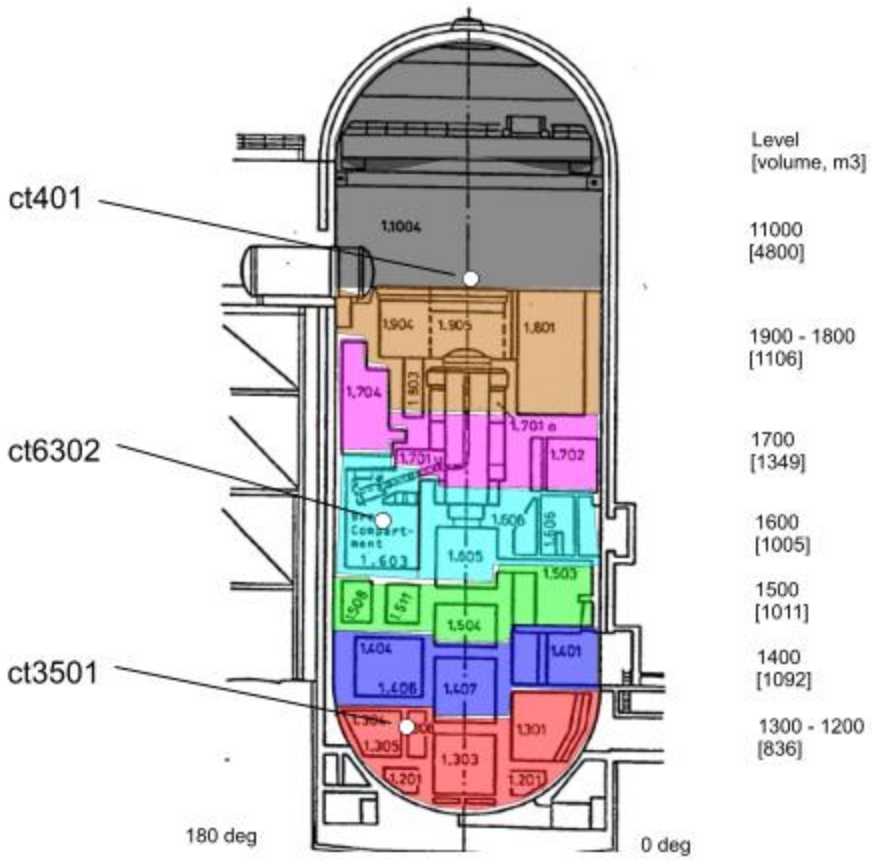

Figure 4-6 **Sketch of the HDR facility for test V44 showing approximate location of local gas temperature sensors (ct401, ct6302, and ct3501).**

4.1.2 Sensitivity Evaluation

The sensitivity of the predicted maximum pressure for test V44 based on selecting various MELCOR models are summarized in Table 4-1.

Table 4-1 Maximum Pressure Calculations for test V44.

	Sensitivity	Peak Pressure (MPa) [%]*
Measured	---	0.244
Reference	33CV, Temperature Flash, NOFOG, Nat. Conv., dynamic film flow	0.273 [20.1]
Flash Model		
Case 1	Pressure Flash	0.273 [20.1]
Aerosol Physics		
Case 2	FOG active	0.270 [18.1]
Case 2a	FOG and RN1 active	0.267 [16.0]
Forced Convection		
Case 3	Forced Convective Vel. (20 m/s max) Levels 1600	0.267 [16.0]
Case 4	Levels 1600 and 1700	0.261 [11.8]
Case 5	Levels 1500, 1600, and 1700	0.256 [8.3]
Condensate Film Thickness Maximum, m		
Case 6	Enforcemax = 0.0005	0.285 [28.5]
Case 7	Enforcemax = 0.0001	0.272 [19.4]
Case 8	Enforcemax = 0.00005	0.267 [16.0]
Nodalization		
Case 9	Single Cell	0.336 [63.9]
Low-estimate		
Case 10	Cases 2, 5, 8	0.252 [5.6]

* Over-pressure error, % = $((P_{calc} - P_{data})/(P_{data} - 0.1MPa)) * 100$

Flashing and Suspended Liquid Water

The flashing models determine the percentage of water which flashes to a vapor state. For the reference case, a temperature flash model is used (default) that determines flashing using a thermal equilibrium calculation for the injected water placed directly into the atmosphere. Furthermore, with the NOFOG keyword included in the CVH input, liquid water suspended initially in the atmosphere drops out at the end of a time step. Since the breakroom is modeled as a separate compartment or control volume, the volume rapidly transitions from an air to pure steam volume during the blowdown. For Case 1, the flashing volume is essentially fully saturated during the two-phase water injection period, and in the breakroom the total pressure equals to the steam partial pressure. These flashing and water removal options then result in the reference case and Case 1 (pressure flash) showing no difference in the predicted peak pressure.

When aerosol physics (RN1 active) is activated as a mechanistic method to remove suspended water in the form of mist or fog, the liquid in the atmosphere is depleted as aerosols undergo agglomeration, gravitational settling, and deposition on structures. Figure 4-7 shows this effect for Case 2 and 2a. The representation of liquid water removal is difficult to quantify, but fortunately this modeling choice has only a small effect on pressure prediction. However, as seen above, the local temperature response (superheating) can be affected when liquid water or mist is modeled. As an example, the temperature profile for sensor ct402 location (Figure 4-3) is re-plotted with the comparisons including the MELCOR temperature calculated with water aerosol modeled (Case 2a). The results, shown in Figure 4-8, with aerosols modeled indicate an improvement in predicting the measured temperatures as superheating is significantly reduced in the upper containment.

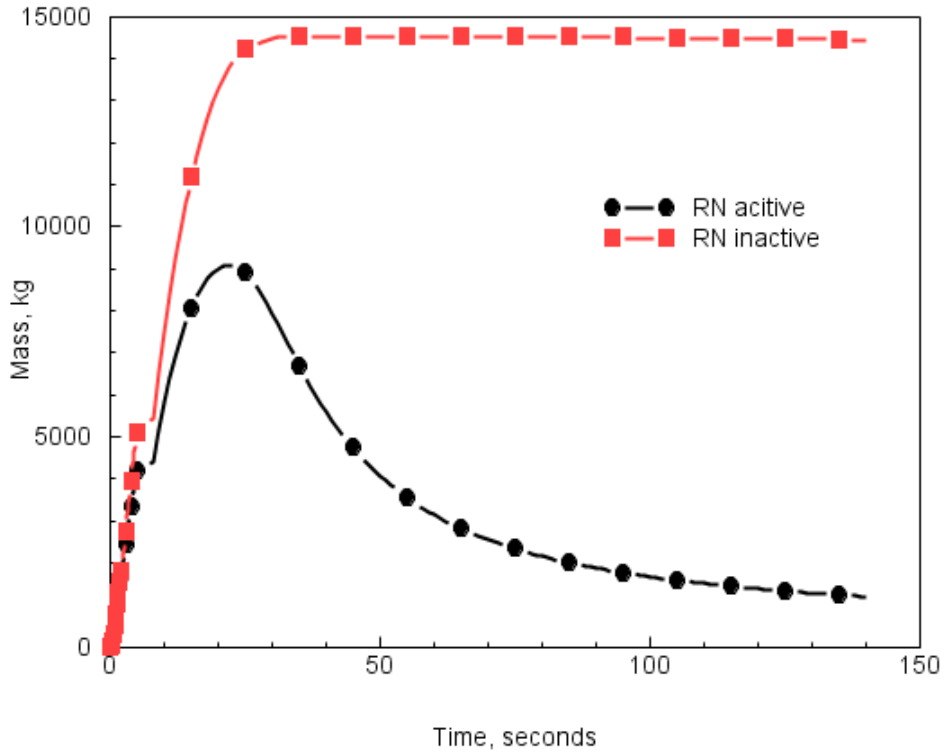

Figure 4-7 **Comparison of the suspended fog mass for test V44 determined for FOG with and without the RN1 package active.**

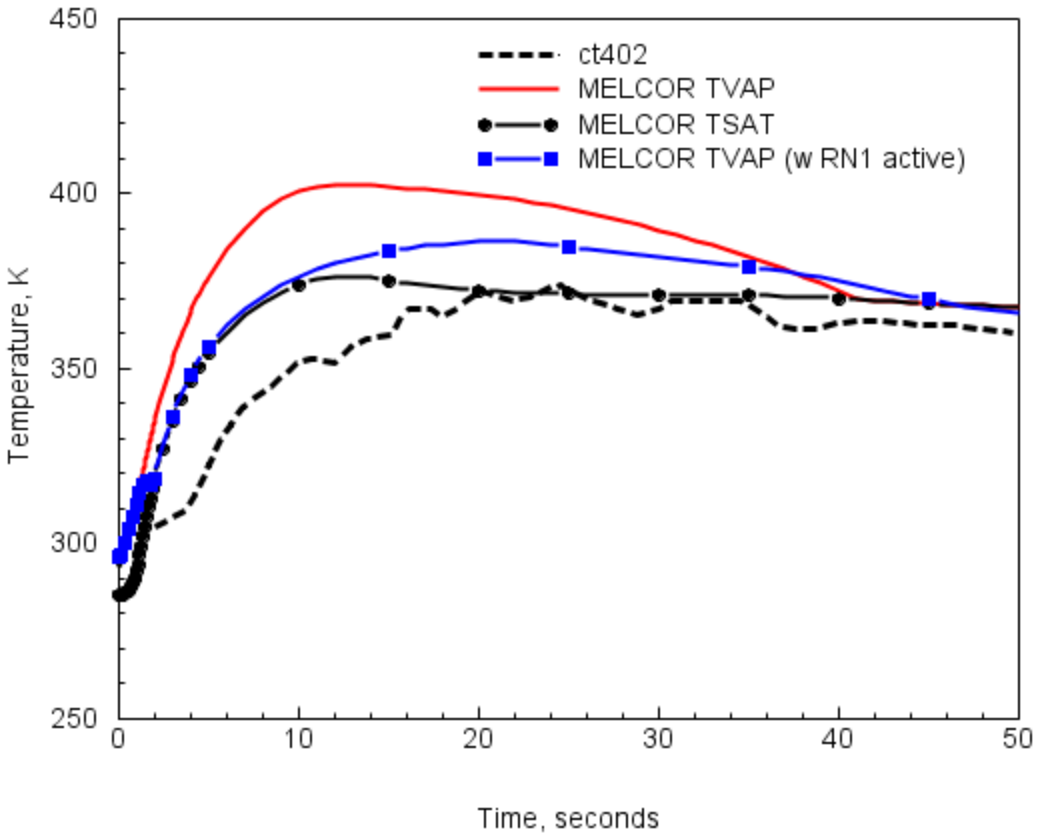

Figure 4-8 **MELCOR calculated upper containment temperature (ct402), showing improved prediction for gas temperature calculated with water aerosols modeled (RN1 active).**

.

Forced vs. Natural Convection

Due to the magnitude of the injection, reasonable judgement would dictate that some degree of forced convection would occur in the breakroom and in regions surrounding the breakroom. We noted above that the forced convective effect tends to diminish as the volume velocity increases. For the sensitivity study, we use a maximum velocity limit of 20 m/s and assume that the velocity time history corresponds to the normalized mass injection profile, Figure 4-9. Further, we consider cases that vary the extent of the region affected by forced convection. Case 3, 4, and 5 assume that the region of force convection expands from only level 1600, to levels 1600-1700, and to levels 1500-1700, respectively. As the region expands, the peak pressure correspondingly decreases as shown in Table 4-1.

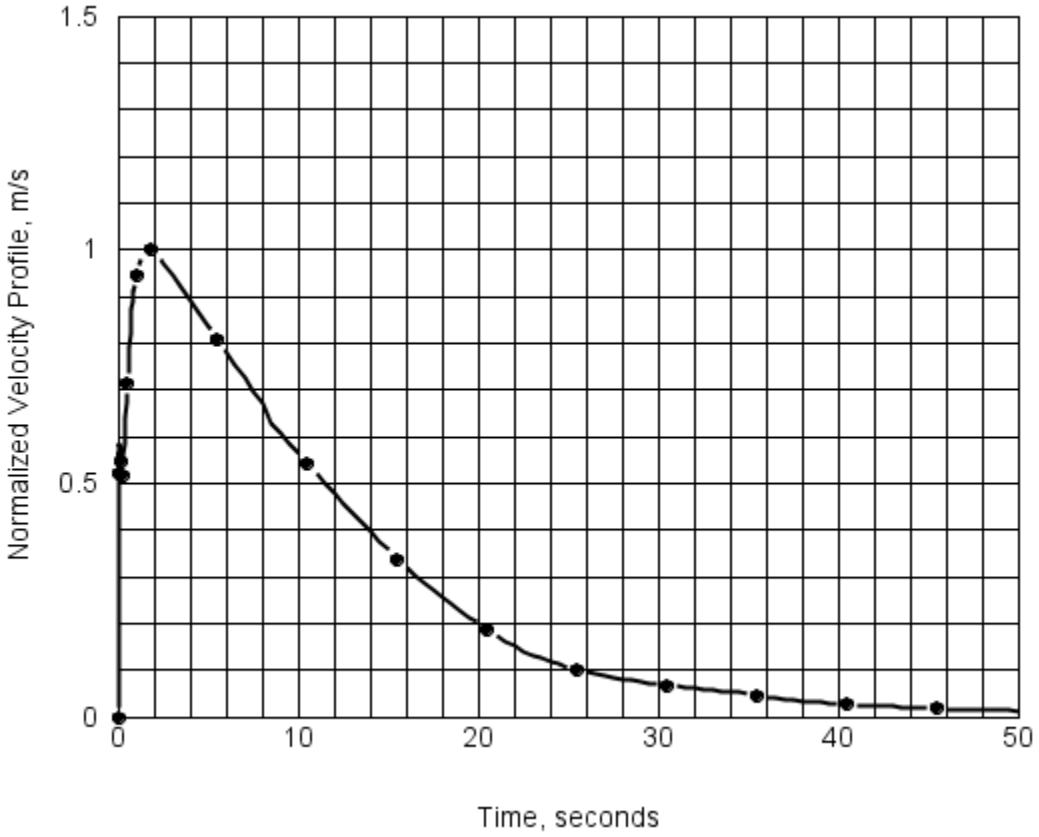

Figure 4-9 Normalized velocity profile based on the mass rate injection for the V44 blowdown source.

Condensate Film Resistance

Condensate film thickness on the wide range of structure geometries and orientations is difficult to quantify. As noted above, condensate resistance to energy transfer is a small contributor to total energy resistance at the surface of a structure when the resistance is dominated by boundary layer diffusion (with relatively high air concentrations), and this would be the case for regions well away from the breakroom. However, for regions near the injection site the steam concentration will be high and the condensate thickness is also expected to be much lower than the film flow model would predict as a result of entrainment due to high atmospheric velocities. Using the Enforcemax keyword the film thickness can be limited to a maximum thickness, and therefore a sensitivity to film thickness can be observed. Cases 6 through 8 show the effect of film thickness limits on the peak pressure prediction. The reference calculation using dynamic film flow is well represented using a maximum condensate thickness of 0.0001 meters.

Nodalization

The effects of nodalization are investigated by comparing the 33CV representation of the V44 test to a single-node representation. A single-node deck is prepared by reducing all control volumes into a single volume with a linearly increasing volume from the lowest to the highest altitude. As noted in Table 4-1 (Case 9), the single-cell calculation results in the highest observed peak pressure. The reduction in nodes to a single volume means that the sourced water is equilibrated with the entire containment atmosphere in a natural convective environment thereby reducing the total rate of energy removal from the atmosphere over the multi-cell representation. Global response reflected in the total energy of the containment atmosphere is increased in the nodalization sensitivity. However, local temperature effects are not conservatively determined with the single cell calculation as shown in Figure 4-10.

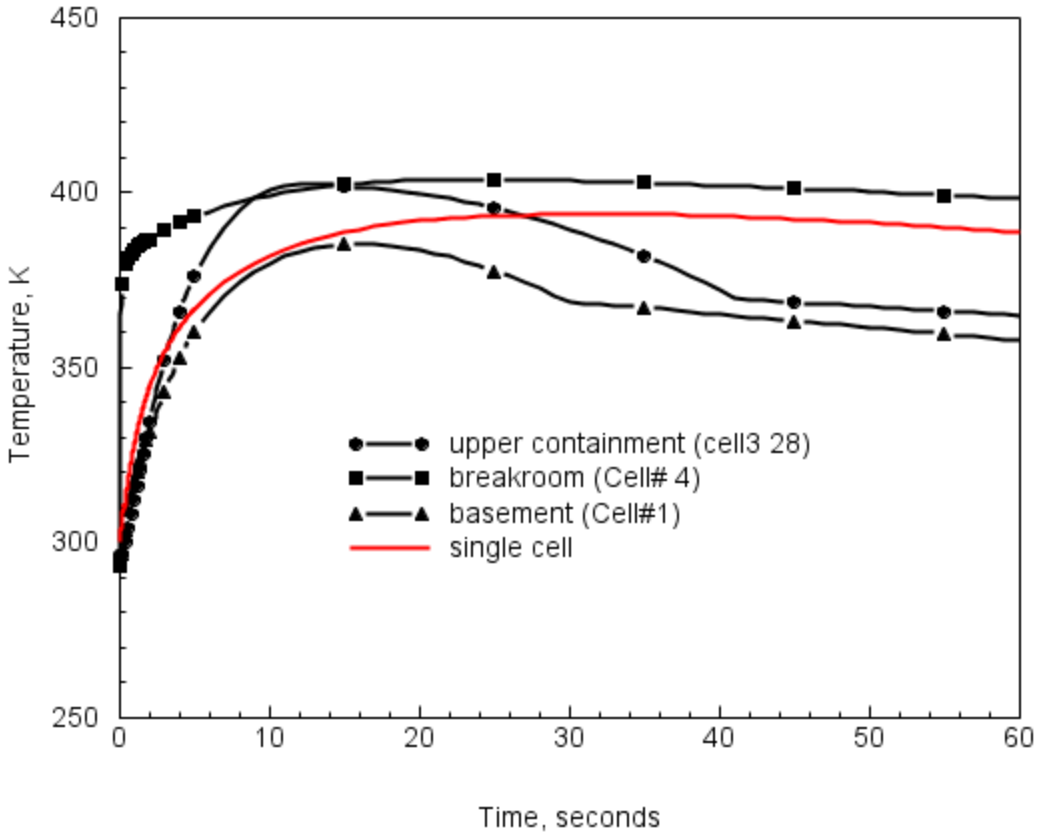

Figure 4-10 **Comparison between the gas temperature profiles produced with the temperature flash no fog model for the 33CV and single-node representations of the V44 test.**

4.1.3 Benchmark

The five cell CONTAIN analyses presented in Til02a were re-calculated for the 33CV nodalization and input settings used for the reference MELCOR case (natural convection, dropout of liquid water, temperature flashing). Since previous CONTAIN V44 test calculations [Til02a] were run using the CONTAIN default maximum film thickness of 0.0005 meters, the Enforcemax keyword was also used, setting the MELCOR maximum film thickness to the CONTAIN default 0.0005 meters. The pressure comparison between the codes is shown in Figure 4-11, and gas temperature comparisons are shown in Figure 4-12. The agreement in pressure is shown to be excellent. The gas temperatures are predicted in a similar manner with some noted difference in the early degree of gas superheating. Issues related to code differences due to over-mixing are more appropriately investigated in longer term tests with light gas injections (i.e., T31.5 and the E-series tests).

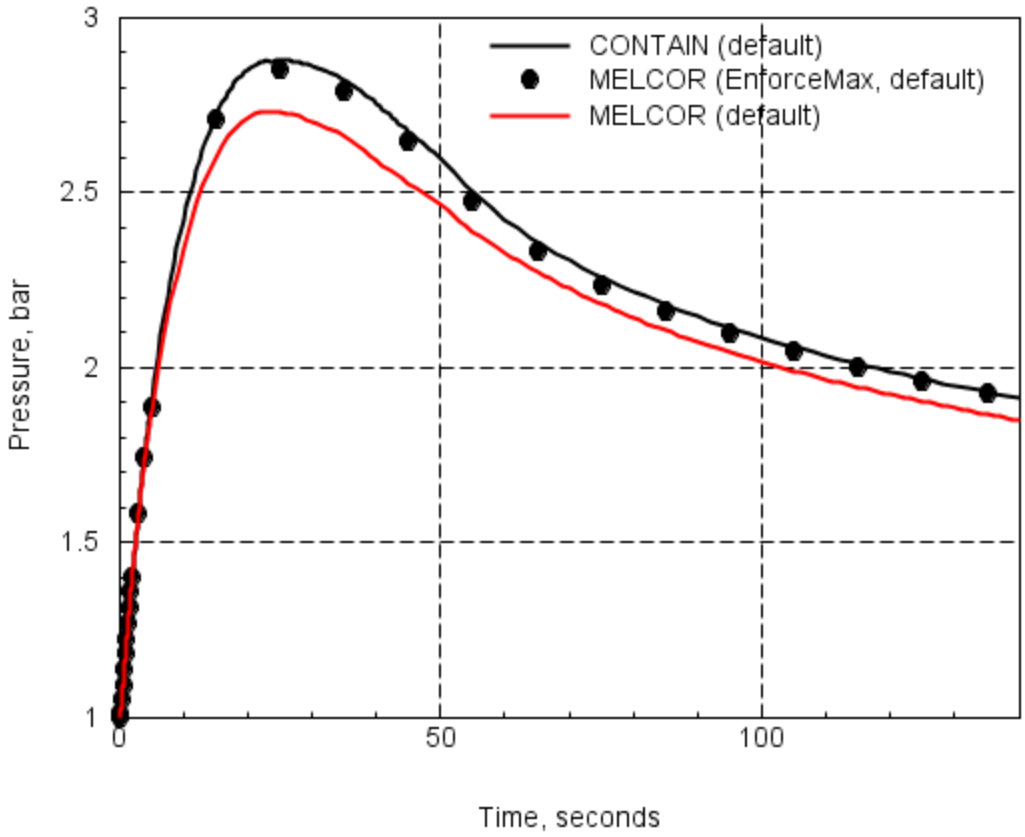

Figure 4-11 **MELCOR calculated containment pressure for test V44, showing the agreement between MELCOR and CONTAIN for input that limits film maximum thickness to the default limit of 0.0005 meters. Setting the MELCOR film calculation for dynamic film flow gives the lower pressure response as a result of a smaller film thickness and reduced condensate thermal resistance.**

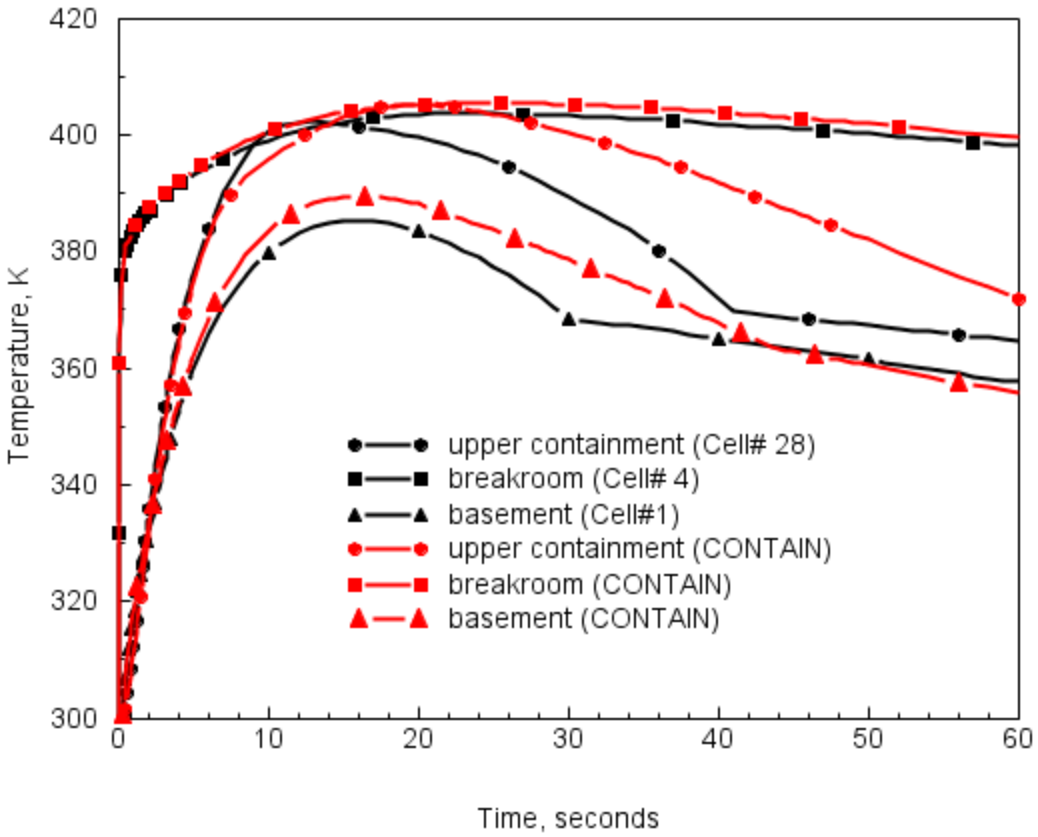

Figure 4-12 **Comparison of MELCOR and CONTAIN calculated containment gas temperatures for test V44 with maximum film thickness set to the default value of 0.0005 meters.**

4.2 Test T31.5 [ISP-23]

For the ISP-23 calculation, the 33CV cell nodalization of the containment is used. ISP-23 differed from ISP-16 in the location of the steam injection location, which was moved from room 1603 to 1704, a larger room one level higher at an elevation of approximately 22 meters. HDR test T31.5 was chosen for ISP-23 with the injection rate similar to ISP-16 (V44), as shown in Figure 4-13. A main focus of the ISP-23 was the containment response during the post-blowdown period. Consequently, a long-term period of measured gas pressure and temperatures extended out to 20 minutes. The locations for local temperature measurement corresponding to the 33CV volumes is provided in Table 4-2, and the approximate locations within the facility are indicated in Figure 4-14. The reference calculation, as with the V44 reference calculation, uses the default method for treating forced convection with large hydraulic areas to effectively zero out cell velocities. Because the ISP-23 test was nodalized to better represent the compartmentalization of the facility, this calculation is a good indication of the code's capability to predict local temperatures during a blowdown and following depressurization period.

Table 4-2 HDR gas temperature sensor locations relative to the 33CV nodalization

Sensor	Elevation, m	33CV volume #	Comment
ct404	40	#30	Upper dome region
ct7403	22	#10	Breakroom (1704)
ct3708	25	#22	Upper-staircase
ct3713	5	#2	Lower-staircase
ct3501	-5	#1	Basement

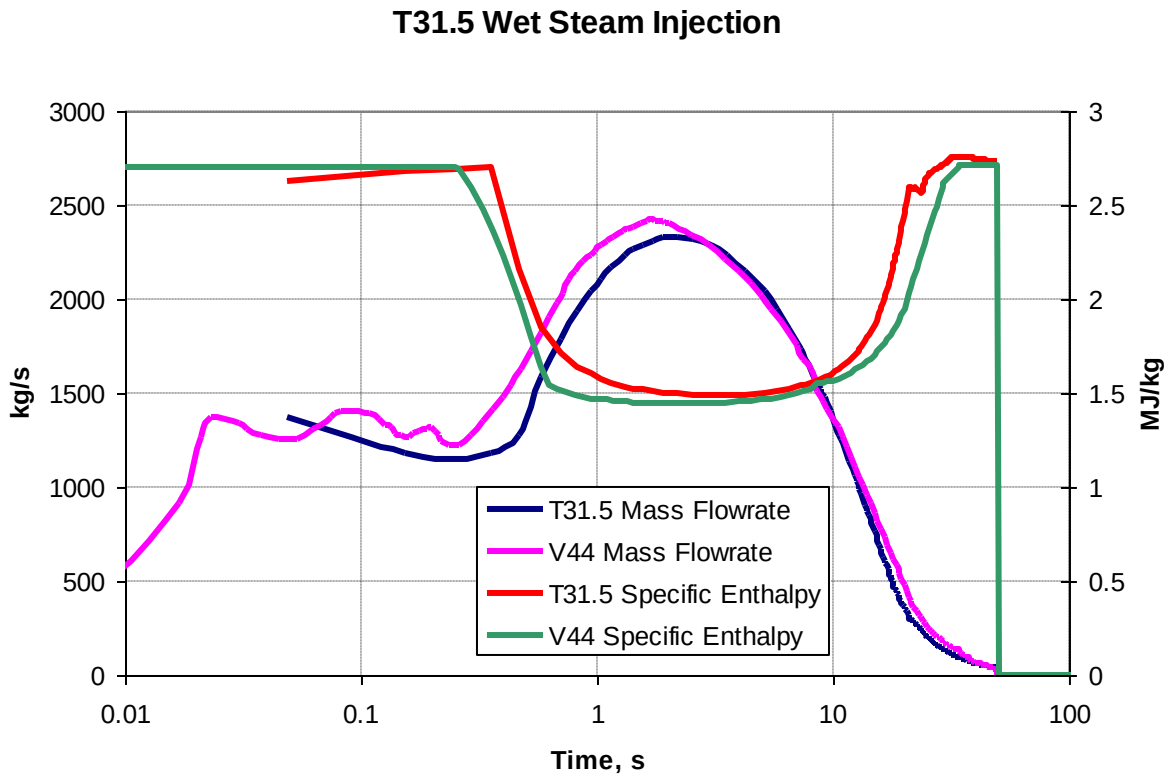

Figure 4-13 **The mass flowrate (kg/s) and specific enthalpy (MJ/kg) of the entering water are presented for the wet steam injection during the T31.5 test and is compared to the V44 test.**

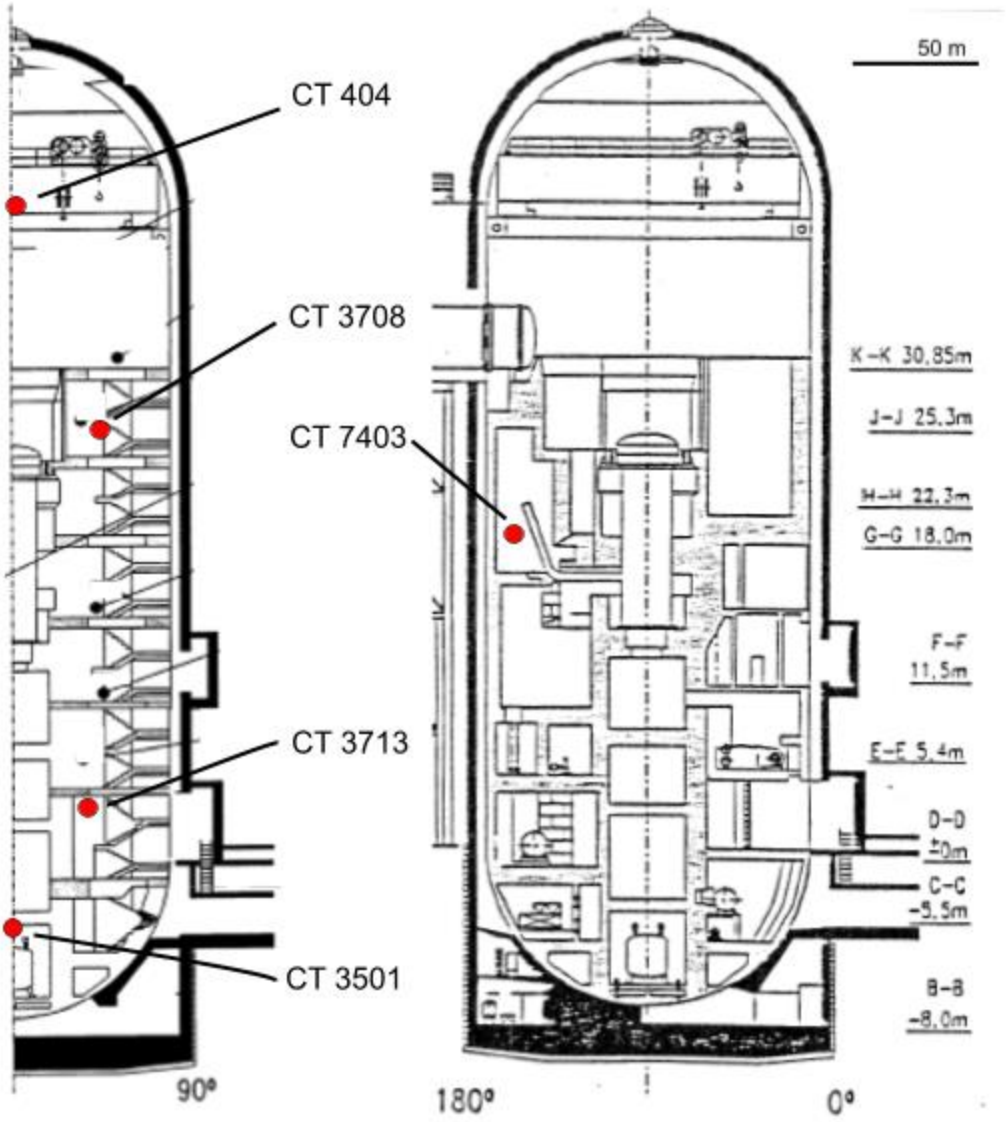

Figure 4-14 Approximate locations for HDR gas temperature sensors, test T31.5.

4.2.1 Reference Case

The HDR containment response analysis for the T31.5 steam injection was performed with 1) the temperature flash model (default), 2) unflashed water dropped out of the atmosphere at the end of a timestep (NOFOG), 3) no control volume velocities, and 4) dynamic film flow. The input settings are identical to the settings used for the V44 reference case above, apart from the location and mass energy source corresponding to the specification for ISP-23 (T31.5). The reference case comparisons with measurements emphasizes the medium and long-term time periods: 0 - 50 seconds and 0 - 1200 seconds. These comparisons are shown in Figure 4-15 and Figure 4-16 for pressure and in Figure 4-17 and Figure 4-18 for local temperature. As with the V44 test analysis, sensitivity cases are included to further an understanding of the test and simulation effort, and these cases are discussed below in Section 4.2.2.

Generally, the reference case calculations provide a good representation of the measured trends for pressure and local temperatures for both the medium and long-term periods, as can be observed in the comparison figures. As with the V44 test, the peak pressure is somewhat over-predicted with the conservative inputs chosen. The depressurization of the containment is very well predicted for the long-term portion of the test. Breakroom temperature is also well represented with the calculation – with the saturation temperature calculated with only a few degrees over the measurements. Some small amount of superheating is calculated just after the blowdown which is not apparent from the measurements. Later in the depressurization period superheating is also noted in the calculation for the breakroom that is also not apparent from measurement trends.

In the upper containment, gas temperature rises much earlier than the measurements, and this could be attributed to the delay time for the temperature sensors with the small sensible heat transfer that takes place during the initial single phase steam/air mixture transport into the upper containment region. The predicted saturation temperature in the upper containment is well predicted while a substantial amount of superheating is evident in the calculation but not in the measurements. The superheating is an expected result from the selection of NOFOG for the reference case input, as discussed in Section 3. The issue concerning calculated superheating which is not observed from measurement is addressed below in the sensitivity study and in the discussion on determining containment loads (pressure and temperature).

At the upper vertical staircase location, the local temperatures, especially saturation temperature, matches the measurements well with only a few degrees over prediction in the medium-term and with values essentially overlapping the measurements for the long-term period. A small degree of superheating is evident during the late long-term period that is not apparent from measurements.

For the lower vertical staircase, the calculated gas and saturation temperature over-predict the measured temperatures by about 20 degrees in the medium-term. The over-prediction of gas temperature continues for the depressurization period; however, the saturation temperature trends toward the measured temperature such that at the end of the long-term period the calculated saturation temperature and measurement nearly overlap.

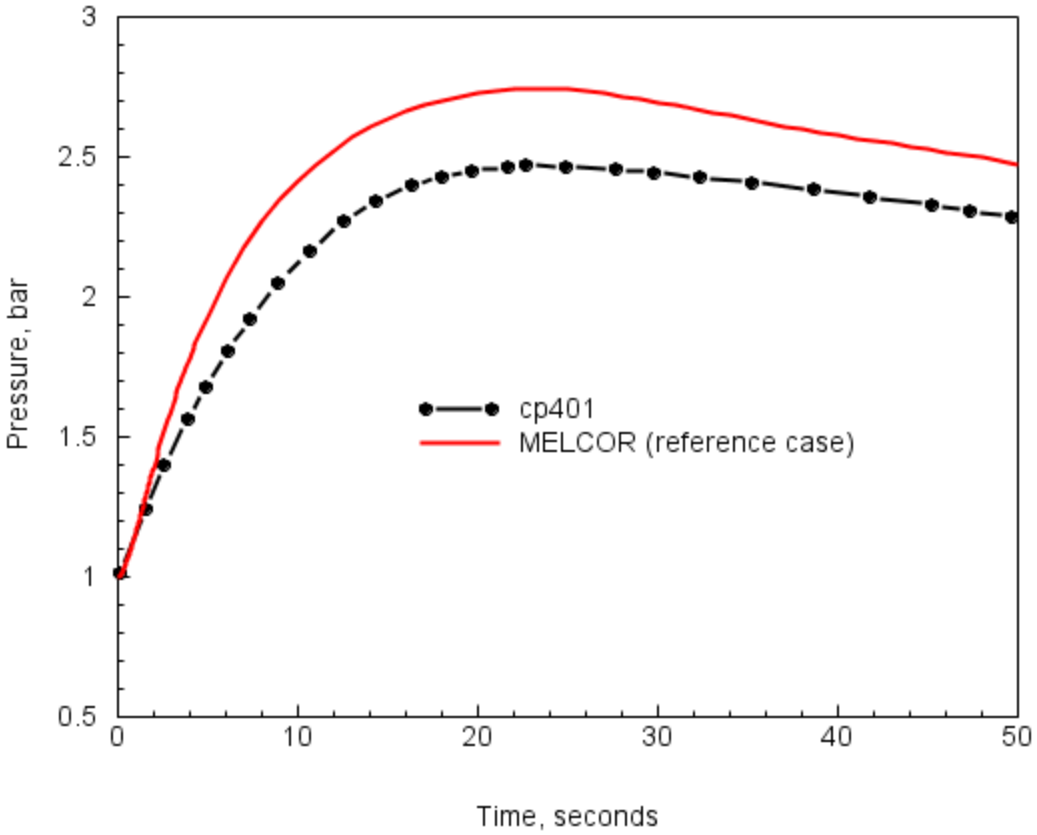

Figure 4-15 **Comparison of the measured and reference case pressure profile for the T31.5 test in the dome region of HDR facility – medium time period.**

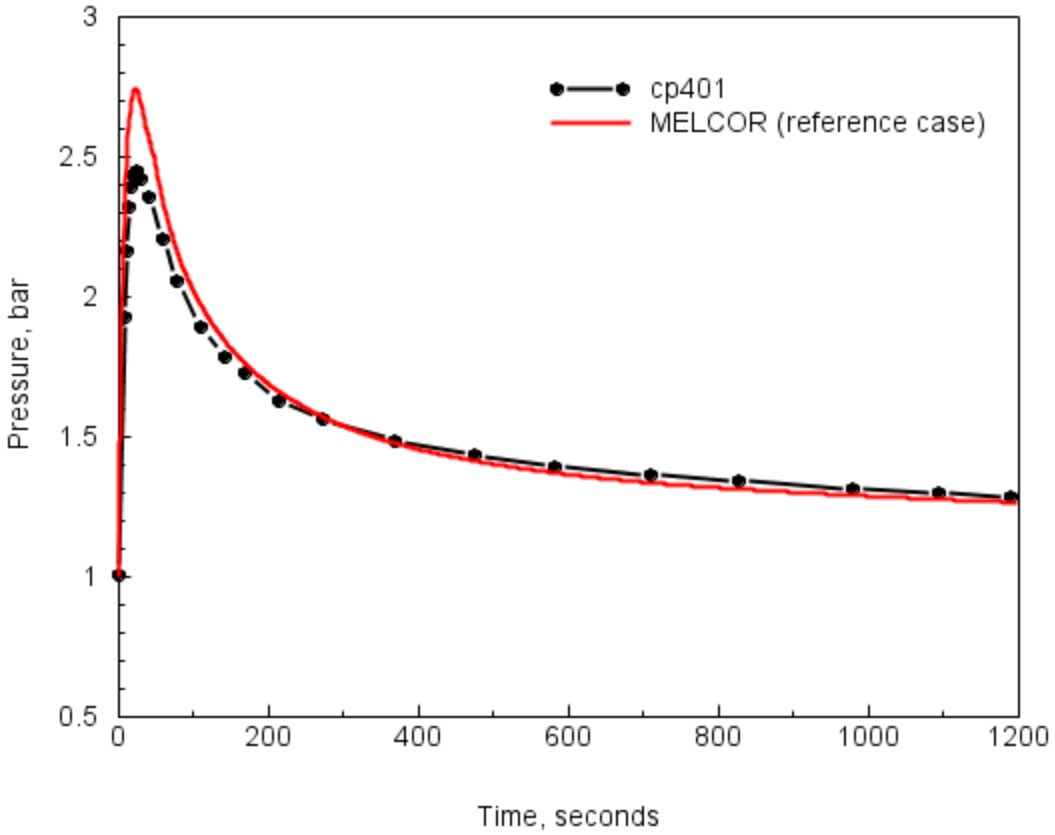

Figure 4-16 **Comparison of the measured and reference case pressure profile for the T31.5 test in the dome region of HDR facility – long time period.**

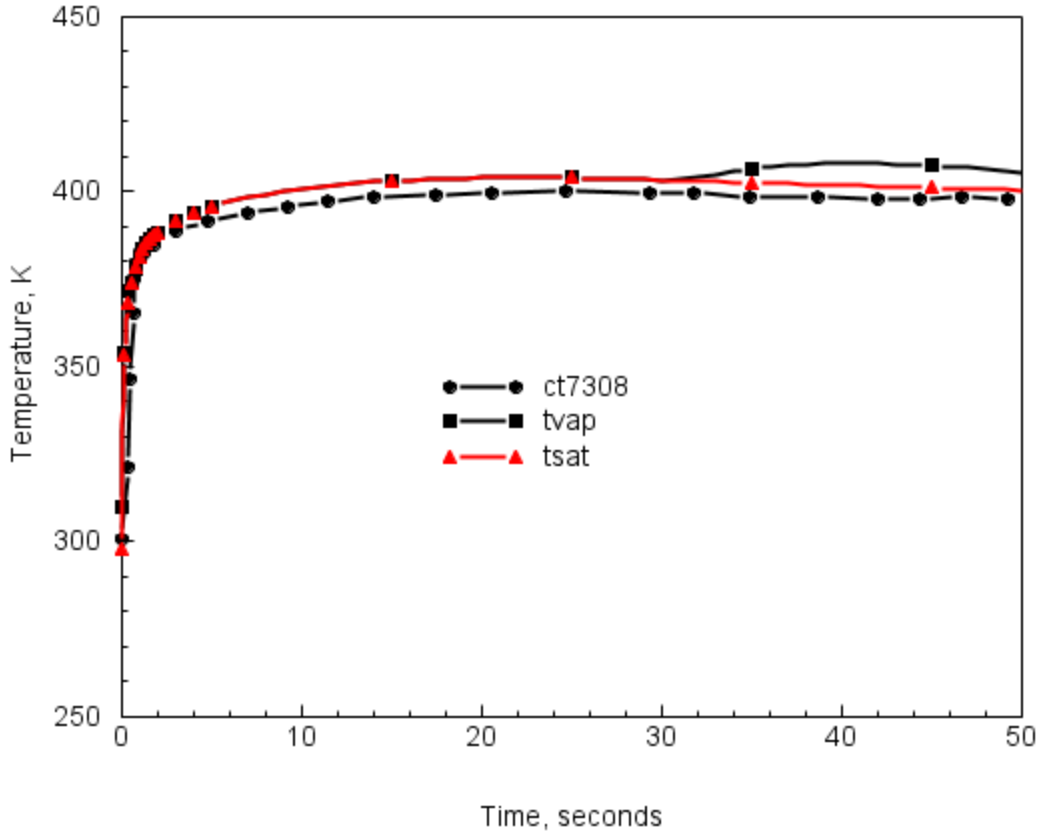

Figure 4-17 Comparisons of the measured and reference case break room temperature profile in the T31.5 test – medium time period.

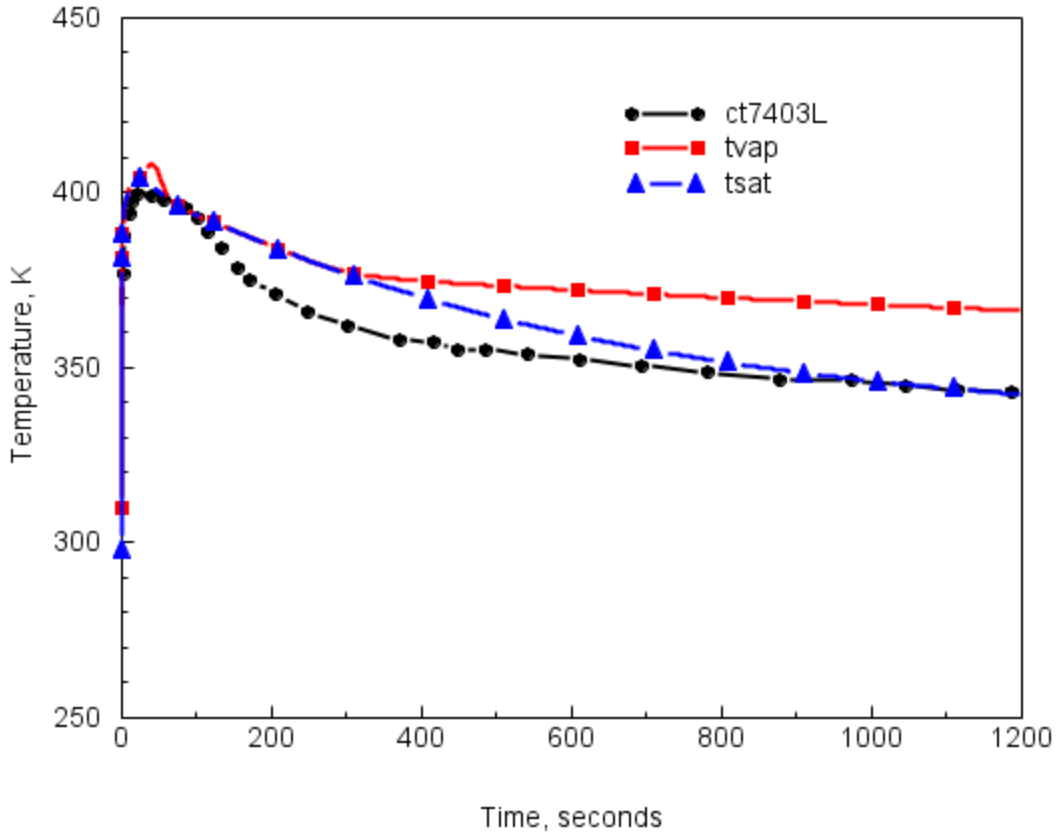

Figure 4-18 Comparisons of the measured and reference case break room temperature profile in the T31.5 test – long time period.

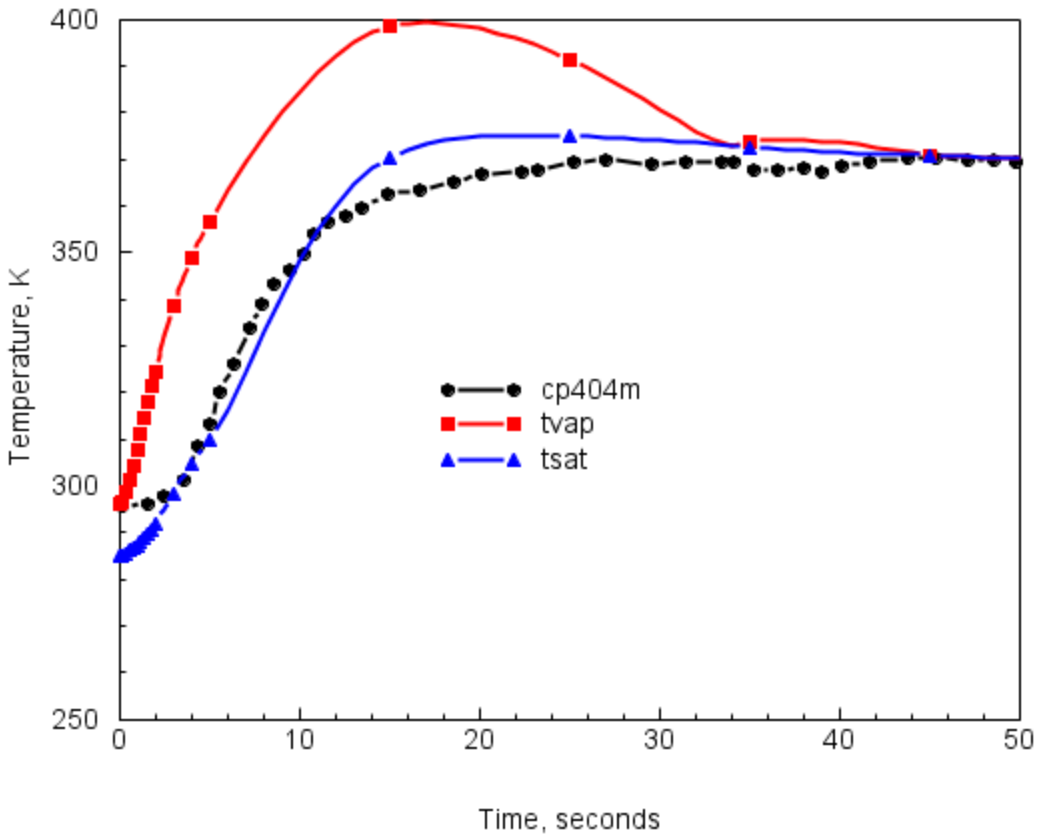

Figure 4-19 **Comparisons of the measured and reference case upper containment (40 meter) temperature profile in the T31.5 test – medium-term time period.**

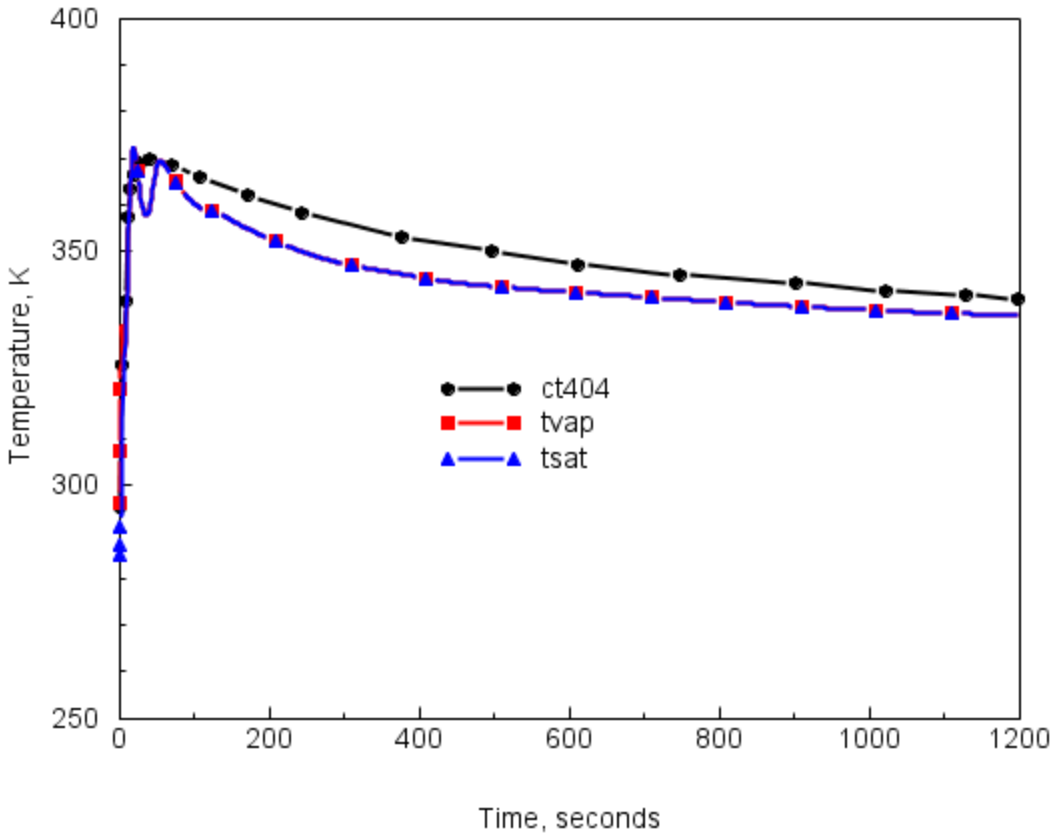

Figure 4-20 **Comparisons of the measured and reference case upper containment (40 meter) temperature profile in the T31.5 test – long-term time period.**

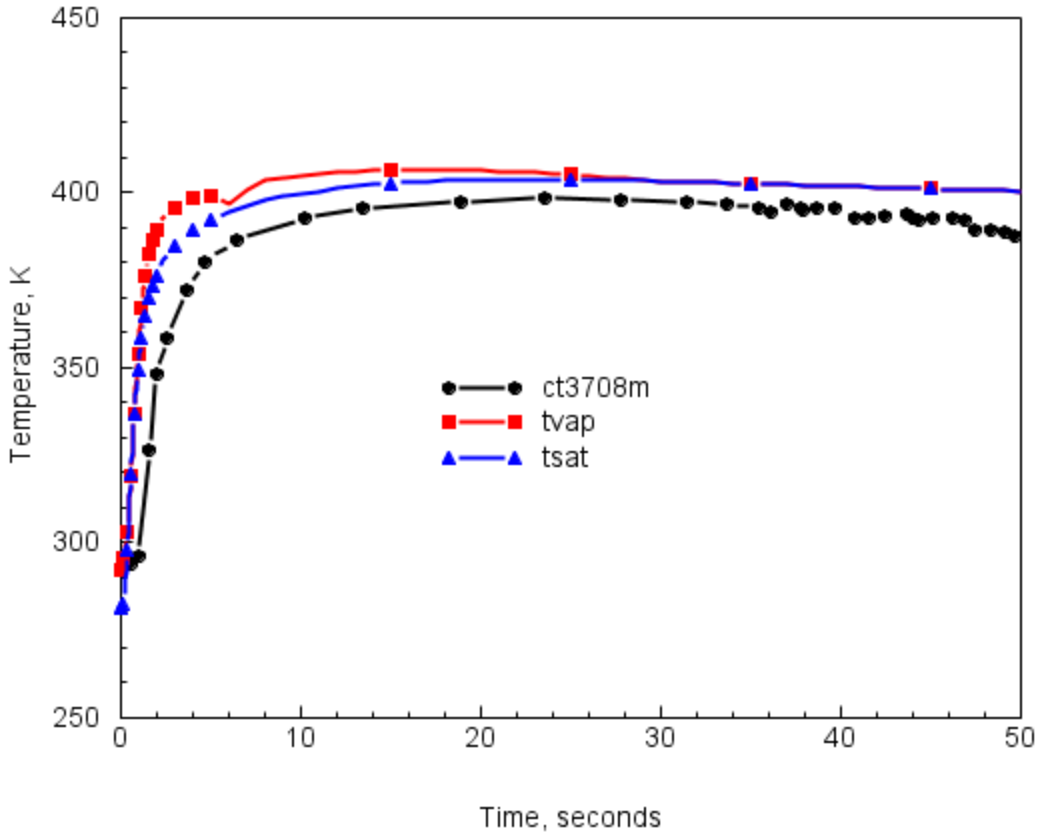

Figure 4-21 **Comparisons of the measured and reference case upper staircase (25 meter) temperature profile in the T31.5 test – medium-term time period.**

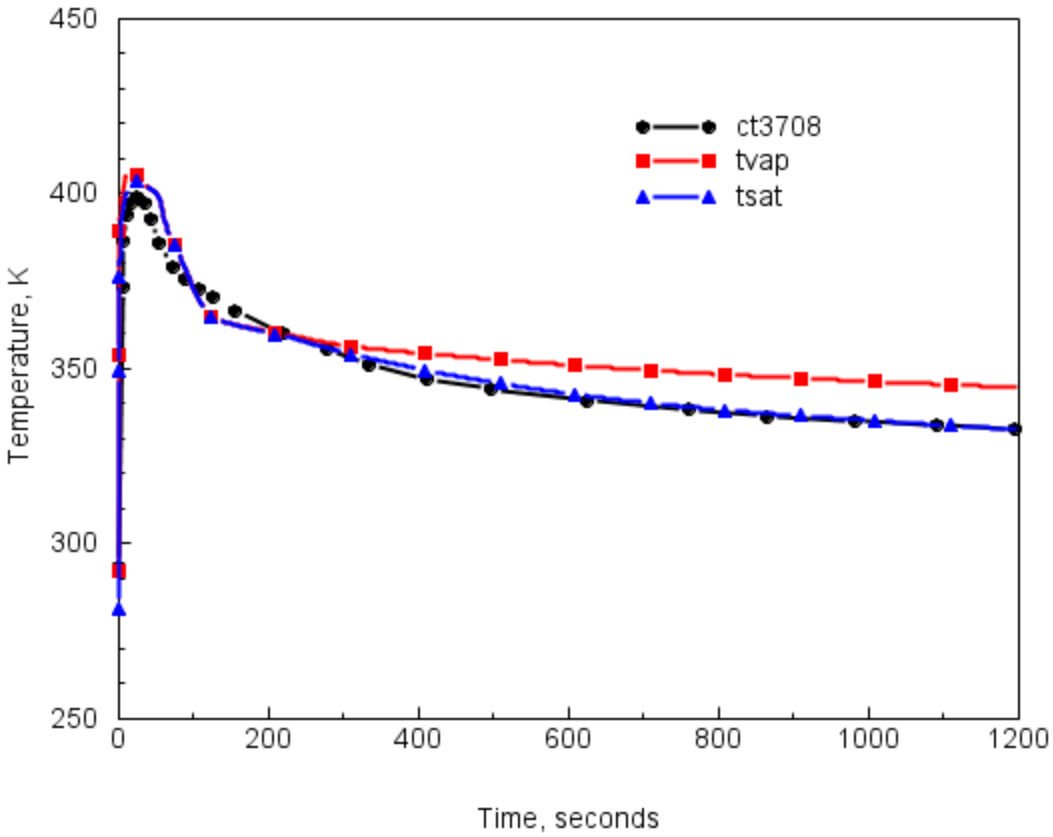

Figure 4-22 **Comparisons of the measured and reference case upper staircase (25 meter) temperature profile in the T31.5 test – long-term time period.**

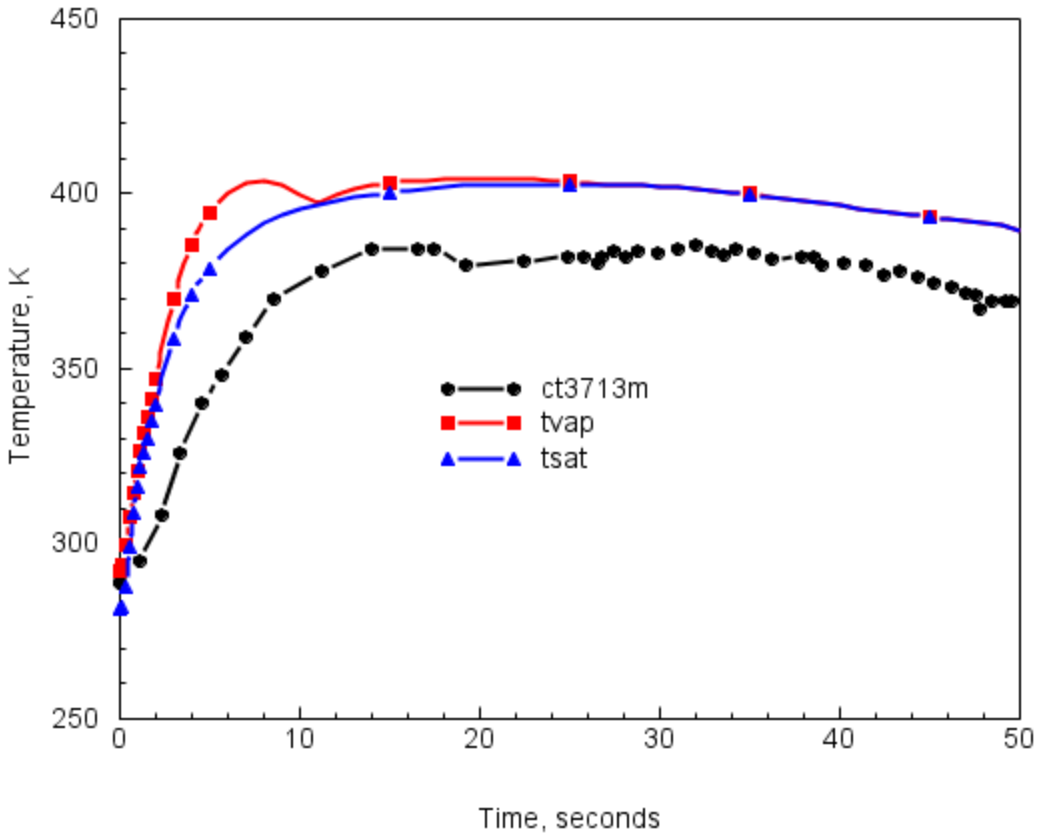

Figure 4-23 **Comparisons of the measured and reference case lower staircase (5 meter) temperature profile in the T31.5 test – medium-term time period.**

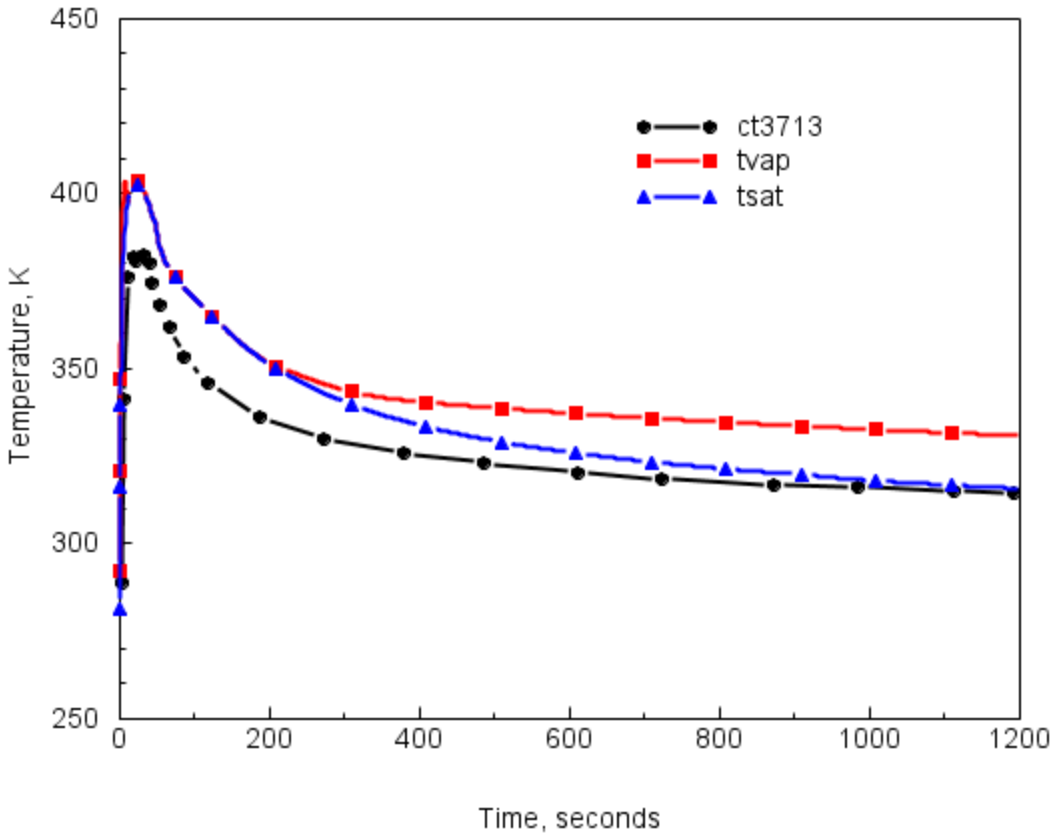

Figure 4-24 **Comparisons of the measured and reference case lower staircase (5 meter) temperature profile in the T31.5 test – long-term time period.**

4.2.2 Sensitivity Evaluation

The pressure predictions within the medium-term and long-term calculation periods for various sensitivity analyses are presented in Table 4-3. Pressure comparison for the medium-term relate to the peak pressure, and for the long-term the comparisons are for the containment pressure at the end of the period, 1200 seconds. For these sensitivity cases, comparisons for the type of flashing is omitted since this sensitivity was well covered with test V44. The suspended liquid sensitivity case is modeled with FOG and RN1 active (aerosol physics with deposition and settling). Two cases are included to show max film thickness set to 0.0005 and 0.00005 meters. A single-cell case is also included, and finally a combination of sensitivity cases 1, 2, and 3 is used to estimate the least conservative model for T31.5 (ISP-23) test.

During the medium-term that includes the blowdown period, the sensitivity cases for test T31.5 show similar trends that were also identified for test V44. What is different for test T31.5 is the focus on post-blowdown behavior, and in this respect we note that in the long-term the sensitivities that were important for pressure response becomes much less important in the post-blowdown period. Issues related to force convection, liquid suspension, and condensate film thickness are blowdown concerns, but in the post-blowdown period these phenomena are essentially absent from the calculation and therefore do not significantly influence the prediction of the global response as reflected by containment pressure.

Shown below are pressure and temperature profiles for a calculation that include not only the effect of FOG modeling on pressure and temperature but also the combination of all sensitivity inputs that result in a lower estimated pressure for the medium-term than the reference case. The plots cover results for both the medium and long-term, and can be compared to the reference case presented in Section 4.2.1 to evaluate the importance of modeling FOG and forced convection. The comparisons demonstrate by modeling choice, the degree of conservatism that is imbedded within the reference calculation by phenomenon. Although it would be difficult to argue that the following figures for the combination (fog, forced convection, and film thickness) are “best-estimates”, the lower estimates for Case 5 are clearly the better representation at least of the medium-term pipe rupture tests in the HDR T31.5 test, and therefore the results, by comparison, show model conservatism for the reference case.

Table 4-3 Pressure Calculations for test T31.5

	Sensitivity	Pressure (MPa)	
		Peak	Long-term**
Measured		0.250	0.128
Reference model	---	0.274 [19.2]***	0.126 [-7.1]
Aerosol Physics			
Case 1	FOG and RN1 active	0.268 [15.1]	0.128 [0.0]
Forced convection			
Case 2	Forced convection*	0.258 [8.2]	0.127 [-3.6]
Film maximum thickness			
Case 3	Enforcemax = 0.00005m	0.268 [15.1]	0.127 [-3.6]
Case 4	Enforcemax = 0.0005m	0.290 [30.1]	0.130 [7.1]
Combination from above			
Case 5	Cases 1, 2, and 3	0.254 [5.5]	0.129 [3.6]
Nodalization			
Case 6	Single Cell	0.320 [50.7]	0.128 [0.0]

* forced velocity profile as V44 calculation, for levels 1600, 1700 and 1800

** measured and calculated at 1200 seconds

*** over-pressure error, % = $((P_{calc} - P_{data})/(P_{data} - 0.1MPa)) * 100$

Suspended Liquid Water

The treatment of suspended liquid water was investigated similar to the V44 test sensitivity analysis, with the reference case input modified to change the NOFOG setting to FOG with the RN1 package activated to allow aerosol physic modeling for liquid water removal from the atmosphere due to agglomeration, deposition and gravity setting. Here the results of this liquid water removal simulation is presented for pressure (Figure 4-25 and Figure 4-26) and local temperature (Figure 4-27 through Figure 4-34). Marginal improvement with measured pressure is apparent mainly for the long-term period. For temperatures, the superheating seen with the reference case is noticeably reduced with the FOG activated, showing better agreement with temperature measurements for both medium- and long-term periods. Still some superheating occurs late in the long-term. The onset of superheating begins approximately when local fog mass goes to zero as liquid mass is depleted due to evaporation, deposition, and settling. For example, fog mass is plotted for the upper containment and staircase in Figure 4-35. Fog mass is present for the entire long-term period in the upper containment, and for this location the gas and saturation temperatures are equal. In the upper staircase the fog mass is depleted at approximately 600 seconds when superheating begins. The energy source for the superheat is sensible heat transfer from cooling metal primarily. Regions that experience significant early structure heating during the blowdown are more likely to have superheating predicted, as in the case of the breakroom and upper staircase. The low staircase has less contact with hot steam/air mixtures, and therefore retains more liquid water in the air and has cooler metal structures. These conditions favor a saturated atmosphere.

Of course the importance of superheating, calculated or observed, needs to be evaluated for possible impact on containment loads. By itself a small amount of superheating would not be significant to an increase in containment pressure loading since pressure is proportional to total containment energy and increases in sensible energy will not change the total energy content greatly. This is reflected in the small peak pressure change between the reference case with superheating and sensitivity case with FOG and aerosol physics activated. In terms of the local gas temperature increases with superheating, the thermal loads on structure or equipment is dependent mainly on latent heat transfer not sensible heat transfers. Latent heat transfer is a function of vapor partial pressure difference between the bulk gas and the film or structure temperature. Figure 4-36 shows the relative latent and sensible heat transfer calculated for metal structures in the breakroom during significant periods of calculated superheating. The percentage of sensible heat transfer compared to total heat transfer to the structures is about 6 to 8%. The thermal loads are therefore much more dependent on the calculated saturation temperature in this case than on gas temperature. Consequently, we focus more attention on the agreement between calculated saturation temperature and measured gas temperature, and for the T31.5 test the agreement is mostly within a few degrees and overall within ~ 10 degrees of measurement in the upper staircase and upper containment.

The typical trends of over-mixing are noted in the lower staircase region where the saturation temperatures are over-predicted by approximately 20 degrees. There is no sensitivity adjustment that can address this trend with justification. Although mixing can be affected by large changes in pathway loss coefficients, these adjustments are too large to be justified for negating the control volume overmixing tendency. Here we limit ourselves to observing that the effect is noted, and appears significant for the lower regions of the containment, that is, below the injection elevation.

In the upper containment and staircase, the saturation temperatures are generally predicted below the measurements, and this behavior is probably due to the inability of the code to resolve a buoyant plume.

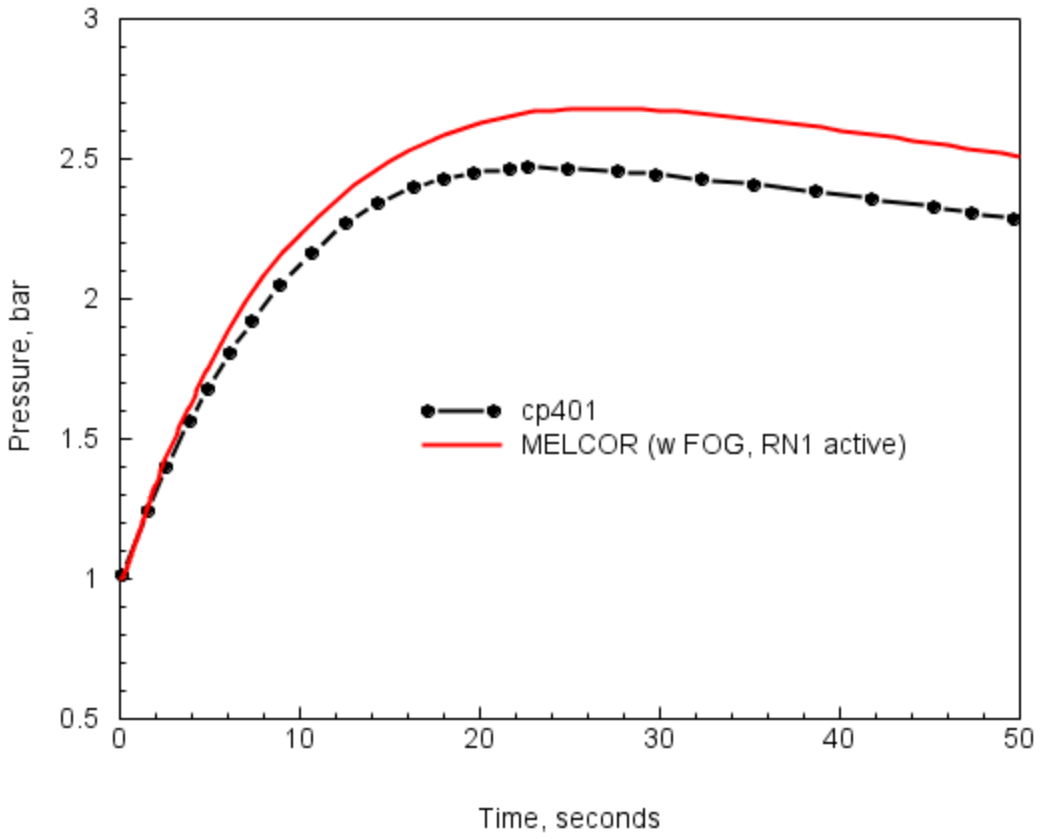

Figure 4-25 **Comparison of the measured and MELCOR FOG sensitivity case for the upper containment pressure profile during the medium-term T31.5 test period.**

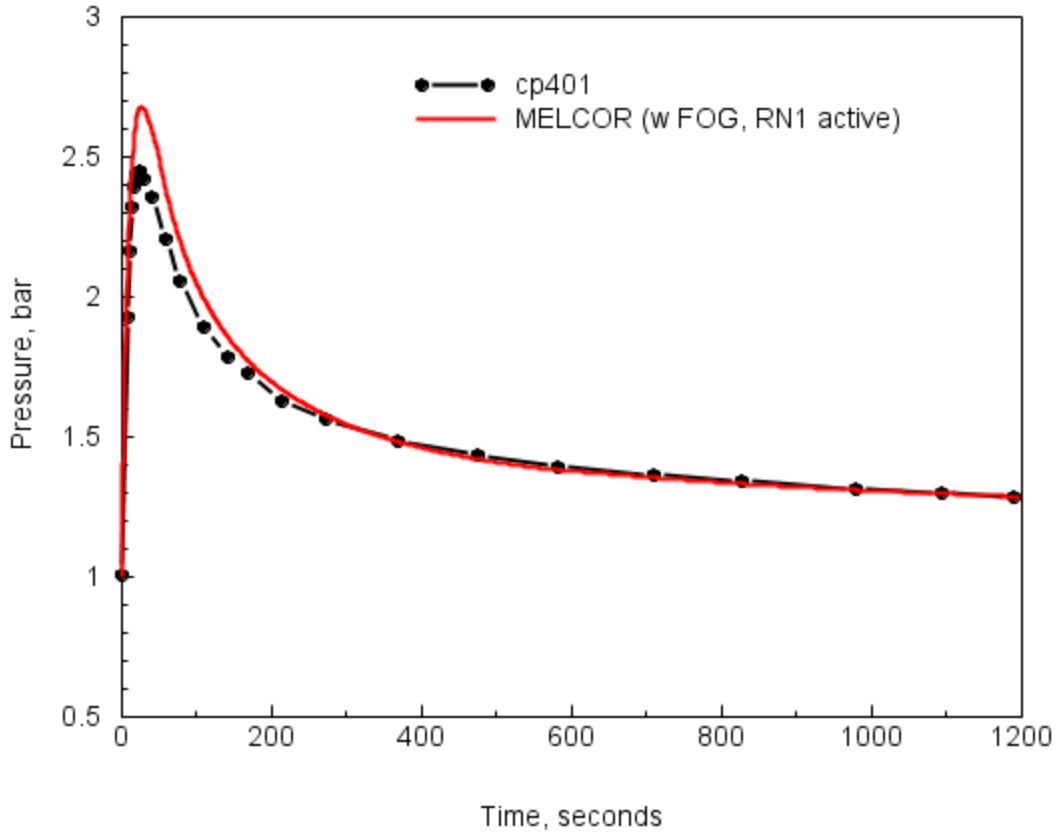

Figure 4-26 **Comparison of the measured and MELCOR FOG sensitivity case for the upper containment pressure profile during the long-term T31.5 test period.**

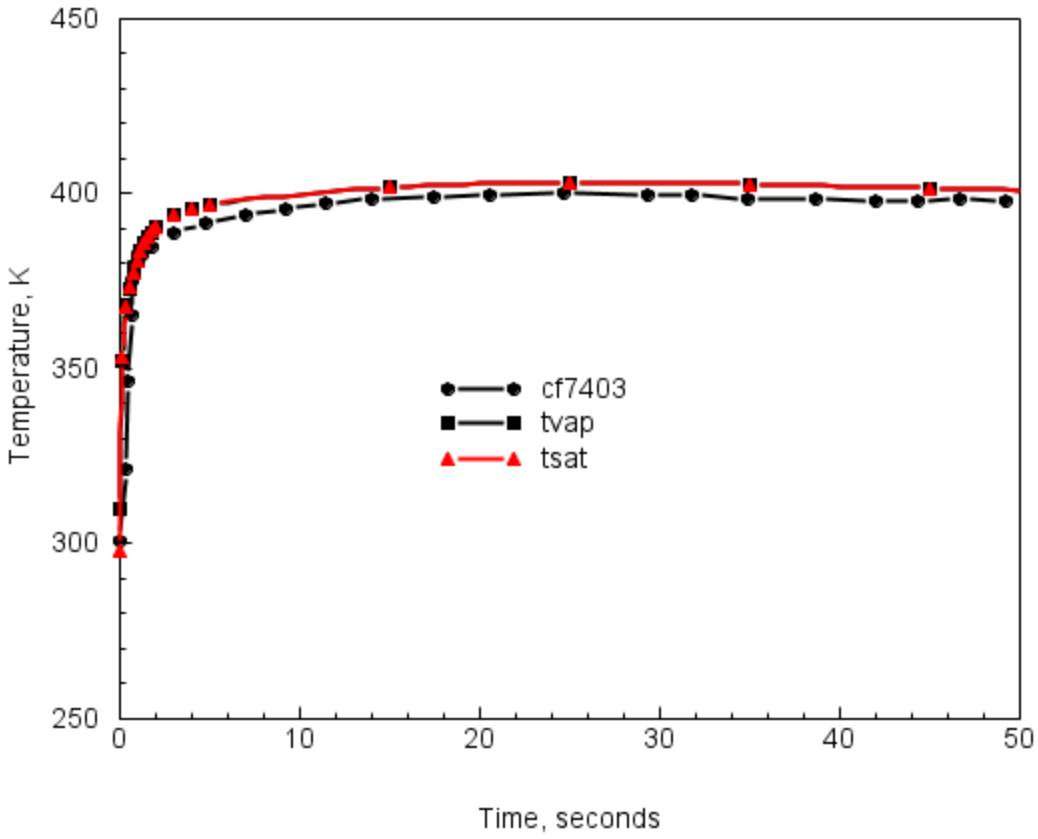

Figure 4-27 **Comparison of the measured and MELCOR FOG sensitivity case for the breakroom gas temperature during the medium-term T31.5 test period.**

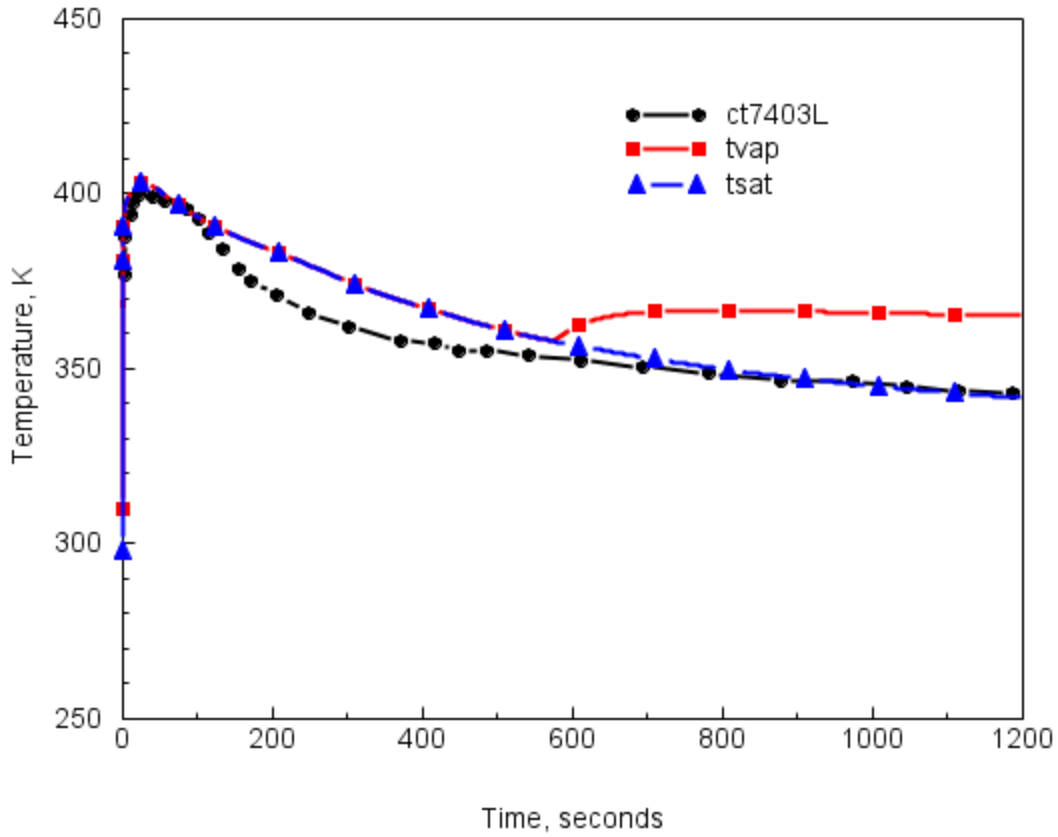

Figure 4-28 **Comparison of the measured and MELCOR FOG sensitivity case for the breakroom gas temperature during the long-term T31.5 test period.**

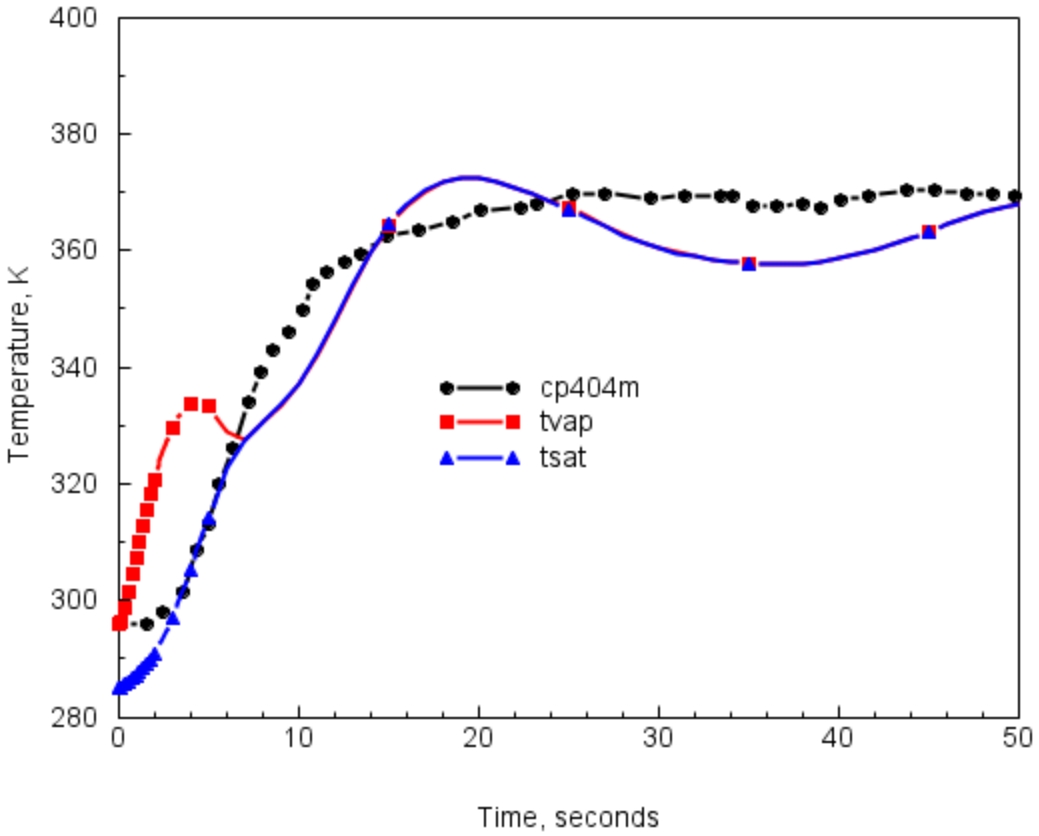

Figure 4-29 **Comparison of the measured and MELCOR FOG sensitivity case for the upper containment gas temperature during the medium-term T31.5 test period.**

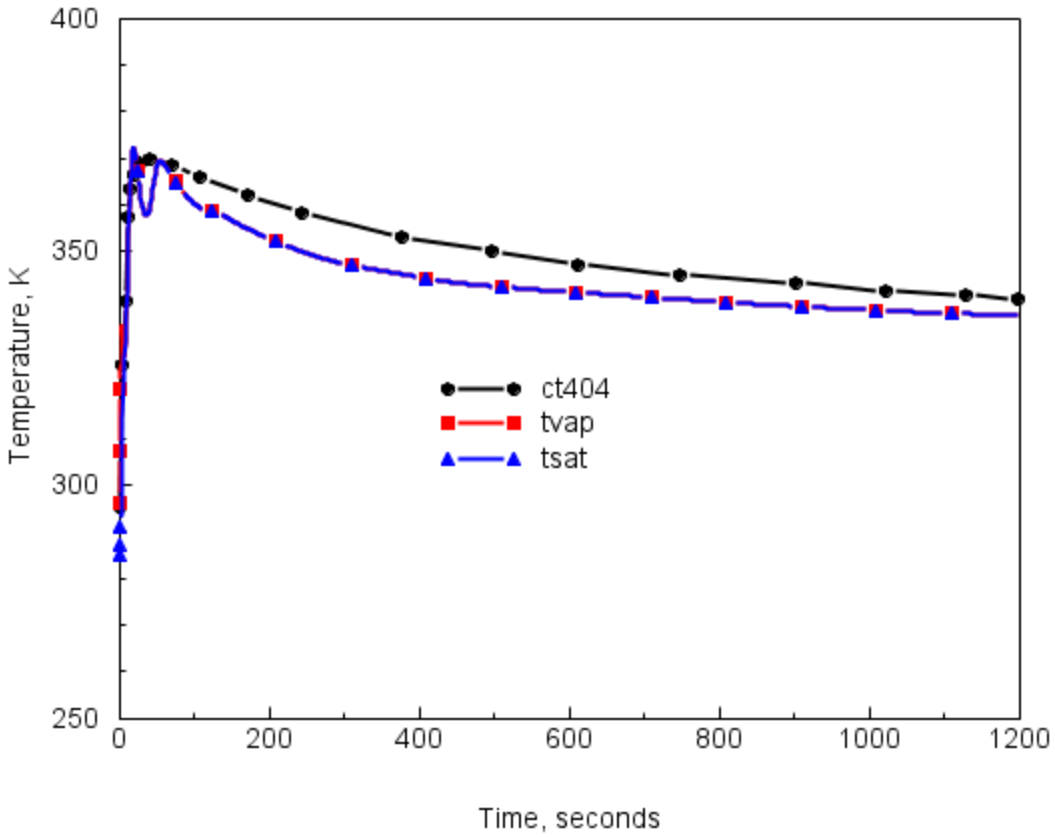

Figure 4-30 **Comparison of the measured and MELCOR FOG sensitivity case for the upper containment gas temperature during the long-term T31.5 test period.**

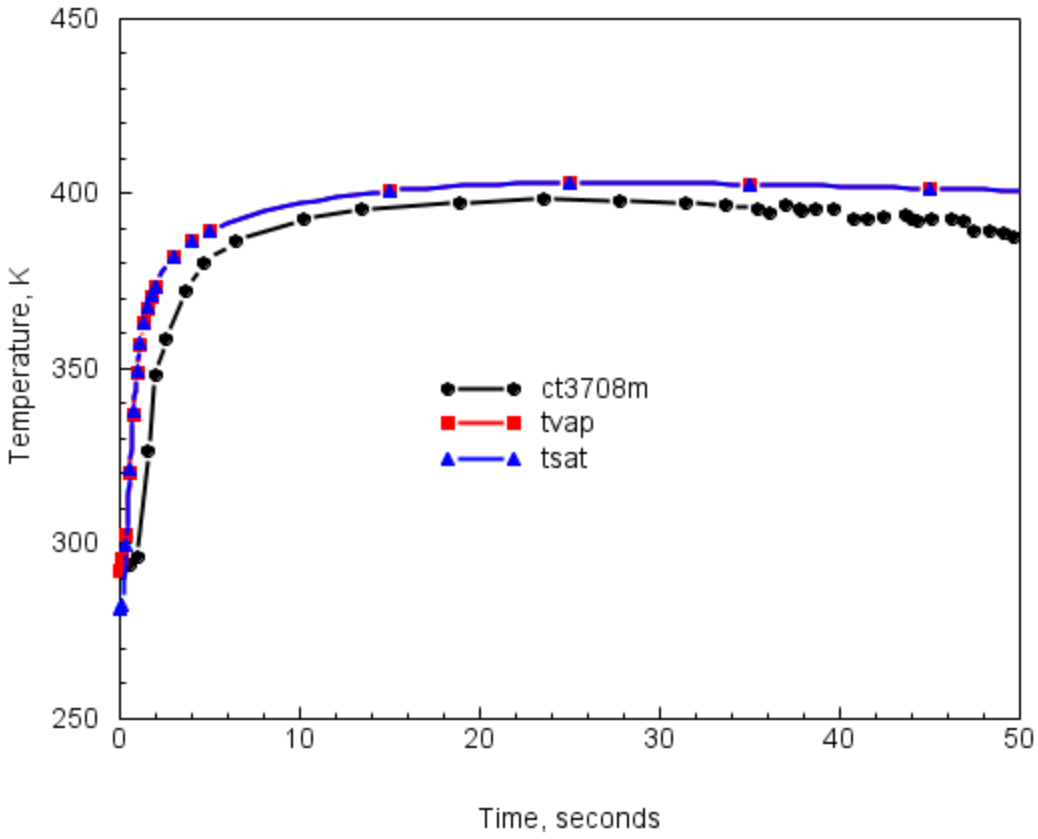

Figure 4-31 **Comparison of the measured and MELCOR FOG sensitivity case for the upper staircase gas temperature during the medium-term T31.5 test period.**

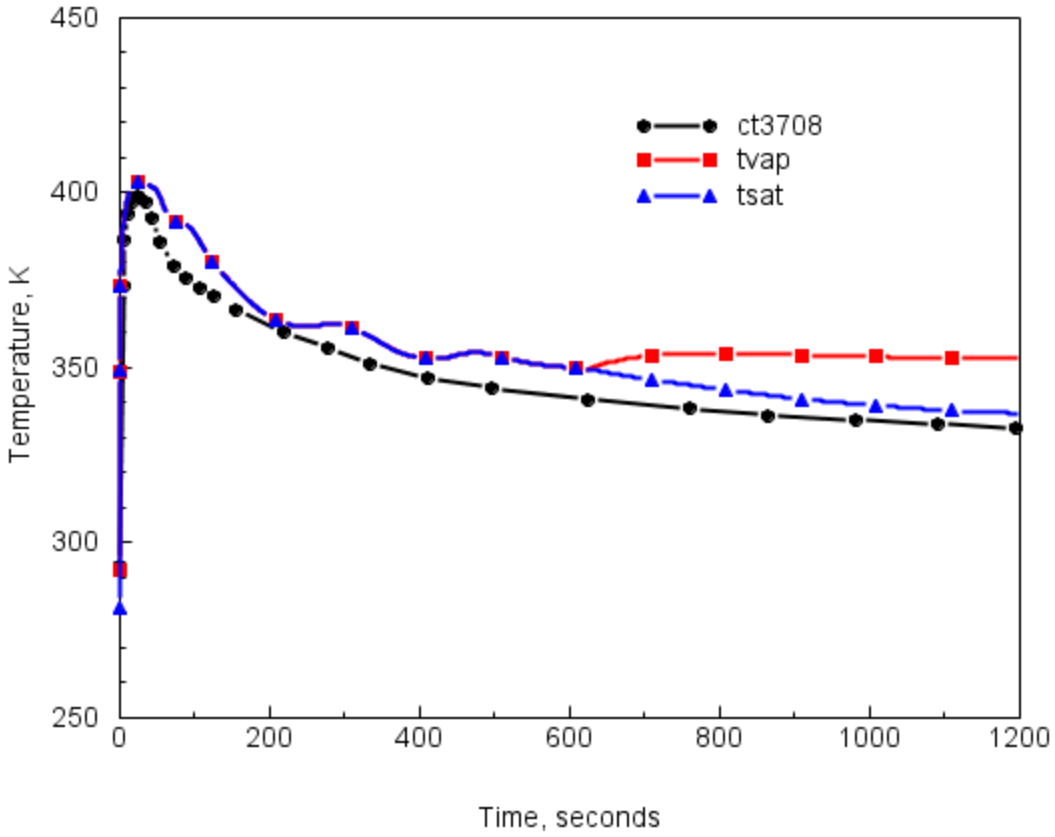

Figure 4-32 **Comparison of the measured and MELCOR FOG sensitivity case for the upper staircase gas temperature during the long-term T31.5 test period.**

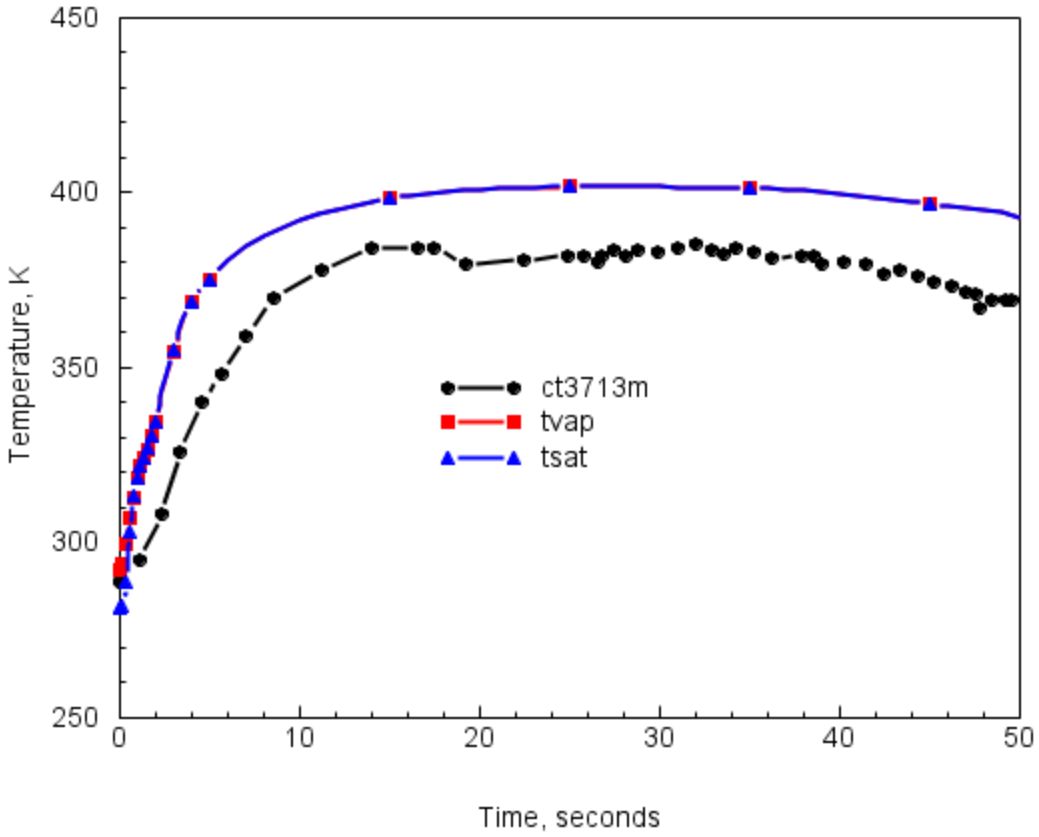

Figure 4-33 **Comparison of the measured and MELCOR FOG sensitivity case for the lower staircase gas temperature during the medium-term T31.5 test period.**

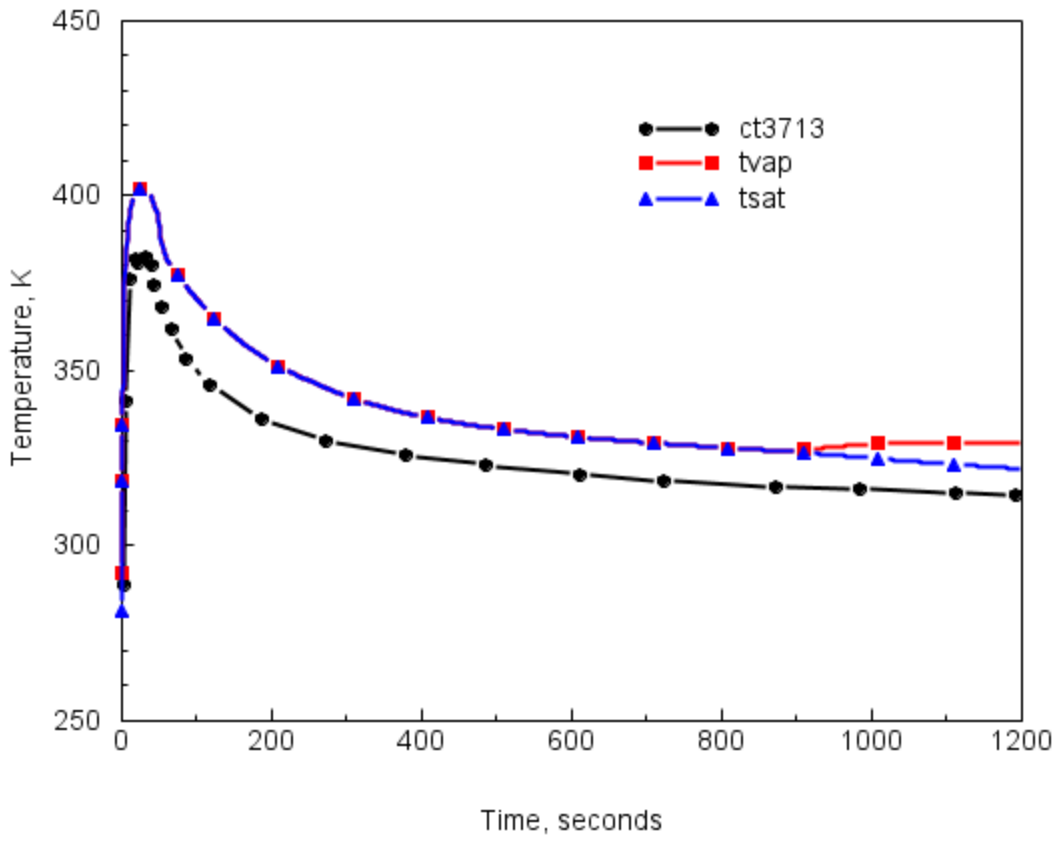

Figure 4-34 **Comparison of the measured and MELCOR FOG sensitivity case for the lower staircase gas temperature during the long-term T31.5 test period.**

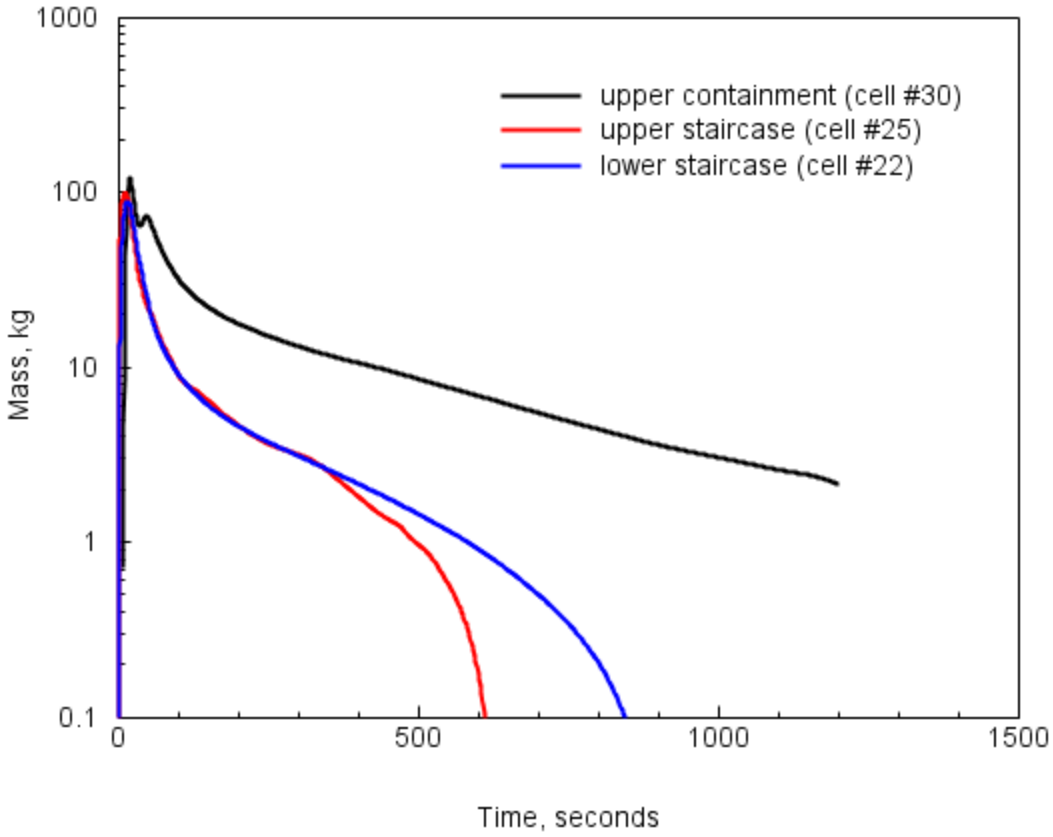

Figure 4-35 MELCOR calculated local fog mass for the T31.5 test with FOG and RN1 active – long-term.

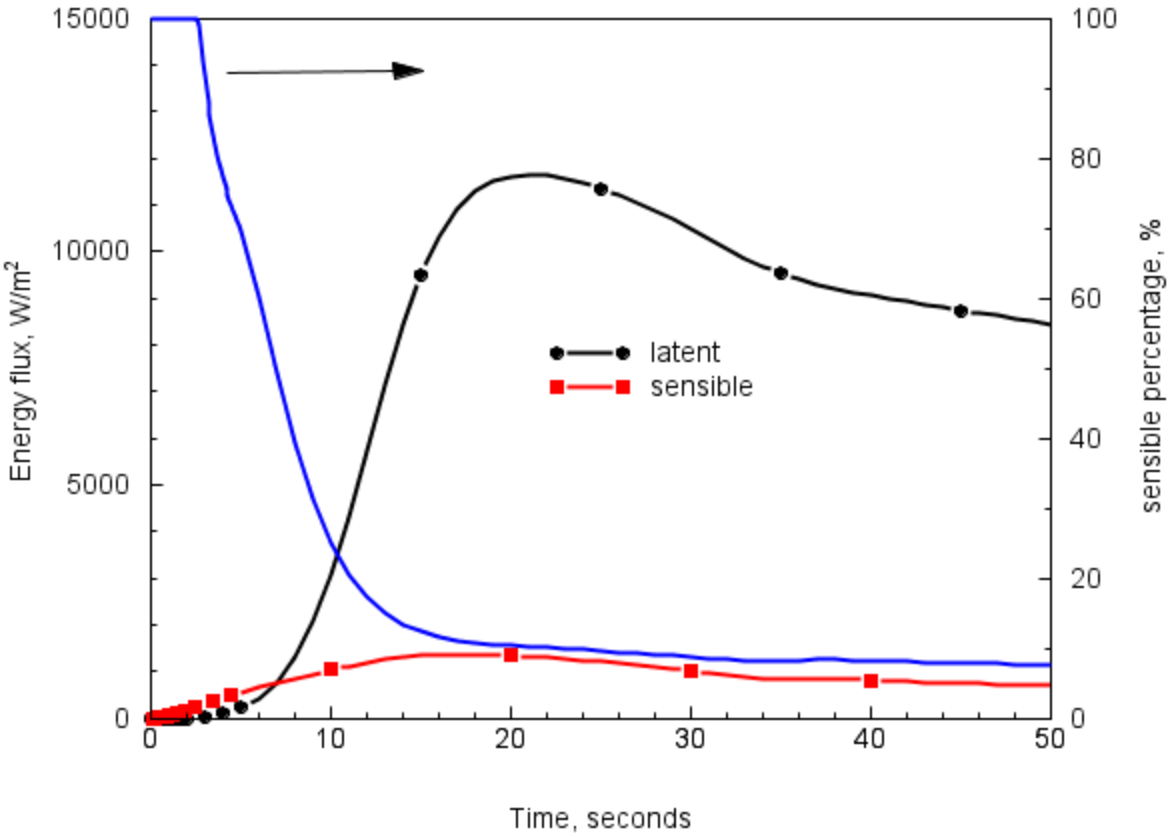

Figure 4-36 MELCOR calculated energy flux to metal structure (30intfe1) in cell#30 for the reference case in HDR test T31.5.

Combined Sensitivity Case.

The reference case is modified in sensitivity Case 5 to include FOG and RN1 active, forced convection in the breakroom level and levels above and below the breakroom (1600,1700,1800), and at maximum film thickness setting somewhat below a dynamic film thickness in the reference case. In the medium-term the effects of these modeling choice is most noticeable in the reduction of calculated pressure with the most significant effect being the forced convective modeling. Shown in Figure 4-37 through Figure 4-46 are the results for the combination case. In the medium-term the pressure profile is well predicted with the peak pressure calculated within ~ 5%. The long-term pressure (time > 300 sec) is calculated with no observable deviation from the plotted pressure measurement. Local temperatures are slightly improved, especially in the medium-term, compared to measurements but the improvement is not as obvious as for the pressure prediction.

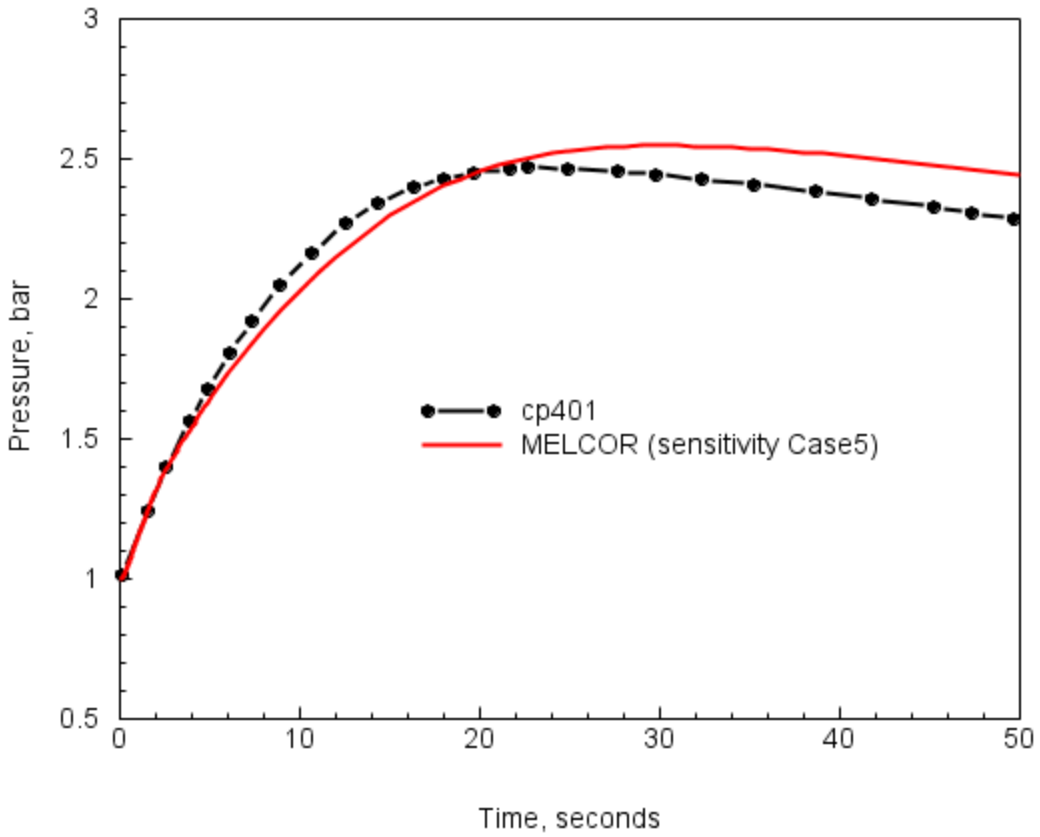

Figure 4-37 **Comparison of the measured and MELCOR combined sensitivity case (Case 5) for the upper containment pressure profile during the medium-term T31.5 test period.**

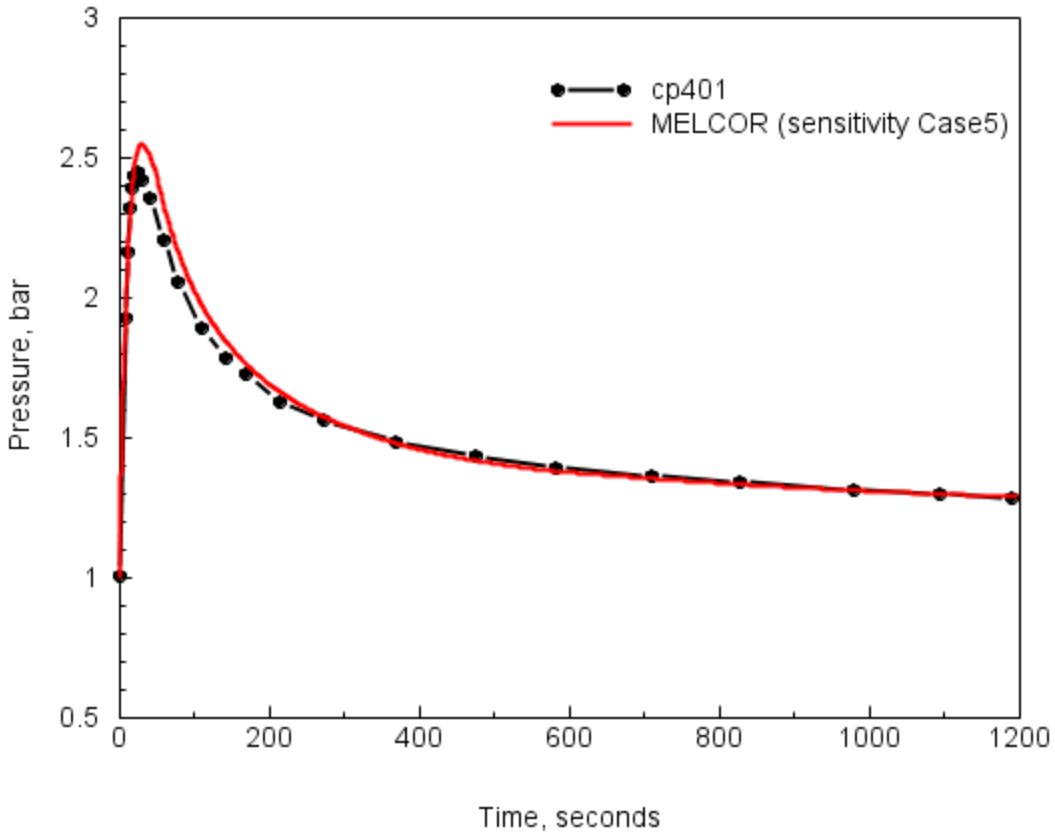

Figure 4-38 **Comparison of the measured and MELCOR combined sensitivity case (Case 5) for the upper containment pressure profile during the long-term T31.5 test period.**

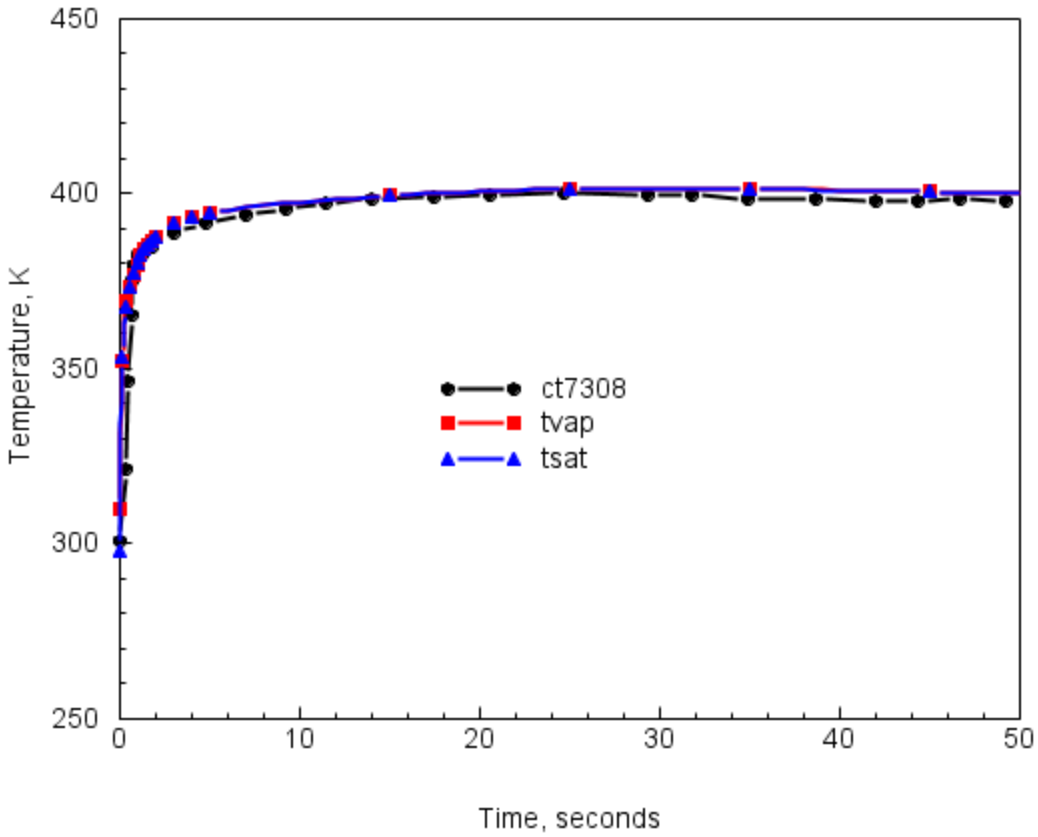

Figure 4-39 **Comparison of the measured and MELCOR combined sensitivity case (Case 5) for the breakroom gas temperature during the medium-term T31.5 test period.**

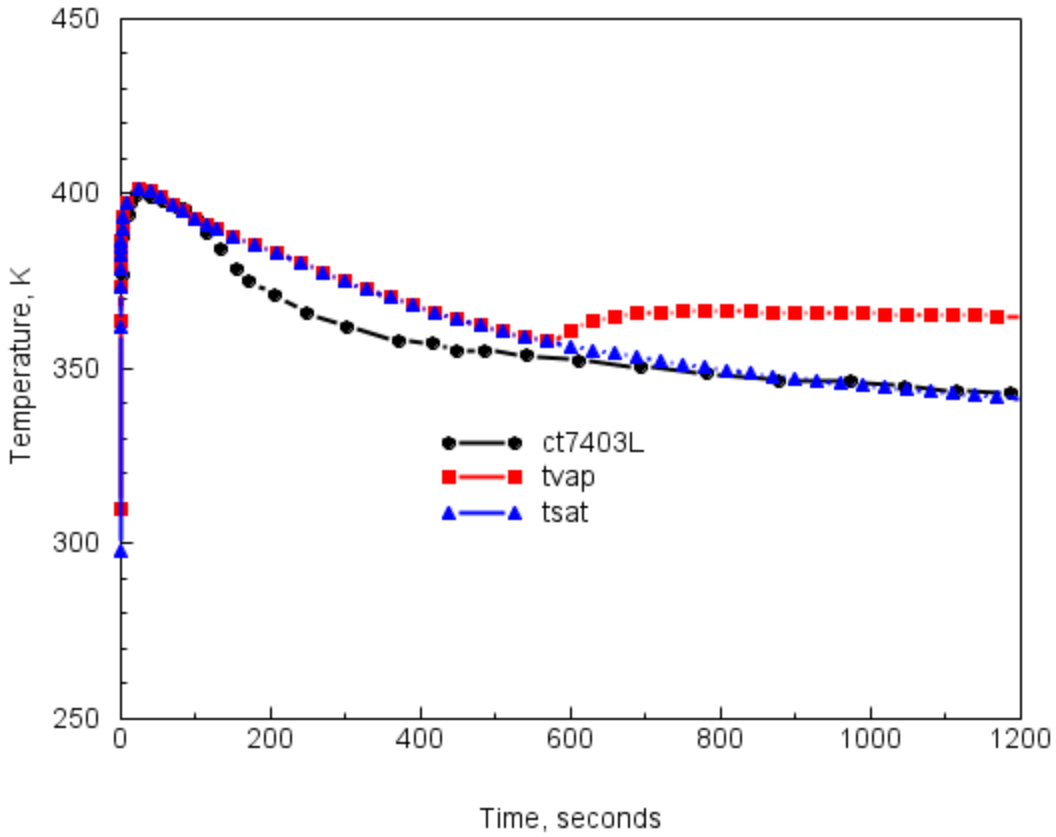

Figure 4-40 **Comparison of the measured and MELCOR combined sensitivity case (Case 5) for the breakroom gas temperature during the long-term T31.5 test period.**

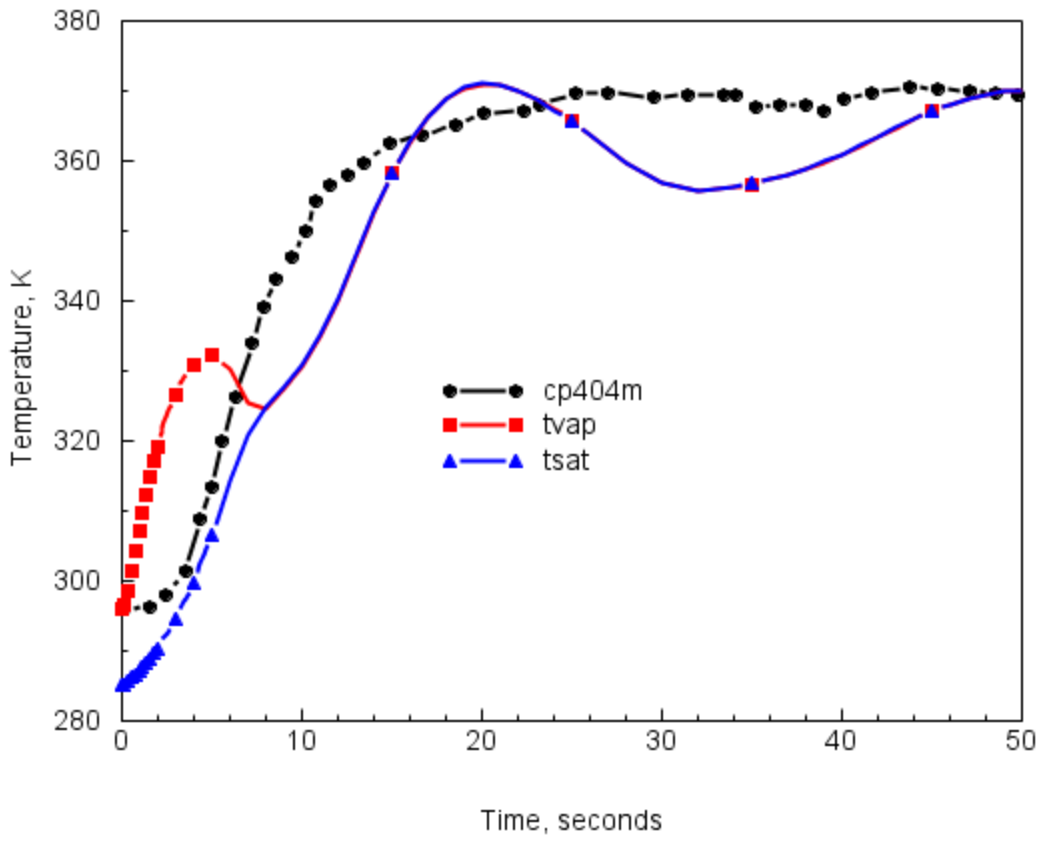

Figure 4-41 **Comparison of the measured and MELCOR combined sensitivity case (Case 5) for the upper containment gas temperature during the medium-term T31.5 test period.**

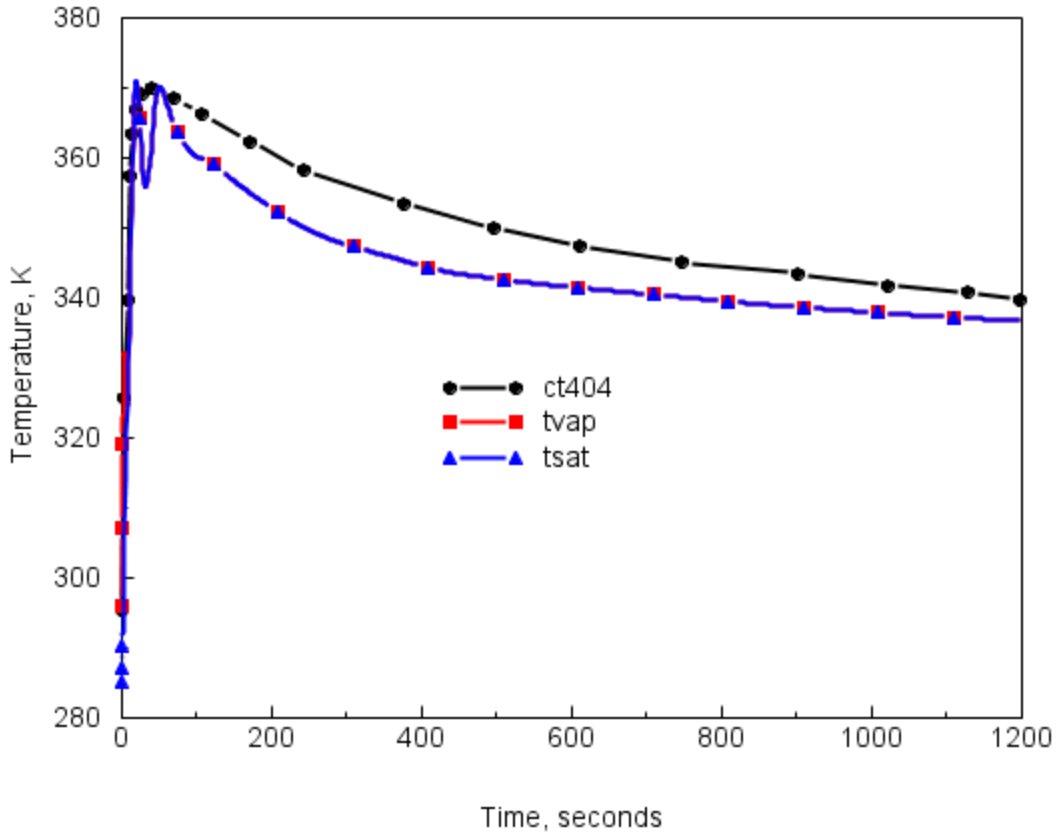

Figure 4-42 **Comparison of the measured and MELCOR combined sensitivity case (Case 5) for the upper containment gas temperature during the long-term T31.5 test period.**

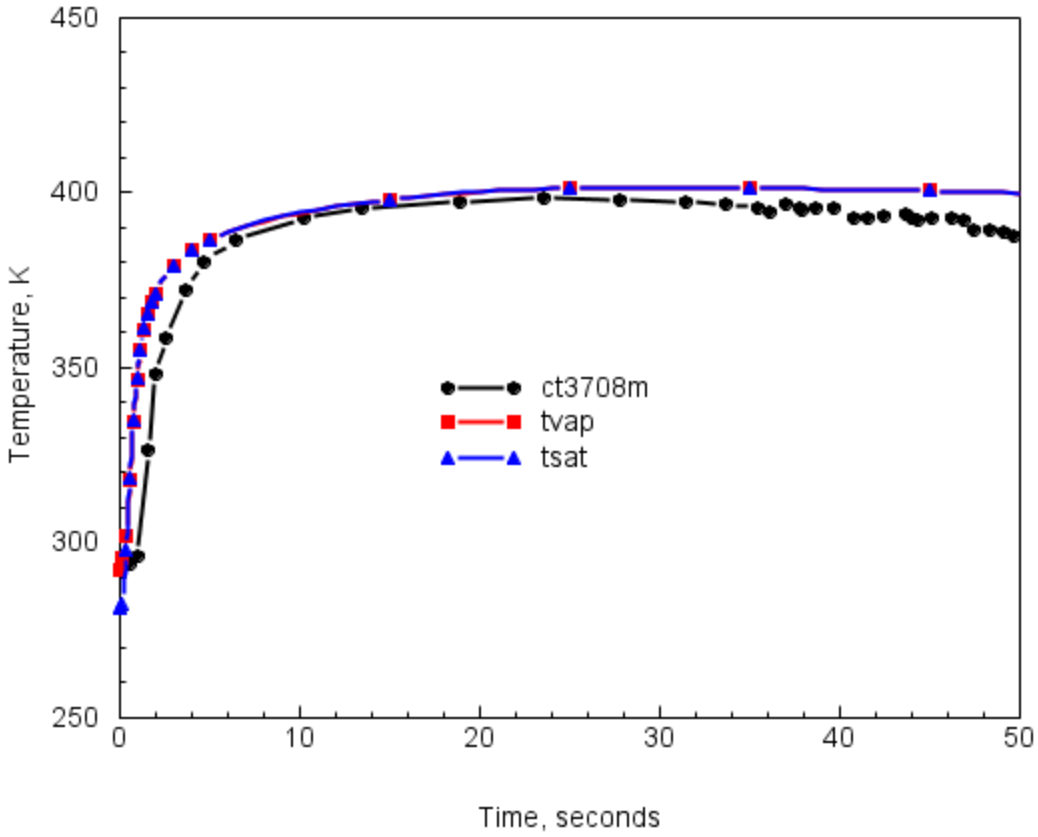

Figure 4-43 **Comparison of the measured and MELCOR combined sensitivity case (Case 5) for the upper staircase gas temperature during the medium-term T31.5 test period.**

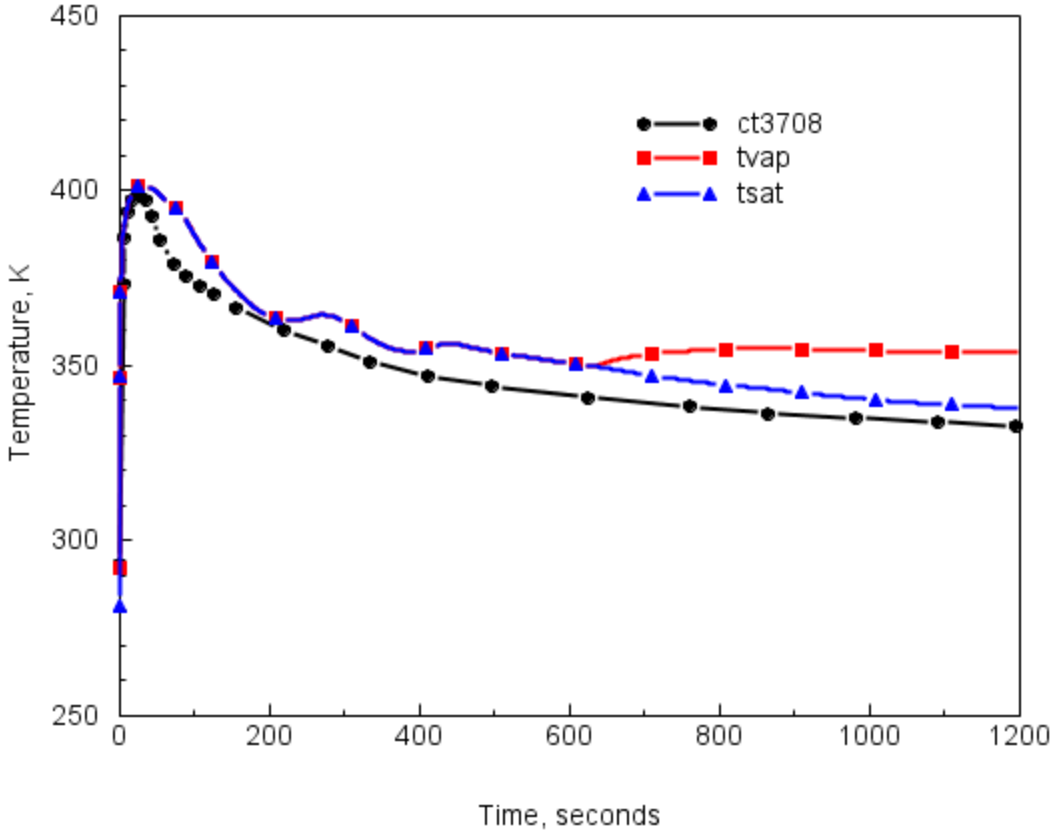

Figure 4-44 **Comparison of the measured and MELCOR combined sensitivity case (Case 5) for the upper staircase gas temperature during the long-term T31.5 test period.**

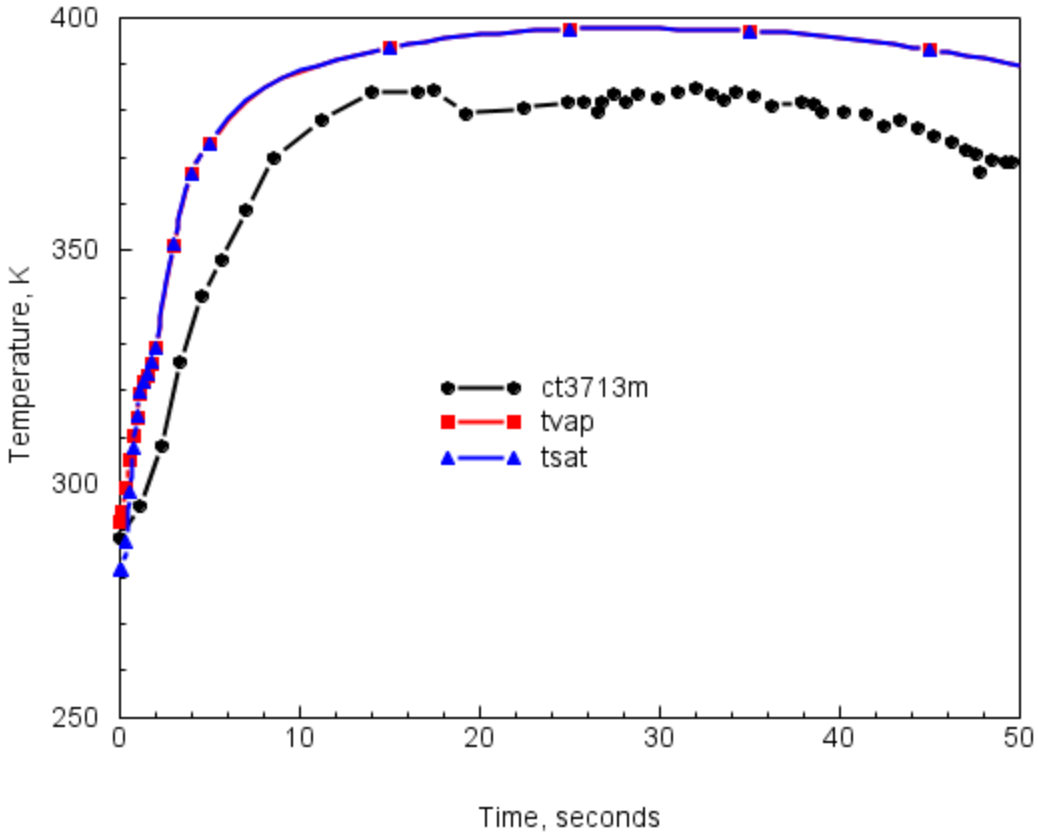

Figure 4-45 **Comparison of the measured and MELCOR combined sensitivity case (Case 5) for the lower staircase gas temperature during the medium-term T31.5 test period.**

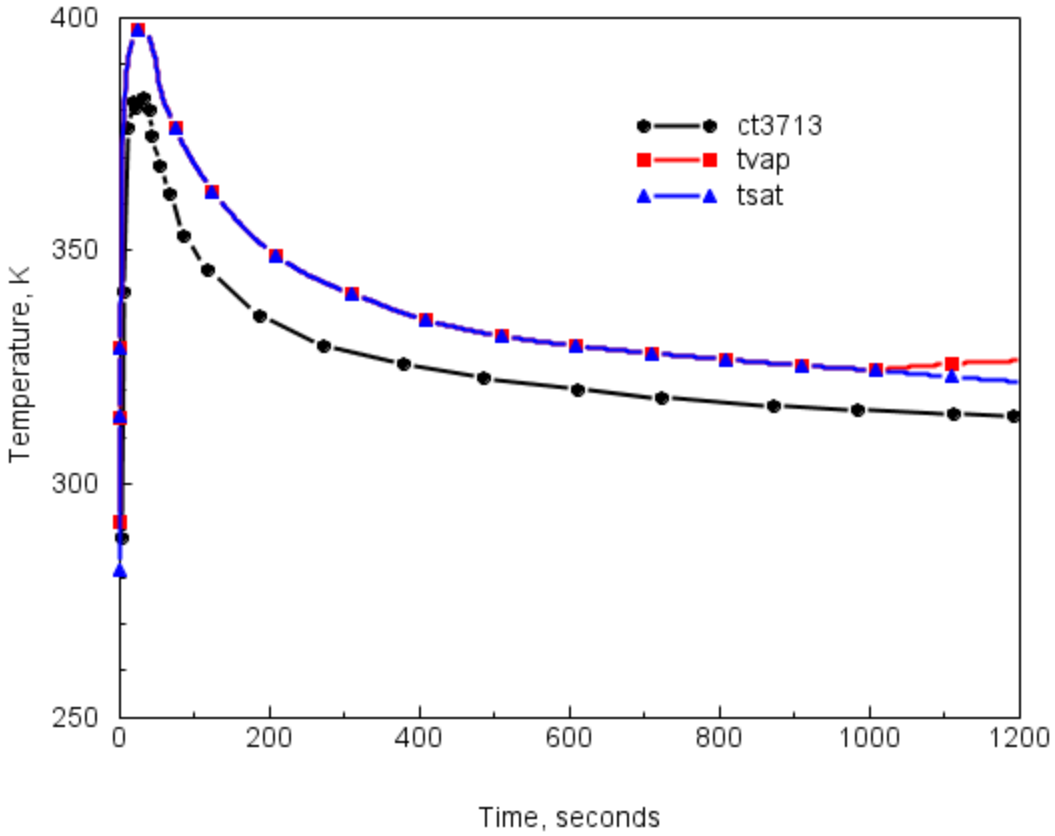

Figure 4-46 **Comparison of the measured and MELCOR combined sensitivity case (Case 5) for the lower staircase gas temperature during the long-term T31.5 test period.**

4.2.3 Benchmark

The 33CV calculation used in the CONTAIN ISP-23 submission was used here for the MELCOR benchmark against the CONTAIN code. This calculation was submitted using the CONTAIN water aerosol model to remove liquid water from the atmosphere in a mechanistic (physical) manner as indicated above for the FOG and RN1 active cases. The CONTAIN case was modeled in the ISP-23 submission without forced convection and with the default condensate film thickness maximum fixed at 0.0005 meters (no dynamic film flow modeled). In Figure 4-47 and Figure 4-48 show the pressure comparison for a similarly modeled MELCOR and CONTAIN calculations for the medium- and long-term periods. Figure 4-49 through Figure 4-54 show benchmark comparisons plots for local gas temperatures in the breakroom, upper containment, and upper and lower staircase regions. The benchmark comparisons for the T31.5 test differ in that the time periods spans the long-term depressurization period and the modeling includes the addition of water aerosols to model fog effects (condensation/evaporation of droplets and removal by deposition and settling).

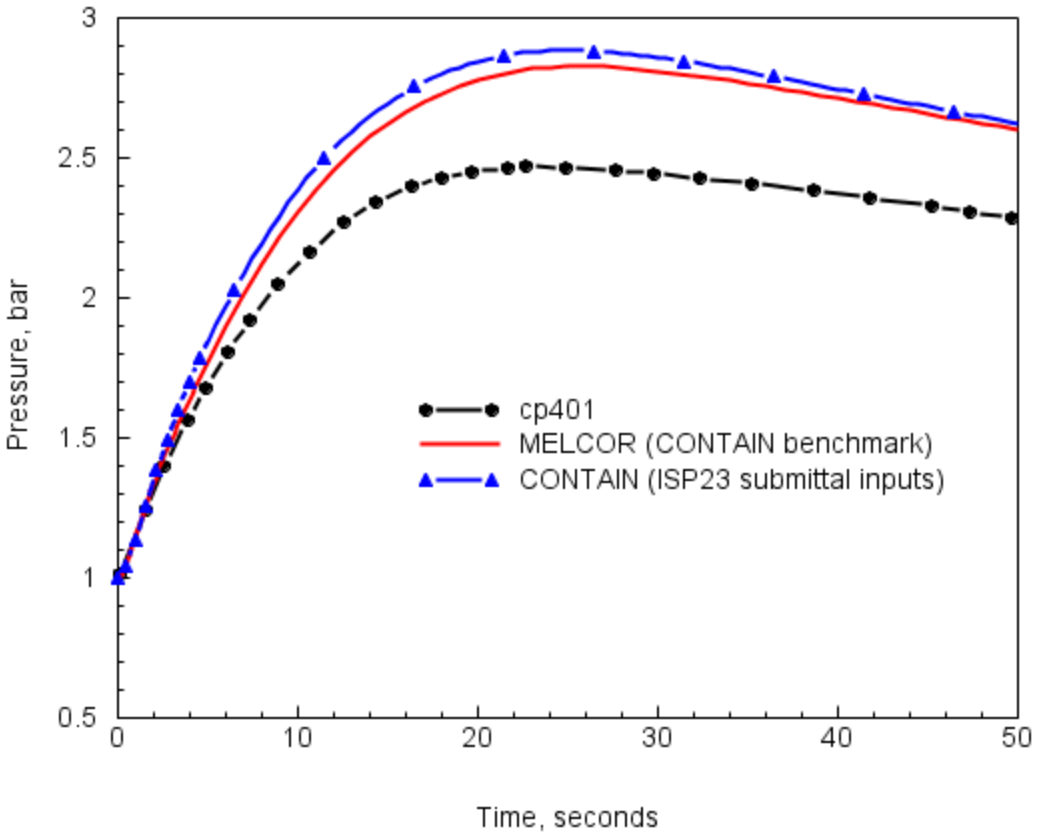

Figure 4-47 Benchmark for MELCOR/CONTAIN codes upper containment pressure profile during the medium-term T31.5 test period.

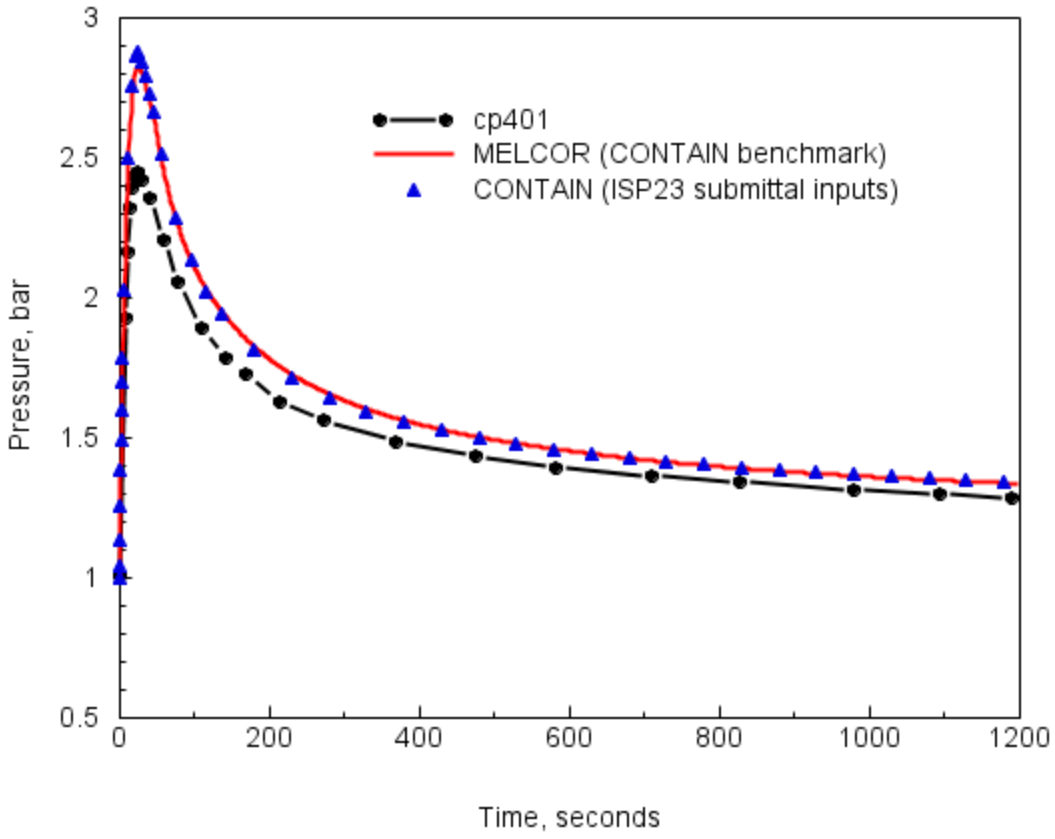

Figure 4-48 Benchmark for MELCOR/CONTAIN codes upper containment pressure profile during the long-term T31.5 test period.

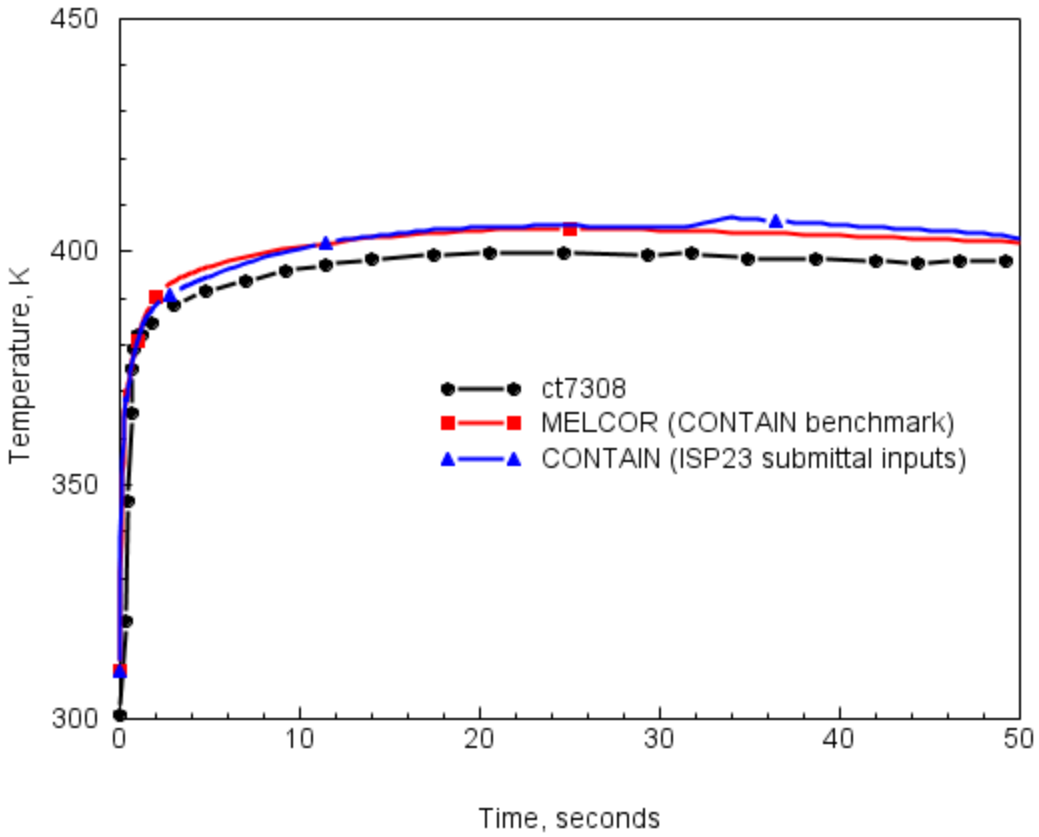

Figure 4-49 Benchmark for MELCOR/CONTAIN codes breakroom gas temperature during the medium-term T31.5 test period.

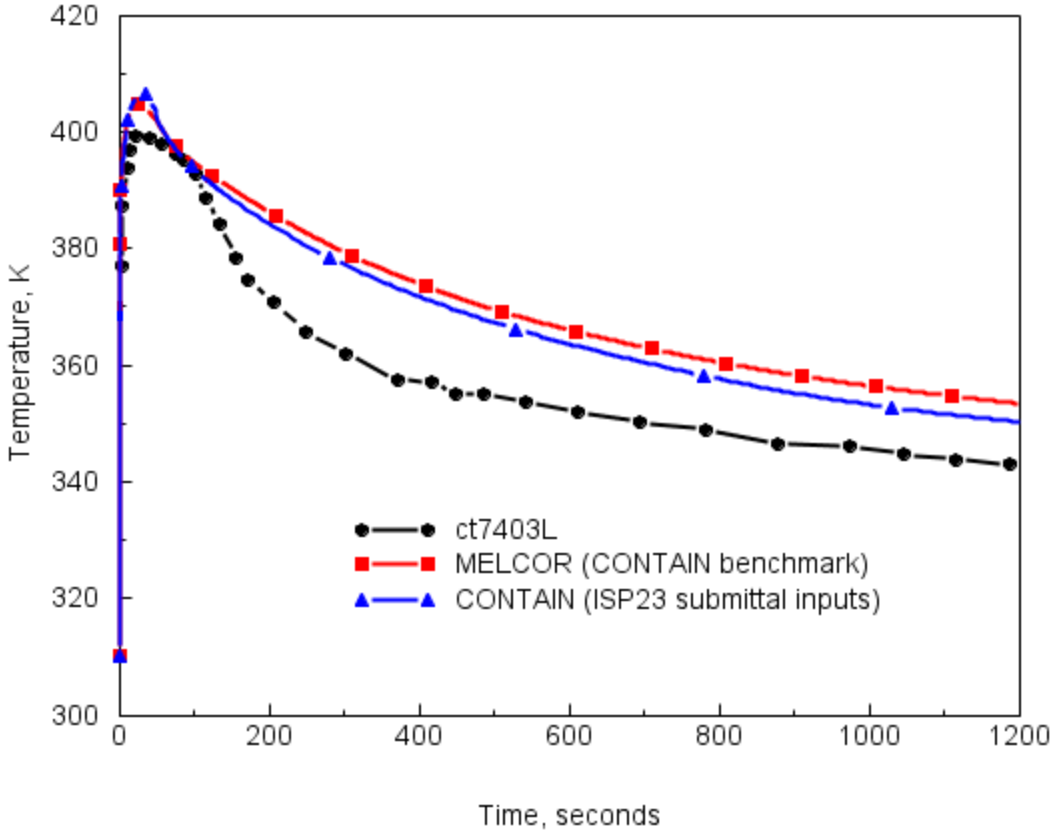

Figure 4-50 **Benchmark for MELCOR/CONTAIN codes breakroom gas temperature during the long-term T31.5 test period.**

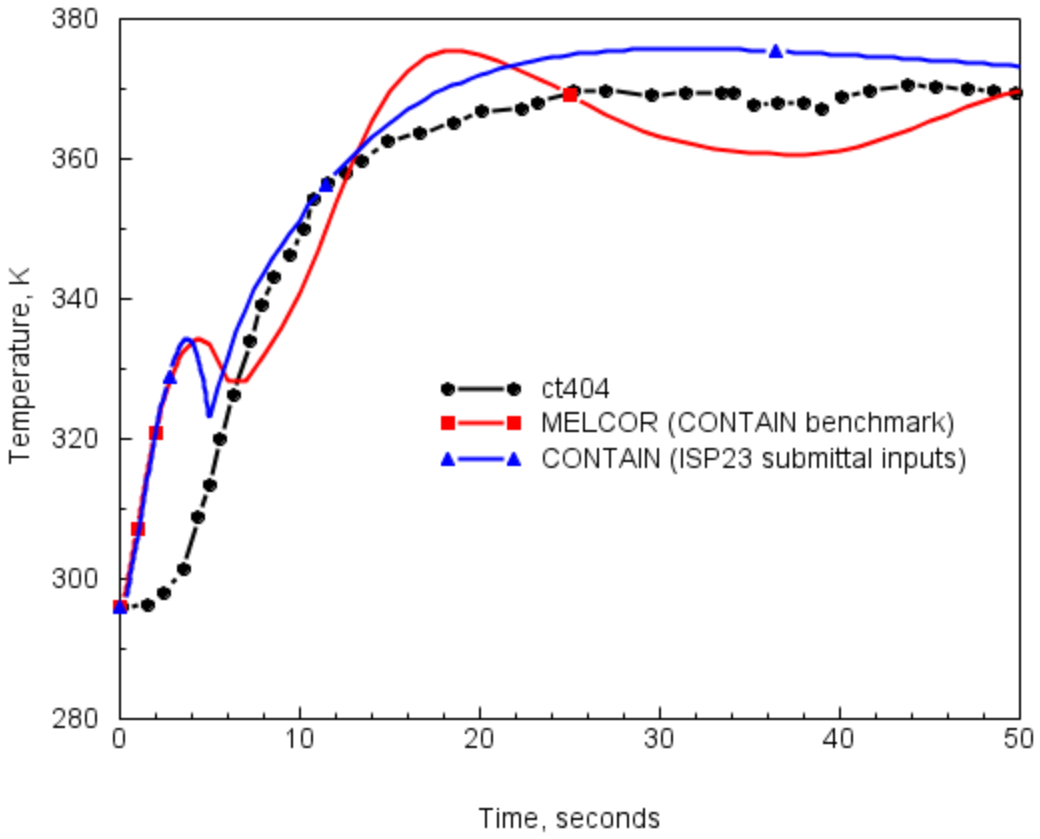

Figure 4-51 Benchmark for MELCOR/CONTAIN codes upper staircase gas temperature during the medium-term T31.5 test period.

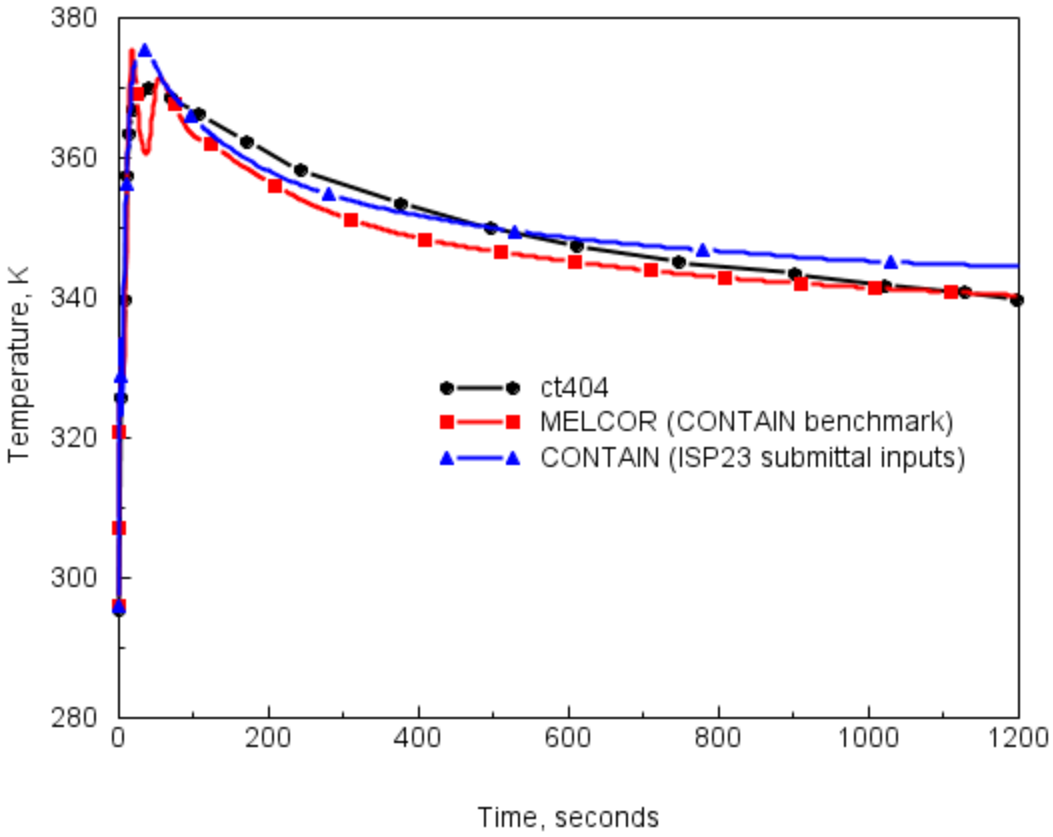

Figure 4-52 Benchmark for MELCOR/CONTAIN codes upper staircase gas temperature during the long-term T31.5 test period.

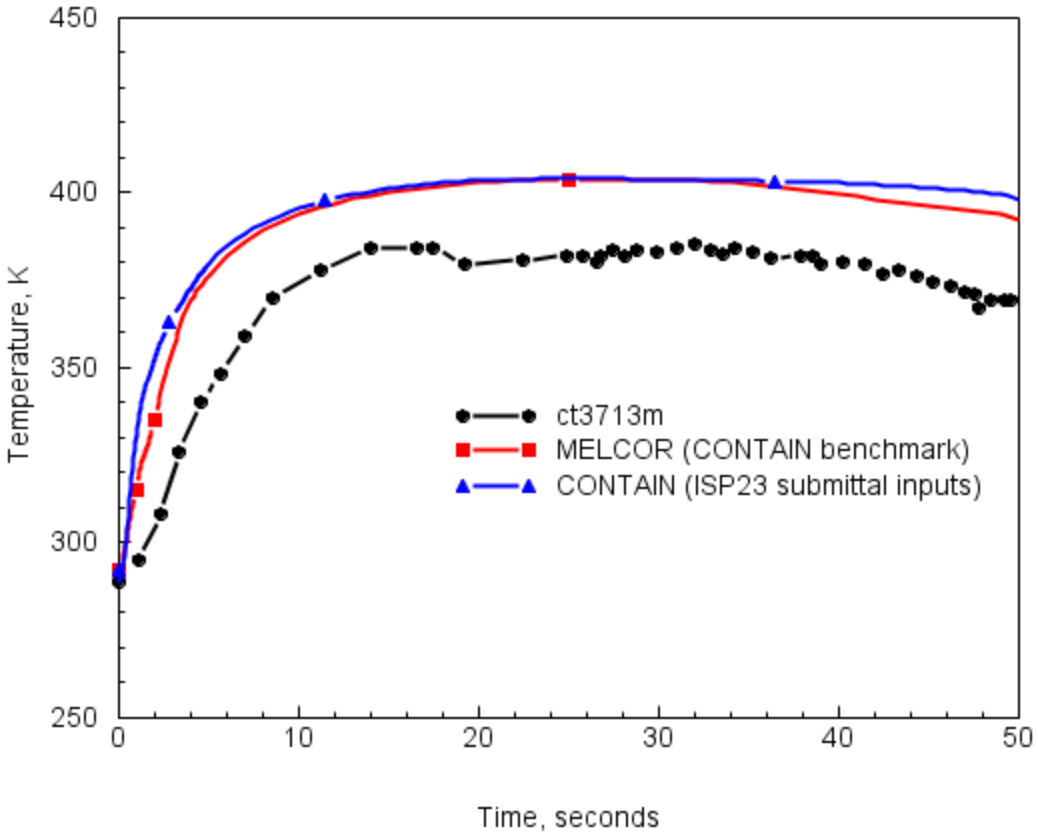

Figure 4-53 Benchmark for MELCOR/CONTAIN codes lower staircase gas temperature during the medium-term T31.5 test period.

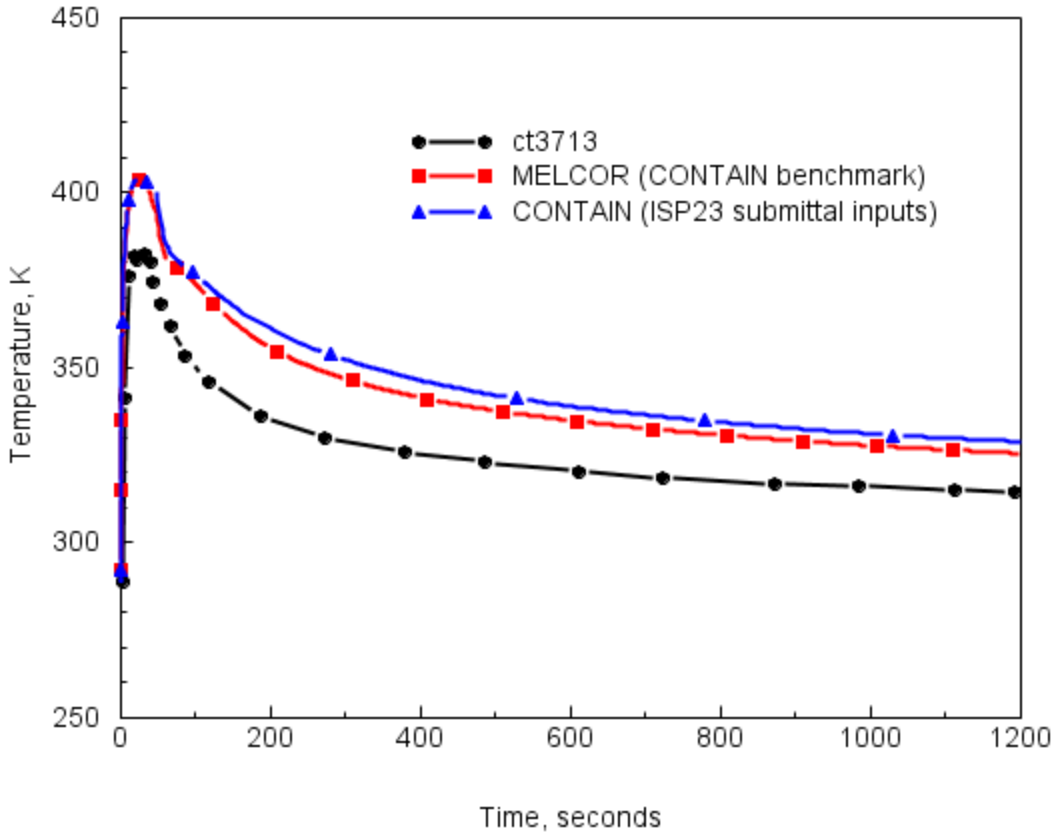

Figure 4-54 **Benchmark for MELCOR/CONTAIN codes lower staircase gas temperature during the long-term T31.5 test period.**

4.3 Test T31.5 (Project HDR Benchmark)

In a separate initiative from the T31.5 (ISP-23) effort, Project HDR sponsored a benchmark exercise for test T31.5 [Val89, Wol89a]. This exercise extended the time period for comparisons from 20 minutes to an hour after the initiation of the blowdown; included in this benchmark was the light gas (hydrogen/helium) injection period that began at about 36 minutes and lasted approximately 15 minutes. The extended test was an attempt to simulate containment conditions that may exist during a beyond DBA scenario. SNL participated in this exercise and the results of those comparisons were reported by Project HDR in Reference [Wol89b]. The exercise represented an important benchmark since it was the first hydrogen distribution test conducted in a large-scale integral test facility. In this section, the focus is on the ability of the MELCOR code to predict regional hydrogen concentrations within the containment during the extended portion of the T31.5 test.

4.3.1 Extended T31.5 Test Hydraulic and Gas Concentration Measurements

The extended T31.5 test begins with an injection of steam followed with the light gas injection at 36 minutes, Figure 4-55 and Figure 4-56, respectively. Steam and light gas injections are located at the same location as the blowdown injection, Figure 4-57. Shown in Figure 4-58 is the pressure profile measured during the T31.5 test which includes the extended period. A small pressure rise at ~ 20 minutes is the atmospheric response to the extended steam injection. Figure 4-59 shows the measured hydrogen concentrations (volume percentage) in the upper containment region above the operation floor at ~ 31 meters, and along the staircase/equipment shaft. The sensors locations plotted in Figure 4-59 are highlighted in Figure 4-60. In the upper containment region, a detailed sensor location map is shown in Figure 4-61. Sensors CG431 and CG432 are located in the equipment pathway connecting the lower containment and dome region, and those readings are influenced by circulation flows in the pathways. For elevations above 31 meters the upper containment is shown to be well-mixed for elevations from 34 to 49 meters, with all readings indicating similar concentration values. Below the injection elevation (22 meters) the hydrogen concentration measurement at 6 meters is very low, indicating a typical stratification pattern that has also been observed in a more general way for the temperatures measured in T31.5 (ISP-23). However, in the case of concentration data, the data represent a better indication of regional mixing rather than temperature measurements, since temperatures are influenced not only by mixing but by condensation/evaporation processes and compression taking place regionally. Consequently, concentration measurements are viewed as a more direct indicator of mixing processes, and that makes the T31.5 extended test period valuable for assessing containment mixing modeling as implemented in simulation codes.

4.3.2 Reference Case

Results are presented here for the global pressure response and hydrogen concentration at locations above and below the HDR operation floor. Table 4-4 provides the key between instruments and their corresponding cell in the 33CV model. Shown in Figure 4-62 is the comparison between measured and predicted pressure, extended out to one hour. As noted above, there is an over prediction in pressure during the blowdown period, mainly due to an underestimation in the heat transfer for periods of forced convection condensation occurring in the vicinity of the blowdown

region. The pressure relaxation however is predicted with very good accuracy, indicating that depressurization, which is dependent on the atmosphere interaction with both short-term (steel) and long-term (concrete) heat sinks is well modeled for a global response.

Shown in Figure 4-63 is the measured and calculated hydrogen concentration in the upper containment. There is a slight delay in the initial increase in the predicted hydrogen concentration. This delay is indicative of a lack of plume modeling in the code which would be expected to enhance the rate of light gas transfer from the break location to the upper containment. Nevertheless, after a few minutes the rate of increase is correctly calculated, and the nearly complete mixing of the upper containment space is predicted. The small under prediction of the peak concentration in the upper containment is a reflection of the tendency of the code to overmix the containment gases during the injection period as noted in the example plume modeling discussion above in Section 3.

Stratification of the hydrogen concentration measured and predicted for the reference case is shown in Figure 4-64. The slight under prediction of the upper containment concentration is attended by a similar over prediction of concentration below the injection elevation. This behavior is typical for observations with control or lumped parameter type codes.

4.3.3 Sensitivity Evaluation

Two sensitivity calculations were run to investigate 1) film thickness modeling and 2) nodalization on predicted hydrogen concentrations. In the first sensitivity, the film thickness was set to the default maximum thickness for the CONTAIN code (0.0005 meters), and therefore the case also served as a representative case for the MELCOR/CONTAIN benchmark. The nodalization case was the extreme case where the facility is modeled as a single cell.

Shown in Figure 4-65 is the pressure comparisons for the film thickness sensitivity case. Figure 4-66 shows the reference and sensitivity comparisons calculations for the upper and lower hydrogen measurements. The reference calculation was performed with dynamic film modeling and for this model the maximum film thickness was much less than the sensitivity case run with Enforcemax = 0.0005 meters. The case with the greater film thickness results in a larger water inventory for long-term evaporation from structures, and therefore has an increased long-term vapor pressure. The higher vapor pressure results in a slight increase in long-term pressure, and a reduction of light gas volume % (α mole fraction).

The single cell pressure profile is compared in Figure 4-67 with the reference case (33CV). Hydrogen concentration calculated for the single cell model is compared in Figure 4-68 with concentrations calculated using the 33CV reference model. Although, the global pressure comparisons are not significantly changed by the reduced nodalization model, hydrogen concentrations are greatly affected due to the large stratification that occurs in this test. Consequently, the complete mixing that is assumed with the single cell model, under predicts maximum hydrogen concentrations in the upper containment and over predicts concentration in the lower containment.

4.3.4 Benchmark

The MELCOR/CONTAIN T31.5 (ISP-23) benchmark was extended to include the Project HDR light gas injection period. Shown in Figure 4-69 is the comparisons for the calculated and measured containment pressure, and the hydrogen concentration comparisons are plotted in Figure 4-70.

Table 4-4 Hydrogen sensor locations and corresponding 33CV cells for the Project HDR T31.5 test. (Highlighted sensors indicate measured locations for comparisons to code predictions)

H2 Sensor	R (cm)	PHI (deg)	Z (cm)	Cell #	General Location
CG431	652	81	3100	28	Upper containment
CG432	657	278	3100	27	
CG433	640	180	3400	28	
CG434	768	358	3400	27	
CG435	241	294	4050	31	
CG436	241	66	4050	32	
CG437	141	315	4900	33	
CG438	141	45	4900	33	
CG5303	652	81	600	22	Staircase
CG6607	657	278	1200	5	Spiral stairs
CG6608	652	81	1200	23	Staircase
CG7401	810	124	1760	10	Breakroom
CG7701	652	81	1650	24	Staircase
CG8401	657	278	2300	7	Spiral stairs, etc.
CG9202	657	278	2650	19	Spiral stairs, etc.
CG9301	652	81	2650	26	Staircase

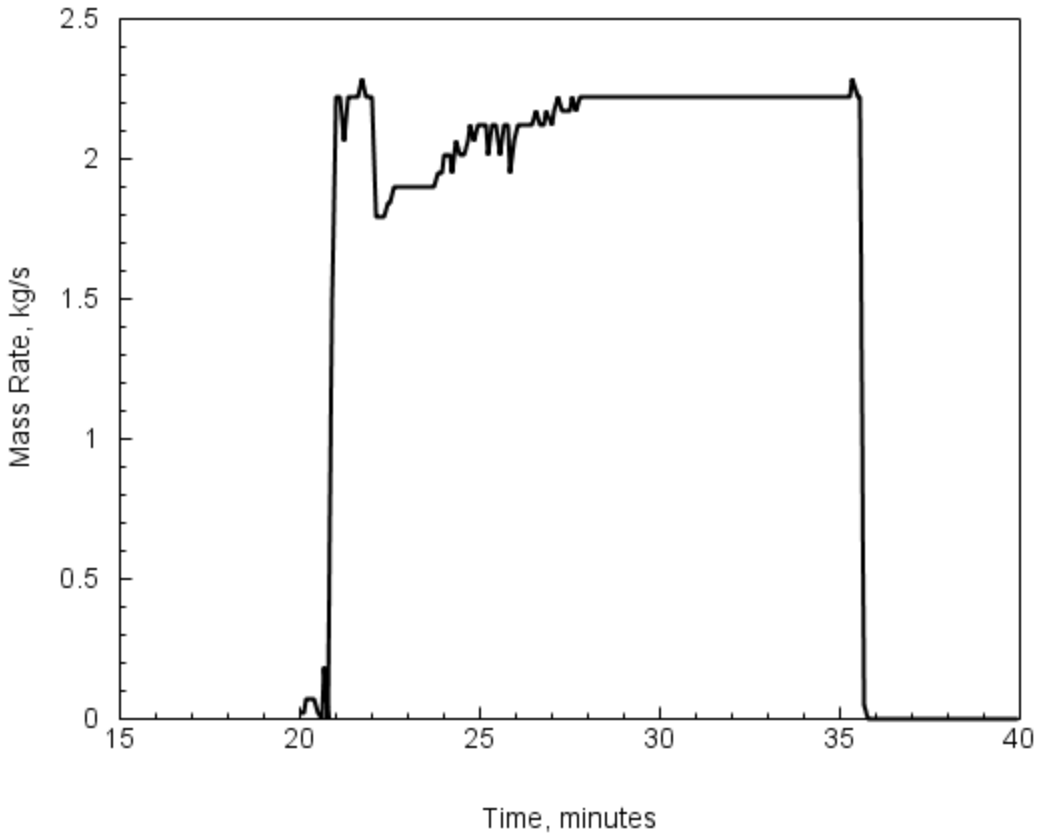

Figure 4-55 Delayed steam injection for the extended T31.5 test period.

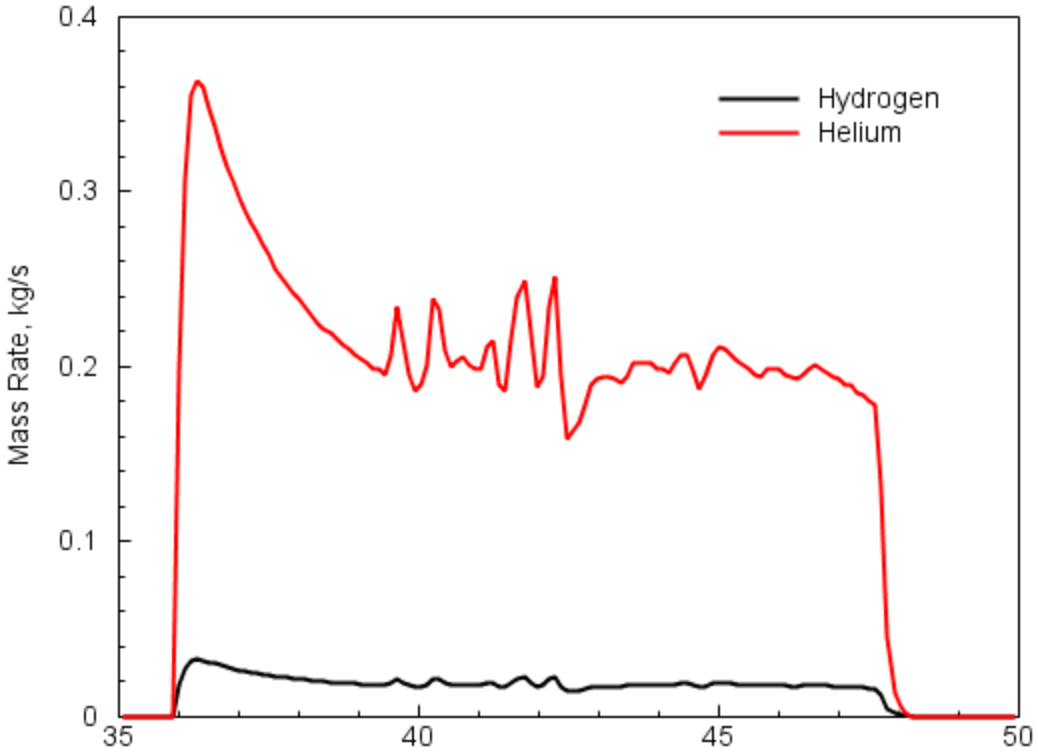

Figure 4-56 Light gas injection (H2/He 15/85 volume %) for the extended T31.5 test period.

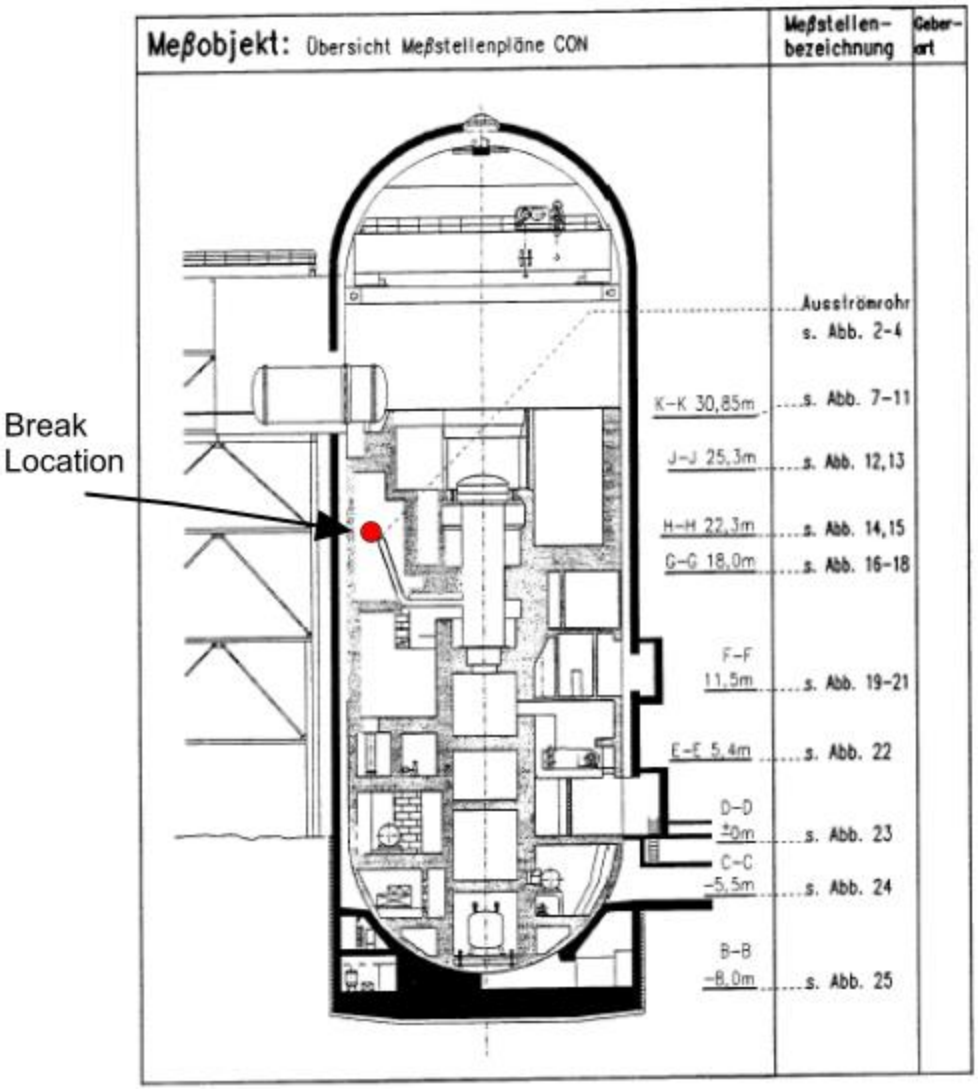

Figure 4-57 HDR facility showing the break location for the blowdown and extended steam/light gas injections [Hol91].

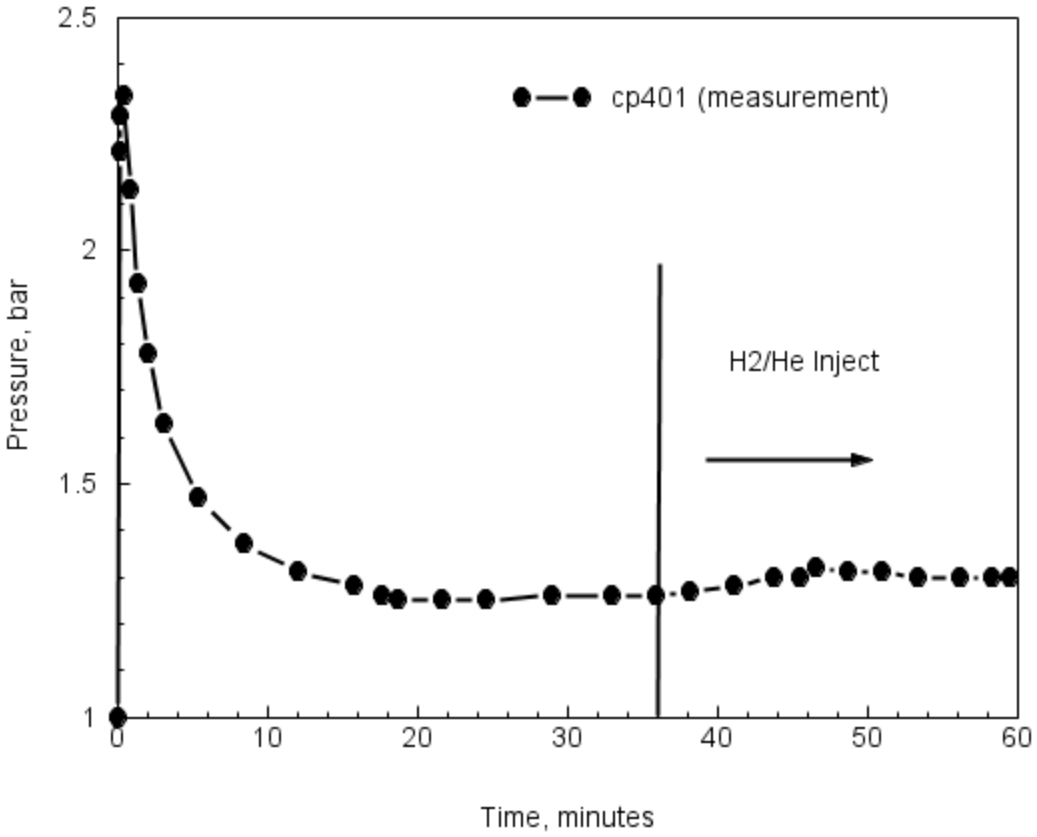

Figure 4-58 Measured containment pressure for the T31.5 test with the extended period (20 to 60 minutes).

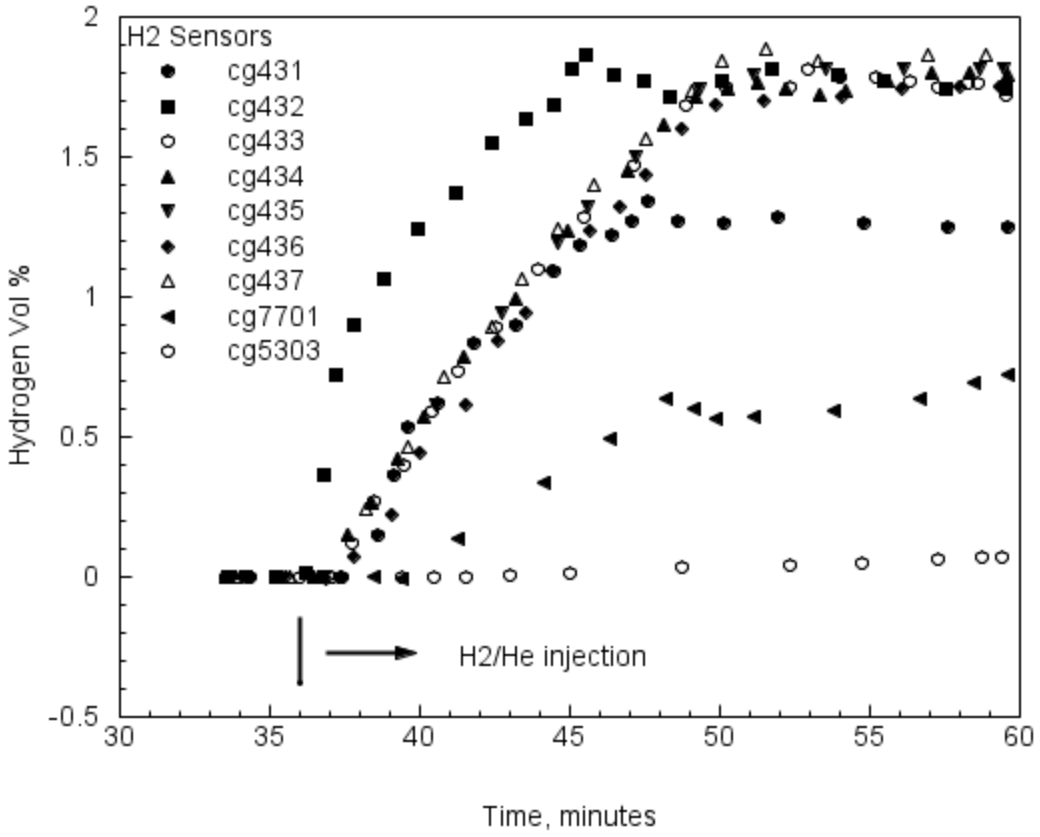

Figure 4-59 T31.5 hydrogen concentration measurements for the upper and lower containment regions during the extended test period.

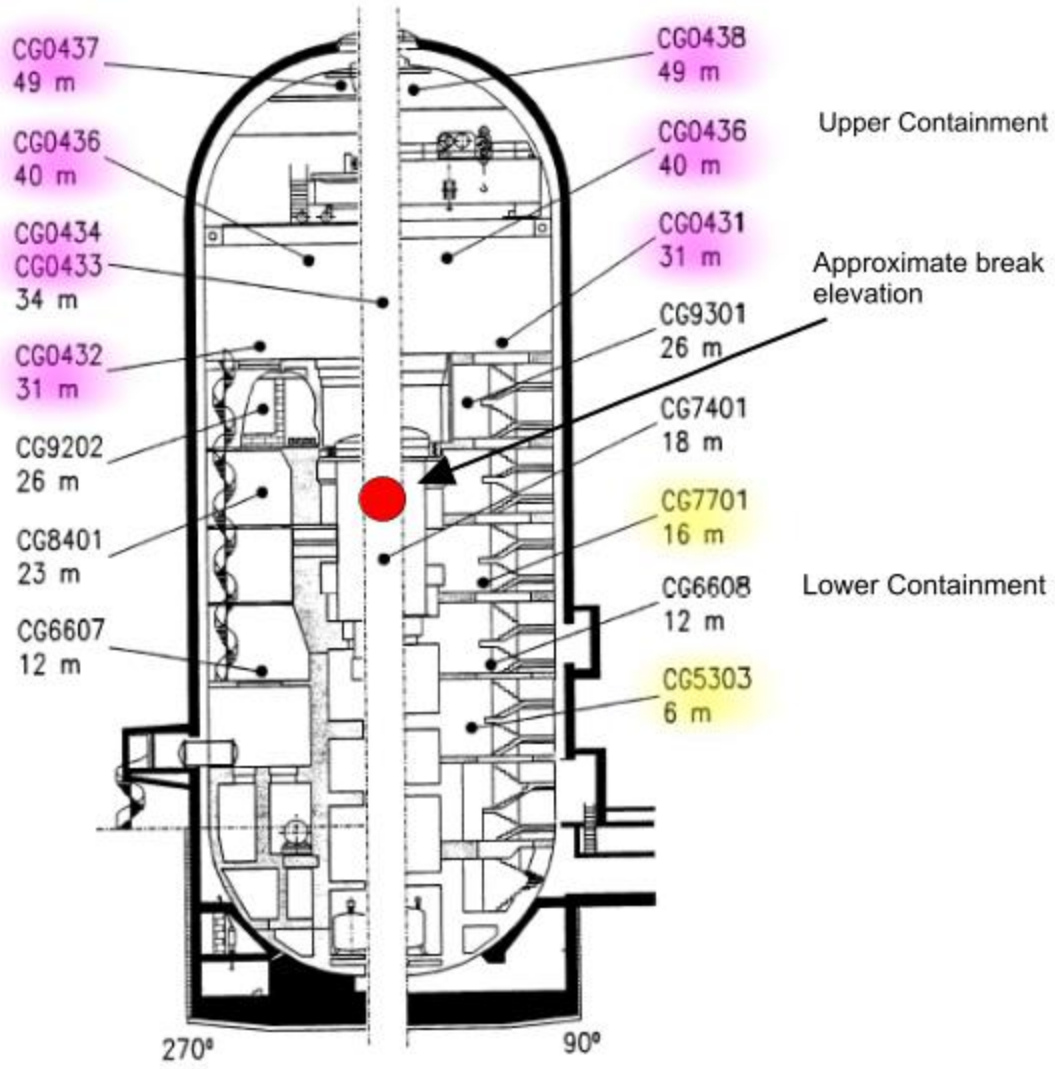

Figure 4-60 Sensors locations for plotting upper and lower containment regions [Hol91].

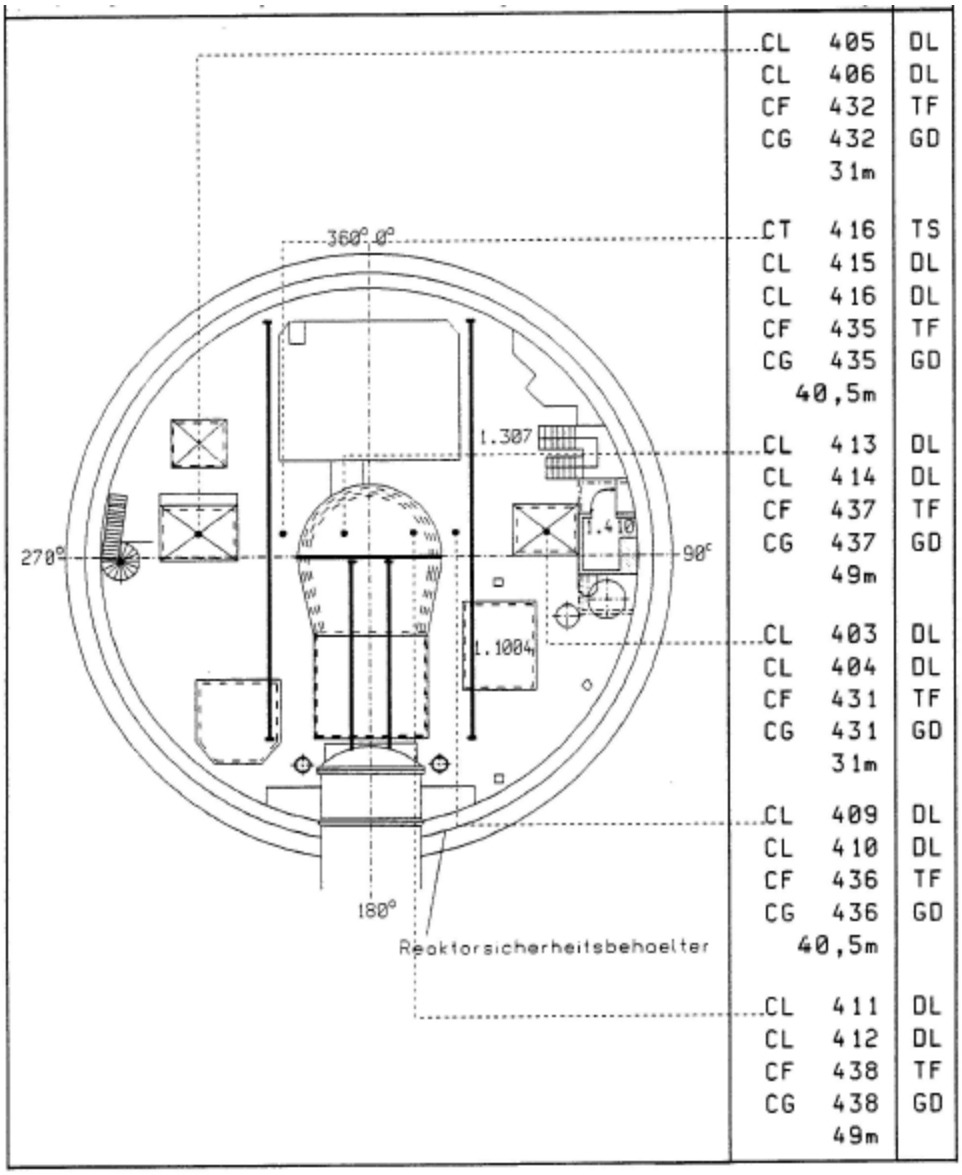

Figure 4-61 Hydrogen sensor map for the HDR upper containment region [Hol91].

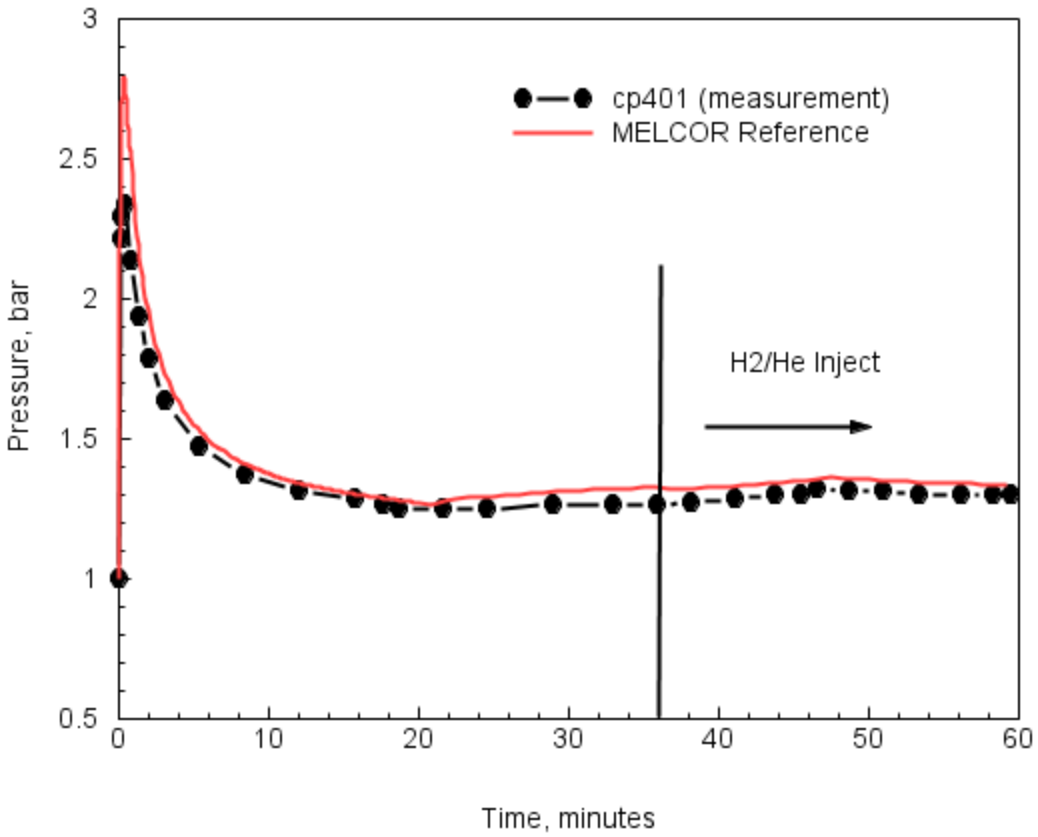

Figure 4-62 **Comparison of measured and MELCOR calculated containment pressure for the T31.5 test during the extended test period (H2/He gas injection).**

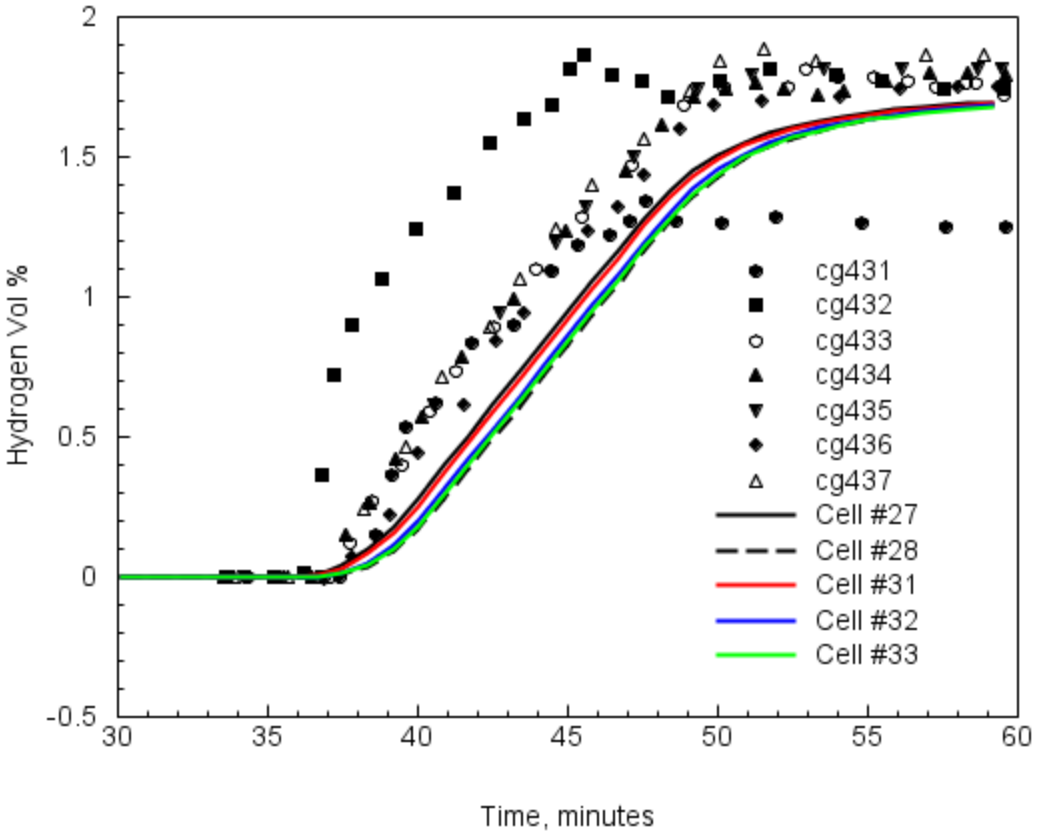

Figure 4-63 Comparison of measured and MELCOR calculated hydrogen concentrations in the upper containment region of the HDR facility during the T31.5 extended test period.

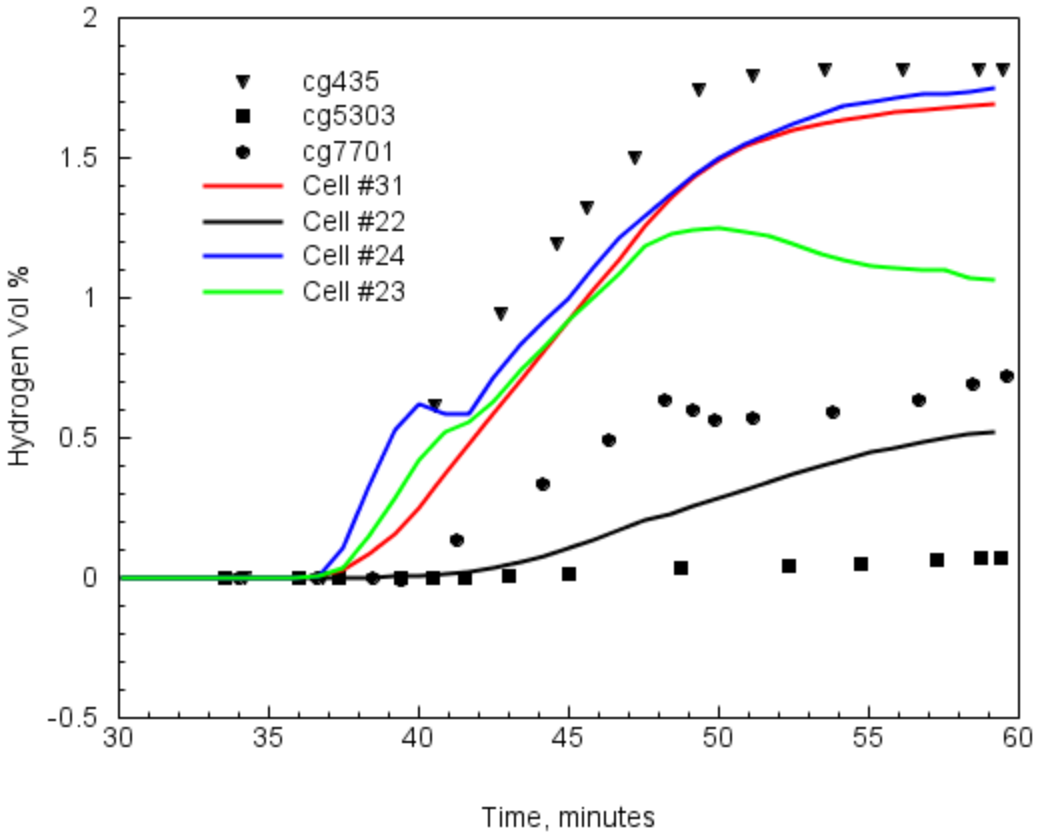

Figure 4-64 **Comparison of measured and MELCOR calculated hydrogen concentrations in the upper and lower containment regions for the T31.5 extended test period. (cg5303 – cell #22, cg7701 – cell # 23, and cell #24 in the breakroom level, cg435 – cell #31)**

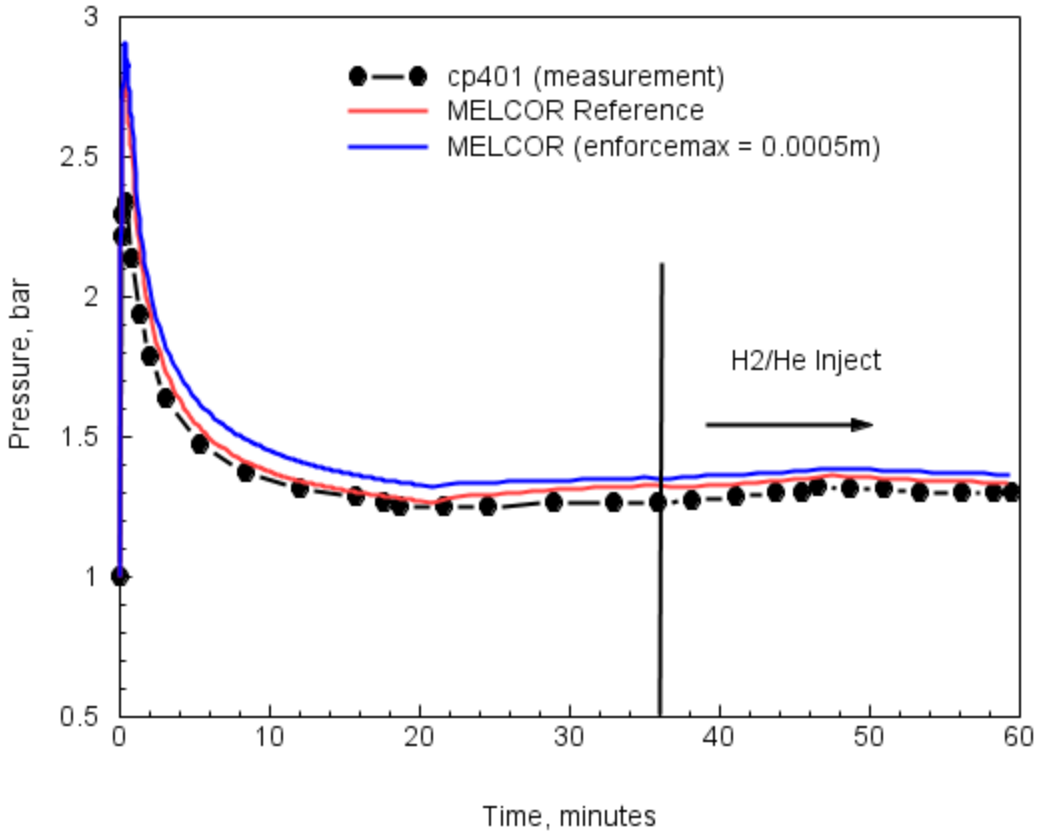

Figure 4-65 **Comparison of MELCOR reference and film thickness sensitivity case (0.0005 m) for containment pressure during the extended T31.5 test period.**

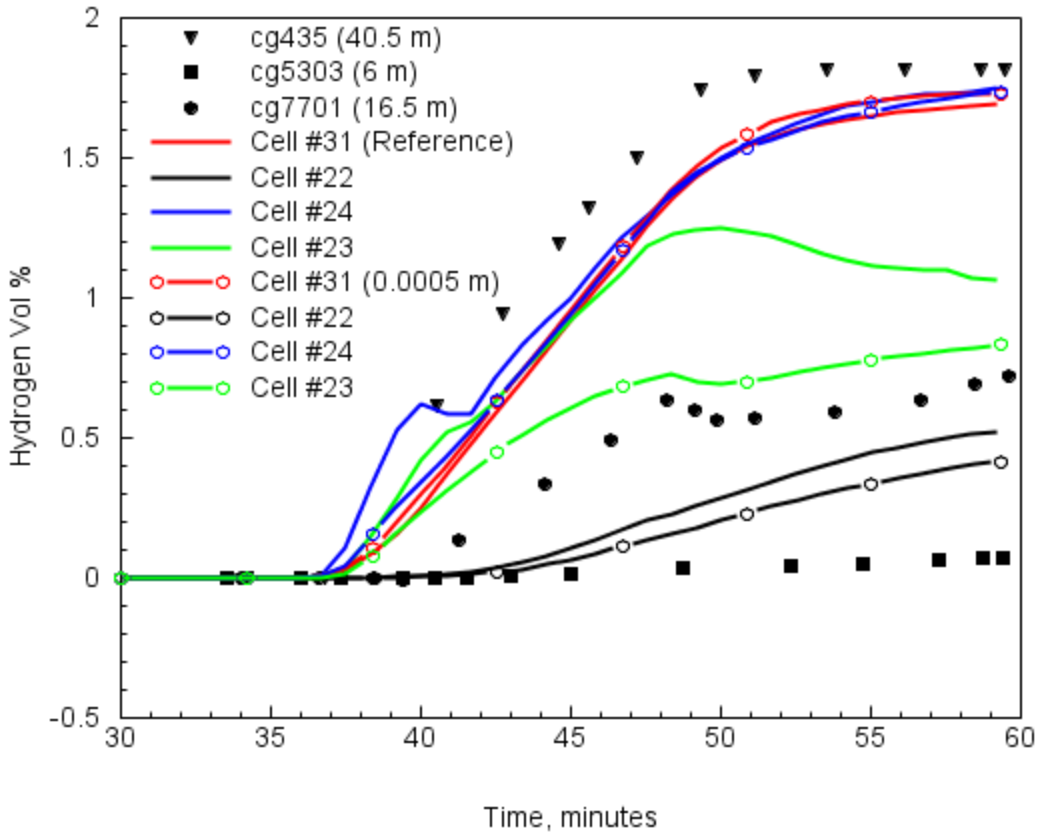

Figure 4-66 **Comparison of the MELCOR reference and film thickness sensitivity case (0.0005 m) for hydrogen concentration during the T31.5 extended test period.**

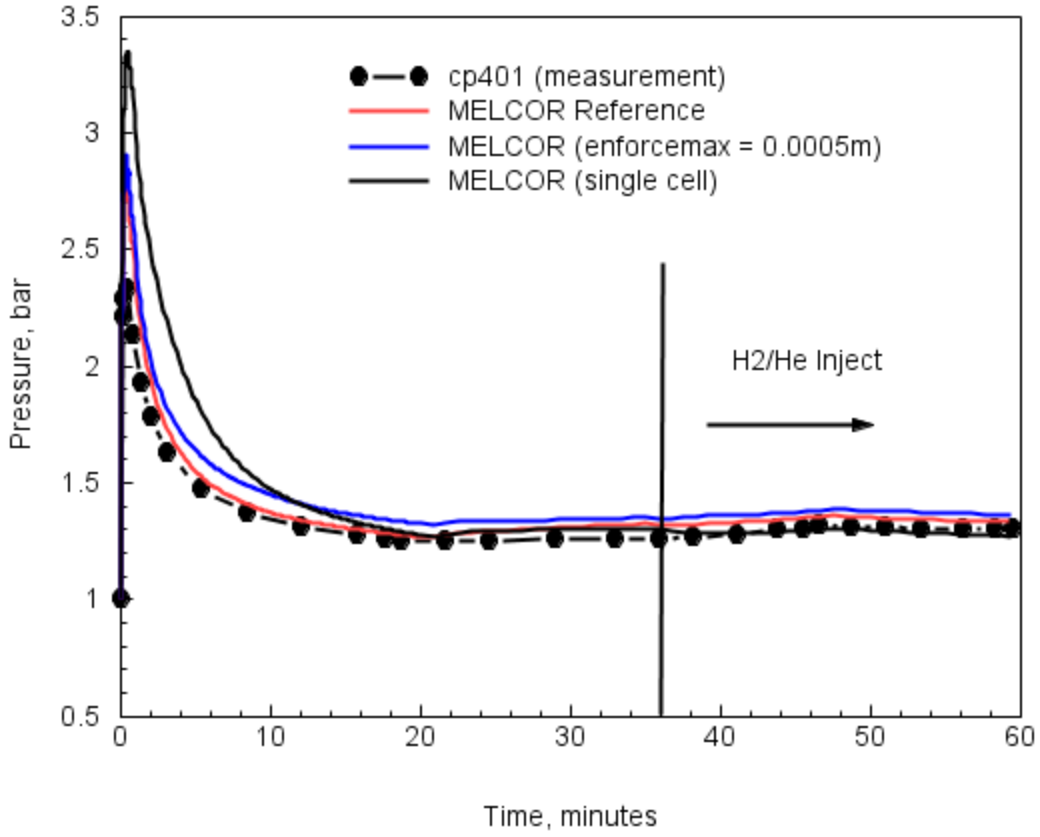

Figure 4-67 **Comparison of MELCOR calculated containment pressure for all sensitivity cases during the T31.5 extended test period (H2/He injection).**

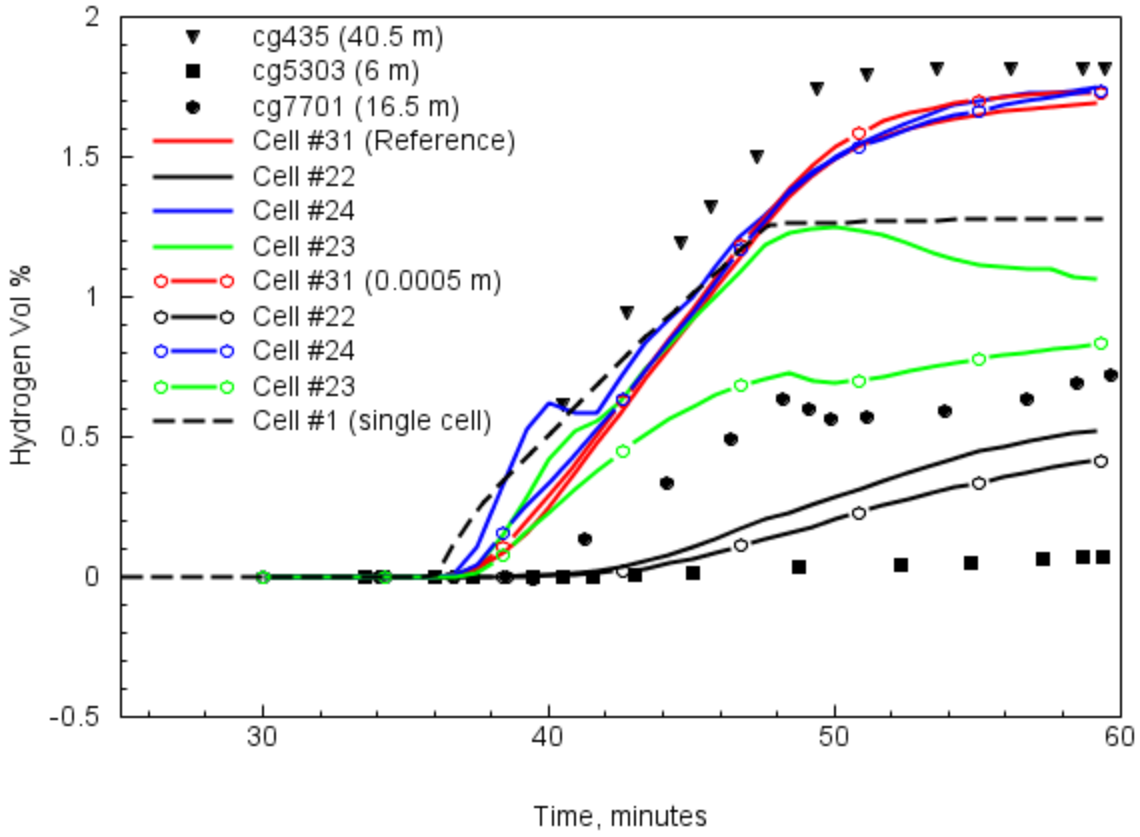

Figure 4-68 **Comparison of MELCOR calculated upper and lower containment hydrogen concentrations for all sensitivity cases during the T31.5 extended test period (H2/He injection).**

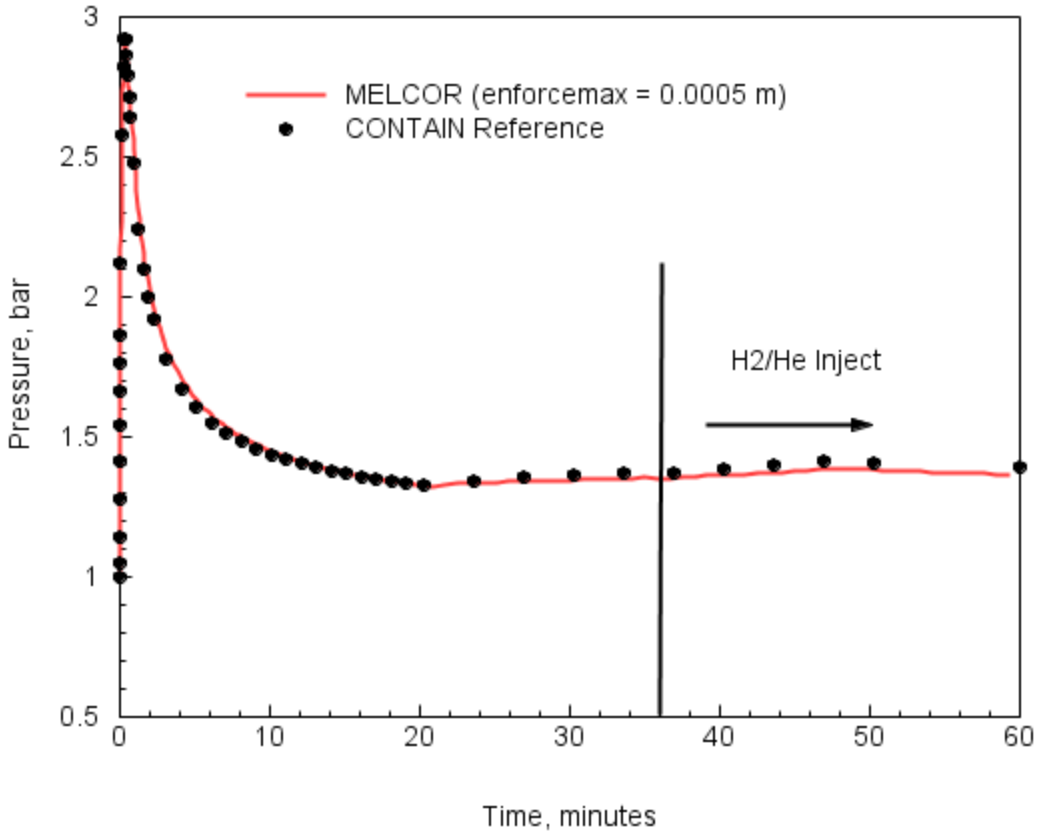

Figure 4-69 MELCOR/CONTAIN benchmark for pressure calculations during the T31.5 extended test period (H2/He injection).

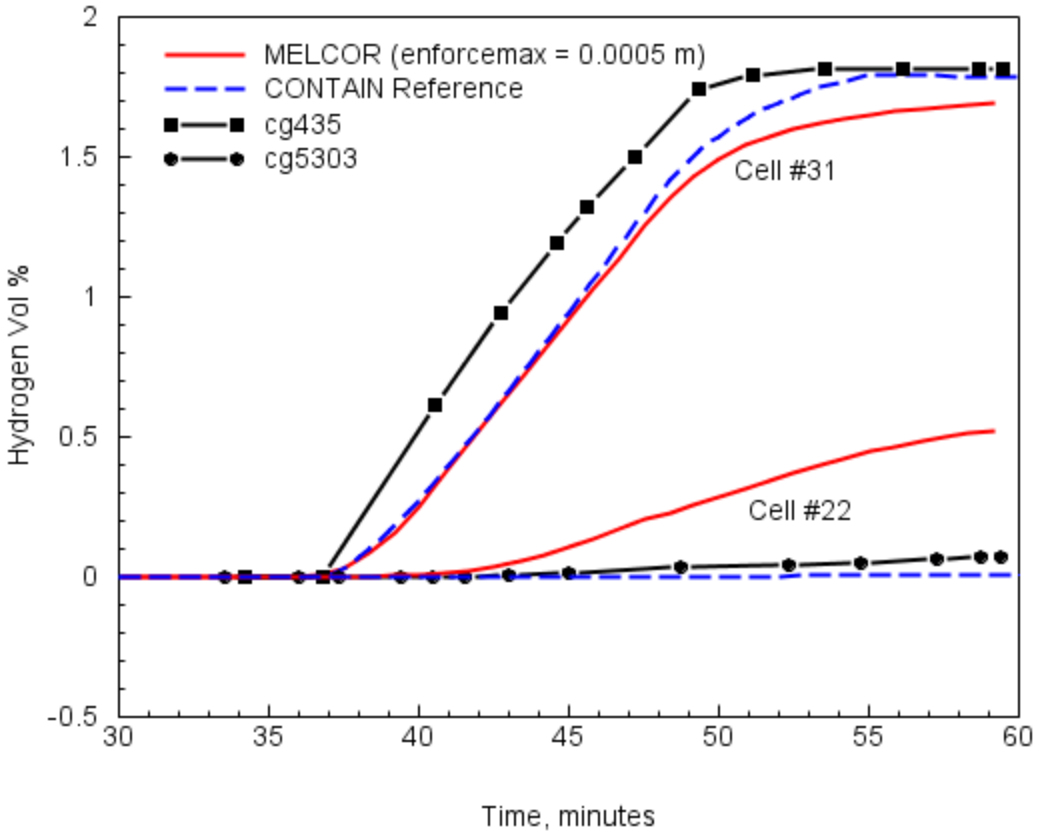

Figure 4-70 **MELCOR/CONTAIN benchmark calculations for the upper and lower containment hydrogen concentrations during the T31.5 extended test period. The CONTAIN code input uses the default hybrid flow solver option that improves on the calculation of weak flows resulting in substantial stratification in the containment.**

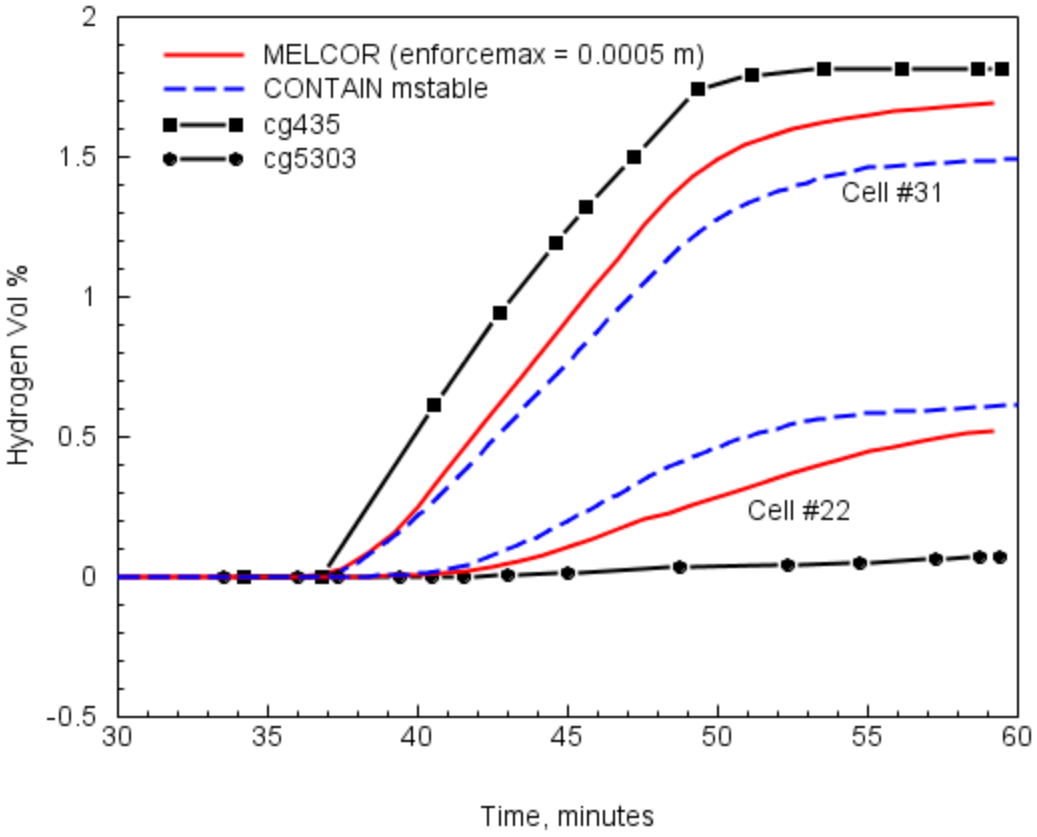

Figure 4-71 **MELCOR/CONTAIN benchmark for upper and lower containment hydrogen concentrations during the T31.5 extended test period (with the CONTAIN mstable flow model that represents a more well-mixed modeling option – and the original flow model used in the CONTAIN 1.0 code).**

4.4 Test E11.2 [ISP-29]

The HDR Test E11.2 is a gas distribution test conducted in the HDR facility, Figure 4-72, to investigate the spatial movement of an injected light gas mixture under simulated severe accident conditions. The experiment is a long-term test requiring approximately 21 hours to complete. A chronology of the operational events during the experiment is given in Table 4-5, and a sketch of the test procedure is shown in Figure 4-73.

A summary of the test energy input (events), energy output (extraneous losses), and monitoring is given below. The information on the test is obtained from various sources. In fact, there is no single document that can be referenced to give a complete and accurate presentation of the test. Early documents describing the test were followed by numerous addendums from PHDR and Technische Universitat Munchen (ISP-29 coordinator) as more information was offered to participants in the code exercises. Addendums included corrections made to previous specified input conditions. Some of the more important reports and letters regarding the experiment are:

- the general description of events, facility and monitoring sensors (References Val89a and Val89b)
- facility leak rate, gap venting (Reference Kar91a)
- corrected external steam rates and cooling system energy flux (Reference Kar91b)
- energy and mass balance errors for E11 series (Reference Wen91)

Taken together these references define the E11.2 test. The test may be divided into five operation or event periods.

E11.2 Operation Event Summary

Period 1. During the heat-up period an external supply of superheated steam (pressure = 9.25 bars and temperature = 224.4 C) is injected into the Room 1805 (1800 level) at a constant rate of 2.1 kg/s for 693 minutes. In the heat-up period, the external steam source is accompanied by a small break blowdown of the HDR facility RPV. The RPV blowdown is characterized by a time dependent mass rate that initially begins at ~ 1.6 kg/s and then decreases to about 0.2 kg/s at the end of the heat-up period. The enthalpy of the blowdown steam ranges from about 2700 to 2800 kJ/kg. The nominal enthalpy of the steam entering the containment from the external steam source is 2888 kJ/kg. Both injection jets are directed horizontally at the outer wall in Room 1805, resulting in a dispersed steam source exiting the room.

Period 2. At the end of the heat-up phase, the external steam injection rate in Room 1805 is reduced to 1.2 kg/s, and terminated after about an hour at the lower rate. Approximately 10 minutes before the external steam is shut off, a gas mixture of 15% by volume of hydrogen and 85% helium is injected into Room 1805 (also directed at the wall). The gas mixture enters at a rate of about 0.1 kg/s and at a temperature of 400 K. The gas injection lasts approximately 30 minutes. During the

last 20 minutes of the injection only the gas mixture is injected into the containment. This period, from the end of the heat-up to the end of the gas injection is referred to as the gas injection period.

Period 3. Within less than a minute from the time that the gas source is terminated, a second steam injection in the bottom of the containment, Room 1405 (1400 level) is started. The source of this steam is the same external supply line as the heat-up external steam source, and the mass rate and enthalpy are the same as in the heat-up period. The lower steam injection last about 3 hours.

Period 4. In about 15 minutes after the termination of the lower steam source, the upper dome shell (above the spring-line) is cooled by external sprays. The outer dome spray period lasts nearly 4 hours. The initial spray rate is 5.83 kg/s, and is incremented (see Table 4-5) three times until a final rate of 10.69 kg/s is reached. The temperature of the spray water is about 10 C.

Period 5. At the end of the spray period, a cooldown period begins and lasts for 4 hours. Later the containment is vented, but that portion of the test is not considered in this report.

4.4.1 Reference Case

The SNL submittal for test E11.2 (ISP-29) was sent in January 1992, and is documented in the ISP-29 report [Kar92] and in a SNL letter report to the USNRC [Til92]. During the early 90's, the E11.2 test was used to assess the hybrid flow solver modeling in the CONTAIN 2.0 code [Mur96]. Reference Mur96 may be consulted for details pertaining to the modification of an early nodalization of HDR facility that resulted in a 15-cell input deck. The nodalization of the E11.2 test is derived from the CONTAIN geometry inputs from Mur96, with some required adjustments to translate into MELCOR control volume definition and format, discussed later. The 15-cell nodalization is shown in Figure 4-74. Some additional details concerning cell volumes, elevation, and compartment makeup of the cells are given in Table 4-6. Figure 4-75 shows how the upper containment region (above ~31 meters) is divided into three cells (7, 8, and 9). A sketch of the HDR facility with the 15 cell nodalization overlay is shown in Figure 4-76.

In the reference calculation, suspended liquid water is modeled using aerosol physics (RN), condensate film flow is treated using the dynamic film model (default), and the thermal properties for steel and concrete correspond to property values listed for the CONTAIN code. In the sensitivity subsection below, various cases demonstrate sensitivity to nodalization, condensate film modeling, and thermal properties.

Similar to the T31.5 deck, slight modifications were incorporated to meet the RN package requirements. One-centimeter-thick concrete floors were added to the 12^{th} and 13^{th} control volumes to give a settling heat structure; although the 12^{th} and 13^{th} control volumes are found in the annulus space, there is no observable sensitivity to this inclusion. Flow-through areas were implemented as well from control volumes 10 to 11 and 11 to 12, as well as the dome region, 9, to control volumes 8 and 7. Control volume 8 and 11 were modified by increasing the height of each by 5mm to meet flow-through area altitude requirements.

Attempts were made to reconcile some compatibility issues between MELCOR and CONTAIN due to CONTAIN specific functionality implemented for the E11.2 analyses, namely the

engineered overflow, cell overflow, and heat structures conductively connected through bcouter/icell/strnum. The CONTAIN modeling for sump overflow has no physical basis as water is simply moved from one control volume to another when an elevation criterion is met. While trying to reproduce this transport method with MELCOR, instabilities were observed for the pool-only flowpaths and it was abandoned. Instead, pooled water is permitted to remain stationary in all control volumes for the MELCOR analysis. Cell overflow, another CONTAIN function implemented in the E series analysis, transported gravitational settling water and film drainage directly to sumps. Overflow film drainage was implemented in the MELCOR analysis using film flow networks to force all film drainage into one of the three sump pool control volumes, 1, 3, and 7, but gravitational settling directly to one of the three sumps was not implemented and instead contributes to pooled water in the respective control volume. CONTAIN, unlike MELCOR, allows heat structures to be logically connected even though the structure may not share exact elevations. The stainless steel containment shell was modeled in this fashion to capture annulus heat removal. This resulted in modifying the stainless steel heat structure elevations and/or axial lengths to meet MELCOR altitude criteria to allow conductive connections. Some of the parent control volume containing the lower stainless steel structures, particularly those in the 13th control volume, had altitudes that did not overlap and thus their heat structures were irreconcilable and left independent.

The ISP-29 test applied containment shell cooling in the annulus region (control volumes 10-13). The original CONTAIN deck did not incorporate a node network and rather applied the spray water only to cell 10. This was emulated in MELCOR by defining a 2-node film flow network to direct the film from the spray source on the outer dome in cell 10 to a dummy heat structure in the environment control volume. Due to film tracking node constraints in MELCOR, the inner dome film flow is being allowed to pool in the 9th control volume rather than being removed to the 7th control volume sump.

With respect to the experimental procedure, two incidents distracted from the ISP-29 participation and modeling effort: 1) an experimental mass rate error for the pre-heat external steam source negated the blind submittal for the ISP, and 2) an initial omission of the sensor line cooling within the facility later noted by Project HDR introduced a degree of uncertainty in the test specification. Recalibration of the steam injection nozzle later corrected the steam injection rate, and an approximation of the distribution of energy extraction from cooling lines addressed the issue of uninsulated cooling lines. The method of treating the sensor cooling lines was to weight local energy removal by the relative number of sensors in rooms and the local partial pressure of vapor calculated during the test. Figure 4-77 depicts the energy removal rate from the entire facility and Table 4-6 lists the percentage of samplers present in each control volume as the cooling fraction. Equation **4-1** was applied to capture the fraction of the heat removal for a control volume. The fraction of the heat removal rate f_n was determined by weighting the steam partial pressure $P_{v,n}$ and cooling fraction cf_n for cell n.

$$f_n = \frac{P_{v,n} cf_n}{\sum_i^n P_{v,i} cf_i} \qquad \text{Equation 4-1}$$

A comparison of the calculated and measured containment pressures is shown in Figure 4-78. The over prediction of the pressure at late time is evident. It should be mentioned that analysts using other lumped parameter and field codes have also observed an over prediction in pressure of a similar amount and this has led to a number of suggested reasons for this disagreement (uncertainty in heat sinks, steam injection rates, coolant line energy extraction, and thermal properties). In the subsection on sensitivities, one of these possible causes is investigated, thermal properties of concrete.

Figure 4-79 shows the comparisons between all calculated and measured local temperatures. Table 4-7 shows the correspondence between temperature measurement location and calculation cells. To better follow the comparisons, the HDR facility nodalization overlay is shown in Figure 4-80 with the approximate loop circulation profiles. One region that is problematical is the region that spans levels 1600 and 1500. This region is where the bottom of the loop circulation sets up due to the injection source in cell #6. Sensors in this area may be just above or below a major cross-flow region and therefore can have a varied response between closely spaced sensors (e.g., ct1101 at 6m and ct6603 at 12m). The coarse nodalization in this region (cells #2 and #3) may not be able to resolve local variations in cross-flow. The following figures (Figure 4-81 to Figure 4-83) group the sensor location with corresponding cells by regions within the facility to better focus the comparisons. Figure 4-81 shows the upper containment and source region, indicating good agreement for the upper containment dome (40 to 50 meters) and fair agreement for the source region that probably suffers from the complicated jet dispersion and plume formation for this region.

As indicated in Figure 4-81, the above-deck temperatures are predicted within approximately 5 degrees. Below deck, the trends are predicted but the absolute comparisons show variations that have not been captured so well by the present nodalization, especially in the lower cross-flow region (e.g., cell #3). A clear variation between calculated and measured values occur in the lower containment where cell #3 shows a significant rise during heat-up (period 1), but the measure temperature is nearly flat. A corresponding Figure 4-84 shows that the calculated temperatures are saturated in the lower containment; therefore, superheating due to compression does not explain the over-prediction. Unlike the large pipe rupture in test T31.5, the E11.2 steam sources simulate small LOCA breaks, where compression heating is minimum. This conclusion is also consistent with the good temperature agreement observed for cell #2 and sensor ct1101 at 6 meters, located just below cell #2. Over-prediction is more likely the result of coarse nodalization in a transition region of cross-flow between the equipment shafts at ~ 270 and 80 degrees where MELCOR is calculating that a strong cross-flow occurs lower in the containment than measured.

One of the more important aspects of the E11.2 test concerns the stability conditions predicted by the code and how these conditions affect gas transport and mixing. Shown in Figure 4-85 are comparisons of measured and calculated light gas (hydrogen and helium) concentrations in the upper and lower containment. The significant stratification of the light gas mixture during injection is predicted, however trends observed for the light gas concentration in the upper containment (elevation >40 meters) during the external spray period is not predicted well. Specifically, the light gas concentration peaking at ~ 24% at about 800 minutes is underpredicted by MELCOR by about 14 percentages points (~ 60% under-prediction). Unlike the measured light gas concentration during the spray period, the MELCOR code predicts a well-mixed upper

containment region throughout the spray period. The inversion of the upper containment concentration, as this region is cooled by the sprays later in the test (> 800 minutes), is not captured by the code. More detailed analysis of the mixing phenomenon occurring during the E11.2 test can be found in References Til02a and Til92.

4.4.2 Sensitivity Evaluation

Sensitivity calculations performed with the MELCOR code investigate pressure, temperature, and light gas concentration variation to 1) thermal property specifications, 2) film thickness models, 3) nodalization, and 4) sensor coolant line exclusion. Table 4-8 through Table 4-10 define the property, film, and nodalization cases, with the last case (Case 5) addressing the cooling line exclusion calculation.

The HDR facility was used for many steam injection tests, some of short duration (sec) tests simulating large pipe ruptures and others of long duration (hours) simulating phenomena occurring in severe accident events. The cumulating effect of these tests on concrete wall paint and condition of the concrete surface layers was in some areas severe, such that the original specification of concrete properties is suspected of being under predicted for conductivity, heat capacity and density. Migration of water into the concrete surface layers is the concern for long-term exposure. When water enters the pores of concrete, these initial assumed thermal properties are expected to increase with corresponding increases in the thermal transport efficiency of the structures. Cases 1 and 2 (Table 4-8) investigate concrete thermal property variation on the code's prediction of the containment pressure response, Figure 4-86. Figure 4-87 shows that the upper containment light gas concentration prediction is essentially unaffected by the concrete thermal property variations as defined in Table 4-8.

During the large pipe rupture tests (V44 and T31.5), the modeling for film condensate thickness was shown to have an effect on peak pressure predictions, with a more conservative maximum film thickness of 0.0005 meters (CONTAIN default) chosen for the more conservative pressure prediction. Figure 4-88 shows the HDR E11.2 test pressure response for the reference case (MELCOR default film model – dynamic film flow) and the EnforceMax = 0.0005 case, Table 4-9. For the severe accident simulation test (E11.2), the more important heat sinks are the concrete structures. These structures interact with an atmosphere that has relatively low steam and high air concentrations. Consequently, the film condensate thermal resistance is a small fraction of the diffusive resistance due to the steam/air boundary layer. As a result, the long-term severe accident simulation is only weakly affected by film thickness modeling. Figure 4-89 and Figure 4-90 show the calculation sensitivity for lower containment temperature and upper containment light gas concentration prediction, respectively. For these two responses, the calculation shows essentially no sensitivity to the film thickness model variation as specified in Table 4-9.

The cross-flow modeling in the lower containment during the heat-up portion of the E11.2 test was discussed above as an issue that may benefit from a more detailed nodalization of the containment. A 48CV geometry model, Table 4-11, replaces the 15CV nodalization used in the reference case and is modeled here as sensitivity Case 4, Table 4-10. Table 4-12 gives the modifications that where necessary to translate the CONTAIN 48CV model to the MELCOR input. Figure 4-91 shows that both the 48CV and 15CV models predict global pressure response with similar result,

slightly higher than measured. The increased definition of the lower containment with the 48CV model however does improve the lower temperature calculation compared to measurements, Figure 4-92. The calculation of the light gas concentration in the upper containment however is not improved with the 48CV model, Figure 4-93.

The neglect to adequately specify the instrument line cooling for the E-series of tests severely compromised the thermal hydraulic validation exercise for ISP participants. The importance of cooling line energy extraction is highlighted for Case 5 where cooling extraction is eliminated from the E11.2 test calculation, Figure 4-94. Because cooling line energy extraction was poorly characterized for the test, modeling global energy (pressure) accurately was difficult and therefore conclusions regarding pressure predictions must be cautioned. Having recognized this limitation regarding global response, the cooling line sensitivity case does indicate that cooling line energy extraction has little impact on light gas distribution calculations which is a major feature of the E-series tests, Figure 4-95.

Table 4-5 Chronology of Operational Events for the E11.2 test

Period	Time, minutes	Description
1 (heat-up)	0.0 693.82 (41629 s)	Start small LOCA and external steam (upper) End LOCA and reduce external steam
2 (gas injection)	739.4 (44364) 749.98 (44999) 772.3 (46338)	Start of gas mixture injection End of external steam injection (upper) End of gas injection
3 (lower steam)	772.93 (46376) 958.77 (57526)	Start of external steam release in R1405 End of external steam release
4 (outer spray)	975.0 (58500) 1095.0 (65700) 1155.0 (69300) 1185.0 (71100) 1203.0 (72180)	Start of outer spray period, mass flow rate = 5.83 kg/s Increase mass flow rate, 7.36 kg/s Increase mass flow rate, 9.17 kg/s Increase mass flow rate, 10.69 kg/s End of spray period and start of natural cooldown
5 (cooldown)	1445.0 (86700)	End of natural cooldown period

Table 4-6 HDR Facility 15-cell Nodalization for E11.2 [Til02a]

Cell #	Volume, m^3	Bottom Elevation, m	Cooling Fraction	Rooms
1	836	-16.376	0.1	1201, 1202, 1203, 1301, 1302, 1304, 1305, 1307, 1308, 1311
2	2113	1.8595	0.24	1405, 1406, 1407, 1403, 1409, 1401, 1410, 1408, 1404, 1317, 1327, 1501, 1506, 1507, 1512, 1513, 1502, 1520, 1503, 1504, 1505, 1508, 1511, 1514
3	1005	7.653	0.16	1603, 1611, 1602, 1609, 1606, 1604, 1607, 1608, 1605, 1337
4	574	21.8066	0.14	17010, 1902, 1804, 1803, 1904, 1905
5	202	15	0.02	1707, 1347
6	279	22.043	0.08	1805, 1903, 1357, 1367
7	2146.766	23.399	0.0835	33332, 33333, 1801
8	901.883	30.845	0.0351	33331
9	2094.35	40.5	0.0814	33334
10	588.16	40.5	0	2011
11	367.166	30.845	0	2012, 2022, 2032
12	654.3	13.995	0	2013, 2023, 2033
13	1033.58	0.8575	0	2014, 2015, 2016, 2024, 2025, 2026, 2034, 2035, 2036, 2017, 2027, 2037
14	1083	16.27	0.06	17011, 1704, 1708, 1703, 1706, 1702
15	Environment	-	-	-

Table 4-7 Temperature sensor locations plotted in the temperature comparison plots.

Sensor	Z, meter	PHI, degrees	Room	Cell# (15-cell deck)
ct430	48	315	Dome (above spring-line	9
ct9302	26.5	80	1903 (staircase)	6
ct7701	16.5	80	1700 level (staircase)	5
ct6603	12	80	1600 level (staircase)	3
ct1101	6	280	1511	2

Table 4-8 E11.2 test sensitivity cases for concrete thermal properties.

Case	Density, kg/m^3	Specific Heat, J/kg-K	Thermal Conductivity, W/m-K
1	HDR specification:		
	2225	879	2.1
Reference	CONTAIN properties:		
	300 K 2400. 400 K 2400.	1000. 1000.	2.4 2.33
2	Concrete properties 15-20% increase (above HDR specification)		
	2559 (15% +)	1067 (20%+)	2.5 (19% +)

Table 4-9 E11.2 test sensitivity cases for film condensate modeling.

Case	Film Condensate Model
Reference	Dynamic film drainage (MELCOR Reference)
3	EnforceMax = 0.0005 meters (CONTAIN Default)

Table 4-10 E11.2 test sensitivity cases for nodalization scheme.

Case	Nodalization
Reference	15CV (MELCOR Reference)
4	48CV

Table 4-11 HDR Facility 48-cell Nodalization for E11.2 [Til02a]

Cell #	Volume, m^3	Bottom Elevation, m	Rooms
1	217	-6.07	1201,1202,1203,1303
2	619	-1.6	1301,1302,1304,1305,1307,1308,1311
3	445	-1.46	1405,1406,1407
4	113	-1.1	1403,1409
5	359	-0.54	1401,1410,1317
6	59	-1.6	1408
7	116	-1.1	1404
8	166	5.4	1501,1506,1507,1512,1513
9	499	4.7	1502,1520,1503,1504,1505
10	295	5.3	1508,1511,1514
11	280	11.9	1603
12	192	10.	1611
13	61	10.	1602
14	59	10.	1609
15	183	10.	1606
16	112	10.	1604,1607,1608
17	78	7.4	1605
18	44	13.85	17011
19	64	20.6	17011O
20	793	14.3	1704
21	90	15.	1708
22	119	15.	1707
23	102	15.	1703,1706
24	54	15.	1702
25	164	25,1	1803,1904,1905
26	343	21.	1801
27	279	23.2	1805,1903,1357,1367
28	125	20.6	1802
29	169	23.1	1804,1902
30	61	5.4	1327
31	40	10.	1337
32	83	15.	1347
33	558.16	40.5	2011
34	124.903	30.845	2012
35	174.36	30.845	2022
36	124.903	30.845	2032
37	218.1	13.99	2013
38	218.1	13.99	2023
39	218.1	13.99	2033
40	232.43	4.55	2014,2015,2016

Table 4-11 (cont.)

Cell #	Volume, m^3	Bottom Elevation, m	Rooms
41	384.3	4.66	2024,2025,2026
42	235.6	4.65	2034,2035,2036
43	384.3	-5.5	2017,2027,2037
44	901.883	30.84	3331
45	901.883	30.84	3332
46	901.883	30.84	3333
47	2094.35	40.5	3334
48	environ	-10	N/A

Table 4-12 Modifications made to the MELCOR 48CV model.

Location	Modifications
Cell#5	HS sso159 separated into sso159a Cell#5(C5) and sso159b (C40), HS sso260 separated into sso260a (C5) and sso260b (C42), HS sso361 separated into sso361a (C5) and sso361b (C37), and HS sso462 separated into sso462a (C5) and sso462b (C40)
Cell#6	HS sso77 separated into sso77a (C6) and sso77b (C42)
Cell#10	HS sso133 axial length (BNDZL) adjust to fit within Cell#10 and Cell#42
Cell#13	Flow Through Area (FTA) to Cell#17; HS sso171 separated into sso171a (C13) and sso171b (C42)
Cell#14	FTA to Cell#17
Cell#15	HS sso190 separated into sso190a (C15) and sso190b (C40)
Cell#24	FTA to Cell#20
Cell#25	FTA to Cell#29
Cell#26	FTA to Cell#25 and Cell#27
Cell#28	Subfloor added for gravitational settling
Cell#30	FTA to Cell#9
Cell#31	FTA to Cell#17; HS sso374 separated into sso374a (C31) and sso374b (C40)
Cell#32	FTA to Cell#22
Cell#33	FTA to Cell#34, Cell#35, and Cell#36
Cell#34	FTA to Cell#37; Adjusted cell height by +.005m
Cell#35	FTA to Cell#38; Adjusted cell height by +.005m
Cell#36	FTA to Cell#39; Adjusted cell height by +.005m
Cell#37	Subfloor added for gravitational settling
Cell#38	Subfloor added for gravitational settling
Cell#39	Subfloor added for gravitational settling
Cell#40	Subfloor added for gravitational settling
Cell#41	Subfloor added for gravitational settling
Cell#42	Subfloor added for gravitational settling
Cell#43	Subfloor added for gravitational settling
Cell#47	FTA to Cell#44, Cell#45, and Cell#46

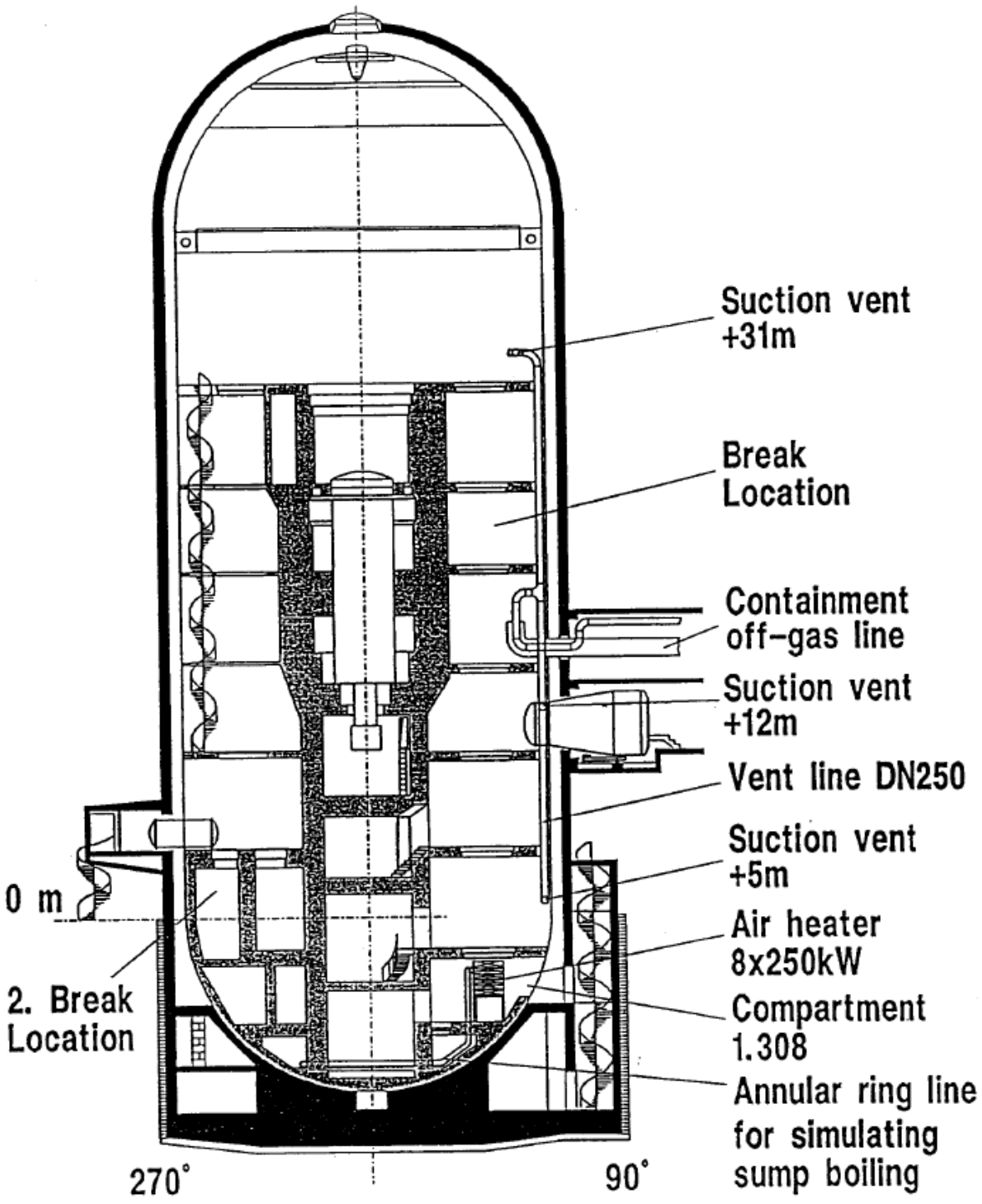

Figure 4-72 E11.2 test facility configuration. [Kar93]

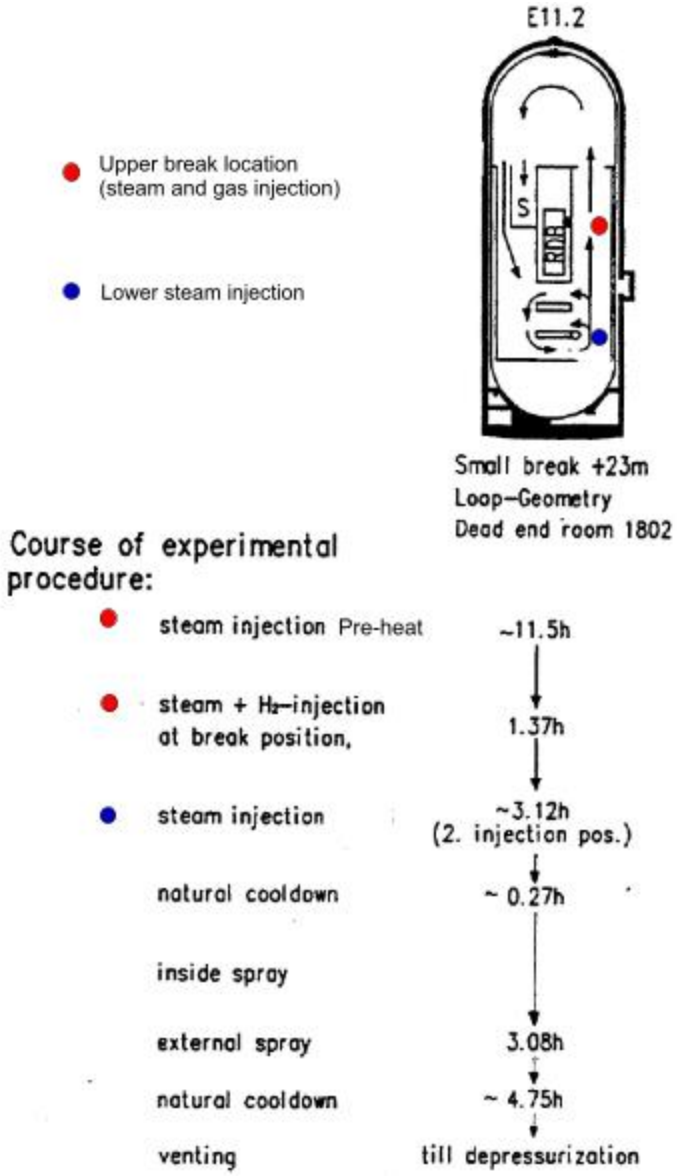

Figure 4-73 **E11.2 experimental procedure, showing approximate locations of injections and sketch of loop-geometry (staircase and spiral stair). No inside spray, external spray on outer dome, above the spring-line.**

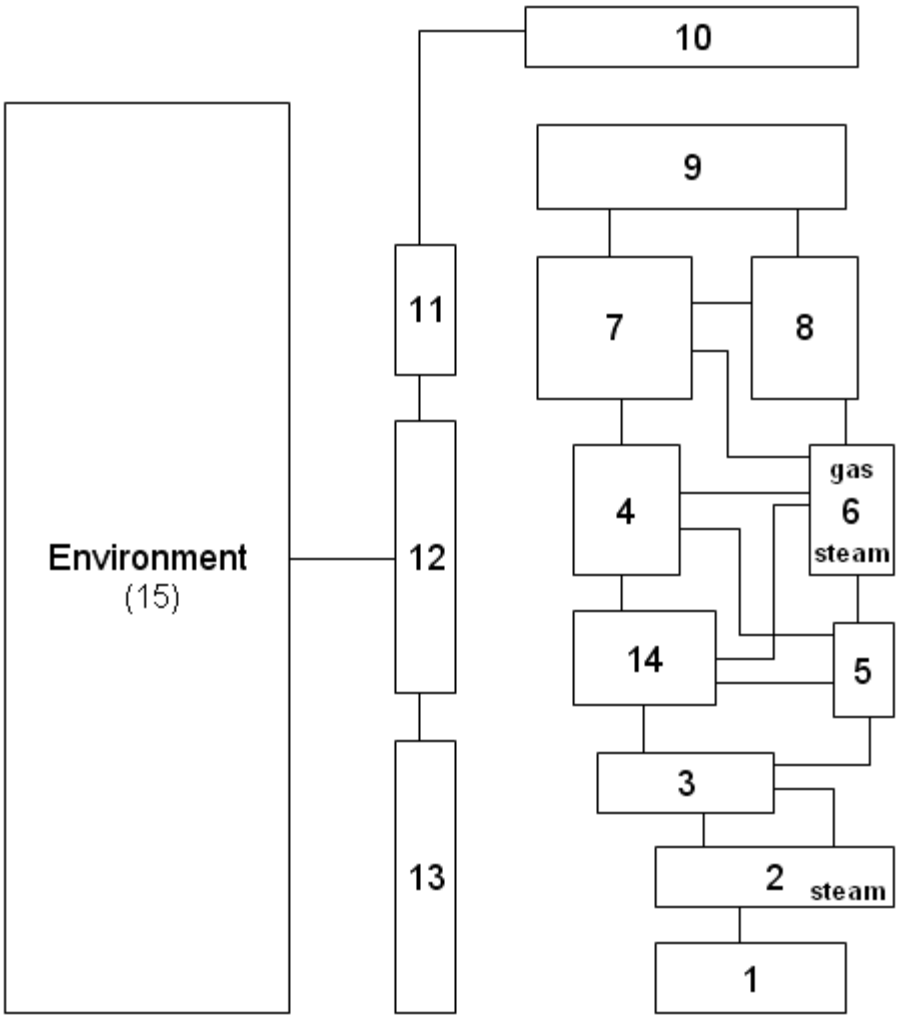

Figure 4-74 15 cell nodalization used for the E11.2 test reference calculation

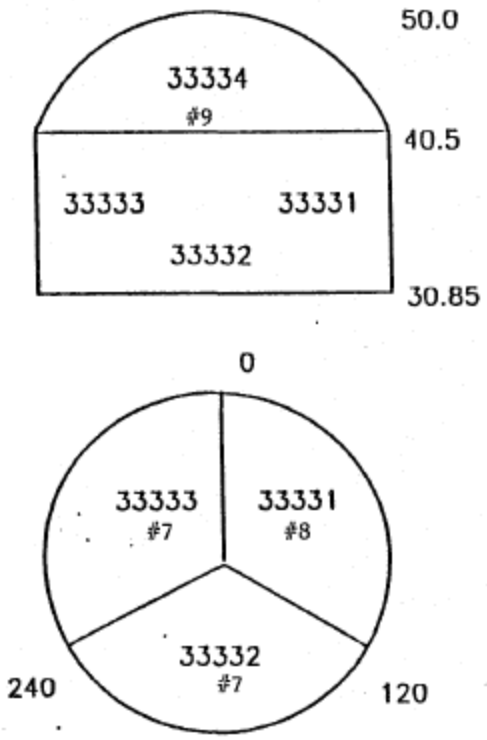

Figure 4-75 Upper containment cell configuration

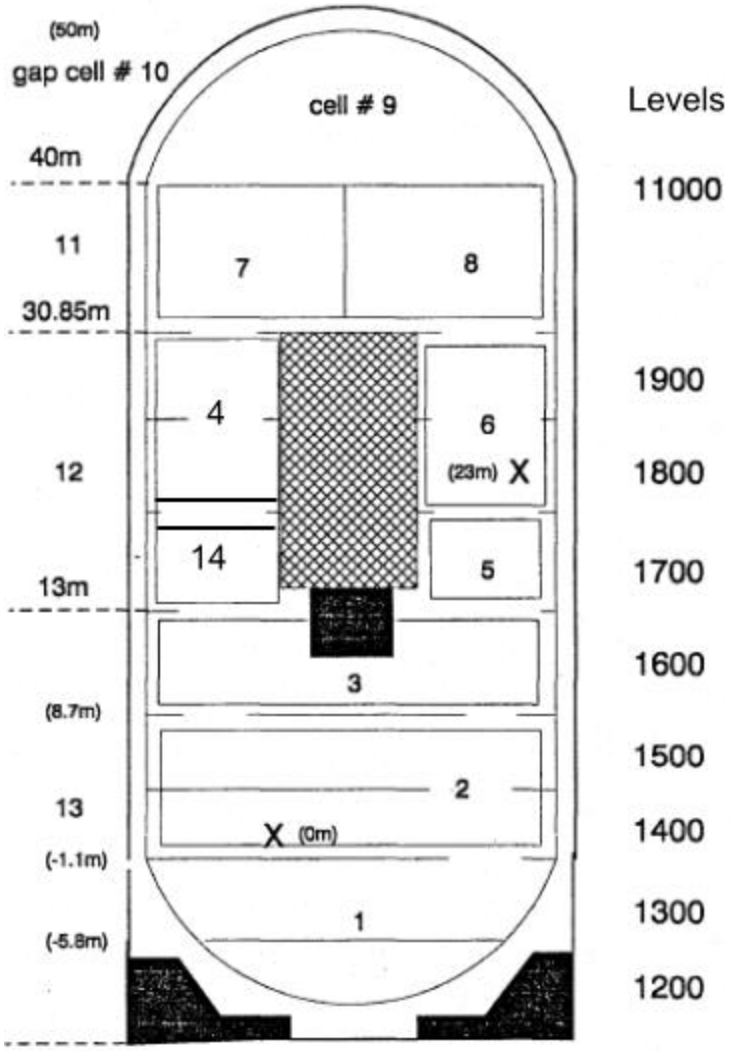

Figure 4-76 Sketch of the HDR facility with the 15-cell node overlay.

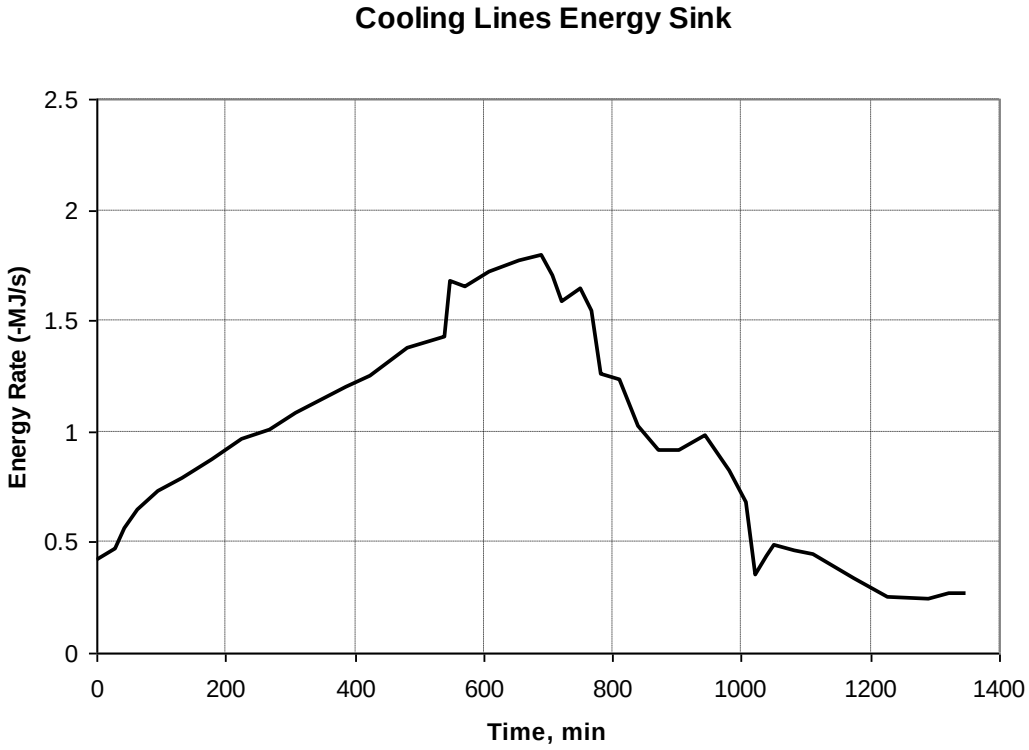

Figure 4-77 Depiction of the total energy removal approximation for the cooling lines supporting the atmosphere sampling equipment during the E11.2 test. [Til02a]

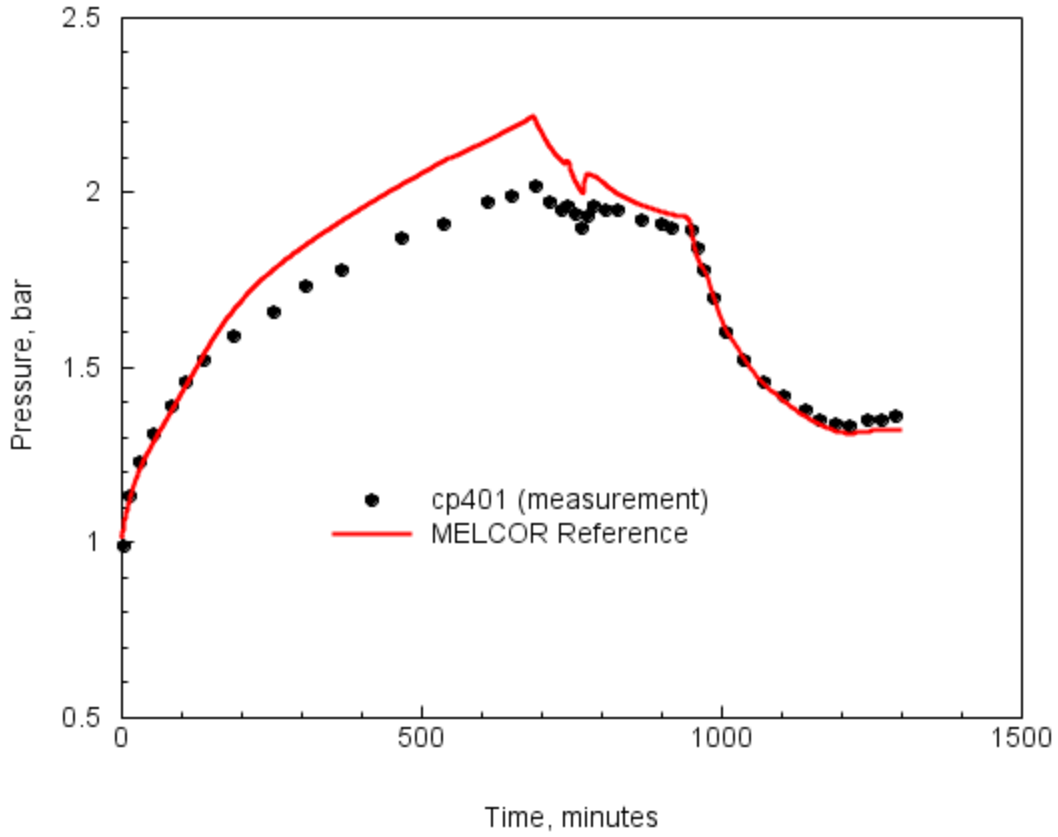

Figure 4-78 MELCOR reference calculation of containment pressure compared to measured values for sensor ct401.

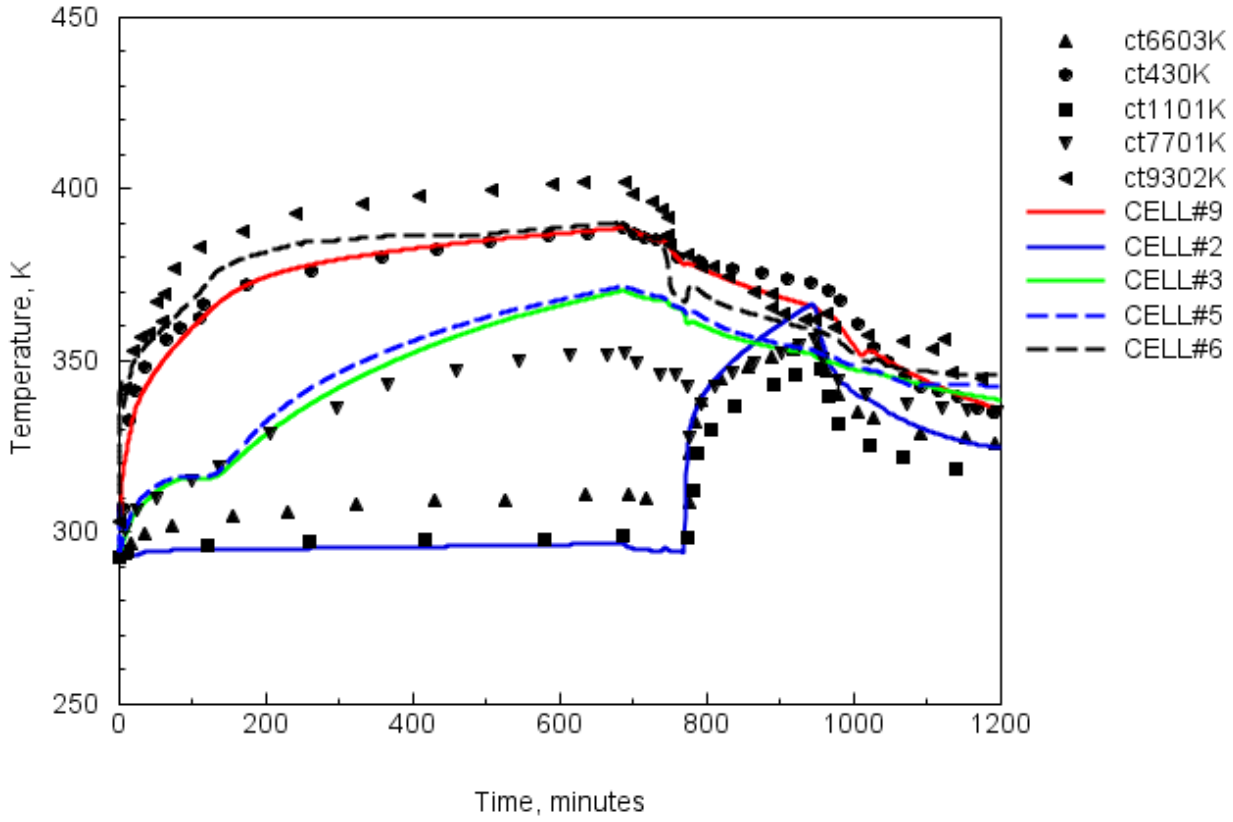

Figure 4-79 **Comparison between the calculated and measured temperature sensors for HDR E11.2 test using the MELCOR reference input.**

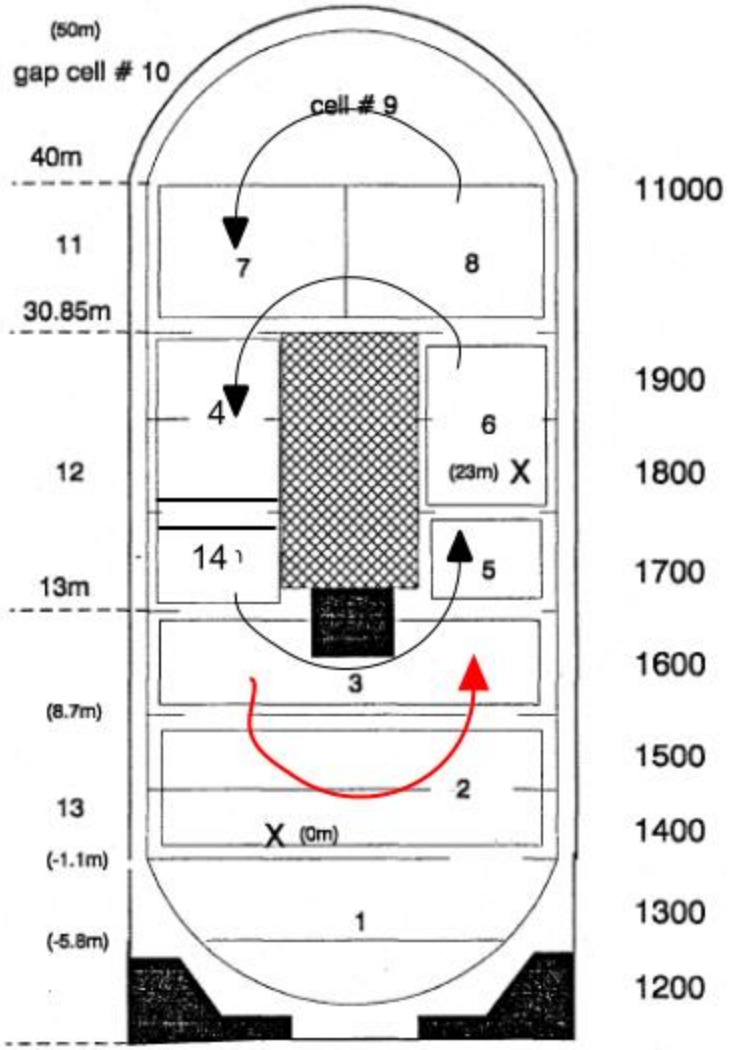

Figure 4-80 Approximate circulation profiles for the E11.2 test.

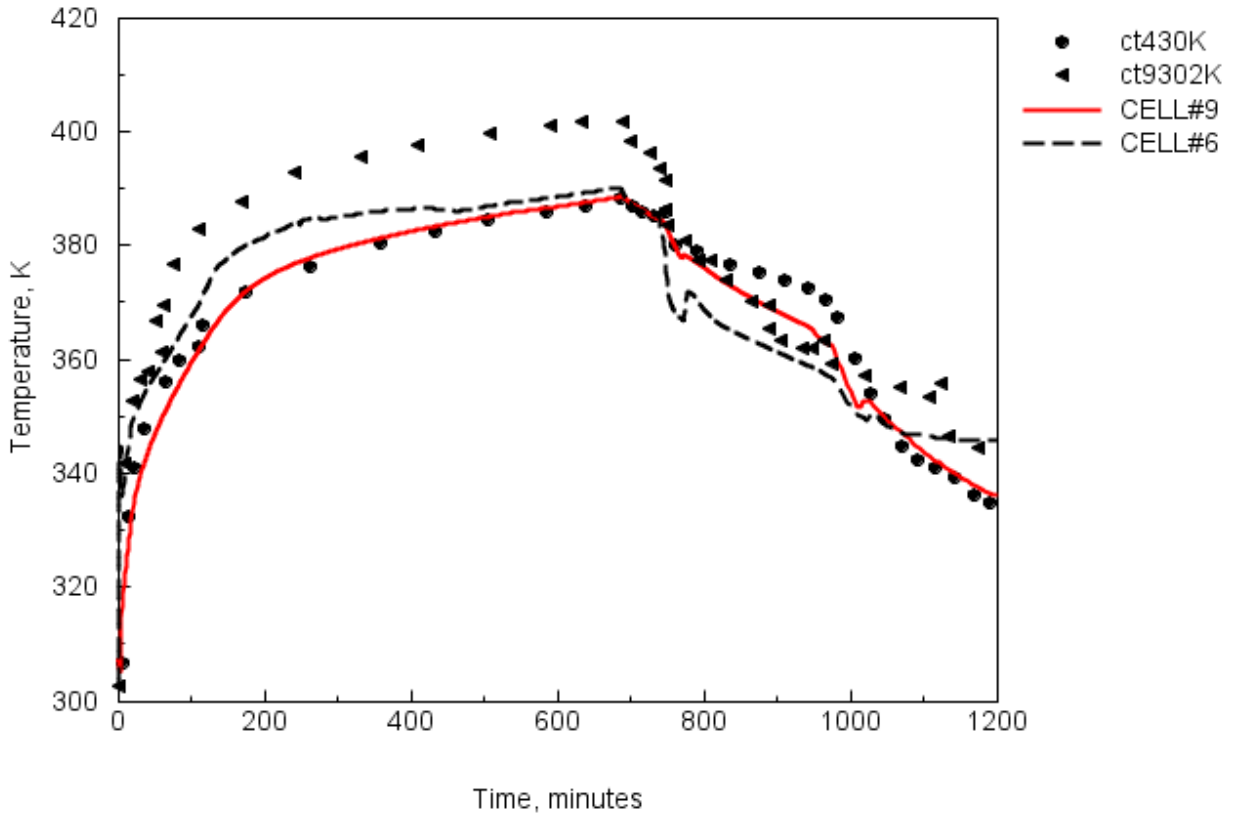

Figure 4-81 **Comparison of reference MELCOR and measured temperatures in the upper containment (40-50 meters) and the upper staircase region.**

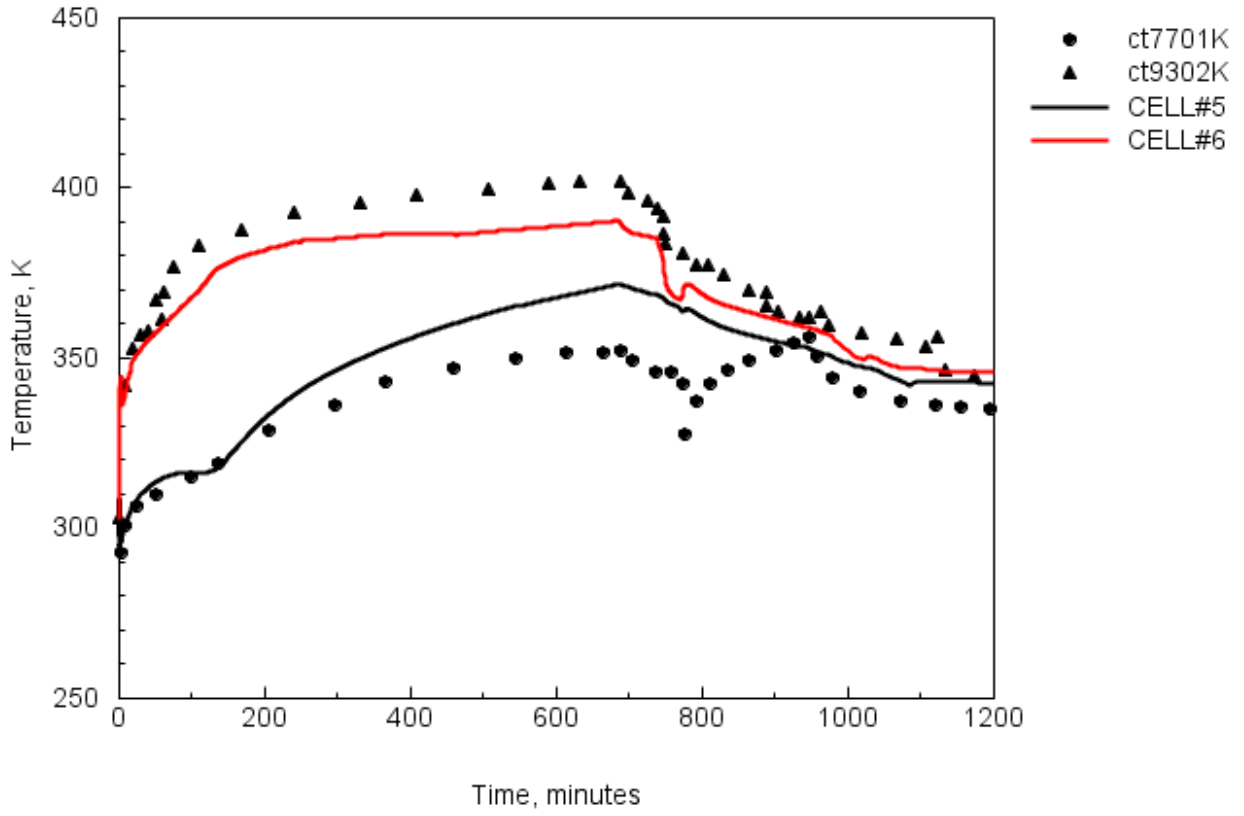

Figure 4-82 Comparison of reference MELCOR and measured temperatures in the upper and mid-staircase region for HDR E11.2 test.

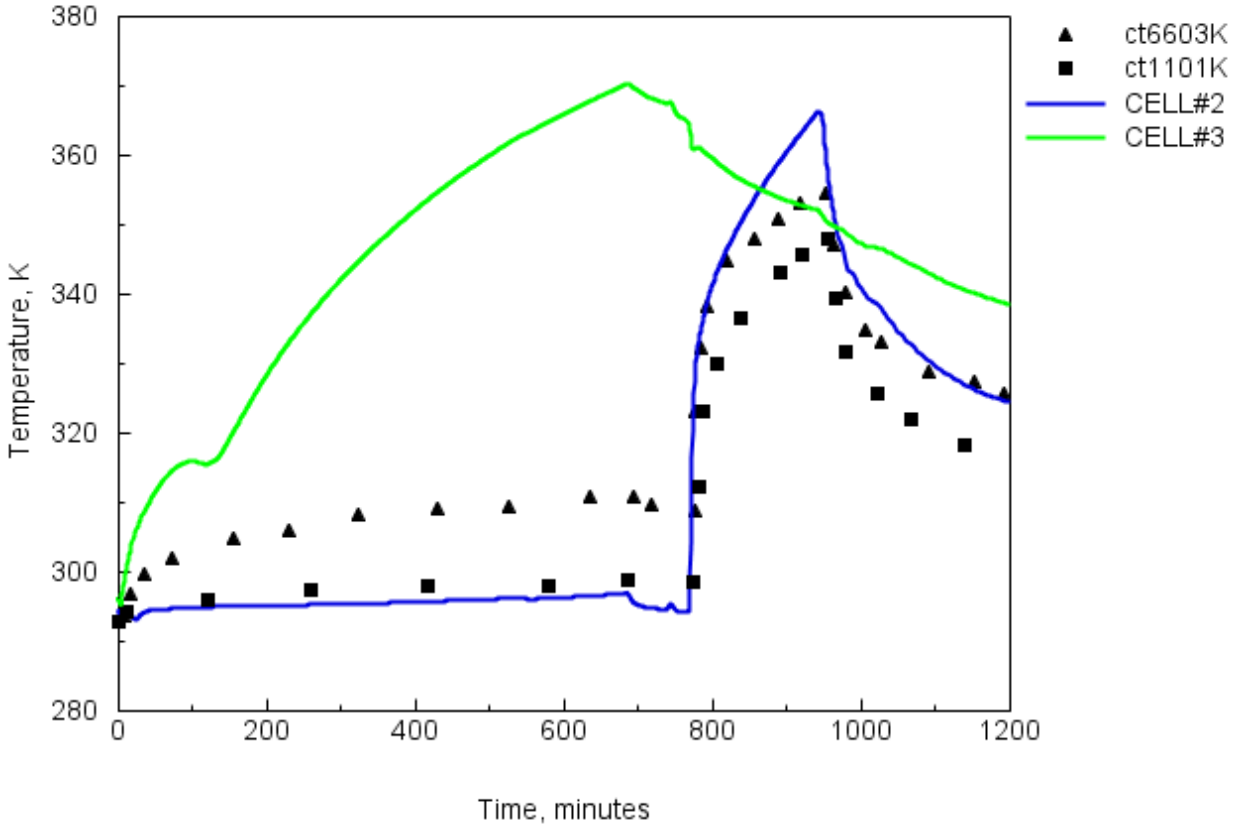

Figure 4-83 Comparison of reference MELCOR and measured temperatures in the cross-flow region of the lower containment for the HDR E11.2 test.

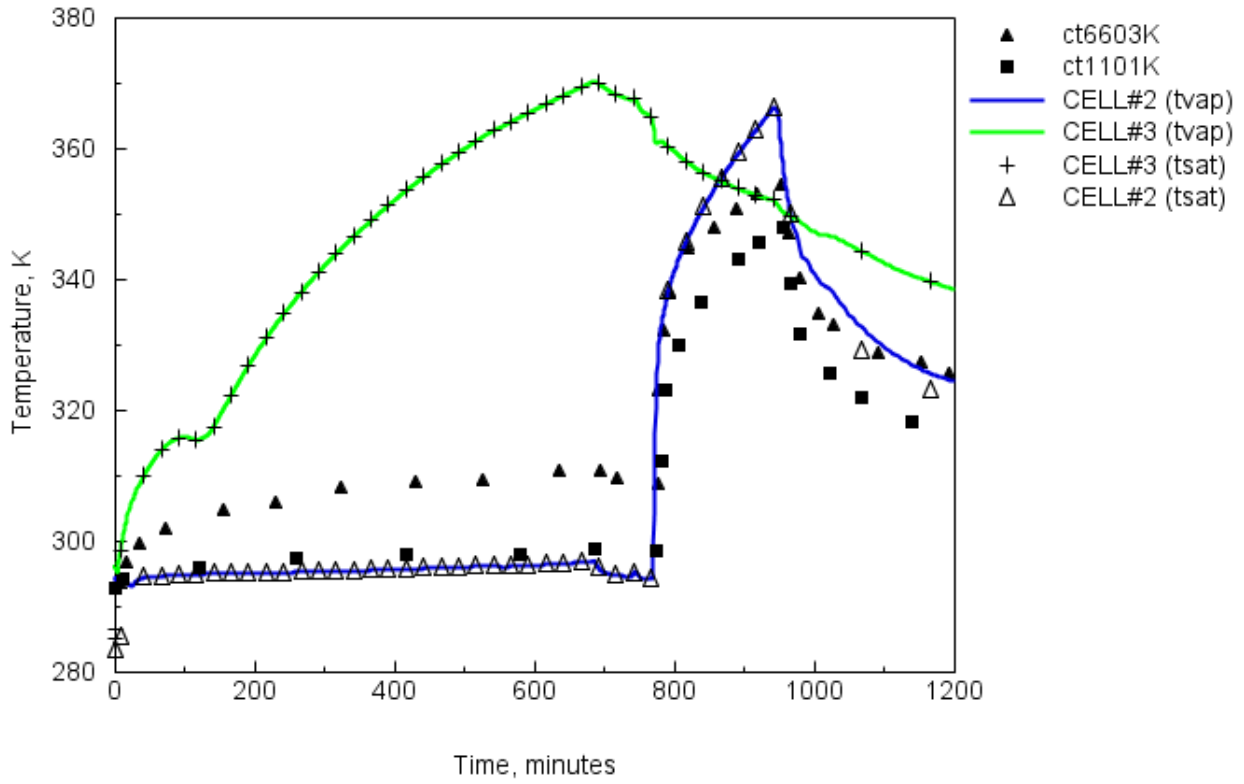

Figure 4-84 **Comparison of reference MELCOR and measured temperatures in the cross-flow region of the lower containment for the HDR E11.2 test, where both gas and saturation temperatures calculated with MELCOR are shown.**

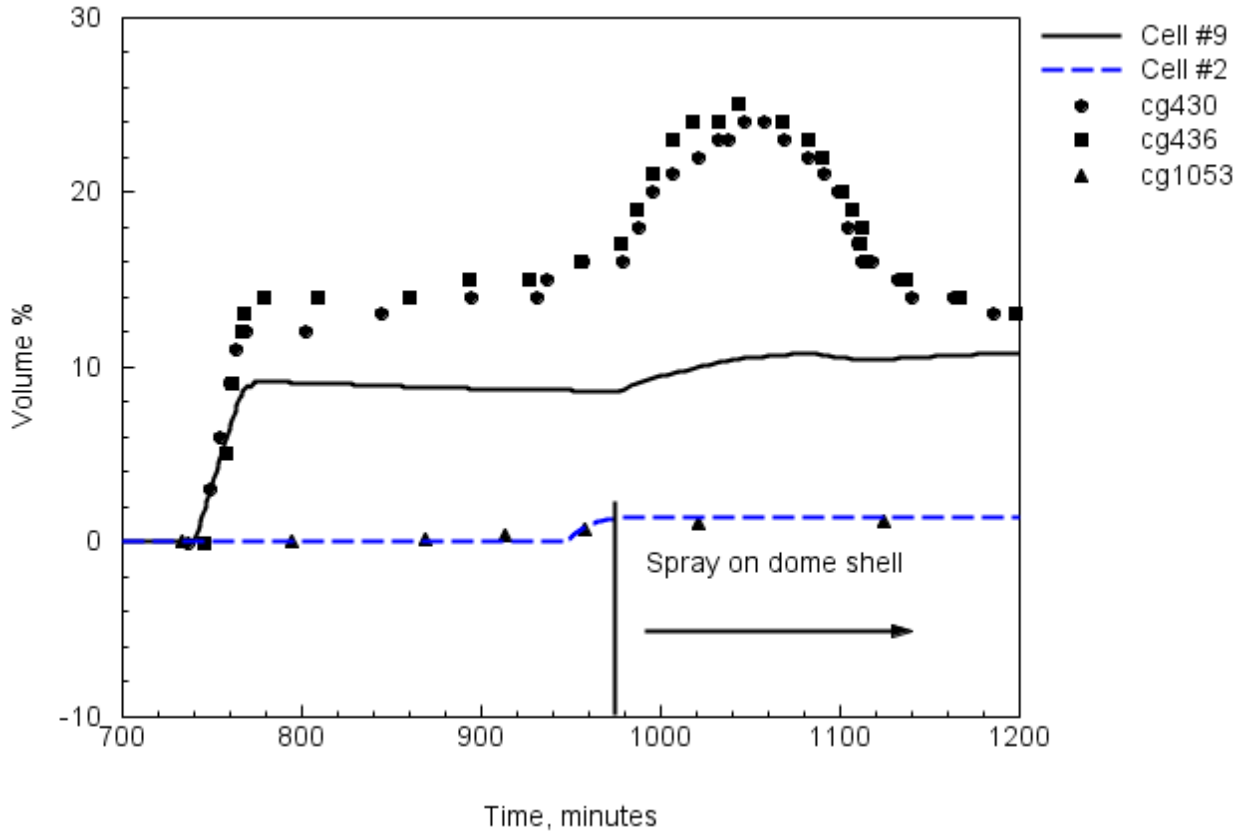

Figure 4-85 **Comparison of reference MELCOR calculated and measured light gas concentration in the upper (cg430,cg436, and cell #9) containment region (40-50 meters) and the lower (cg1053 and cell #2) containment region (6 meters) for the HDR E11.2 test.**

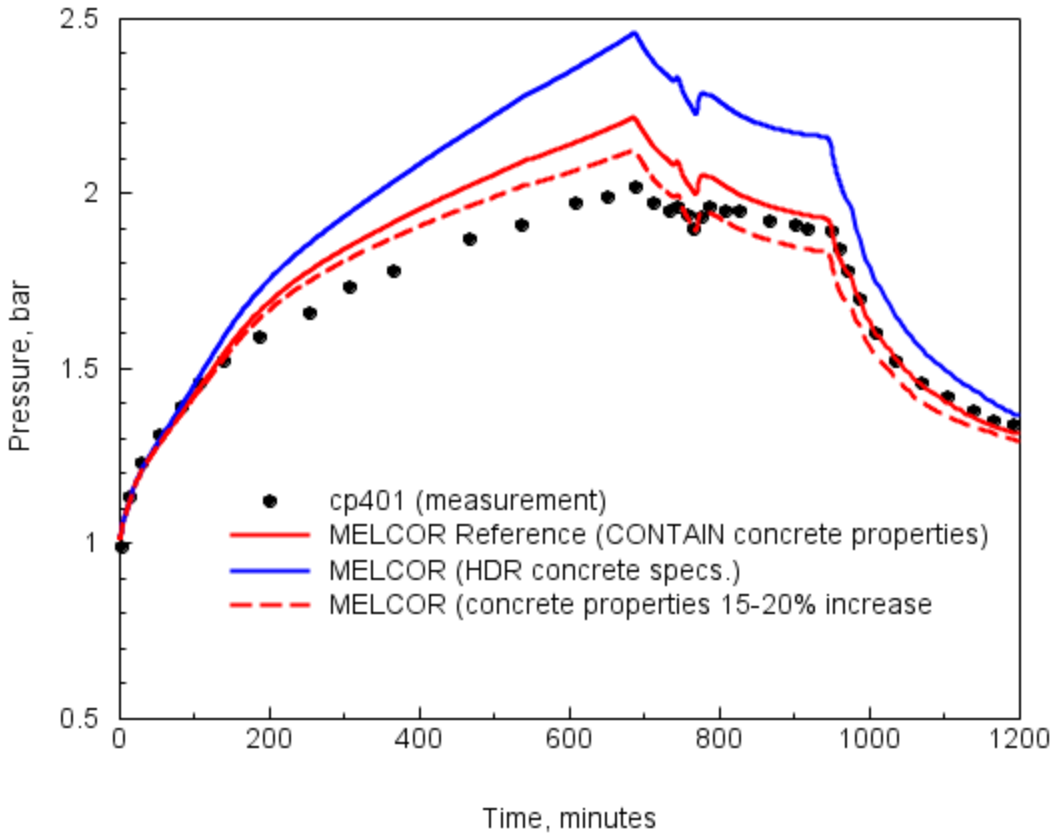

Figure 4-86 **MELCOR calculations of HDR pressure response for various concrete property inputs (see Table 4-8 for the specific property values by case number). The order of sensitivity cases listed, beginning with HDR concrete specification, correspond to cases 1 and 2, respectively.**

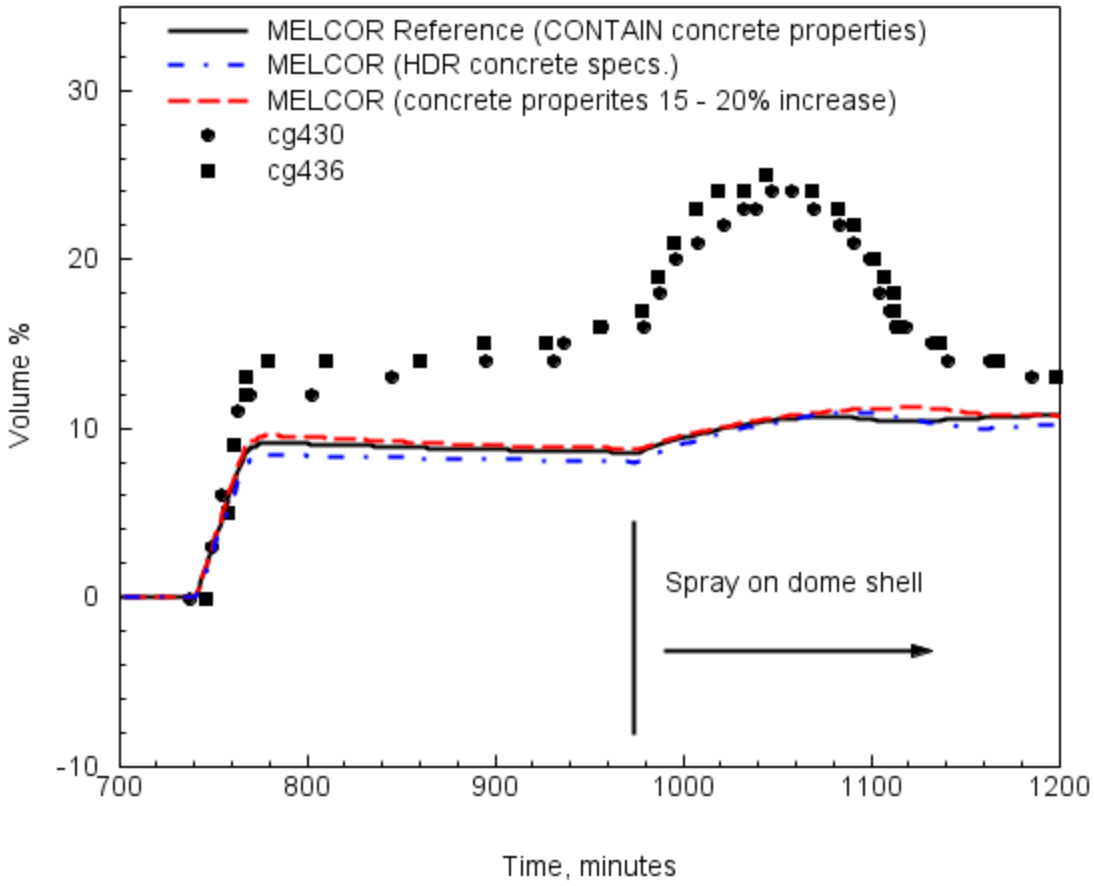

Figure 4-87 **MELCOR calculations of HDR light gas response in the upper containment for various concrete property inputs (see Table 4-8 for the specific property values by case number). The order of sensitivity cases listed, beginning with HDR concrete specification, correspond to cases 1 and 2, respectively.**

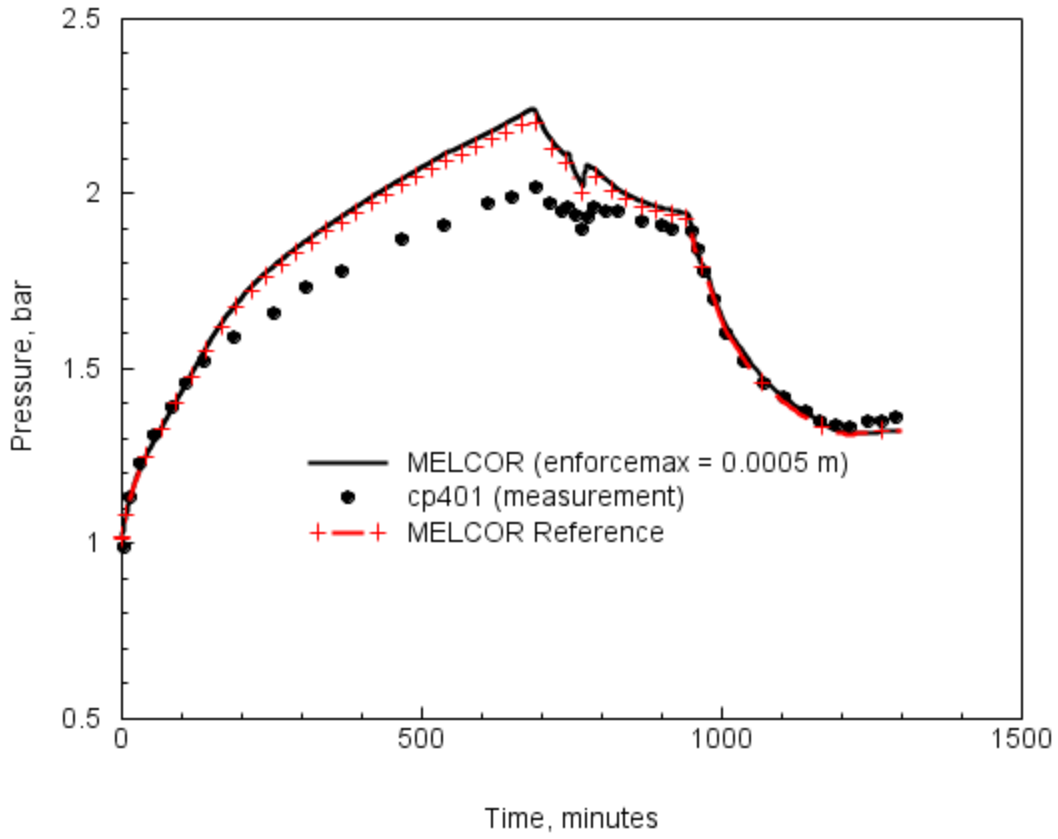

Figure 4-88 Comparison of the MELCOR pressure calculation sensitivity to film condensate thickness modeling for the HDR E11.2 test.

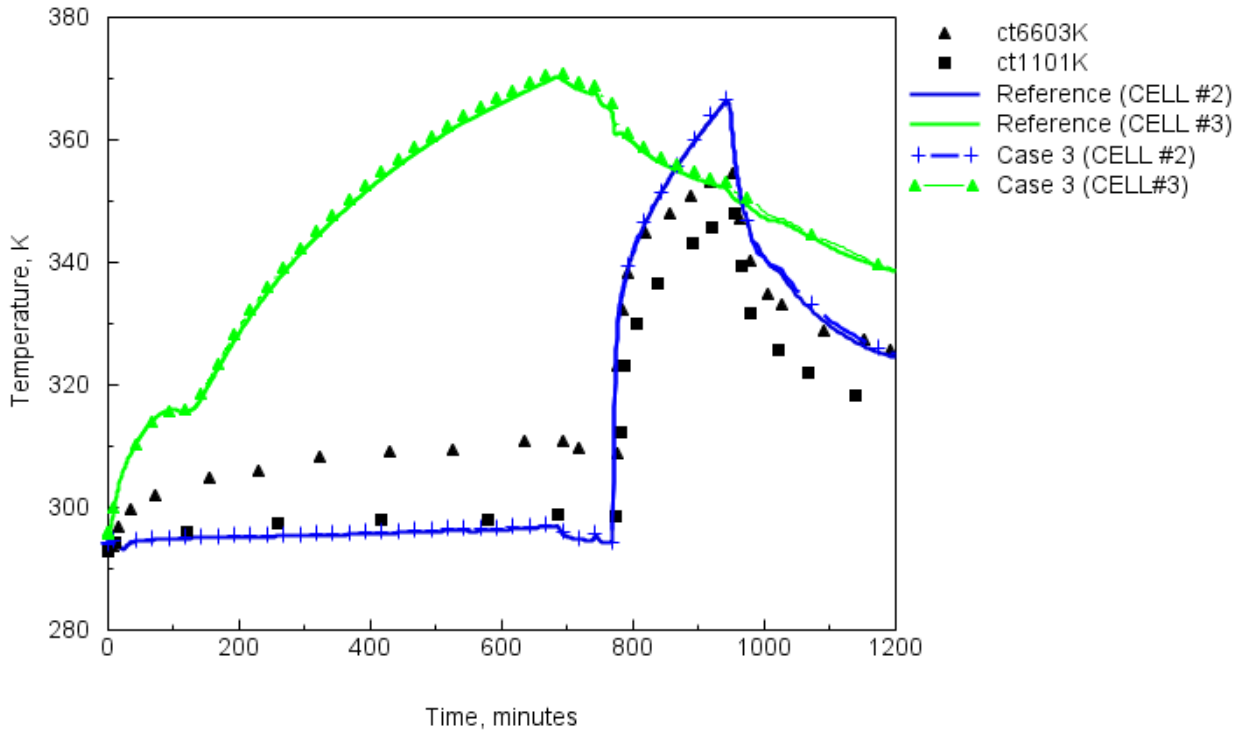

Figure 4-89 **Comparison of the MELCOR lower containment temperature calculation sensitivity to film condensate thickness modeling for the HDR E11.2 test. Case 3 corresponds to the film condensate thickness modeled with EnforceMax = 0.0005 meters, and the Reference case with the default dynamic film flow model.**

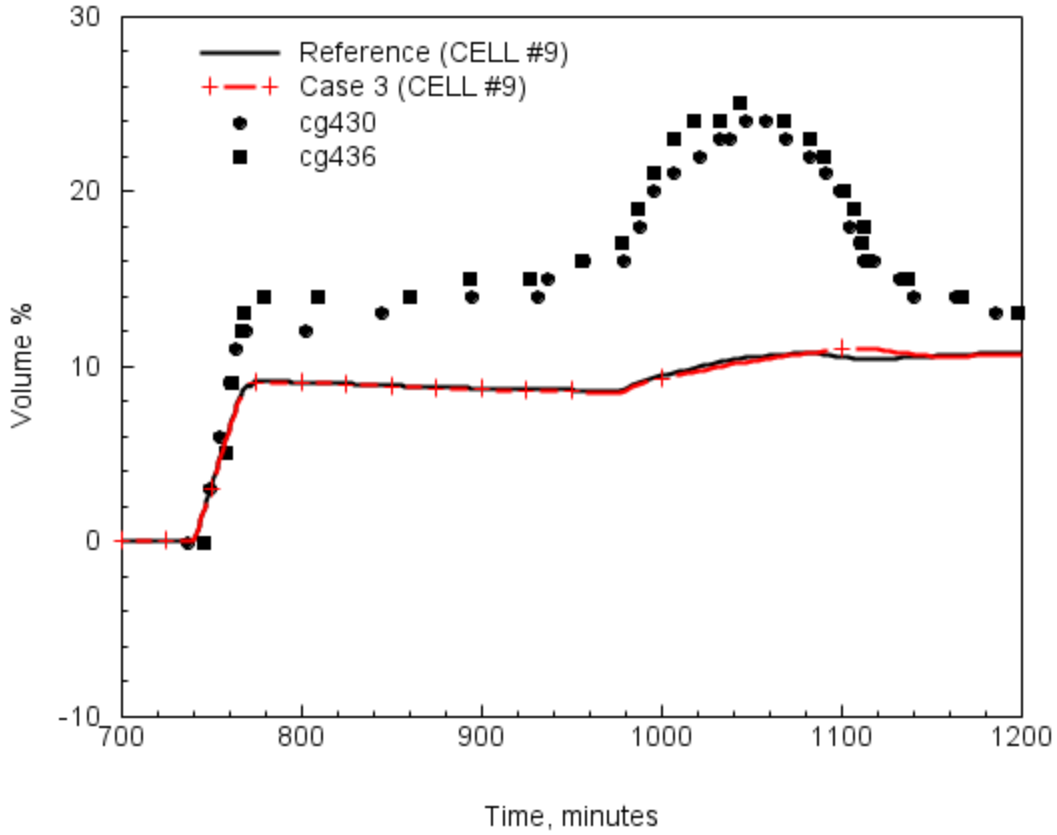

Figure 4-90 **Comparison of the MELCOR upper containment light gas calculation sensitivity to film condensate thickness modeling for the HDR E11.2 test. Case 3 corresponds to the film condensate thickness modeled with EnforceMax = 0.0005 meters, and the Reference case with the default dynamic film flow model.**

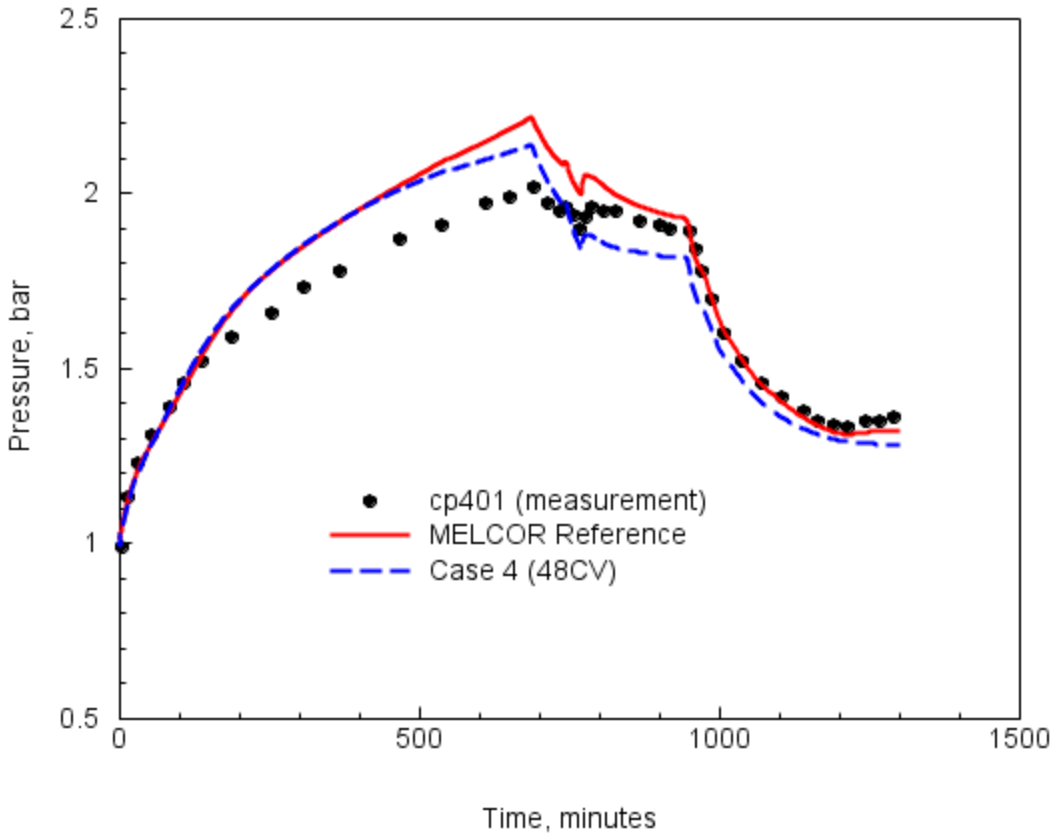

Figure 4-91 MELCOR calculated containment pressure sensitivity to HDR facility nodalization (15CV vs. 48CV).

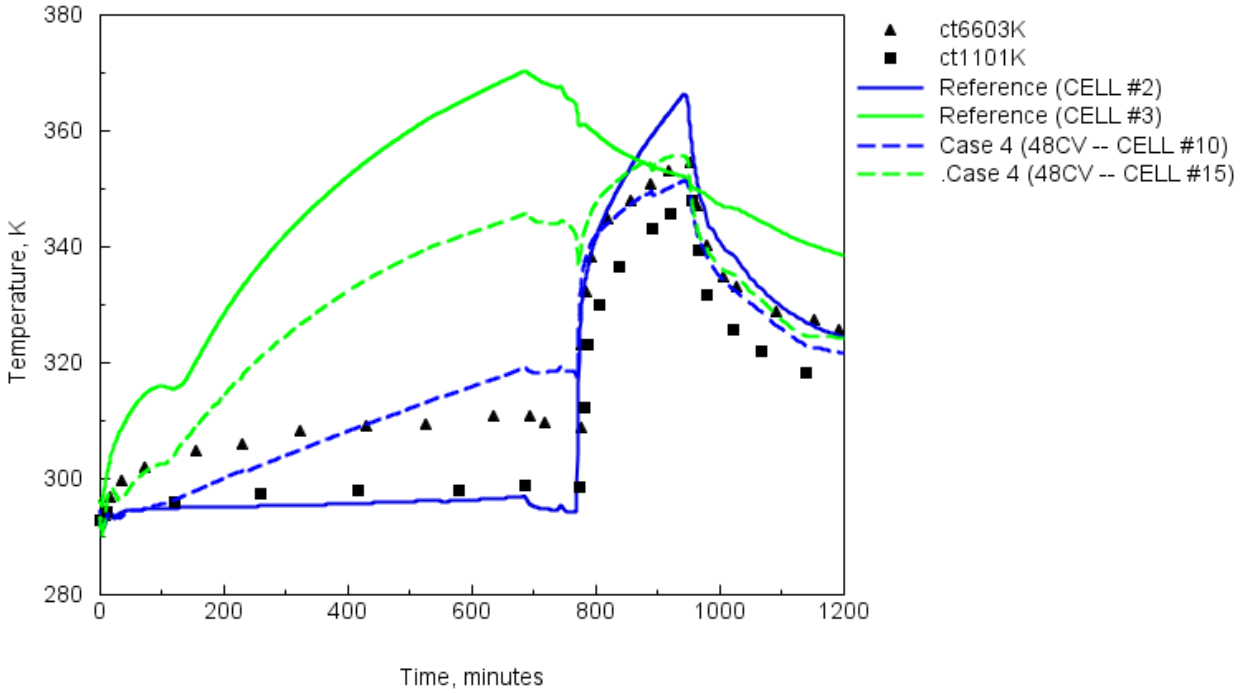

Figure 4-92 **MELCOR calculation of lower containment temperatures, showing sensitivity to HDR facility nodalization (15CV vs. 48CV), especially for the lower containement steam injection period starting at 790 minutes where the additional detail provided by the 48CV modeling does indicate an improvement in local temperature comparison with measurement.**

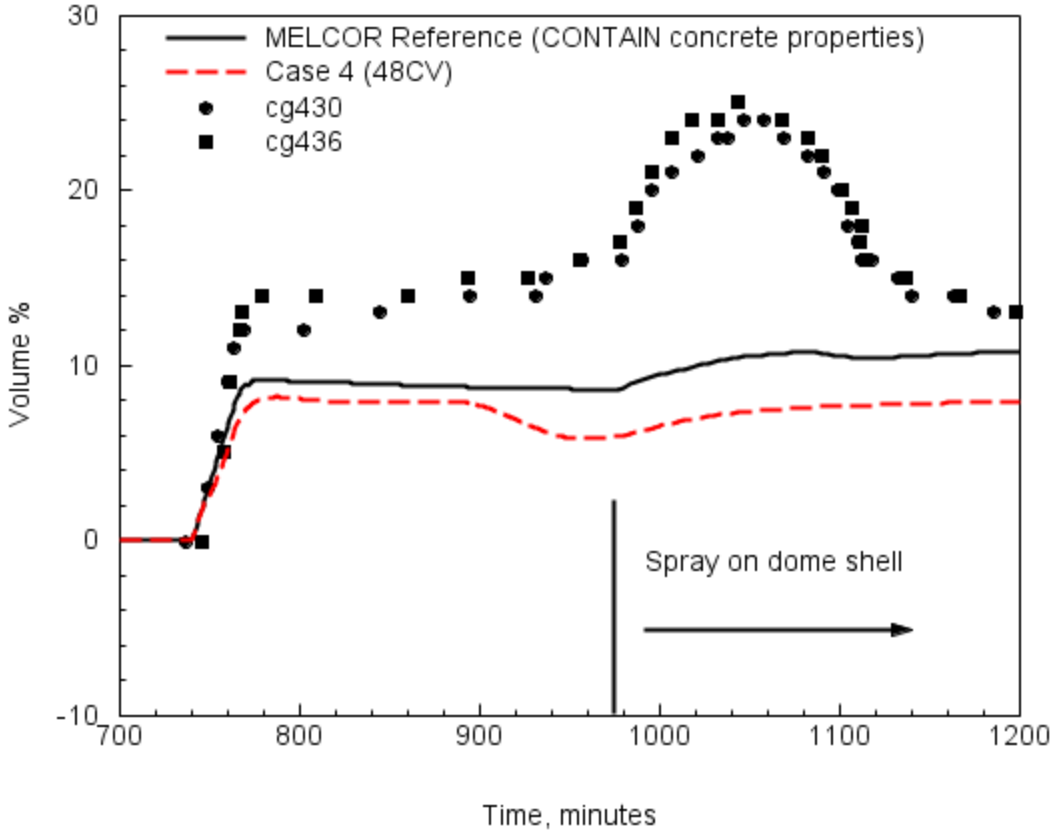

Figure 4-93 **MELCOR calculated light gas concentration in the upper containment for nodalization sensitivity, showing no improvement of the reference (15CV) case versus the 48CV calculation.**

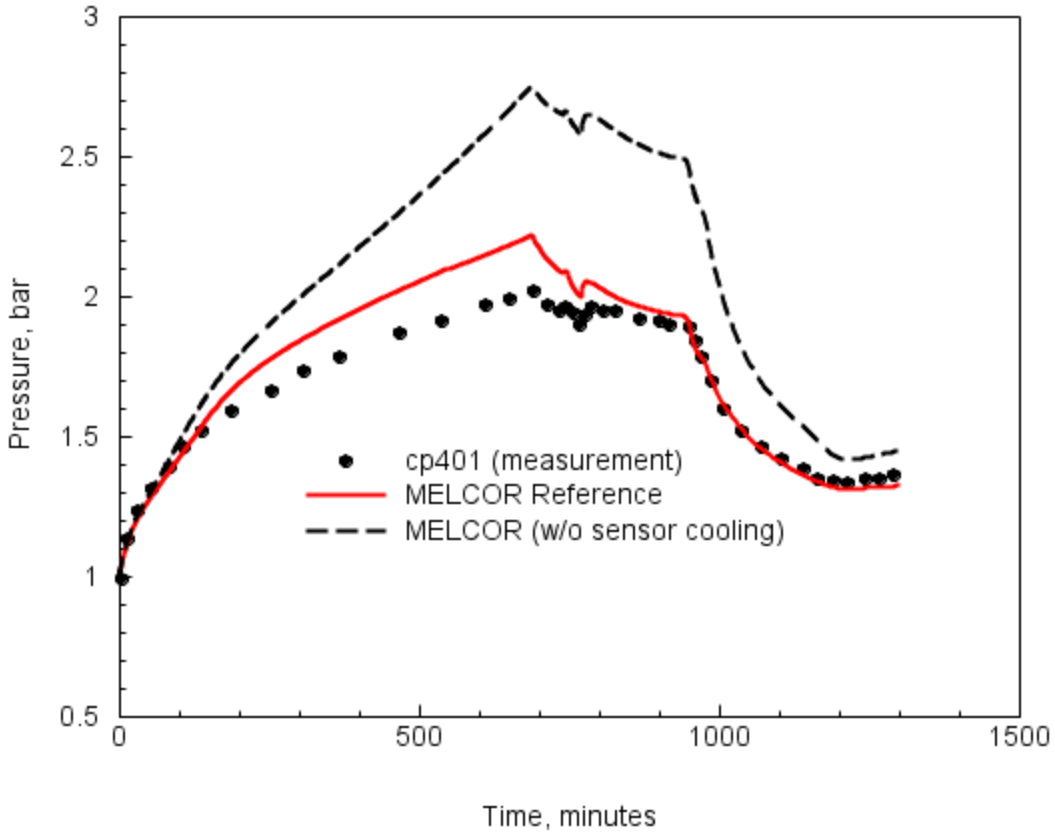

Figure 4-94 MELCOR pressure calculation sensitivity (Case 5) to sensor line cooling for HDR E11.2 test.

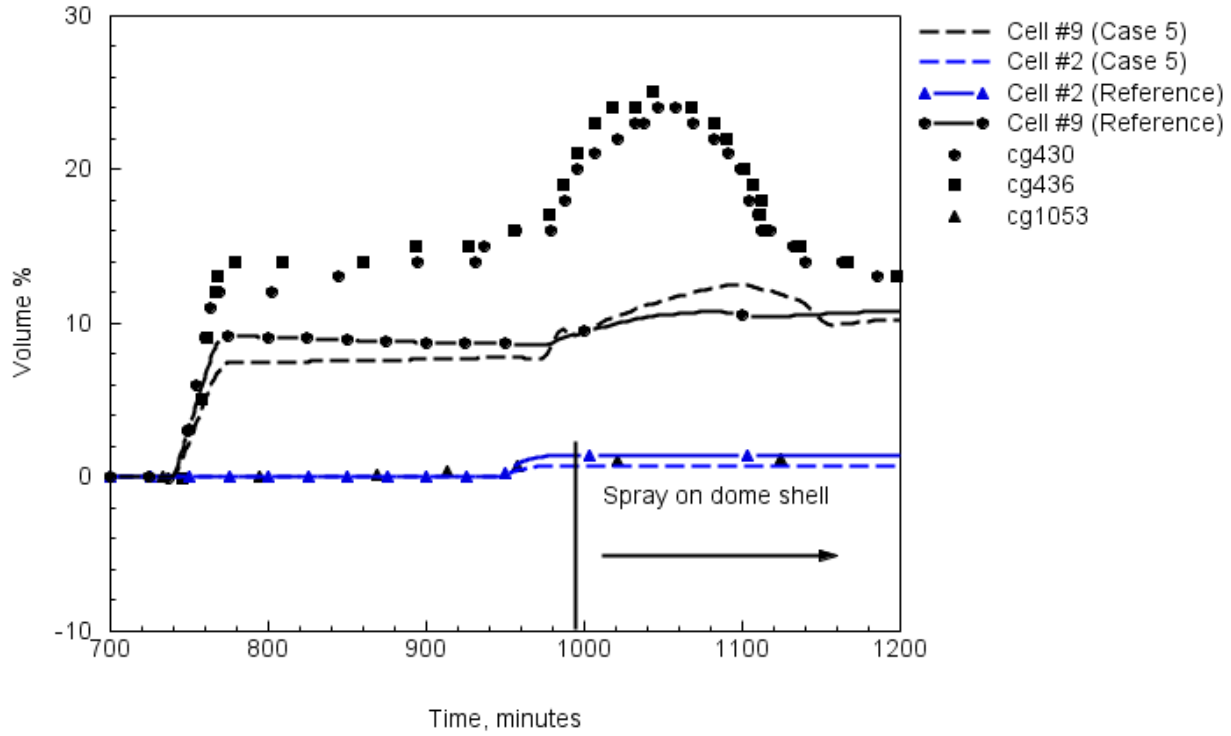

Figure 4-95 MELCOR light gas calculation sensitivity to sensor line cooling for HDR E11.2 test (Case 5 – w/o sensor cooling).

4.4.3 Benchmark

Figure 4-96 depicts good agreement between the calculated global pressure observed in the CONTAIN (mstable) and MELCOR reference case as the calculations approach the peak pressure in the containment and depressurize. The default momentum equation flow solver for CONTAIN is the hybrid flow solver. The flow solver is discussed in detail in Reference Mur96, and an older version of the solver is provided as an optional model in the code. That model tends to predict more mixing of stratification layers and is referred to as the "mstable" model. Mixing behavior for both CONTAIN and MELCOR was briefly discussed in Section 3 for a sample plume illustration. For the E11.2 test, the mixing behavior modeled with the "mstable" option in CONTAIN more closely represents the MELCOR calculation for global pressure. And from the standpoint of global behavior the "mstable" modeling appears to better represent the loop cross-flow in the lower containment and cooling in this region of the containment. However, when comparing the local conditions for the light gas concentration in the critical region of the upper containment, CONTAIN with the hybrid flow solver compares more favorably with the experiment data especially during the spray period when the upper containment light gas concentration peaks, Figure 4-97. Again, the CONTAIN "mstable" calculation with over-mixing corresponds better to the MELCOR calculated light gas concentration predicted during the release and spray period.

While CONTAIN was able to predict the peak light gas concentration experienced in the dome of the upper containment, MELCOR deviates soon after the light gas release due to over-mixing and the inability to model plume behavior. The activation of the dome external spray begins to increase the gas concentration in both CONTAIN and MELCOR due to the condensation of water vapor in the dome region, but much less for MELCOR than CONTAIN and the experiment measurement. Eventually, the density inversion of the light gas in the dome region results in rapid mixing between control volumes 7, 8, and 9 in CONTAIN, while the experiment experienced slower transition to a well-mixed condition. MELCOR with over-mixing, however, does not capture this inversion phenomenon as well as the CONTAIN code with the hybrid flow solver.

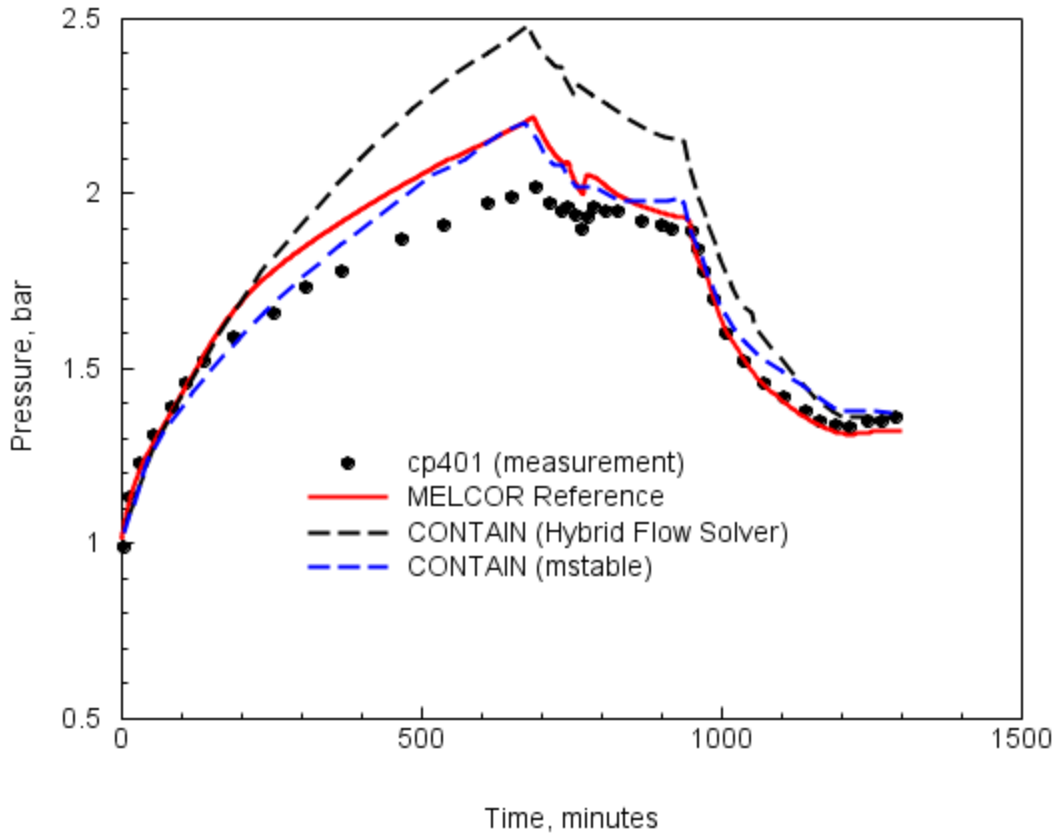

Figure 4-96 Comparison of MELCOR and CONTAIN pressure calculations for the HDR E11.2 test.

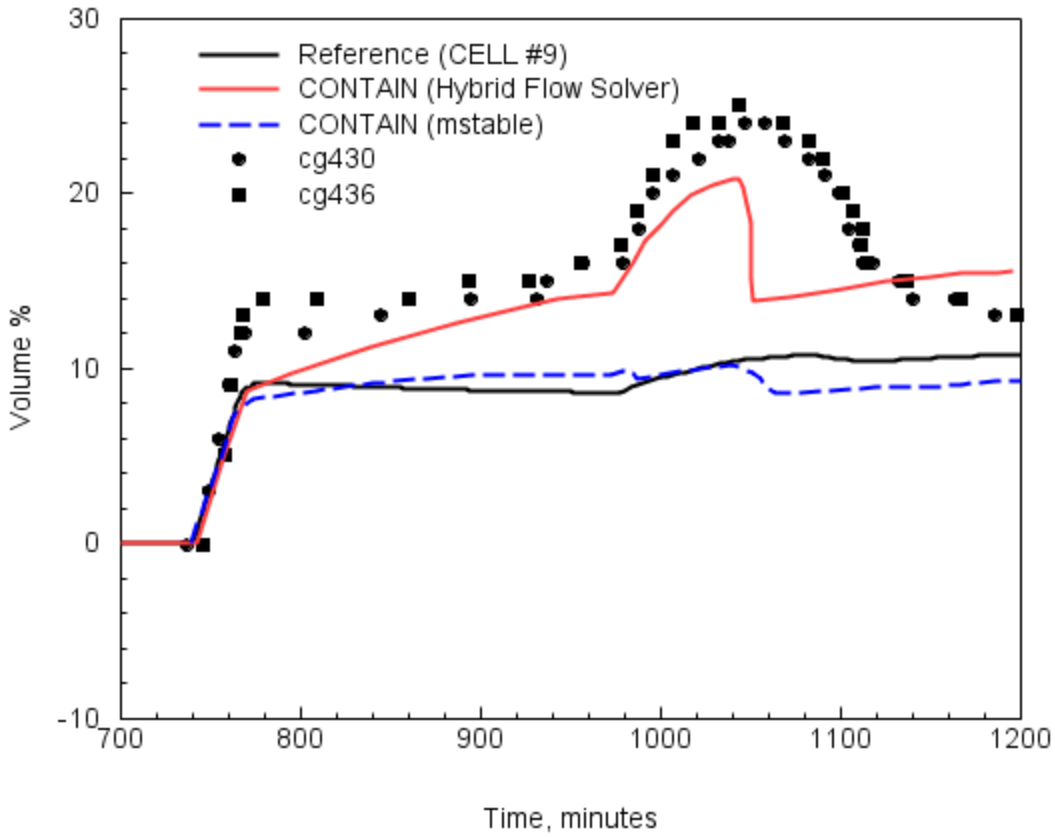

Figure 4-97 Comparison of MELCOR and CONTAIN calculations for light gas concentration in the HDR upper containment (above 40 meters) during the HDR E11.2 test.

4.5 Test E11.4 (Project HDR Benchmark)

The E11.4 test was used as a benchmark exercise for codes, sponsored by Project HDR [Val92, Gre92]. The experimental procedure for the E11.4 test is shown in Figure 4-98. The main difference between the E11.2 and the E11.4 test was 1) the different injection locations for the steam and light gas mixture and 2) the duration of the heat-up period. In the E11.4 test, a single injection location was moved to the lower containment (room 1405), Figure 4-99. The low injection position meant that the containment would not exhibit the severe stratification observed in the mid-elevation injection of E11.2. The E11.4 test also includes an extended heat-up period of about 34 hours, 3 times the length of the heat-up period for E11.2.

The E11.4 test was part of the E series, like ISP-29, to investigated containment mixing. Unlike the ISP-29, the steam sources for the E11.4 test originate near the base of the facility which improves overall containment mixing, reducing the importance to adequately model stratification within the facility. This experiment provides reassurance that lumped parameter codes which generally suffer from over-mixing should be able to calculate system response well when injections are located low in the containment.

Since E11.4 was not submitted as an ISP, information adequately characterizing the experiment was more difficult to obtain. For the purpose of this report, water sources were extracted from a prior CONTAIN sensitivity analysis input file of the E11.4 test. This allows the ~ 34 hour heat-up phase to be calculated and a validation analysis performed for MELCOR from a thermal hydraulic perspective.

4.5.1 Reference Case

The MELCOR reference case for test E11.4 uses the 15CV nodalization scheme as used to model the HDR E11.2 test. Instrument cooling was modeled as describe for E11.2 but using the E11.4 measured cooling rates which were slightly different from E11.2, Figure 4-100. The heat-up phase steam mass flow rates are shown for the RPV blowdown (small break) and the external steam source. At approximately 800 minutes into the test an interruption of the external steam supply for 200 minutes occurred, Figure 4-101, caused by a defective steam valve that was later repaired.

Shown in Figure 4-102 is the comparison between the measured and predicted containment pressure during the heat-up period of the test. The break in the pressure increase at about 800 minutes is the result of a failure in the steam supply valve. The valve was repaired and the heat-up period of the test continued. Clearly, the agreement between measured and calculated pressure over the heat-up period of the test is quite good. After 34 hours (2040 minutes) the absolute error in pressure is 6.2%, while error in the over-pressure prediction is 12.7%. These errors are essentially within the measurement accuracy of the pressure transducers (3-10 kPa). We can compare the two pressure measurements and predictions for E11.2 and E11.4 over the first 11 hours (660 minutes) of the tests (during the E11.2 heat-up period), Figure 4-103. Over the similar heat-up periods, each test has the same steam injection mass and energy. The E11.4 pressure is lower since more long-term heat sink material (concrete) is exposed to steam in E11.4 due to the uniform mixing in this test as contrasted to the E11.2 test that showed significant stratification. This figure also shows an outstanding difficulty with the E11 series of code calculations - there is

very good agreement in pressure with the E11.4 test while the calculations for E11.2 show a significant over prediction. This observation has been made by analysts using other lumped parameter codes [Lee99] and even finite control volume codes employing thousands of nodes [Roy95].

The uniform mixing resulting from the low injection is shown in Figure 4-104 where measured temperatures are plotted for the lower and upper containment. In the lower containment region two measurement locations are plotted: the measurement ct5304 is located in room 1503 away from the staircase; measurement ct5301 is located in the equipment shaft near the staircase. A review of the breakroom (1405) location at level 1400 is shown in Figure 4-105. Movement of the steam in the rising plume is shown to favor the pathway that directs the flow up from level 1400 to the staircase/equipment shaft at the 80 degree mark on level 1500, Figure 4-106. The steam/gas mixture in the plume, rising up through the equipment shaft, is seen to have a slightly higher temperature than in the room adjacent to the shaft where major heat sinks are located. In the case of the calculations, the temperature trends from the lower to upper containment are well predicted. The lower containment temperature is under predicted early in the transient, and less so during the late portion. Presumably this under prediction is the result of the rather coarse nodalization in the lower containment. We also see in the figure that the calculation behaves similar to the observation in measurements between the shaft and adjacent room region; where the lumping of a number of rooms on the 1500 level together amplifies the variation in temperatures at this level. In contrast, the upper containment temperature calculations are essentially within the measurement uncertainty of 1-2 degrees near the end of the heat-up period.

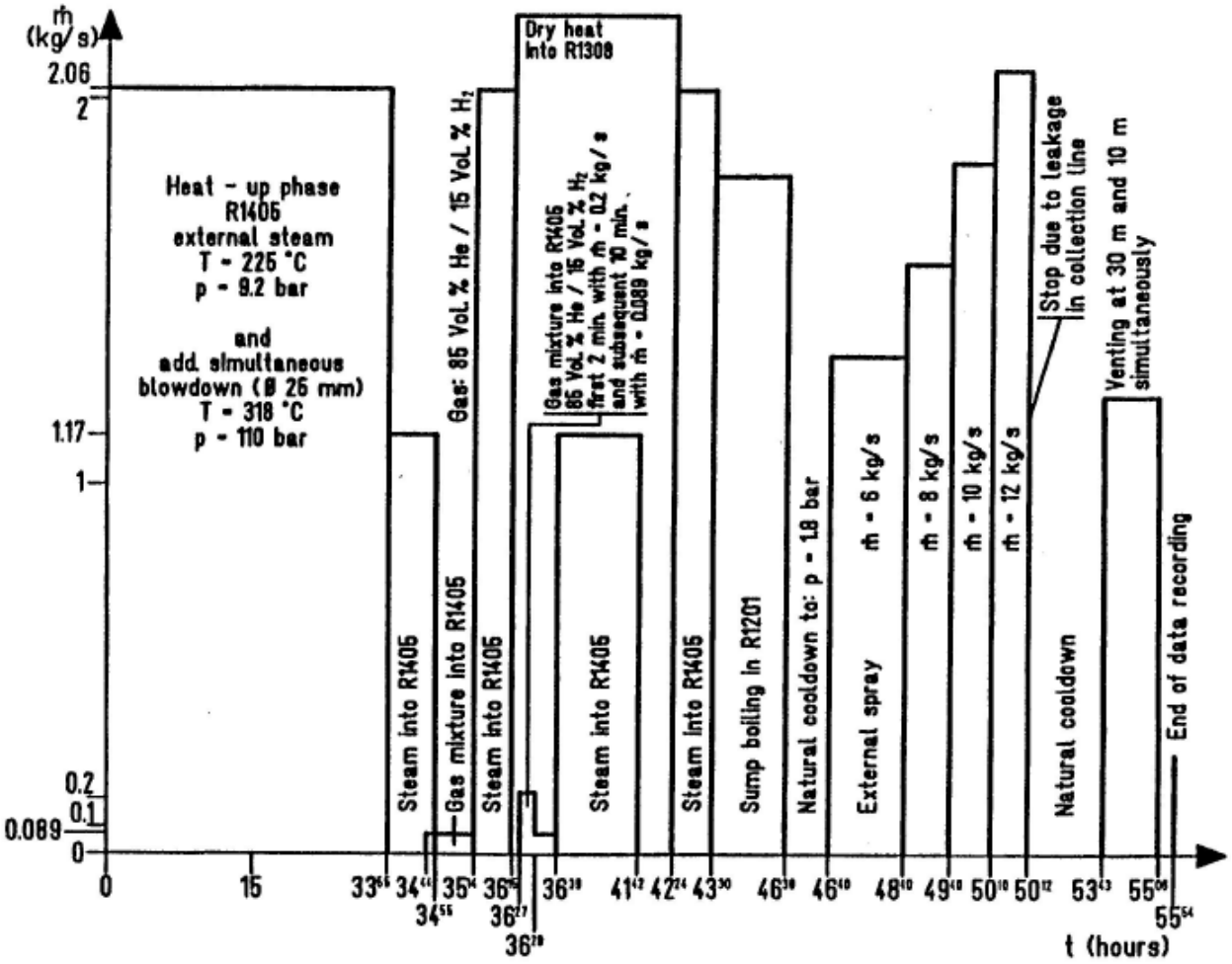

Figure 4-98 HDR E11.4 test procedure [Til02a].

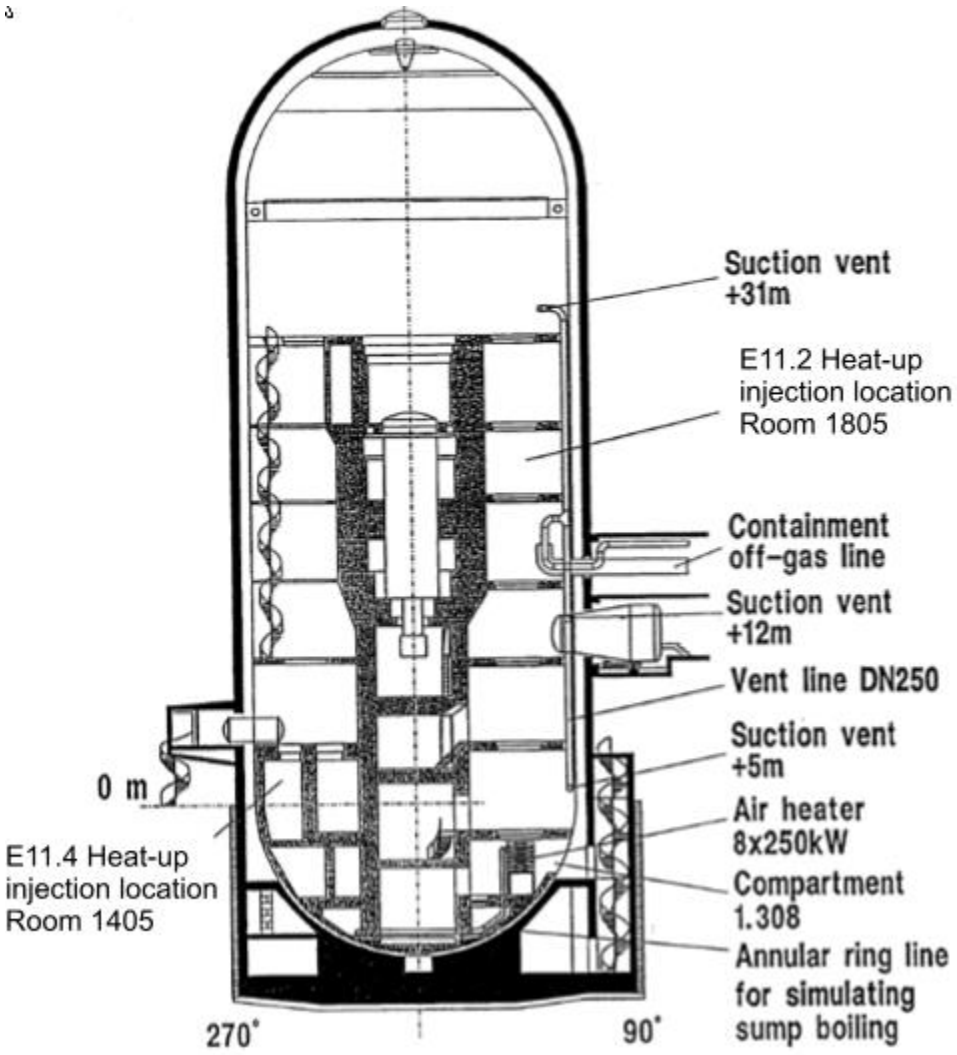

Figure 4-99 HDR facility for E-series tests showing the relative steam injection locations for the heat-up portion of the tests.

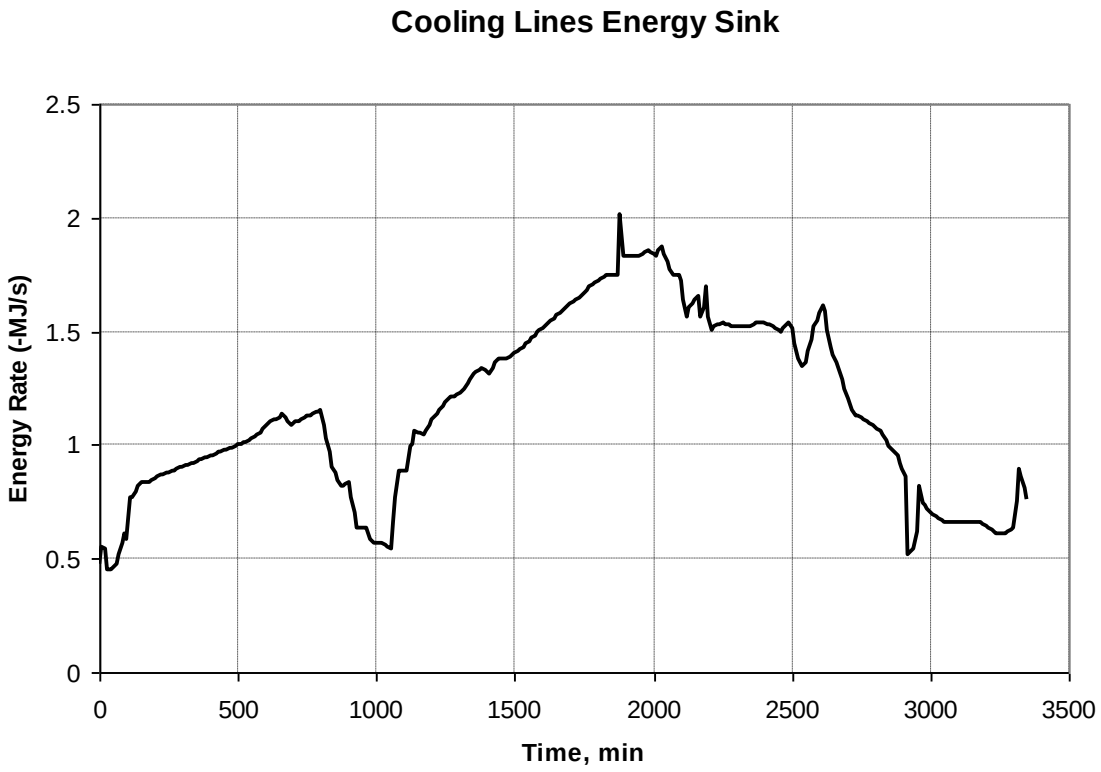

Figure 4-100 Depiction of the total energy removal for the cooling lines supporting light gas sampling equipment during the E11.4 test.

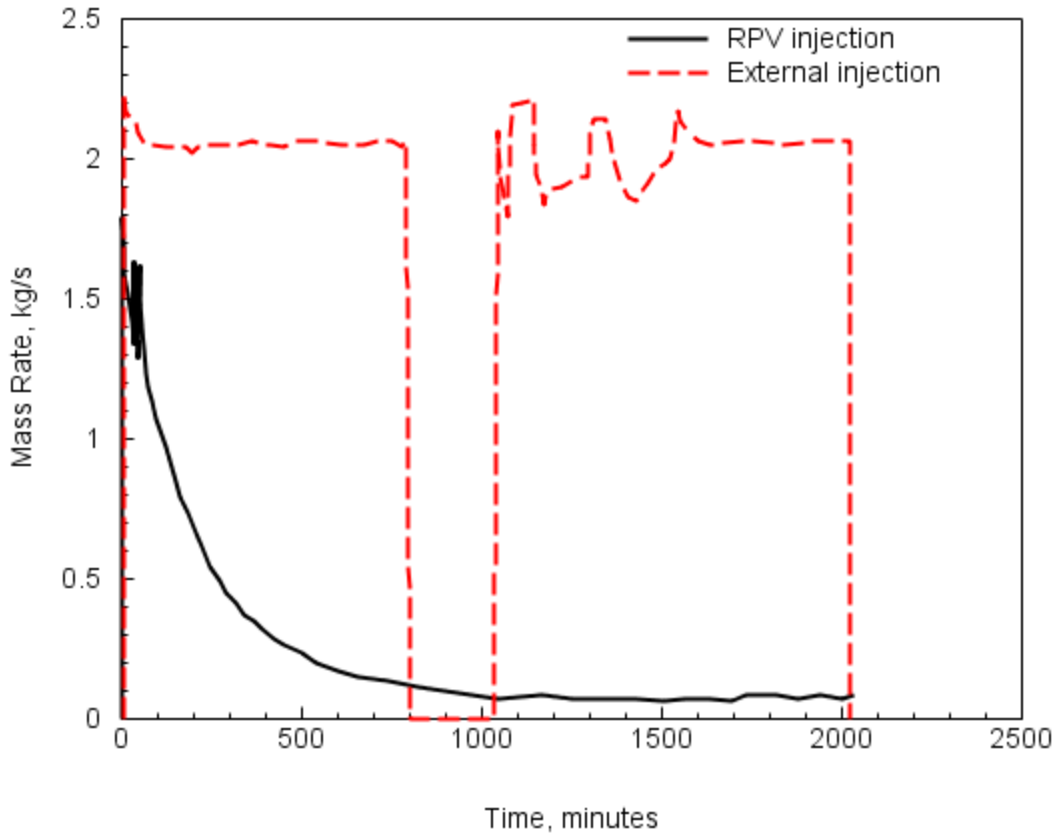

Figure 4-101 E11.4 RPV and external steam sources during the heat-up portion of the test.

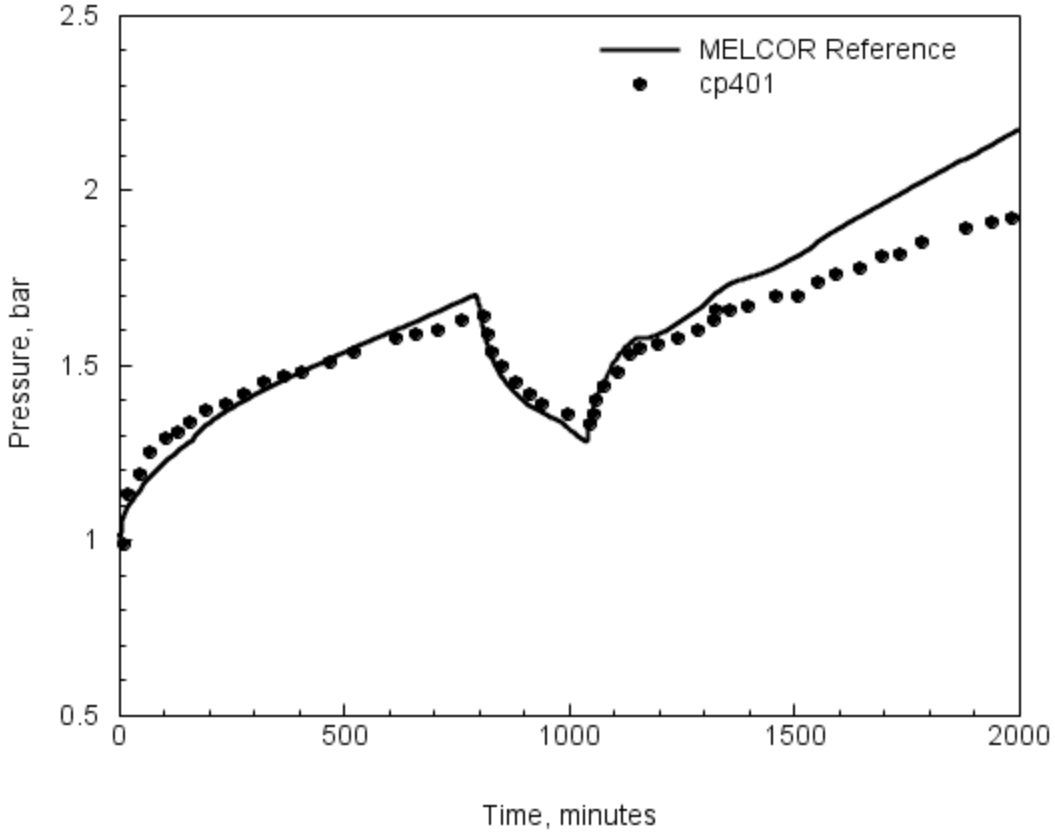

Figure 4-102 Comparison of MELCOR pressure calculation with measurement for the HDR E11.4 heat-up period.

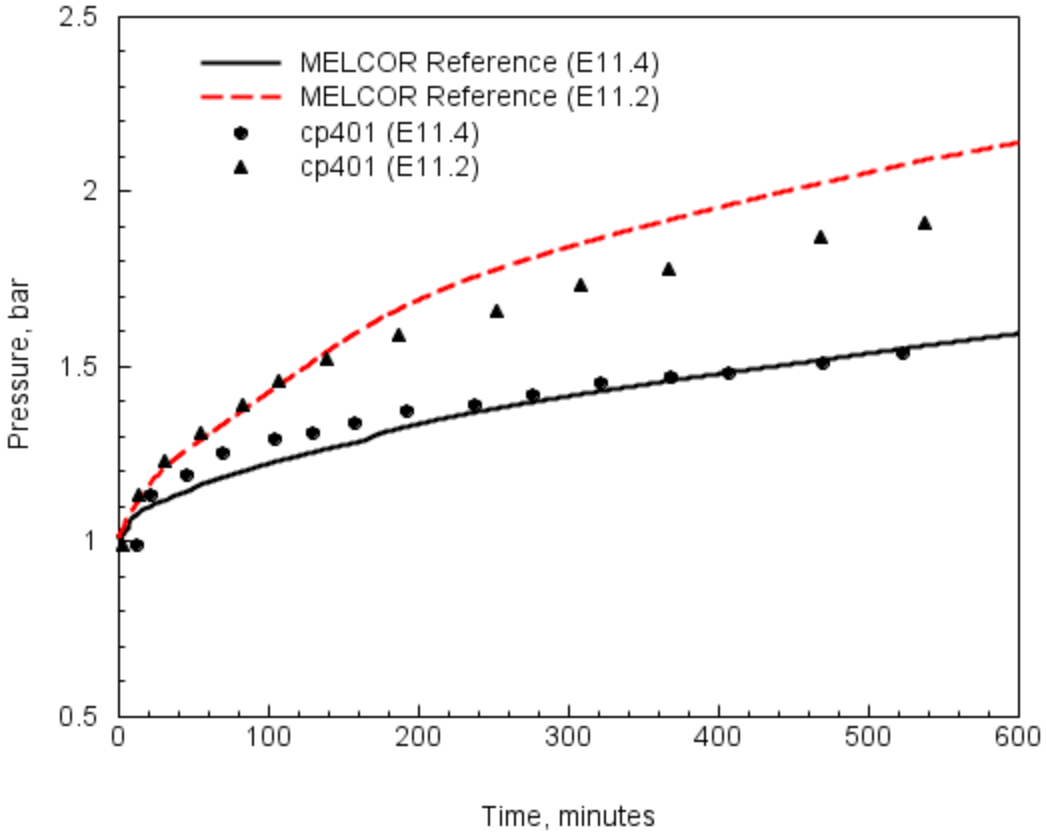

Figure 4-103 Comparison between the E-series pressure measurements and MELCOR reference calculations during a portion of the test heat-up period.

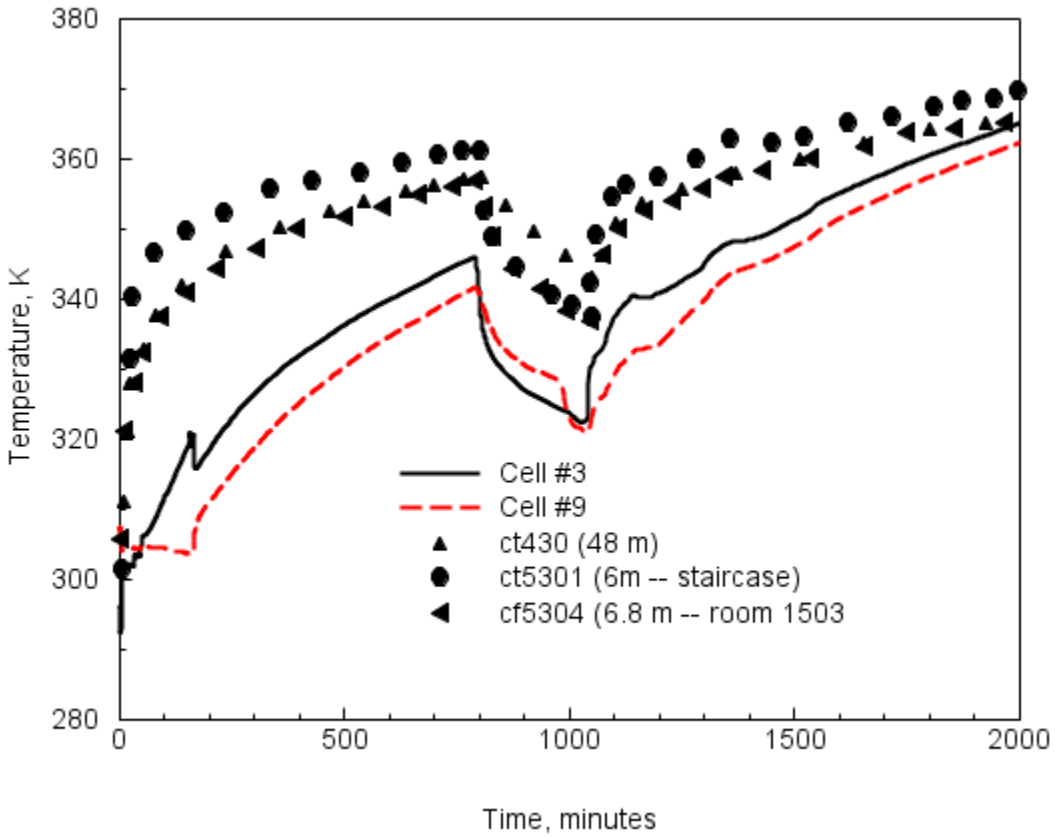

Figure 4-104 Comparison of MELCOR calculated and measured local temperatures during the heat-up period of the E11.4 test.

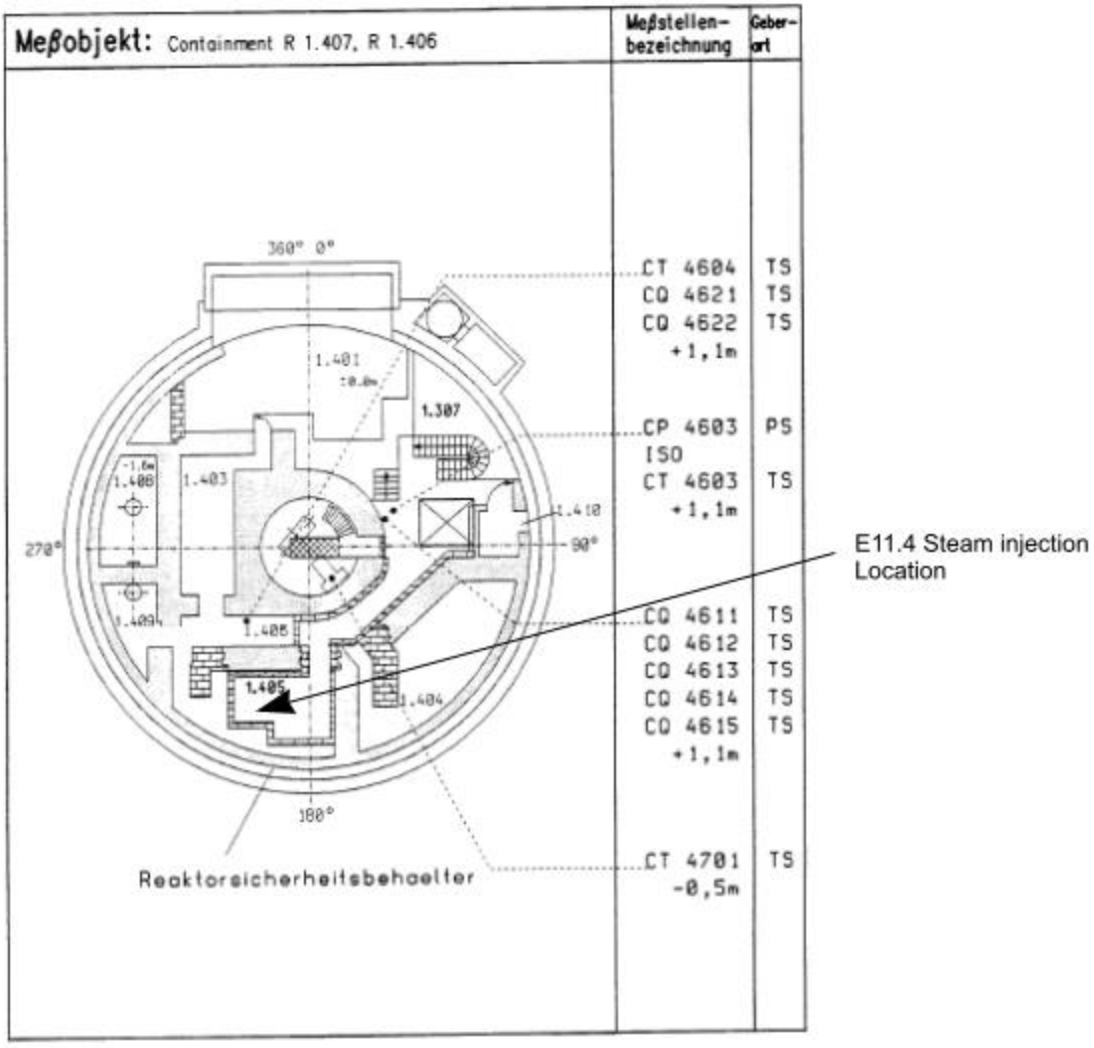

Figure 4-105 Steam injection room for the E11.4 test.

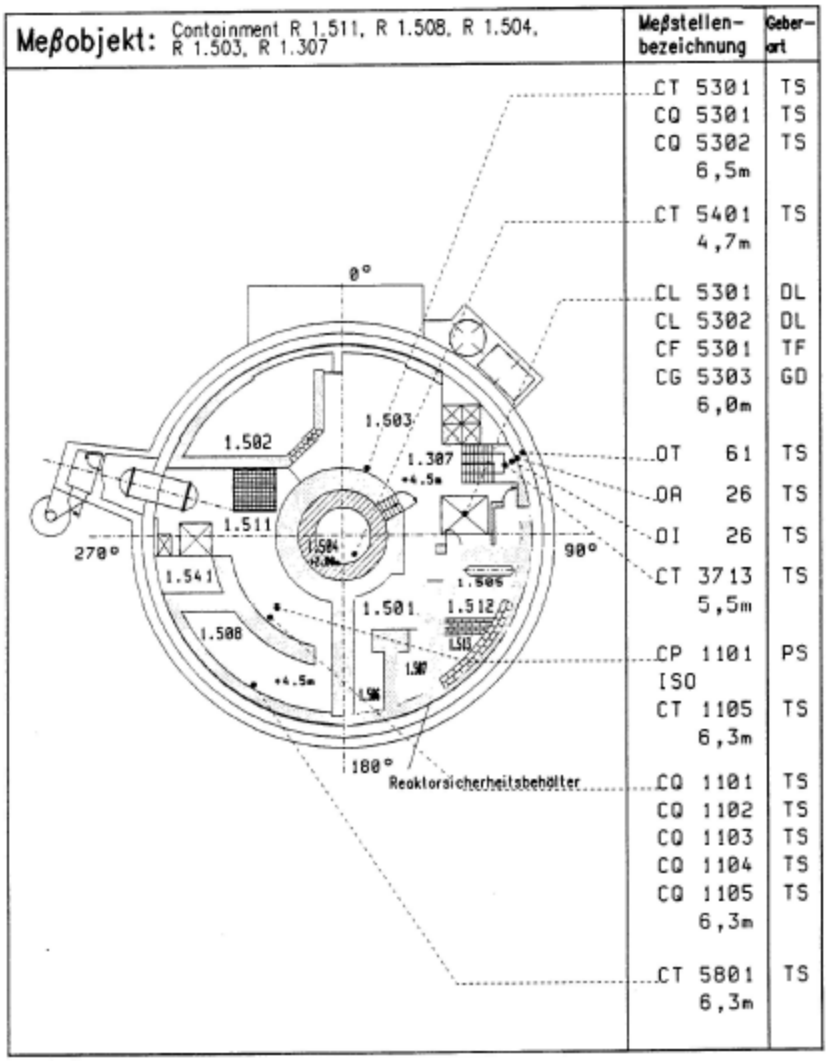

Figure 4-106 Level 1500 in the HDR facility with the ct5301 sensor located in the vicinity of the staircase and the ct5304 sensor located in room 1503 some distance away from the staircase and out of the pathway of the rising steam plume.

4.5.2 Sensitivity Evaluation

Three sets of sensitivity calculations were performed for the HDR E11.4 test involving the following modeling categories: 1) concrete thermal properties 2) film thickness modeling (dynamic vs. EnforceMax), and 3) nodalization scheme (15CV vs. 48CV). The choices are identical to those sensitivities discussed above for the E11.2 test.

Concrete Thermal Properties

Shown in Figure 4-107 is the pressure comparison for the reference calculation that was run with CONTAIN concrete properties and an identical calculation with concrete properties specified by Project HDR. As noted previously, the CONTAIN properties have a higher density, specific heat capacity, and conductivity, which would be more consistent with concrete having some migration of water taking place during the heat-up period. The Project HDR specified properties correspond to dry concrete.

Film Thickness Modeling

The reference case was calculated with the condensate film on structures determined using the dynamic film flow model. In the sensitivity case the film is calculated in a manner similar to the CONTAIN default method with the film thickness building to a maximum thickness of 0.0005 meters. In MELCOR, the CONTAIN method is invoked using the keyword EnforceMax. For slow pressurizations that simulate severe accidents the containment does not have local regions with high steam concentrations; therefore, the major resistance for condensation to structures is the atmospheric diffusion boundary layer next to the structure surface. Consequently, energy transfer during the test is only slightly affected by film resistance. Figure 4-108 shows this low degree of sensitivity to condensate film modeling.

Nodalization

The reference case nodalization scheme was coarsely specified in the lower and mid-containment levels. To better approximate local conditions in the regions above the source injection, the containment was subdivided into more cells as detailed in Table 4-11. Figure 4-109 and Figure 4-110 show the pressure and local temperature comparisons for the two nodalization schemes. There is no improvement in the pressure prediction by a more detailed nodalization, but there is a significant improvement in the local temperature calculation with the 48CV model. It is difficult to use the global energy transfer as a measure of goodness for a calculation since there are a number of reasons why energy transfers may be either over or under predicted (as demonstrated with the sensitivity case for thermal properties of wet vs. dry concrete).

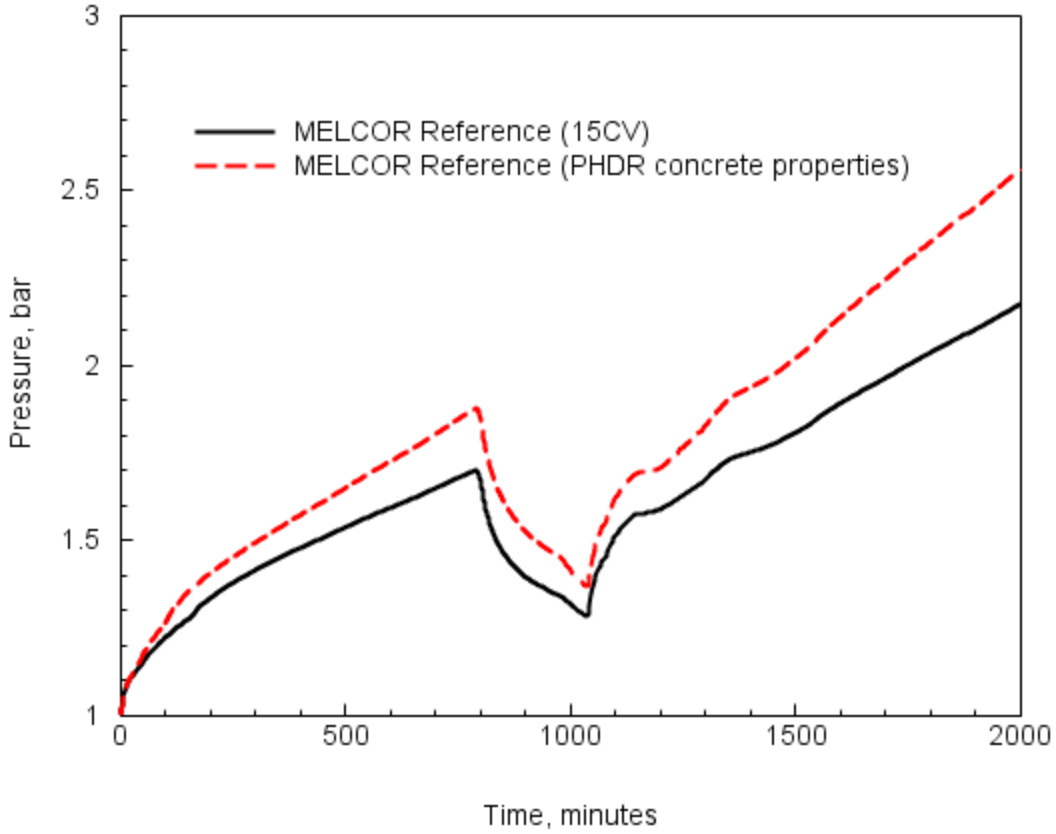

Figure 4-107 **Comparison of MELCOR calculated pressure for the reference case run with CONTAIN concrete thermal properties and an identical calculation run using the PHDR concrete properties. In this comparison the higher valued CONTAIN properties simulate wet material versus the PHDR material that is assumed to be dry.**

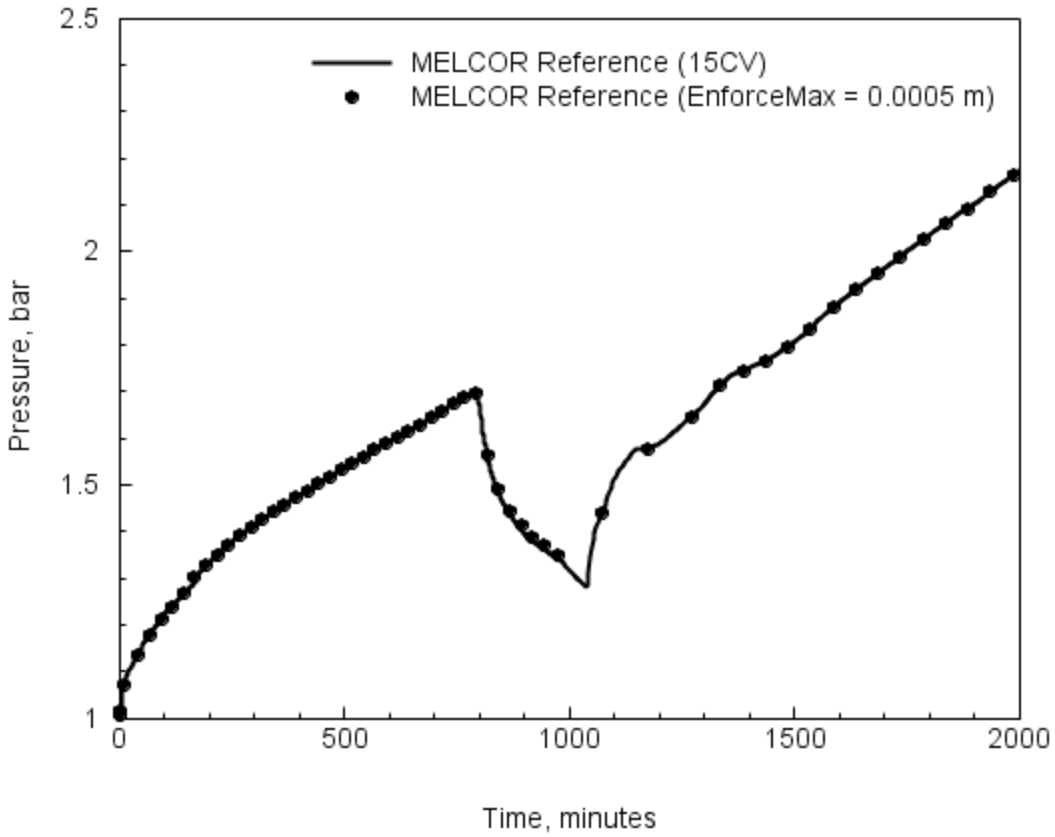

Figure 4-108 Comparison of MELCOR calculated pressure for the reference case with dynamic film modeling and a sensitivity case run with the film maximum thickness set using EnforceMax = 0.0005 meters (CONTAIN default).

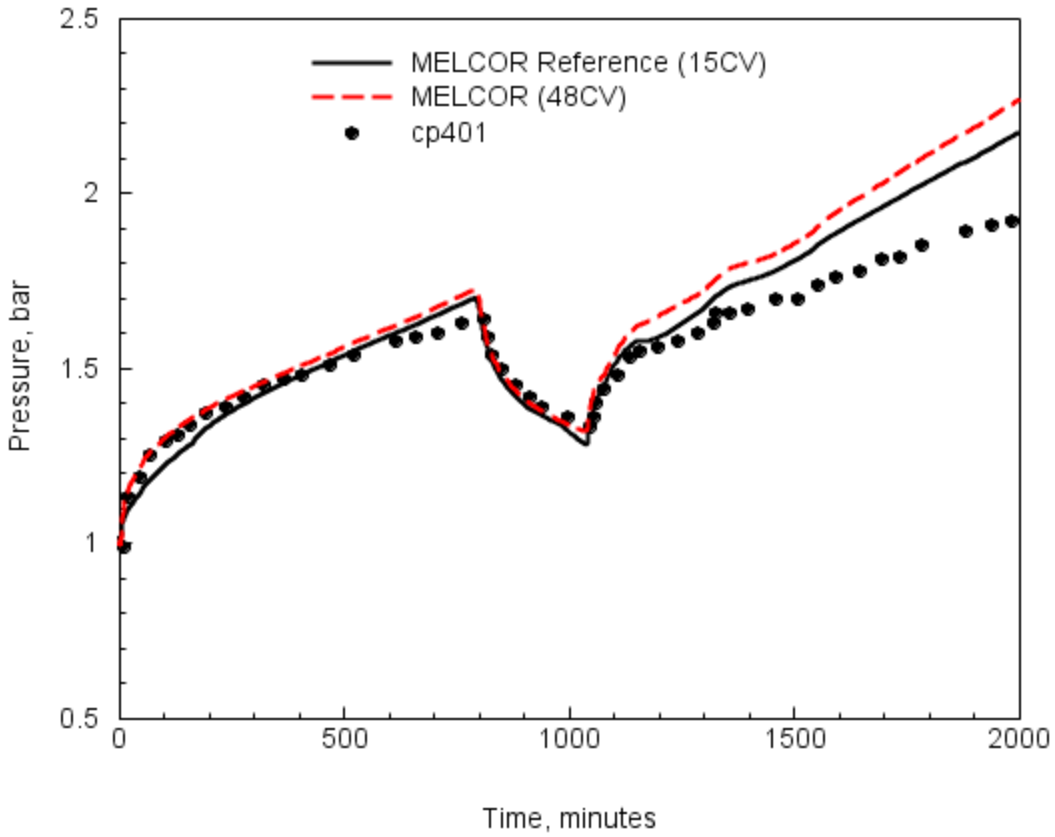

Figure 4-109 Comparison of MELCOR calculated pressure for the reference case nodalization 15CV and a more detailed 48CV nodalization scheme.

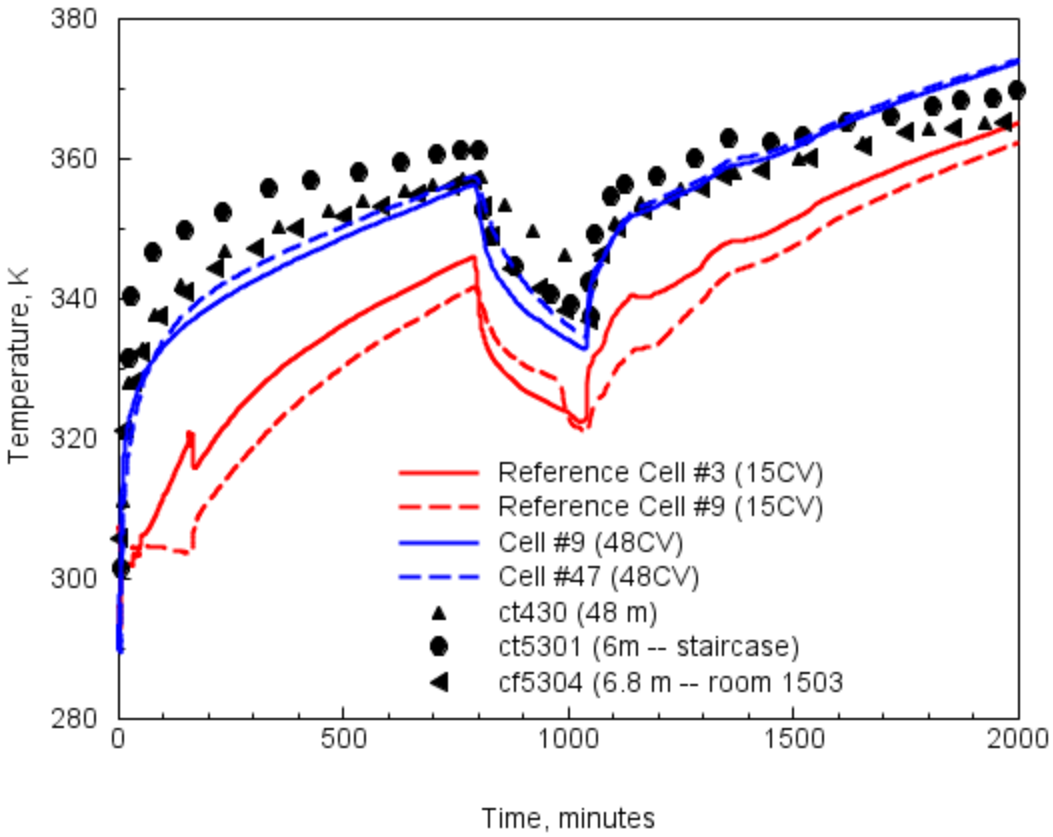

Figure 4-110 Comparison of MELCOR calculated temperatures for the reference 15CV nodalization and the more detailed 48CV nodalization scheme.

4.5.3 Benchmark

The CONTAIN calculation for the HDR E11.4 test was run with a 48CV input deck. Shown in Figure 4-111 is the pressure comparisons for the 48CV nodalization scheme calculated with MELCOR and CONTAIN. The CONTAIN pressure calculation shows an overall better prediction of the pressure; however, the improvement is slight since the advantage of the hybrid flow solver is minimum for a nearly well-mixed containment space, due to the low injection source in test E11.4. Figure 4-112 shows the temperature comparisons for the lower and upper containment regions. The general behaviors are predicted well, with a slight under prediction for the lower containment temperature that may be an outcome of the reduced circulation that is typically a feature of the CONTAIN hybrid flow solver. Both codes however do a good job of prediction both pressure and local temperature for the HDR E11.4 test for the very long heat-up period.

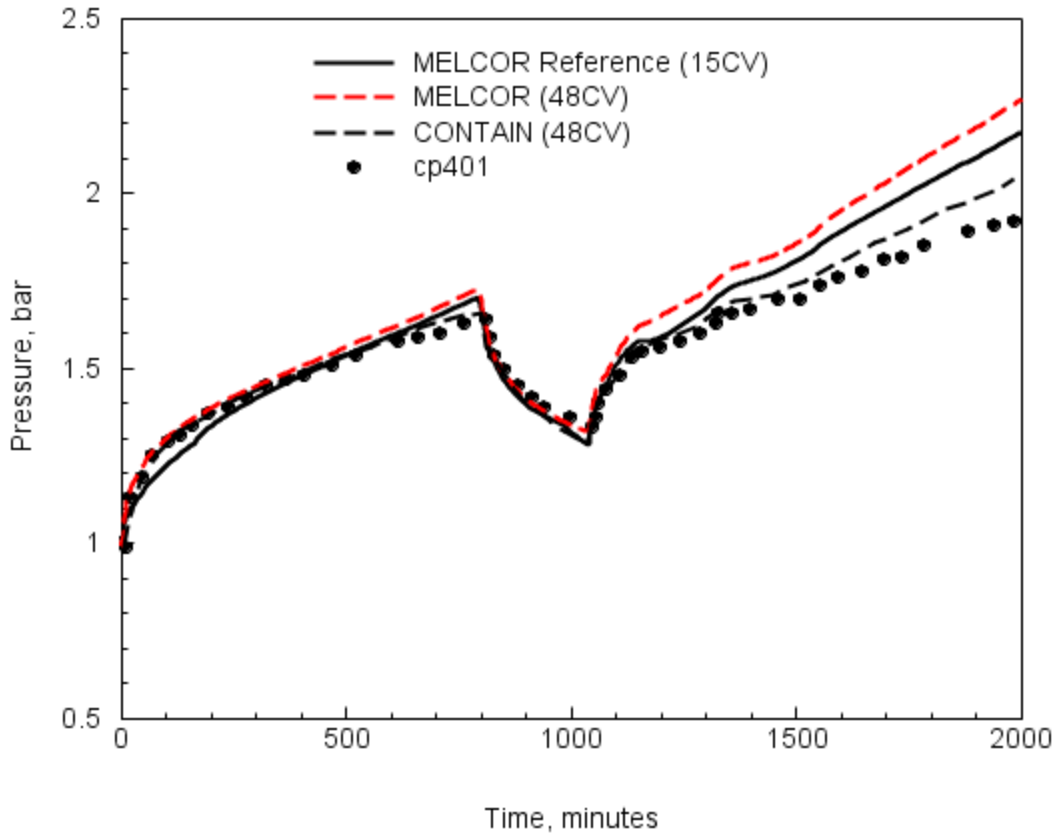

Figure 4-111 Comparison of MELCOR and CONTAIN pressure calculations for the HDR E11.4 test.

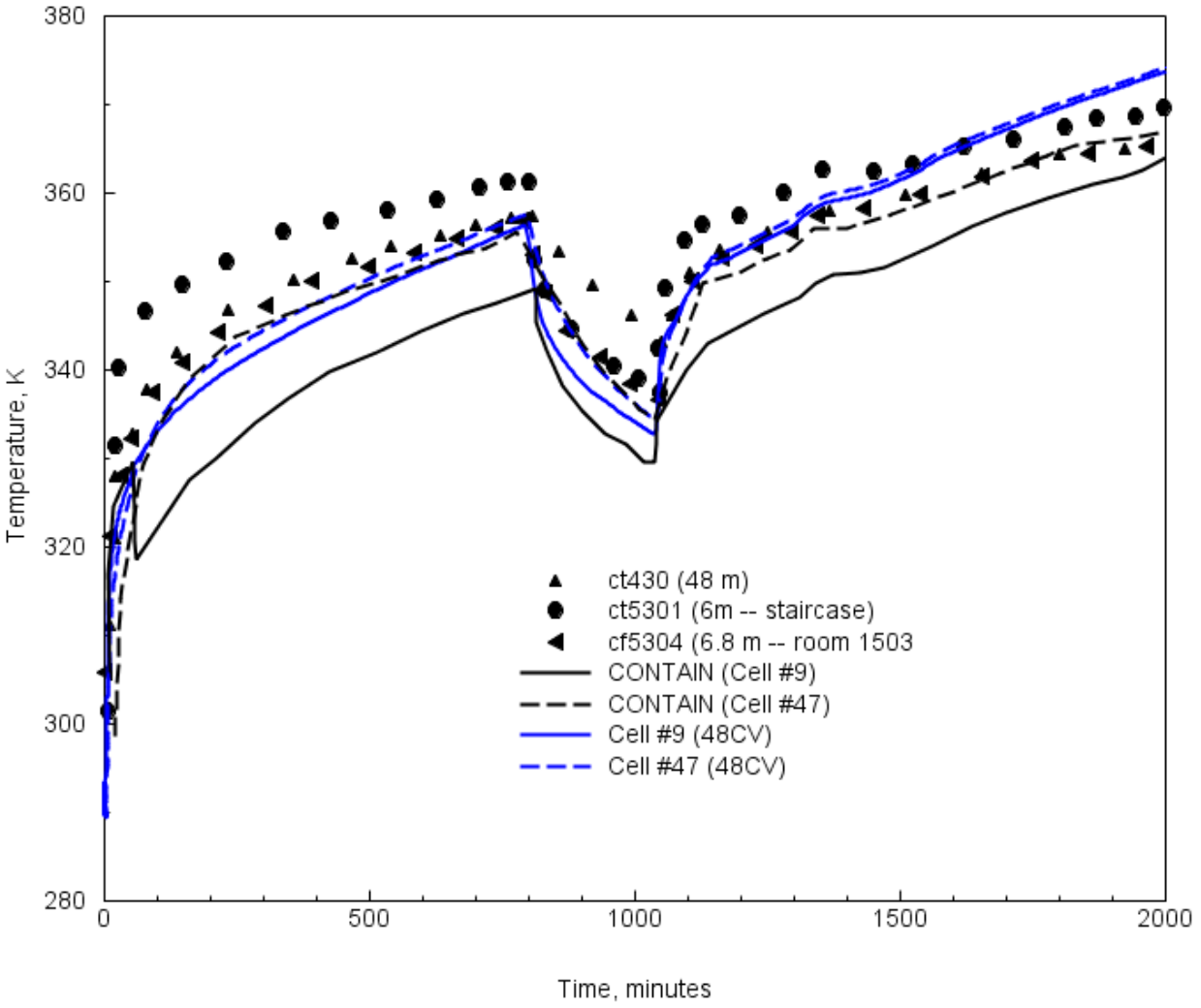

Figure 4-112 Comparison of MELCOR and CONTAIN temperature calculations for the HDR E11.4 test.

5. SUMMARY OF FINDINGS AND CONCLUSIONS

In order to assess the adequacy of containment thermal-hydraulic modeling incorporated in the MELCOR code, a large scale HDR containment test facility was analyzed. These tests are a series of blowdown experiments in a large scaled test facility; including some tests with the addition of hydrogen release which are intended to simulate a variety of postulated breaks inside large containment buildings. The key objectives of this MELCOR assessment are to study: (1) the expansion and transport of high energy steam-water releases, (2) heat and mass transfer to structural passive heat sinks, and (3) containment gas mixing and stratification.

A series of single-cell and multi-cell calculations were performed to demonstrate the effect of code, user, and experimental uncertainties on predicted gas pressure and temperatures. The result of this effort is a conclusion that the MELCOR code is capable of providing reasonable predictions and is comparable to the CONTAIN code in this area. This study has also demonstrated the complexity associated with building an ASM of a containment experiment or postulated accident, with implicit demands on the user knowledge base. A few modeling short-comings were identified, but these typically involved low ranked phenomena or were of a nature that conservative results were obtained. However, over-mixing was observed in local temperature comparisons and more noticeably in gas concentrations in the severe accident representative tests, resulting in determination of lower gas concentrations.

5.1 Reference Calculations

The reference calculations are presented as baseline examples to introduce discussions on modeling while providing a reference for subsequent discussions involving sensitivity calculations. In most instances, the reference calculations are established using modeling choices that would typically be applied in the analysis of containment response of postulated accidents, that is closer to "best-estimate" predictions but inherent conservatisms are recognized, e.g., natural convection condensation modeling during blowdown experiments.

In all the reference calculations, the maximum containment loads (pressure and temperature) were either calculated with very good accuracy, or in the case of blowdown pressure and temperatures, calculated with conservatism(s) using the default options in the code. There were no cases where the maximum pressures were under predicted.

V44 (ISP-16).
The V44 test was characterized by a two-phase blowdown within a relatively small break room. Therefore, the amount of suspended liquid water in the break room atmosphere during the short-term period during the blowdown is expected to be high. The suspended liquid effect is to increase break room pressure over an otherwise pure steam/gas atmosphere by raising the fluid density. Predicting the effects of suspended liquid water on the pressurization of the break room is the focus of the short-term analysis by MELCOR, where the suspended liquid is modeled via the aerosol physics model (RN package). In this case, the inclusion of liquid mass in the fluid density prediction is shown to improve somewhat the pressure and pressure differential predictions over a sensitivity case where liquid water is removed from the atmosphere. The CONTAIN code, that neglects aerosol mass in its interaction of aerosol/gas transport equations, more appropriately

simulates a MELCOR case that eliminates suspended water in the atmosphere (i.e., dropout and NOFOG). Similitude, with respect to improved short-term pressure response of the V44 test predicted by both CONTAIN and MELCOR, is observed when liquid water is retained in the atmosphere by parameter settings rather than invoking aerosol physics.

The peak pressure measurement is observed to be over-predicted by both the MELCOR and CONTAIN codes using the small (33 cell) nodalization of the HDR facility. A single-cell MELCOR calculation showed even a larger over-prediction trend. Parametric simulation of forced convective condensation tended to reduce the degree of over-prediction, but the lack of convective velocity data for the test makes quantifying this phenomenon (forced convection) problematical. It is note, however, that both the MELCOR and CONTAIN codes predict equivalent medium-term pressure and temperature profiles.

T31.5 (ISP-23 and Project HDR exercise).
The HDR test T31.5 was similar to the V44 test with the exception that the pipe rupture was into a significantly larger break room. Consequently, the density of suspended water within the break room during the short-term blowdown period was therefore smaller. With a smaller contribution to the fluid density, the short-term pressurization for both MELCOR and CONTAIN codes showed improved agreement for pressurization compared to the V44 analyses.

The Project HDR exercise that extended the T31.5 calculations into the long-term period (0 to 60 minutes), confirmed that MELCOR was over-mixing the gas/steam concentration compared to both measurements and CONTAIN predictions for local temperature.

E11.2 (ISP-29).
The HDR test E11.2 was a simulation of a small break LOCA scenario to assess severe accident thermal hydraulic conditions with a light gas release (hydrogen simulant). The steam release time was extended to hours in order to provide pre-heating of the facility. The pre-heating period was analyzed with the MELCOR code using a 15-cell nodalization of the facility. The release location for pre-heat steam was approximately mid-elevation within the HDR facility. Consequently, stratification tended to dominate as the phenomenon affecting the accurate prediction of facility pressurization. Unfortunately, other issues with the test procedure (characterization of instrument cooling) and uncertainties with concrete wall properties diminished the ability to quantify stratification modeling as the main contributor to the observed variations between measured and calculated pressurization. In any case, the E11.2 test did focus attention on modeling long-term gas distributions using a lumped parameter code, especially the ability to predict light gas distribution within a facility pre-conditioned by a small break LOCA event.

The comparisons between light gas concentration observed and calculated emphasized the shortcoming of a lumped parameter for extreme cases where regional stratification and plume behavior dominate mixing processes. During the light gas injection period the MELCOR code tends to underestimate light gas concentration measured in the dome region of the facility and overestimate concentrations in the lower regions of the facility. This is a classic example of the over-mixing tendency of the lumped parameter model. In contrast, the CONTAIN code with the hybrid flow solver shows improvement in its ability to predict light gas concentrations throughout the facility. It is also noted that the over-mixing behavior is much more obvious when observing

the comparison for light gas distribution than local temperatures. This observation may be partly explained by the compensating effect of heat and mass transfer on temperatures contrasted by a much smaller effect on gas distributions. Therefore, the ability to predict gas distributions should be a better reflection on the capability of the code to accurately model mixing processes.

E11.4 (Project HDR test).
The E11.4 test was another small break LOCA event simulation, but with the pre-condition steam injection at a low elevation location. The low injection tended to minimize stratification within the facility producing regional conditions more representative of a well-mixed atmosphere, at least more mixing than the E11.2 test with the mid-elevation injection. Consequently, the MELCOR predictions of local temperatures were improved for the E11.4 test, and the pressurization calculations also showed a marginal improvement over the E11.2 test application. When compared to the CONTAIN code regional temperature predictions, the MELCOR code showed a slight improvement in the ability to predict temperatures in the lower elevations of the facility, which again can be explained by the well-mixed conditions observed and that are slightly under-predicted in this case with the CONTAIN hybrid flow solver.

5.2 Sensitivity Calculations

Sensitivity calculations are performed to assist in determining the relative importance of components to the calculational assessment. Assessments of the code modeling are aided significantly by the modeling methodology in the code; that is a physically-based modeling method which is the foundation of the MELCOR code (for example, the HMTA modeling method), allows for meaningful variation of physically identifiable parametric inputs. However, in the more complicated integral case studies, such as HDR, the user induced uncertainties often dominate as the likely source of simulation uncertainty.

Overall, the sensitivity calculations affirmed several common finding demonstrated prior to this study using other codes, such as CONTAIN.

The HMTA method of modeling heat and mass transfer for atmosphere-to-structure and atmosphere-to-spray droplets is a validated method for the conditions expected in containment atmospheres. This finding was made possible in part by user access to physically based parameter choices that are available in the code through input options. In all cases, default options were found appropriate for predicting the variety of mass and heat transfer conditions expected in domestic plants during postulated accidents.

In terms of the enhancement effects, that is, those that increase maximum containment loads, the default options were always found to result in conservative estimates. Additionally, modeling options which enhanced the conservatism of estimates, e.g., selection of flashing model, liquid entrainment, etc. provide guidance for performing peak pressure analyses.

Nodalization, an area of user influence, was quantitatively shown as affecting both short-term differential pressure calculations and long-term gas mixing behavior. Some significant over predictions in lower compartment temperatures were observed when water redistribution and atmosphere interaction were neglected. These over predictions show the difficulty associated with

predicting degrees of superheat throughout a facility. Since these cases involved only small atmospheric energy increments, the local over predictions resulted in small incremental pressure deviations, and also imply small errors in postulated equipment heating.

Additionally, we have studied the effects of material property specifications and initial and boundary conditions on thermal hydraulic and gas distributions. For instance, the effect of too little steam circulation below the mid-elevation injection in the E11.2 experiment has been noted as one of the more probable reasons for late-time over pressure prediction that has been repeatedly mentioned in the open literature. That, coupled with what appears to be an obvious problem regarding the use of low humidity thermal properties for concrete heat sinks with deteriorated surface coatings, would improve the pressure comparisons presented for the reference calculation.

Although a few sensitivities have been conducted using a single cell representation of test facility, this simple geometric model is generally shown as being too inaccurate for the analyses required in most testing procedures. Multi-cell analyses are clearly preferred when the injection location is elevated (such as HDR V44, T31.5, and E11.2). In all studies where stratification was observed, the hybrid flow solver (which uses a combination of donor and average flow path density to determine gravity heads) performed favorably when compared with experimental data, but to an older method of formulating gravity heads by using averaged densities only. The over-mixing of gases predicted by the old method has been simulated through a user input option and the improvement with the default hybrid flow solver has been confirmed. The studies on gas transport, especially as denoted by comparisons of measured and calculated steam and light gas concentrations, show that the lumped parameter (inter-compartmental) representation is adequate for performing containment safety analyses (in most cases, stable mixing conditions are expected to occur).

5.3 User Guidelines and Implications for Plant Analyses

From the perspective of full plant analyses, the distortion of geometric and source scaling in the tests generally benefit the viewpoint that lumped parameter codes are reliably conservative computational tool for predicting containment responses in design basis plant analysis. It was shown that in both HDR (HDR V44 and T31.5) that the default option for the HMTA model results in significant (20-50%) over-predictions of maximum pressures during experimental blowdown events. In each facility and test procedure, however, the amount of short-term heat sinks and source rates were distorted in such a way that the energy transfer processes during the blowdown event are overly emphasized. Therefore, the tendency of the code to over predict pressure (an indicator of atmospheric energy content) will be reduced for plant analyses as the importance of energy transfer to structures is also reduced due to geometric and time scaling. The over predictions that have been observed in this assessment report are therefore upper bounds on the degree of over prediction expected in plant analyses (assuming the default options for calculating flows along structures and the algorithm for mixed convection are used).

The HDR facility has been used as a testing platform for codes calculating gas transport processes. Its utility however for validation has probably been over emphasized in the literature, especially with respect to the severity of several gas distribution tests that, as a result of geometric scale distortions are not considered representative of postulated conditions expected in domestic

containments. This statement is applied to the elevated injection test of the E-series. As noted, the HDR facility is 1) configured as a very complex, compartmentalized facility, with 2) a large aspect ratio, and 3) tested, in the case of the E11.2 test, using a procedure (location of the injection) and sensitive loop geometry (from the standpoint of gravitation heads and exposed heat sinks) that puts a great deal of importance on the requirements to model small circulating flows for prolonged periods. In comparison to domestic containment designs, the HDR facility is too complex; having too high of an aspect ratio, and in the case of E11.2, used for a scenario that probably over emphasizes the impact of small circulating convection loops, compared to the types of postulated plant accident scenarios. The distribution test E11.2, therefore, is an interesting test for the extreme testing of gas transport and mixing code models. The non-prototypic aspects of the facility and test procedure are the principal factors that make the E11.2 test an extreme test.

Each test characterized by a low injection points where good mixing was exhibited, the MELCOR calculated predictions of the thermal hydraulics and hydrogen distributions were in very good agreement with data. In domestic plants, the likely locations for injections initiated by postulated LOCAs are situated low inside containment, and therefore the containment should be close to a well-mixed environment.

One of the more useful aids to new users of a code are a set of input decks that transition from the simple to the more complex simulations that represent actual plant containments along with postulated accident scenarios. For this reason, and archival purposes, the input decks for all reference calculations are maintained in a supplement document [Til18]. These decks may be consulted to acquire insights in determining the models and input that may be considered for performing plant containment analyses.

In general, containments should be analyzed using a multi-cell representation of the free volume when local versus global features are an important factor (pressure differentials, equipment qualification, etc.). Maximum pressure predictions can often be calculated conservatively using a single-cell representation of the containment; however, it was noted in this report that depressurization (i.e., the pressure relaxation period after the blowdown phase) may not be predicted conservatively with such a restrictive geometric model. Multi-cell models do not necessarily mean a large number of cells; most gas and liquid water transport effects of importance to plant assessments can be modeled with 15 to 20 cells, while 3 to 6 cells in the open region above the operation deck is acceptable in most cases.

The default heat transfer calculations in MELCOR and CONTAIN differ when calculating the Nusselt number and, by extension, the mass transfer due to the heat and mass transfer analogy. First, the convective heat transfer calculation is performed with different coefficients. To adjusted the convective heat transfer correlation, the default external flow multiplication constant used in MELCOR was set by adjusting sensitivity coefficient 4110(1) to a value of 0.14, similar to CONTAIN, and all convective heat transfer calculations performed in this report are presented with the external flow option. Second, CONTAIN calculates the Nusselt number as the greater of the natural and forced convection correlations, but the default approach applied in MELCOR uses Reynolds vs. Grashof number criteria to select the convection regime as either natural, mixed, or forced. The mixed regime is a linear interpolation between the natural and forced convection Nusselt number. As the criterion and inclusion of a “mixed” regime are not present in CONTAIN,

sensitivity coefficient 4060(1) was set to -1.0 to perform both the regime determination and Nusselt number calculation similar to CONTAIN, i.e. the maximum calculated Nusselt number for either forced or natural convection.

Variations in the values of pathway loss coefficients are generally in the range of C_F = 1 to 1.5. Long-term gas mixing, driven by buoyancy forces does not appear sensitive to nominal variations in these coefficients. However, subcompartment analyses (differential pressures) may be more sensitive to these coefficients, and difficult to determine a priori since highly transient water carryover effects are not modeled in the code. For this reason, an upper bound for loss coefficients (i.e., $C_F \sim 1.5$) should be used for breakroom exit pathways. Most analyses performed during quasi-steady state periods however can be formulated using a $C_F \sim 1$; this includes free (or open regions) and compartmentalized volumes.

It has been noted in this report that a tendency to over-mix an injected steam source can affect the accuracy with which a lumped parameter code like MELCOR can predict containment pressurization. However, for predicting large pipe rupture peak pressures that have steam flow driven by momentum forces the code errors due to mixing are typically less important than the neglect of a forced convection component to heat and mass transfer. Consequently, flow parameter settings via pathway loss coefficients to limit mixing within the containment during a blowdown are not recommended when the targeted application is peak containment loads.

When the pipe rupture is in a relatively small compartment and the injection is two-phase, a higher break room pressure and pressure differential is calculated and better approximated by simulating the suspended liquid water within the break room by either invoking the MELCOR aerosol physical models in the RN package, or more simply setting the maximum fog dropout density limit to a high value without invoking the aerosol physic package. Either method is essentially equivalent during the first few seconds of the blowdown when condensed water in the atmosphere is anticipated to be in a suspended state.

Later in the blowdown sequence, tens of seconds, aerosol removal by deposition will deplete the atmosphere of much of the suspended liquid water by the time that the peak containment pressure occurs. Therefore, if the targeted application is peak containment pressure, either the aerosol models via the RN package or the simple fog dropout model, NOFOG, causing liquid water removal at the end of timestep will give essentially identical pressure loading results.

In the case of two-phase blowdowns, there is also a decision that a user has to make regarding how the separation of phases should be modeled during the blowdown. The modeling choices are referred to as flashing options, whether temperature or pressure flash models. Sensitivity cases have been run for both the V44 and T31.5 two-phase blowdowns. For each test the specific setting for flashing model made only a small difference in peak facility pressure calculation. In each case however, there was a slightly higher peak pressure calculated for the temperature versus pressure flash model option. Therefore, temperature flash modeling where the two-phase blowdown is injected as water vapor into the atmosphere is the preferred model. Phase separation using the pressure flash model is more appropriately reserved for high energy line breaks in small rooms where the quality of the source stream is low and the degree of flashing is relatively small.

The subcompartment studies of the V44 and T31.5 tests showed a deficiency in the calculated differential pressure between the break room and adjoining compartments due to using the default choke flow model, further discussed in Appendix B. This model originally assumed the suspended liquid mass would not significantly alter the atmospheric density; therefore, the formulation ignored the effects of suspended liquid mass. However, with consideration of the break room scale and the high energy break, the suspended liquid density exceeded the default maximum fog density, which was relaxed for these analyses, promoting the inclusion of a new critical model which considered the effects of suspended liquid. The HFM was therefore added to the code and is recommended for all analyses. The HFM has improved comparisons with the V44 and T31.5 test results and is similarly present as the default CONTAIN model allowing for greater parity when performing analyses.

Although the HDR tests for small break LOCA tests have indicated some variations in containment load predications (pressure and temperatures) between the codes due to differences in models affecting gas mixing, these differences are likely reduced for situations where containment gas distributions approximate more well-mixed conditions. Such responses have been demonstrated in this report by comparing the MELCOR/CONTAIN pressure and temperature predictions of the E11.2 and E11.4 tests. Consequently, the absence of an improved gas stratification model such as the hybrid flow solver implemented in the CONTAIN code is of less importance for domestic plants having a more open containment space than the HDR facility, and which also have LOCA injections located at low elevations. Both the more open space containments and low elevation injections favor a well-mixed containment atmosphere. Therefore, both geometry and injection locations for actual plants would suggest that containment analysis performed with the MELCOR code would indicate improved performance with respect to containment loads observed calculated for the HDR tests, both short- and long-term.

In summary, as a result of code prediction for the HDR facility tests, and code benchmark exercises for these tests, MELCOR code input and parameter settings have been evaluated for various containment loading conditions: short-term pressure differential, peak pressure and temperature, long-term pressurization/de-pressurization, and local temperature profiles that may be of use for equipment qualification (EQ). Sensitivity calculations have been performed to identify conservative parameter settings and preferred nodalization schemes. Listed in Table 5-1 are recommended code inputs derived from code performance evaluations during the HDR tests analyses. The recommended input settings assume a multi-cell model of the containment, which has been demonstrated as an appropriate geometric model to address the various loading conditions mentioned above. A conservative assessment of loads, within the context of design basis containment analysis applied to PWR plants during LOCA type events, has been a focus for the recommended input settings. However, more extensive analyses and refined recommendations may be required for specialized applications, for example, in applications involving subcompartment analyses.

Table 5-1 Summary of MELCOR/CONTAIN Model and Parameter Settlings for Parity (P) and Corrective (C) actions.

Phenomena/ Process	MELCOR	CONTAIN	Comments
Mixing (intra-compartment):			
Buoyancy/ stratification	Implicit flow solver for lump-parameter formulation	Hybrid flow solver applied to lump-parameter equations	MELCOR flow solver implementation tends to over-mix stratified atmosphere more than the CONTAIN implementation. No parity fix or setting is available within the MELCOR code; whereas, CONTAIN allows for an mstable implementation that enhances mixing slight more than the MELCOR implementation – producing a bracketing of the MELCOR flows.
Transport (inter-compartment):			
Two-phase flow (pool/gas)	Combined flow in single flow path	Separated flow (pool and gas in separate paths)	MELCOR flow path geometry includes pathway heights to allow both gas and pool flow interface definition; whereas, CONTAIN models separate pool and gas pathway center elevations and includes inventory factors to adjust pool and/or gas flows accordingly. No parity fix is available to exactly match two-phase pool/gas flows.
Two-phase flow (disperse liquid/gas)			
Critical flow	Default model unable to reference - (C); Optional homogeneous frozen model (HFM) – (P)	homogeneous frozen model (HFM) – (P)	MELCOR default model for critical two-phase dispersed flow (atmosphere plus fog) is a non-conservative model that has no counter-part in open literature. Code reference manual incorrectly labels the model as a default critical model as the homogeneous equilibrium model (HEM) [To be corrected in future releases]. Recommend using the optional HFM, with parameter setting: CVH-ATMCS FMOD (version 2.x)
	Discharge Coefficient = 0.7 – (P)	Vena contracta factor = 0.7 – (P)	Discharge coefficient to account approximately for non-isentropic and non-ideal nozzle effects
Two-phase water injection:			
Flashing	Default water property is non-ideal EOS – (P)	Default water property is ideal EOS; optional non-ideal EOS activated for parity – (P)	Non-ideal EOS for water is based on water properties consistent with Keenan and Keyes Steam Tables for both codes. Recommend using non-ideal EOS for CONTAIN to establish parity between codes.
	Default flashing model is temperature flash (CV_THR IPFSW – FOG, 4406(1) = 50.)	Default flashing model is temperature flash (default model retains liquid water suspended in atmosphere)	Parity is observed for these models whether the nodalization is single or multi-cell. However, maximum pressure and temperature is typically not calculated with flashed liquid water retained in atmosphere. SC4406(1) is relaxed by increasing the maximum fog density to stop partial drop out of fog.
	Multi-cell configuration; blowdown cell with default temperature flash and CV_THR IPFSW = NOFOG – (P)	Single-cell configuration; pressure flash with optional SRV model – (P)	Unflashed water is dropped out in the CONTAIN code before mixing with containment atmosphere; whereas, MELCOR mixes unflashed water before dropout. The CONTAIN method can be simulated in MELCOR with a multi-cell configuration where the relatively small blowdown cell has fog removed in upstream flow before entering larger containment volume.

Table 5-1 (cont.)

Phenomena/Process	MELCOR	CONTAIN	Comments/Recommendations
Condensation heat and mass transfer:			
Non-condensables	Boundary layer Grashof number – (C)	Grashof transport properties evaluated with consistent boundary location definition	Small degree of conservatism with MELCOR Grashof definition
Film thickness	Single network film tracking as default – (P)	Single network film tracking as option – (P)	
	Film maximum depth model using EnforceMax – (P)	Default film overflow at maximum depth – (P)	MELCOR can model the maximum film thickness film treatment similar to CONTAIN to provide parity using the new EnforceMax record.
Convective heat transfer:			
Mixed Forced/natural	Default is linear interpretation between (Nu_{forced}, $Nu_{natural}$); option for max (Nu_{forced}, $Nu_{natural}$) – (P)	Default is max (Nu_{forced}, $Nu_{natural}$) – (P)	The CONTAIN default for mixed forced/natural flow appears to be a more appropriate formulation based on analysis of Wisconsin flat plate tests. Specify a negative value for SC4060(1) and MELCOR will use the larger Nusselt number.
Forced flow	Cell velocity based on default cell hydraulic area = volume/height; option to set hydraulic area, CV_ARE (2) CVARA – (P)	Cell velocity based on default cell hydraulic area = (volume)**2/3; STRUC HYDAREA – (P)	Cell velocities are typically of use for modeling duct (AP1000) and tube (ESBWR) forced convective condensation/evaporation heat transfer. Within containment volumes, for conservative analysis forced convective process are neglected by effectively setting the cell hydraulic area to a large value, so that $Nu_{forced} << Nu_{natural}$
Natural	Reset multiplier on Nusselt correlation = 0.14 – (P)	Default multiplier on Nusselt correlation = 0.14 – (P)	Significant validation test comparisons favor the CONTAIN default multiplier. Use SC4110(1) to specify the multiplier as 0.14 in MELCOR.

Table 5-1 (cont.)

Phenomena/Process	MELCOR	CONTAIN	Comments/Recommendations
Engineered Safety Features:			
Fan cooler	MARCH 2.0 fan cooler model with extensions, such as a factor to partition sensible and latent heat removal. Parity with CONTAIN code not readily apparent, except through sensitivity coefficient parameter 9001(2)	Mechanistic fan cooler model for partitioning sensible and latent heat removal based on heat and mass transfer analogy	MELCOR default sensible heat transfer coefficient is set to unity. A more appropriate setting appears to be 0.15 as indicated through parity studies. [The CONTAIN mechanistic fan cooler model will be available in MELCOR in future releases.]
Heat Exchangers	Integral model for parallel and counter flow heat exchanger based on the "Number of Transfer Units" (NTU) formulation	Integral model for parallel, counter, cross, and shell heat exchangers based on (NTU) formulation	Cross and shell heat exchangers not modeled in the MELCOR heat exchanger formulation.

6. REFERENCES

Fir85 Firnhaber, M., “ISP16: Rupture of a Steam Line within the HDR-Containment leading to an Early Two-Phase Flow – Results of the Post-Test Analyses,” CSNI REPORT No. 112, June 1985.

Gre92 Green, J. and Almenas, K., "Modeling of the HDR E 11.4 Experiment Using CONTAIN 1.12," Report to USNRC from College of Engineering, Nuclear Engineering Program, Materials and Nuclear Engineering, University of Maryland, College Park, Maryland, March 1992.

Hol91 Holzbauer, H., Wolf, L., and Cron, T., “Investigations on Long-Term Behavior of the Atmosphereand on Hydrogen Distribution in a Reactor Containment after a Large LOCA, Final Evaluation Report, Test Group CON, Experiment T31.5,” (in German), Technical Report PHDR 95-91, Karlsruhe, FRG, December 1991.

Hum15a Humphries. L. L., et al., “MELCOR Computer Code Manuals – Vol.1: Primer and User’s Guide, Version 2.1.6840,” SAND2015-6691 R, Sandia National Laboratories, Albuquerque, New Mexico, August 2015.

Hum15b Humphries. L. L., et al., “MELCOR Computer Code Manuals – Vol.2: Reference Manuals, Version 2.1.6840,” SAND2015-6692 R, Sandia National Laboratories, Albuquerque, New Mexico, August 2015.

Hum15c Humphries. L. L., et al., “MELCOR Computer Code Manuals – Vol.3: MELCOR Assessment Problems, Version 2.1.7347,” SAND2015-6693 R, Sandia National Laboratories, Albuquerque, New Mexico, August 2015.

Kar89 Karwat, H., "ISP23: Rupture of a Large-Diameter Pipe within the HDR-Containment," Vol. 1 and 2, CSNI Report No. 160, Committee on the Safety of Nuclear Installations - OECD Nuclear Energy Agency, Paris, France, 1989.

Kar91a Karwat, H., Letter to ISP-29 Participants, dated 12 February, Technishche Universitat Munchen, 1991.

Kar91b Karwat, H., Letter to ISP-29 Participants, dated 4 July, Technishche Universitat Munchen, 1991.

Kar92 Karwat, H., "OECD-CSNI-ISP29, Distribution of Hydrogen within the HDR Containment under Severe Accident Conditions -Final Comparison Report," Organization for Economic Cooperation and Development -Committee on the Safety of Nuclear Installations, August 1992.

Lee99 Lee, S. J., et al., “Benchmark of the Heiss Dampf Reaktor E11.2 Containment Hydrogen-Mixing Experiment Using the MAAP4 Code,” Nuclear Technology, Vol. 125, pp. 182-195, February 1999.

Mur96 Murata, K. K., and Stamps, D. W., “Development and Assessment of the CONTAIN Hybrid Flow Solver,” SAND96-2792, Sandia National Laboratories, Albuquerque, NM, 1996.

Mur97 Murata, K. K., et al., “Code Manual for CONTAIN 2.0: A Computer Code for Nuclear Reactor Containment Analysis,” NUREG/CR-6533, SAND97-1735, Sandia National Laboratories, Albuquerque, New Mexico, December 1997.

OECD99 Prepared by an OECD/NEA Group of Experts, “SOAR on Containment Thermal Hydraulics and Hydrogen Distribution,” June 1999.

Roy95 Royl, P., et al., “Validation of GASFLOW for Analysis of the Steam/Hydrogen Transport and Combustion Processes in Nuclear Reactor Containments,” Proceedings of the 13th Conference on Structural Mechanics in Reactor Technology, Porto Alegre, RS, Brazil, August 13-18, 1995.

Til92 Tills, J., "Analysis of the HDR Test E 11.2," Letter Report to USNRC from Department 6421, Sandia National Laboratories, Albuquerque, NM, May 1992.

Til02a Tills, J., Notafrancesco, A., and Murata, K., “An Assessment of CONTAIN 2.0: A Focus on Containment Thermal Hydraulics (Including Hydrogen Distributions),” SMSAB-02-02, USNRC ADAMS Accession Number ML022140438, July 2002.

Til02b Tills, J., Notafrancesco, A., and Murata, K., “CONTAIN Code Qualification Report/User Guide for Auditing Design Basis PWR Calculations,” SMSAB-02-03, USNRC ADAMS Accession Number ML022490381, August 2002.

Til08 Tills, J., Notafrancesco, A., and Longmire, P., “An Assessment of MELCOR 1.8.6: Design Basis Accident Tests of the Carolinas Virginia Tube Reactor (CVTR) Containment (Including Selected Separate Effects Tests), SAND2008-1224, Sandia National Laboratories, Albuquerque, NM, February 2008.

Til09 Tills, J., Notafrancesco, A., and Phillips, J., “Application of the MELCOR Code to Design Basis PWR Large Dry Containment Analysis,” SAND2009-2858, Sandia National Laboratories, Albuquerque, NM, May 2009.

Til18 Tills, J., Phillips, J., and Notafrancesco, A, “An Assessment of MELCOR 2.1: Containment Thermal-Hydraulic Tests in the Heissdampfreaktor (HDR) Facility : Supplemental Documentation of the Input Decks,” SAND2018-9883, Sandia National Laboratories, Albuquerque, NM, Sept. 2018.

Val83 Valencia, L., and Kanzleiter, T.F., “Blowdown Investigation in a Reactor Containment – Rupture of a Steam Pipe – Quick Look Report for Tests V42, V43, and V44,” Technical Report PHDR 38-83, Kernforschungszentrum, Karlsruhe, Germany, May 1983.

Val89a Valencia, L., Wolf, L., “Preliminary Design Report – Hydrogen Distribution Experiments E11.1 – E11.5,” Project HDR Safety Program, Karlsruhe, PHDR Work-Report Nr. 10.003/89, March 1989.

Val89b Valencia, L., “Input Data Set for E11.2 (Blind Calculations),” Project HDR Safety Program, Kernforschungszentrum, Karlsruhe, November 1989.

Val92 Valencia, L., et al., "Design Report - Hydrogen Distribution Experiments, E 11.1 - E 11.5," PHDR-Working Report No. 10.004/89, Kernforschungszentrum, Karlsruhe, Germany, August 1992.

Wen87 Wenzel, H. H., et al., "Blowdown- und Wasserstoffvertieilungsversuche Versuchsgruppe CON Versuch T31.5," PHDR 3.520/88, Kernforschungszentrum, Karlsruhe, Germany, December 1987 (in German).

Wen91 Wenzel, H., et al., “Quality Considerations of Major Direct and Indirect Measured Quantities During the Experiments of Test-Group E11,” PHDR Safety Program, Kernforschungszentrum, Karlsruhe, PHDR-Working Report No. 10.002/91, June 1991.

Wol83 Wolf, L., Valencia, L., and Kanzleiter, T., “Overview of the HDR-containment tests,” NUREG/CP-0048, Vol. 3, Proceedings of the U.S. Nuclear Regulatory Commission Eleventh Water Reactor Safety Research Information Meeting, Gaithersburg, Maryland, October 24-28, 1983.

Wol89a Wolf, L. and Valencia, L, "Experimental Results of the Preliminary HDR Hydrogen Distribution Test T31.5, Proceedings of the 4th International Topical Meeting on Nuclear Reactor Thermal Hydraulics, Karlsruhe, Germany, Vol. 2, p. 967, October 10-.13, 1989.

Wol89b Wolf., L. and Valencia, L., "Hydrogen Mixing Experiments in the HDR-facility," NUREG/CP-0 *105, Proceedings of the U.S. Nuclear Regulatory Commission Seventeenth Water Reactor Safety Research Information Meeting,* Rockville, MD October 1989.

APPENDIX A. PHENOMENA DESCRIPTIONS

The following descriptions of containment phenomena are intended to aid the reader in associating and understanding key phenomena discussed in this report. The phenomena are organized according to the layout of containment component and processes discussed in Section 3 and presented in Table 3-1 and Table 3-2.

A.1 Phenomena Identification for the Atmosphere Component

Pressurization/Depressurization

Multi-component gas compression/expansion

This phenomenon describes the physical behavior of compressible gas mixtures. It can be quantified through application of the energy equation and equation of state for gas mixtures. The phenomenon applies to a homogeneous mixture that is undergoing pressurization or depressurization primarily as a result of large additions or removal of single- or two-phase fluids. For example, in the case of a rapid blowdown of superheated steam into a single volume compartment, pressure and temperature are typically determined mainly through the accommodation of the injected gas mixture within the volume. Likewise, rapid depressurization of a containment due to catastrophic containment failure or venting will be determined by the phenomenon of gas depressurization as a result of an expansion processes. Since the atmospheric gas mixture can be two-phase, the phenomenon can also include the bulk processes associated with two-phase thermodynamic equilibrium that involve the partitioning of water between vapor and liquid during thermodynamic state changes.

Aerosol mass and energy exchange

Suspended aerosols can affect the state of the atmosphere in two ways. First, as a liquid they provide internal energy storage primarily as a result of the latent energy that is represented by their presence in the atmosphere, and the aerosols serve as a mass repository for condensed water vapor. As water aerosols form (due to bulk condensation) they are either deposited or settle out of the atmosphere. Therefore, by aerosol behavior processes (deposition, diffusion, agglomeration and gravitational settling) condensed water is removed from the atmosphere. When water aerosols are suspended in the atmosphere, the gas mixture tends to remain in a saturated state (condensation or evaporation). Secondly, as solid aerosols are injected into the atmosphere during a severe accident, the aerosols themselves may contain significant fission products inventories (Csl and CsOH aerosols), and they can alter the atmosphere state through decay heating of the atmosphere. This phenomenon description implies a broad range of supporting interacting phenomenon often categorized as aerosol behavior. However, the main phenomenon, referred to here, concerns the processes by which mass and energy is exchanged between suspended aerosols and the containment atmosphere.

Spray mass and energy exchange

Sprays are an engineering safety feature used in many plants to suppressed containment pressurization, acting as a contact mass and thermal sink to 1) condense steam and 2) cool the atmosphere. The mass and energy exchange processes associated with spray droplets are different from aerosols since the sprays are larger in size than aerosols and therefore are generally not in

thermal equilibrium with the gas mixture and, compared to aerosols, have residence times in the atmosphere of relatively short duration. AC power is required for spray operation.

Volume displacement due to pool filling/draining
The volume of atmosphere of a compartment may change as a pool is formed or drained. As the reactor coolant system, ECCS, and spray system liquid water is transferred to the containment building, the containment free volume will be reduced slightly. However, individual room volumes in the lower regions of the containment may be significantly affected such that these regions may undergo extensive flooding. The volume will increase again if the pool drains by gravity or by pumping to other compartments.

Atmosphere cooling by fan-cooler
Fans force gas mixtures to pass over cooling coils that extract sensible and latent heat (with accompanying condensate mass) from the atmosphere. AC power is required for fan cooler operation.

Mixing (Intra-compartment)

Jet-plume gas interaction/entrainment (localized)
Jet and plume behavior are involved processes driven by buoyancy, momentum, and shear forces. The interaction and entrainment that characterize the phenomenon is dependent on very localized momentum transport processes that occur in a free shear flow environment. For most injection scenarios, an unobstructed jet of hot or light gas will quickly develop into a buoyant plume. Since behavior of this jet-plume is dependent on the jet or buoyancy-driven momentum transport and entrainment processes, this component of the mixing process is classified separately.

Buoyancy/stratification (regional)
Buoyancy/stratification refers to circulation processes that take place outside of plume boundaries in the ambient gas region that usually represents most of the volume within a compartment. The phenomenon again involves buoyancy but in this instance the buoyancy of the fluid is distinguished not by local mixing patterns or large circulation loops; rather, the main feature of the mixing is described in terms of stability limits and stratification wherein a vertical density profile is established and maintained within an open compartment. A fully developed stable stratification for instance would have less dense gases overlying denser gases.

In situations where a light gas is injected into a heavy ambient gas, forming a buoyant plume, the ambient mixing will rapidly develop a stable stratification provided that the injection rate is not too large. In a fully developed state, circulation will have formed essentially a two layered distribution of lighter gases above the heavier gases. The circulation processes that are responsible for this end state typically do not depend on the details of plume or the entrainment processes near the plume boundary but depend on a basic phenomenon characterized by buoyant-driven flow (excluding momentum transport) within the ambient gas mixture. This type of mixing process is distinguished from other localized processes (jet-plume) and larger scale mixing and transport processes that involve convective loops established by gas/wall interactions or buoyant flows between various containment compartments, respectively.

Buoyancy/wall interaction (regional)
This mixing processes involves large circulation patterns that develop within a compartment as a result of the heating and cooling of gases along walls. Whereas the above mixing processes can be described completely assuming an adiabatic wall boundary, this process is dependent on mixing via circulation patterns developed as a result of gas/wall heat and mass transfer. For example, in an enclosure with a hot vertical wall that is opposite from a cold wall, a circulation loop will be set up where gases near the hot wall rise and along the cold wall fall. Even without a calculational model, it is quite apparent that a convection loop affecting mixing (constituent concentrations) will develop; in this case, the dominating phenomenon is buoyancy with mixing behavior dependent on the convection loops that develop.

Diffusion (turbulent)
This phenomenon is defined as a gas mixing process whereby a gas constituent mixes across an interface between two relatively well mixed fluids purely as a result of turbulent diffusion across the relatively small transition layer. In general, within the bulk containment atmosphere, diffusion is of second order importance compared to other containment mixing phenomena because the dimensions of the free volumes are large and the concentration gradients are, in most cases, quite small. Molecular diffusion, which is a much slower process, is generally not included in this category.

Spray dynamics
The interaction of falling spray droplets with the atmosphere will induce gas mixing processes. Small air vortices can be formed as the result of the hydrodynamic drag created by drops falling through the atmosphere - these vortices can in tum induce gas mixing. Large numbers of droplets together can form a virtual stream which creates a downdraft in the atmosphere gas by momentum transfer, thereby creating a regional convection loop.

Fan dynamics
Fan coolers are installed in some containments to provide air cooling by removing sensible and latent heat from the atmosphere gas/vapor mixtures at they pass over cooling coils. The mechanical action of the fans on the gases and vapors will induce mixing in the containment.

Transport (inter-compartment}

Buoyancy
Buoyancy is defined as a process or characteristic of an atmosphere by which less dense gases rise and denser gases fall. In the compartment mixing processes, buoyancy is considered the driving process primarily responsible for regional mixing patterns, such as stratification. On yet a larger scale, involving the transport of gases between compartments, buoyancy can also be a significant driving term that determines large convective loop flows within a containment. These loop flows transport gases and aerosols throughout the containment, and can also affect compartment mixing processes through the various inflows and outflows that develop.

Form and Frictional losses
Given a pressure differential between compartments, the rate of gas flow through a coupled path will depend on form and frictional drag that resists fluid motion. The characteristics of the flow

path may include transient features as implied by rupture disks, or composite form and frictional losses required for ventilation ducts and shafts.

Aerosol coupling
Aerosols are transported between compartments as the gas in which they are suspended flows from one compartment to another. Although the suspended aerosols (water or solid) are considered to be an integral part of the atmospheric component typically referred to as "gas" in the context of flows, they actually represent a separate field -- particles are coupled to the gas field by drag and inertia forces. In addition to the coupling forces, the presence of aerosols increases the effective density of the transported gas/aerosol mixture between compartments. Coupling is therefore a general term to group all phenomena (drag, inertia, density effects, etc.) that affect both the transport of aerosols in flow paths and also the gas flow as a result of the presence of aerosols in the flow. (Note: aerosol coupling as a result of decay heating, for radioactive aerosols, has been considered previously for pressurization/depressurization processes under the phenomenon heading, aerosol mass and energy exchange.)

Liquid water carry over
During rapid blowdowns, a portion of the two phase water injection will be in a liquid water form (large mass size compared to water aerosols) suspended in the flow stream and transported out of the break compartment.

A.2 Phenomena Identification for the Structure Component

Interior heat transfer

1-D transient conduction
1-D transient conduction requires the solution of the generalized one-dimensional Fourier's energy transport equation for solids. The conduction solution should include all thermal resistances such as paints, composites (steel lined concrete), and small air gaps that create a contact thermal resistance.

2- or 3-D transient conduction
2- or 3-D transient conduction is similar to the 1-D transient conduction description with addition of two or three dimensions to the Fourier's energy transport equation.

Interior mass transfer

Outgassing (concrete)
At elevated temperatures, both H_2O and CO_2 gases will be released from concrete structures that are not lined. Both evaporable and bound water are the sources for a steam release.

Surface Sensible Heat Transfer

Spray/aerosol deposition or impingement
Spray droplets may contact wall surfaces as they fall through the containment building and therefore be a source of mass and enthalpy transfer to the surface films. Water aerosols may also

be deposited on wall surfaces transferring mass and enthalpy. These deposition processes are a result of various effects, including settling, diffusion to surfaces, thermophoresis (a Brownian process causing migration of aerosols toward higher temperatures) and diffusiophoresis (deposition induced by condensation of water vapor on surfaces). Solid aerosols that contain fission products when deposited on surfaces can also transfer some portion of their decay heating to those surfaces on which they remain.

Free convection

Free convection for the process of sensible heat transfer at a structure surface refers to energy transfer as a result of buoyancy induced flow along the surface. In this transfer process, the induced flow is developed in a boundary layer adjacent to the heated or cooled structure. The induced boundary layer flow may be either laminar or turbulent.

Forced/mixed convection

Forced/mixed convection for the process of sensible heat transfer at a structured surface refers to energy transfer as a result of gas flow over the surface. When the gas flow is caused primarily by forces other than induced buoyancy in the boundary layer (fans, inter-compartment pressure differentials, free jets, etc.) the convection is referred to as forced. In cases where the induced buoyancy and forced flows each represent a significant transfer phenomenon required for describing the energy exchange, the processes are combined and this regime is referred to as mixed convection.

Radiation (structure to atmosphere)

This type of thermal radiation exchange involves sensible energy transfers between structures and an absorbing-emitting gas. The gas description may include the compartment atmosphere or more locally, a high temperature gas injection source.

Radiation (structure to structure)

Thermal radiation in this case refers to sensible energy exchanges between structures within an enclosure containing a participating gas.

Liquid film resistance

Film resistance refers to the thermal resistance that the film represents to the transfer of energy from the film surface to the wall structure. The resistance for a given film thickness will generally depend on the film flow regime, that is, whether the film flow is laminar or turbulent.

Liquid film advection

Liquid film advection refers primarily to mass and energy transfers in the film as a result of the film flowing along the structure surface.

Surface Latent Heat and Mass Transfer (condensation/evaporation)

Free convection

Latent heat and mass transfer is characterized by the transfer of vapor from/to the bulk to/from the liquid water film surface through a concentration boundary layer (diffusion resistance layer) that is formed as a result of induced buoyancy flow. The driving force for the film surface transfer is

the difference between the partial pressures of vapor at the surface and bulk. It is noted that mass transfers as a result of condensation can affect the containment volume concentrations by effectively enriching the noncondensible gas concentrations. This can be especially important for the hydrogen-air-steam mixtures since condensation will increase the hydrogen-air concentrations and can also de-inert a mixture.

Forced/mixed convection
Latent heat and mass transfer for forced/mixed convection is similar to that indicated for free convection except that the concentration boundary layer across which the vapor is transported has developed as a result of forced gas flows along the surface. When this boundary layer thickness is affected by both the forced and induced buoyancy flows, the flows have a combined effect and the entire mass transfer process is characterized as being in a mixed convection regime.

Transport (film flow)

Liquid film advection
From the standpoint of containment water inventories, liquid film flow will affect the amount of water on structures and the partition of water between all three containment components.

Interfacial shear (film/gas interaction)
When film and gas flow velocities are significantly different (relative velocities), the frictional drag of the gas flow can transfer momentum to the film flow. This interaction can therefore affect the transport of liquid along the surface. This type of interaction, by changing the flow characteristics of the film, can also affect the film thermal resistance and advection.

A.3 Phenomena Identification for the Pool Component

Mixing

Buoyancy/stratification
Temperature variations in the pool may preclude uniform mixing due to the buoyancy effect that tends to stratify the pool layers. This phenomenon is similar to the buoyancy/stratification processes occurring in the atmosphere as a result of gas layer density variations.

Bubble dynamics
Steam or air injection into pools (suppression pools, quench tanks) can agitate the pool, breaking up stratified layers.

Transport

Filling and draining
This process includes the addition and removal of water from pools mainly by gravitational flows (drain-down of condensate, overflow, or pipe flow). Pumping of liquids may also be included in this category.

Displacement (pressure driven)

Liquid may be displaced, as gases, through the action of pressure forces. For instance, the dynamics of vent clearing and suppression pool swell would be included in this category.

Interior Heat Transfer

Convection (flooded structures)
Structures that are flooded during an accident will have their surfaces heated or cooled by pool water. This heat transfer process will typically be characterized as convection (generally assumed to be free convection).

Boiling
Water in pools overlying or in contact with vertical hot surfaces may undergo local boiling, producing a source of steam to the atmosphere. Steam injected into pools may also result in local pool boiling; and, deposits of significant quantities of fission products may boil-off small pools. The boiling process will produce a source of steam to the atmosphere.

Steam condensation (bubbles)
Steam injected into pools (suppression pools) will form bubbles that will rise to the surface. Depending on the pool temperature and depth, a portion of the steam injected will condense, heating the pool water. The steam not condensed will exit from the pool and be considered a source of steam for the overlying atmosphere.

Surface Sensible Heat Transfer

Free convection
Sensible heat transfer at a pool surface may occur as a result of buoyancy induced flow above the surface. In this transfer process the induced flow is developed in a boundary layer adjacent to the heated or cooled pool surface. The induced boundary layer flow may be either laminar or turbulent.

Forced/mixed convection
Sensible heat transfer at a pool surface may occur as a result of gas flow over the surface. When the gas flow is caused primarily by forces other than induced buoyancy in the boundary, the convection is referred to as forced. In cases where the induced buoyancy and forced flows are both significant features required for describing the heat transfer, the processes are combined and this regime is referred to as mixed convection.

Spray/aerosol deposition
Spray droplets may deposit onto a pool surface as a result of gravitational settling and therefore transfer significant mass and enthalpy to the pool. Likewise, solid and water aerosols may also be deposited on pool surfaces. Solid aerosols may contain fission products which will add sensible energy to the pool as they decay (mass addition can usually be neglected). Water aerosols formed in the atmosphere can deposit on the pool surfaces thereby transferring mass and enthalpy to the pool.

Surface Latent Heat and Mass Transfer (condensation/evaporation)

Free convection

Mass transfer as characterized by the transfer of vapor from/to the bulk to/from the pool surface through a concentration boundary layer (diffusion resistance layer) that is formed as a result of induced buoyancy flow. The driving force for the film surface transfer is the difference between the partial pressures of vapor at the pool surf ace and bulk.

Forced/mixed convection

Mass transfer as indicated for free convection except that the concentration boundary layer across which the vapor is transported has developed as a result of forced gas flows along the surface. When this boundary layer thickness is affected by both the forced and induced buoyancy flows, the flows have a combined effect and the entire mass transfer process is characterized as mixed convection.

APPENDIX B. SUBCOMPARTMENT STUDY

B.1 Introduction

The MELCOR 2.1 code has been applied in the HDR pipe rupture tests (V44 and T31.5), which have also been documented as International Standard Problem (ISP) exercises ISP-16 and ISP-23 [B-1 and B-2]. In this appendix the test result for differential pressures generated between the break room and adjoining compartments is investigated to determine the ability of the MELCOR code to predict maximum differential pressure. The conclusions of this study are useful in analyzing a variety of subcompartment case studies involving high energy line breaks in compartmentalized containments where the injected steam is either dry or wet. This HDR analysis effort has been preceded by similar studies using the CONTAIN code [B-3, B-4] and MELCOR code [B-5], and those studies serve as guidance for this work as well as providing an important benchmark to the current MELCOR 2.1 code results.

This appendix is divided into three sections: background (modeling, facility and experiment results) as well as V44 and T31.5 analyses. Section B.2 briefly covers the background for modeling inertia flow for choked and unchoked conditions by codes such as CONTAIN and MELCOR. The facility and experimental results are also addressed in this section. The analyses and sensitivity studies for tests V44 and T31.5 are discussed in Sections B.3 and B.4, respectively, as well as benchmarking to a previous CONTAIN case study [B-3].

B.2 Background

Modeling and Phenomena. Differential pressure calculations obtained with codes like CONTAIN 2.0 and MELCOR 2.1 are performed using an inertial flow model. As an example the CONTAIN formulation is presented below. The CONTAIN model can be described by the simplified governing equation for fluid flow rate Wij from compartment i to j as

$$W_{ij} = Min(W_{iner,ij}, W_{cr,ij}) \qquad \text{Equation B-1}$$

where the inertia flow rate $W_{iner,ij}$ is calculated from a momentum equation given by

$$\frac{dW_{iner,ij}}{dt} = \left[\Delta P_{ij} - \frac{K|W_{iner,ij}|W_{iner,ij}}{2\rho_u(A_{ij})^2}\right]\frac{A_{ij}}{L_{ij}} \qquad \text{Equation B-2}$$

and the critical or choked flow rate $W_{cr,ij}$is given by the augmented Homogenous Frozen Model (HFM)

$$W_{cr,ij} = A_{ij}\nu_{ij}\sqrt{\gamma_u P_u \rho_u \eta_u} \qquad \text{Equation B-3}$$

where,

W = total mass flow of gases, coolant vapor, and homogeneous dispersed liquid coolant;
ΔP = differential pressure;

K = irreversible flow loss coefficient;
ρ_u = upstream flow path density (including dispersed liquid coolant);
A = flow path area;
L = inertia length;
γ_u = upstream ratio of C_p/C_v for the gas/vapor mixture;
η_u = $\left[\frac{2}{1+\gamma}\right]^{\frac{\gamma+1}{\gamma-1}}$;
ν = vena contracta or augmentation factor

MELCOR similarly applies the minimum between the its inertial and critical flow model flow rate, similar to Equation B-1. The subscripts i and j refer to the connecting compartments or control volumes. The inputs in both CONTAIN and MELCOR (orifice flow paths) are the flow path area, characterization of the loss coefficients, and the inertia length. In case of the V44 and T31.5 tests the upstream compartment is the break room. Inertia lengths for orifice type pathways are approximated values which have been estimated in previous CONTAIN studies by the formula

$$L_{ij} = \sqrt[3]{Min(V_i, V_j)} \qquad \text{Equation B-4}$$

where,

V is the volume of a compartment associated with the connecting pathway.

The critical flow equation above is referenced to the model used in the CONTAIN code. For pure gases this modeling is an isentropic ideal gas representation of choking where the gas flows are limited by the sonic speed in the pathway, or vena contracta. When dispersed liquid coolant is present in the flow field the sonic speed on the fluid is reduced below the gas sonic speed. The HFM (with no heat or mass transfer between gas and liquid) uses the same equation for choking as for single phase gas, but the gas/steam density is replaced by the fluid density that includes dispersed liquid mass. For two-phase gas/mixture and dispersed liquid flows through orifices, the HFM has been shown to be a good modeling approach for determining critical flow for a wide range of flow qualities. For applications in containment analyses (applied to licensing, for example), the HFM is augmented by a multiplying factor to approximate a Homogeneous Equilibrium Model (HEM) that is known to be a conservative (under-estimate) model for determining two-phase critical flow through orifices. Therefore, the augmented HFM is typically used for subcompartment analyses, and the empirically derived augmented factor that accounts for non-isentropic as well as HFM/HEM differences is ~ 0.7. To determine whether choking flow has actually occurred in an experiment where the pressure differentials are measured, the augmenting or vena contracta factor can be varied to investigate how choking affects pressure differential calculations. Note, that most containment flow pathways are not always represented accurately by sharp-edge orifices or perfect nozzles; therefore, in reality the vena contracta or augmenting factor for accurate choking modeling may vary from the factors commonly used for subcompartment application. Consequently, this factor included in the modeling is typically investigated by a range of sensitivity calculations. For licensing applications a conservative value of 0.7 is generally chosen. For the MELCOR 1.8.6 code, there was no modeling of two-phase dispersed liquid sonic speed for the atmosphere “phase”; rather, the fluid sonic speed was always

the gas/steam mixture sonic speed. In MELCOR 2.1, an HFM identical to the CONTAIN model was added and incorporated into calculations by invoking an optional keyword (FMOD) in the CVH package input. Currently, a recommendation to include this option as the default setting for the code is being considered.

In terms of important phenomena for subcompartment analysis of high energy line breaks, the most important phenomena are inertial flow, limited perhaps by single- or two-phase critical flow. Due to the short periods that are typically involved (few seconds), heat and mass transfers in the compartments are not important. Because two-phase flow (dispersed liquid drops in the fluid) can occur which when accounted for can effectively limit gas/vapor exit from the break room, other phenomena affecting the flow field upstream also becomes important, such as flashing and entrainment of liquid within the field. For these tests, the flashing is modeled as a temperature flash (constant enthalpy process) and entrainment is bound by two limits, 0 and 100% entrainment. There is no modeling available that can account for degrees of entrainments in complicated break room geometries; therefore, the assessment is based on limits and sensitivity calculations.

Facility and Experiment. The break rooms for the V44 and T31.5 tests are rooms 1603 and 1704, respectively. Shown in Figure B-1 is the break room (1603) and adjoining room (1708) for the V44 test. The pressure differential is measured with DP sensor cp6301. Differential pressure is also measured between the room 1603 and adjoining room 1704, Figure B-2, using DP sensor cp6303. For the T31.5 test the break room and adjoining room are shown in Figures B-2 and B-3. For this test the differential pressure is measured between break room 1704 and 1707 is sensor cp 7415. It should be pointed out that there are significant differences between each of the break rooms; break room 1603 is a rather small room (280 m^3) and break room 1704 is much larger (793 m^3). Additionally, break room 1603 is more open with few open space obstructions, while break room 1704 is full of small metal obstructions (exposed pipes, hangers, and equipment). Differential sensors cp6301 and cp6303 are placed near constructed pathways that are simple straight pathways, while sensor cp7415 measures the pressure differential near an open door pathway that is not a straight connection pathway. Tables B-1 and B-2 are detailed lists of flow path data for each test provided by Project HDR and used in this and previous subcompartment study calculations [B-1]. These pathway lists provide pathway input (area and loss coefficients) and a description of each connecting path.

The short-term pipe rupture steam injections for tests V44 and T31.5 are shown in Figure B-4 and B-5. Both injection mass rates and specific enthalpies are nearly identical. While the injections are typically described as wet steam injections (due to the relatively low enthalpy), both tests have an initial dry steam injection (elevated enthalpy) period that occurs during the first second after the pipe rupture disks break.

Shown in Figure B-6 are the measured pressure differentials for tests V44 and T31.5. The figure shows the significant difference in the two experiments, where the V44 test shows a much larger pressure differential that has a clearly defined second maximum after the early peak during the dry steam injection. The smaller pressure differential in the case of the T31.5 shows a maximum at the time of dry steam injection and a second maximum during the wet steam injection that is much less pronounced than in the case of the V44 test. These response behaviors are analyzed in the following sections.

B.3 HDR V44 Test Calculations

The reference case for the HDR V44 subcompartment calculation included the following input settings: 33CV nodalization, temperature flashing (default), FOG active (no RN), two-phase choking using HFM (FMOD), augmentation factor ν set to unity, Table B-1 pathway areas and K values, and natural convection for sensible and latent heat transfers. Shown in Figure B-7 is the comparison of calculation and measurement for the differential pressure between the break room 1603 and adjoining room 1708. To determine whether the MELCOR reference case experienced any period of choking, the augmentation factor was increase from 1 to 2. Those calculated differential pressure comparisons (ν = 1 → 2) show no difference in results; meaning that no choking was occurring in either case. However, when the augmentation factor was reduced to 0.7 a choking period was noted both for the dry and wet steam injection, as shown in Figure B-8. The conclusion was that the response observed with the differential pressure for the reference case was due to unchoked flow through the pathway. The good agreement for the early dry steam injection period with the reference case indicated that the loss coefficient for the pathway was appropriately set, and that the trend line for the calculated differential pressure during the wet steam injection was in general agreement with the measurement, pointing to the importance of continued liquid water suspension in the flow stream. Another case where the fog was eliminated (NOFOG active) showed a diverging calculation with measurement, Figure B-9; again indicating that the presence of fog was an important contributor to the improved comparison shown for the reference calculation during the wet steam injection. Although short periods of choking could not be ruled out, the presence of choking in the test appeared unlikely. This conclusion left the remaining issue of why, even with 100% entrainment, was the two-phase flow period under-predicted or offset a fix amount from the measurement but having a similar trend line.

In the CONTAIN analysis of this test [B-3 and B-4], it was hypothesized that during the two-phase flow period the loss coefficient for two-phase flow increases due to dispersed liquid in the flowing fluid. In the case of two-phase flow the single phase coefficient is known to increase but the transition and amount of increase is difficult to assess for a rapidly varying flow field. In reference [B-4] it was argued that the increase should vary approximately in proportion to the time varying ratio ρ_u/ρ_g , where ρ_g is the gas/vapor mixture density. Shown in Figure B-10 is the time history for this ratio as calculated for the reference case. In the limit where the ratio is unity, the loss coefficient is the single phase coefficient, but as the ratio increases and reaches a fixed value the two-phase coefficient should stabilize at a constant value. This limiting constant value for the two-phase coefficient is empirically determined based on the agreement between the calculated and measure differential pressure, when the two-phase loss coefficient is adjusted. To effectively incorporate a time varying loss coefficient, the flow path area is modified with time according to the trend line for the density ratio in Figure B-10. In the MELCOR code this is accomplished using the Valve input keyword in the FL package along with a control function to provide a time varying pathway open fraction. This technique was also used in the CONTAIN analysis for this test (i.,e., time varying area to effectively adjust the loss coefficient), and for that case good agreement with the measured differential pressure was obtain with a 35% increase in the loss coefficient when the density ratio leveled out during the wet steam injection. Shown in Figure B-11 are the comparisons of measured and MELCOR calculated differential pressures for various

cases: reference case, NOFOG case, K time varying increase by 35% at two-phase limit, and CONTAIN reference case with K time varying by 35%.

The phenomena associated with the V44 differential pressure response are complicated and the analysis is subject to uncertainty since measured pressure response is only an indirect indicator of the phenomena dominating in the test. Phenomena that were considered are: choking, entrainment, and two-phase flow within the break room pathways (i.e., via loss coefficients). The analysis of the test results with the MELCOR code suggests that of the phenomena considered, the most important are entrainment and two-phase flow. For the calculated atmospheric ratios of total suspended mass to gas/steam mass, and increase in the single phase loss coefficient of ~ 35% during two-phase flow appears to provide a good representation of the maximum pressure differential measured in the test between the break room and an adjoining room R 1708. Additionally, the MELCOR differential pressure history during the wet steam injection are shown to be slightly lower than an equivalent CONTAIN calculation, and that small offset appears to be related to a variation in the difference in calculated suspended liquid mass during a portion of the wet steam injection.

B.4 HDR T31.5 Test Calculations

The comparison of measured differential pressures for HDR V44 and T31.5 tests, Figure B-6, showed significant variation in both maximums and trend lines. In the case of V44, the observed maximum pressure was observed at about 65% great than in the T31.5 test; and, the maximum in the V44 test occurred during the wet steam injection while for the T31.5 test the maximum occurred during the earlier dry steam injection. During the walk-down through the facility it was noted that the open space of the T31.5 break room was clutter with various pipes, hangers, and miscellaneous equipment that would represent obstacles to the break room fluid flow field. In contrast, the V44 break room open space was relatively free of suspended obstacles. Another contrasting feature between the tests was the different free volume sizes: V44 free volume is 280 m3 and the volume for the T31.5 break room is 793 m3, and increase in the volume of the V44 test of 183%. Since, the injection mass and energy was nearly equivalent for the tests, the injected energy density rate was significantly higher for the V44 test, Figure B-13. The combination of high energy density and open space favored the suspension of continued entrainment of the unflashed water during the wet steam injection period for the V44 test, but lower energy density and obstructions in the case of the T31.5 test suggests a condition where the suspended unflashed water would more likely rapidly removed from the atmosphere by de-entrainment mechanisms such as gravitation settling and impact interactions. Whatever the mechanisms might be, it seems reasonable that for the T31.5 test the liquid water loading in the break room atmosphere would be less than occurring for the V44 test. And this suggested reason would explain the time shift of differential pressure maximum observed between tests. As shown below, the MELCOR differential pressure calculations (with sensitivity cases) support this conclusion.

Shown in Figure B-14 is the MELCOR reference differential pressure calculation for the instrumented pathway #176 that connects the T31.5 break room 1704 with the adjoining room 1603 compared to the differential pressure sensor cp6303 reading (see Figure B-2). The reference case for HDR T31.5 subcompartment analysis including the follow settings: 33CV nodalization, temperature flashing (default), FOG active (no RN), two-phase choking using HFM (FMOD), with

the augmentation factor ν set to unity. In contrast with the calculation results for the V44 test, during the wet steam injection, here the calculation with 100% unflashed liquid entrainment over predicts the differential pressure which would suggest that either the actual entrainment was either less than 100% or perhaps the calculation is predicting two-phase choking when it does not occur. A series of sensitivity calculations investigates this matter, Figure B-15. A number of conclusions are suggested by these calculations:

1) Comparing cases [Fog (v= 1) and Fog (v=2)], choking is not occurring either during the dry or wet steam injection with the reference calculation;
2) Comparing cases [Fog (v=1 and NOFOG (v=1)], entrainment percentage in the test is bounded by these two cases indicating a removal mechanism either by gravitation settling or impact, or both occurring during the wet steam injection, and for the dry injection the differential pressure is well predicted using the HDR loss coefficients for the break to adjoining rooms;
3) Comparing cases [Fog (v=1) and Fog (v=0.7)], the test conditions in the break room while not choked for either the dry or wet steam injection, is quite close to choking conditions as evidence by the conservative setting producing both single and two-phase choking.

Figure B-16 shows the comparison between the MELCOR reference differential pressure calculation for pathway #92 that connects the T31.5 break room 1704 with the adjoining room 1707 compared to the differential pressure sensor cp7415 reading (see Figure B-3). Pathway #92 is the zigzag door passage that is shown in Figure B-3. The zigzag pathway results in a slightly higher loss coefficient evaluation than the instrumented pathway #176 (K = 2.04 compared to pathway #176 K = 1.23). Consequently, the differential pressure is both measured and calculated higher than pathway #176. Shown in Figure B-17 are the sensitivity calculations for pathway #92, suggesting the conclusions reached above for this pathway also.

Figure B-18 and B-19 are calculations using the reference case settings except that the Fog density is determined using the MELCOR aerosol physics package (RN active). The results for differential pressure are shown to be nearly identical to the reference case, indicating ~ 100% entrainment with water aerosols and the corresponding increase in fluid density for flow through the pathways.

B.5 References

B-1. Firnhaber, M., "International Standard Problem ISP16: Rupture of a Steam Line within the HDR-Containment leading to an Early Two-Phase-Flow, Final Comparison Report and Appendix IV.," CSNI Report No. 112, Committee on the Safety of Nuclear Installations, OECD Nuclear Energy Agency, Paris, France.

B-2. Karwat, H., "International Standard Problem ISP23: Rupture of a Large-Diameter Pipe with the HDR-Containment, Final Comparison Report," CSNI Report No. 160., Committee on the Safety of Nuclear Installations, OECD Nuclear Energy Agency, Paris, France.

B-3. Tills, J., Notafrancesco, A., and Murata, K., "CONTAIN Code Qualification Report/User Guide for Auditing Subcompartment Analysis Calculations," SMSAB-02-04, Office of Nuclear Regulatory Research, Nuclear Regulatory Commission, September 2002.

B-4. Tills, J., Notafrancesco, A., and Murata, K., "An Assessment of CONTAIN 2.0: A Focus on Containment Thermal Hydraulics (Including Hydrogen Distribution)," SMSAB-02-02, Office of Nuclear Regulatory Research, Nuclear Regulatory Commission, July 2002.

B-5. Notafrancesco, A., Esmaili, H., and Tills, J., "Application of the MELCOR Code to Design Basis Subcompartment Analysis," RES/FSTB 2011-02, Office of Nuclear Regulatory Research, Nuclear Regulatory Commission, May 2011.

Table B-1. Flow paths from break compartment for HDR V44									
Open#	From Comp#	To Comp#	From Vol#	To Vol#	Area m^2	α*	K	C_{FC}	Comment
110	1603	1704	4	10	0.37	0.55	3.31	1.65	pipe channel with weir sill in comp. 1704
133	1603	1708	4	11	0.43	0.65	2.37	1.18	upper part of opening #162
140	1603	1704	4	10	1.64	0.6	2.78	1.39	opening situated in opening #143
143	1603	1701u	4	8	3.02	0.7	2.04	1.02	opening in the upper part of break compartment 1603, crossed by break pipe
145	1603	1701u	4	8	0.173	0.65	2.37	1.18	channel parallel to opening #143
163	1603	1606	4	6	1.104	0.7	2.04	1.02	zigzag passage with stairs and open lead-shielded door
165	1603	1605	4	7	0.19	0.7	2.04	1.02	wall opening and steel pipe
176	1603	1704	4	10	0.238	0.9	1.23	0.62	instrumented (DK) channel with rounded inlet
180.2	1603	1704	4	10	0.152	0.7	2.04	1.02	zigzag channel in ceiling of break compartment 1603
183.1	1603	1704	4	10	0.183	0.7	2.04	1.02	rectangular opening
183.3	1603	1704	4	10	0.01	0.65	2.37	1.18	five bore holes

* discharge coefficient (determined by GRS – Gesellschaft fur Reaktorsicherheit, Germany [B-3].

Table B-2. Flow paths from break compartment for HDR T31.5									
Open#	From Comp#	To Comp#	From Vol#	To Vol#	Area m^2	α*	K	C_{FC}	Comment
92	1704	1707	10	12	1.5	0.7	2.04	1.02	Zigzag passage with stairs (lateral edges rounded) and instrumented door
96	1704	1804	10	18	0.43	0.9	1.23	0.62	Instrumented (DK) channel with rounded inlet
98	1704	1804	10	18	0.02	0.6	2.78	1.39	Bore with measuring cables
100	1704	1904	10	14	0.015	0.6	2.78	1.39	bore
102	1704	1701o	10	9	1.62	0.75	1.78	0.89	Opening in biological shield
103	1704	1805	10	16	0.088	0.6	2.78	1.39	Two bores close to opening #102
109	1704	1903	10	21	0.31	0.7	2.04	1.02	Ventilation duct leading from R1704 via two elbows to R1903 and to main ventilation duct
140	1704	1603	10	4	1.26	0.8	1.56	0.78	Opening siturated in opening #143
176	1704	1603	10	4	0.236	0.9	1.23	0.62	Instrumented (DK) channel with rounded inlet
180.2	1704	1603	10	4	0.152	0.7	2.04	1.02	Zigzag channel in ceiling of R1603
227	1704	1805	10	16	0.08	0.65	2.37	1.18	Pipe channel, insulating material partially squeezed
228	1704	1804	10	18	0.0015	0.7	2.04	1.02	3 lead-in holes for drives

* discharge coefficient (determined by GRS – Gesellschaft fur Reaktorsicherheit, Germany [B-4].

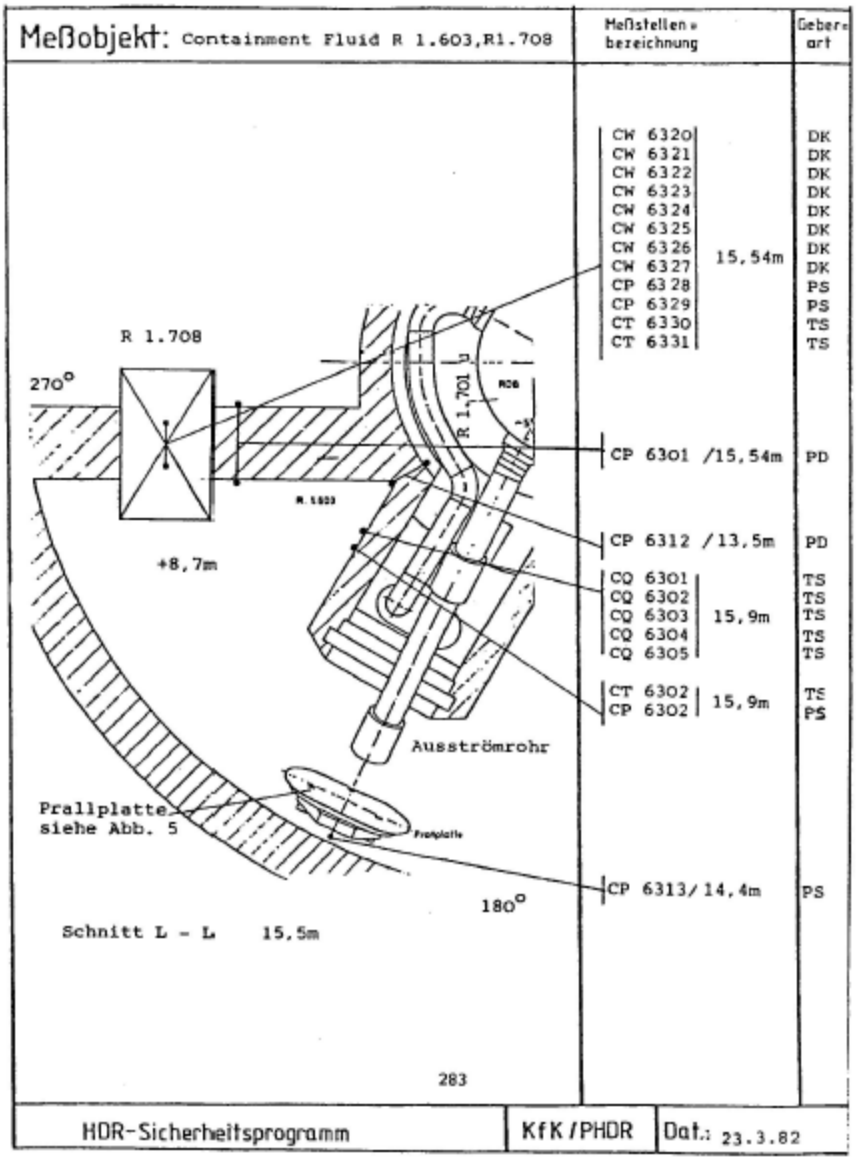

Figure B-1 **HDR V44 test break room (1603) and adjoining room 1708. Sensor CP 6301 measures the pressure differential between rooms 1603 and 1708.**

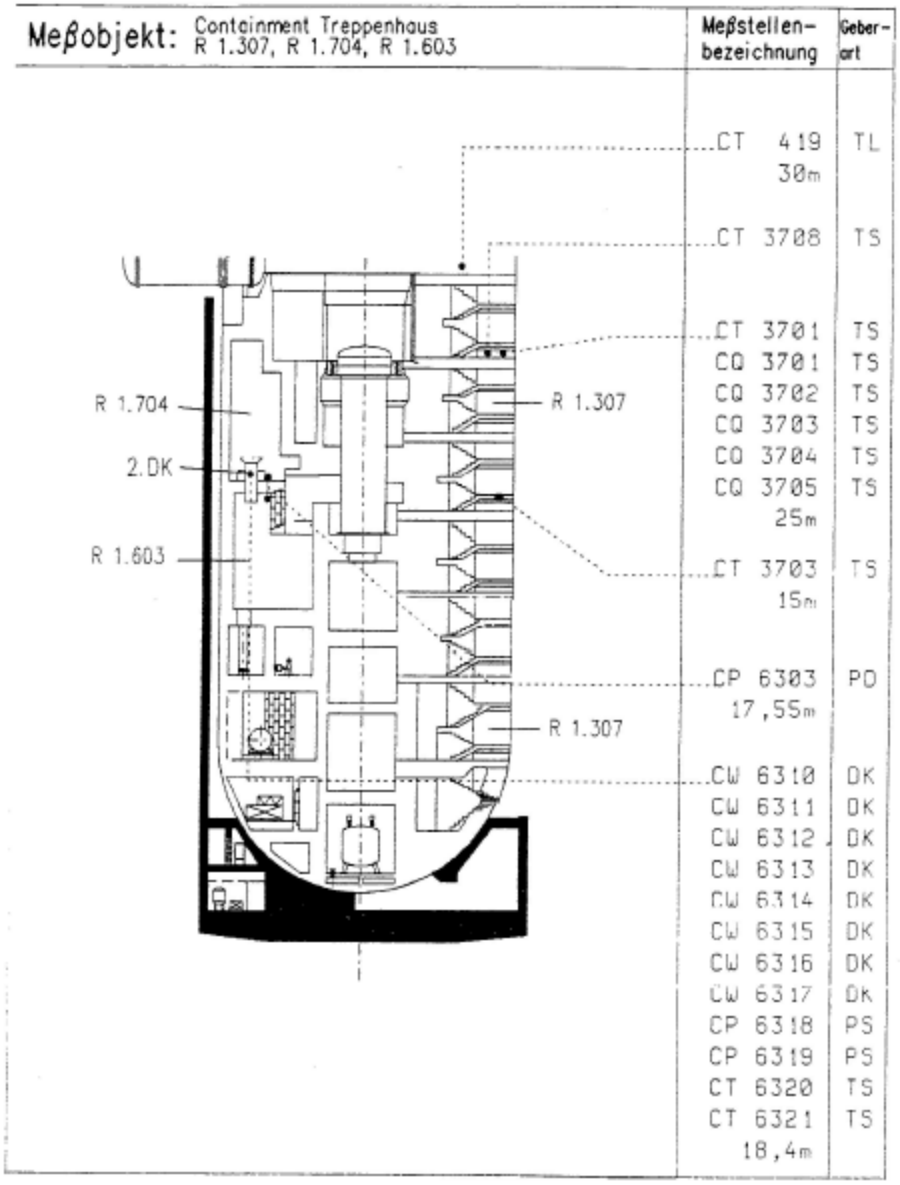

Figure B-2 **HDR V44 test break room (1603) and adjoining room (1704). Sensor CP 6303 measures the pressure differential between rooms 1603 and 1704.**

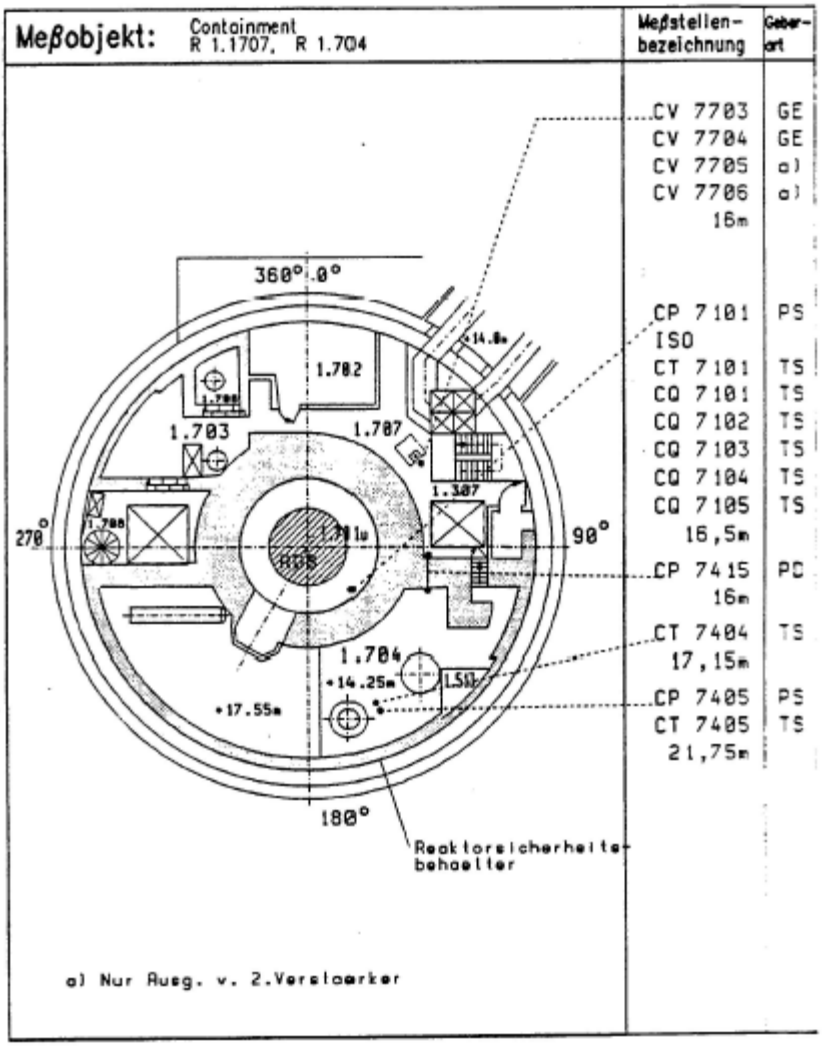

Figure B-3 **HDR V44 test break room (1704) and adjoining room (1707). Sensor CP 7415 measures the pressure differential between rooms 1704 and 1707.**

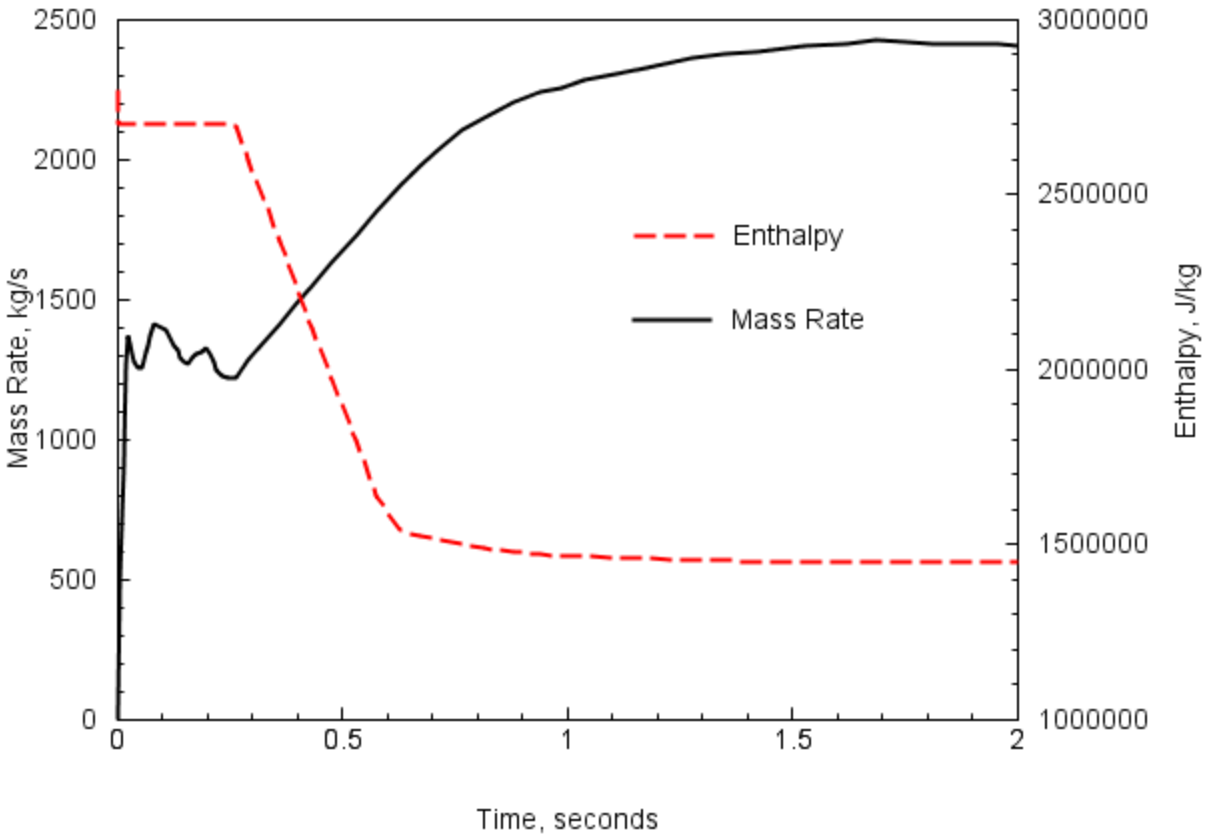

Figure B-4 Short-term steam injection mass and energy for HDR test V44.

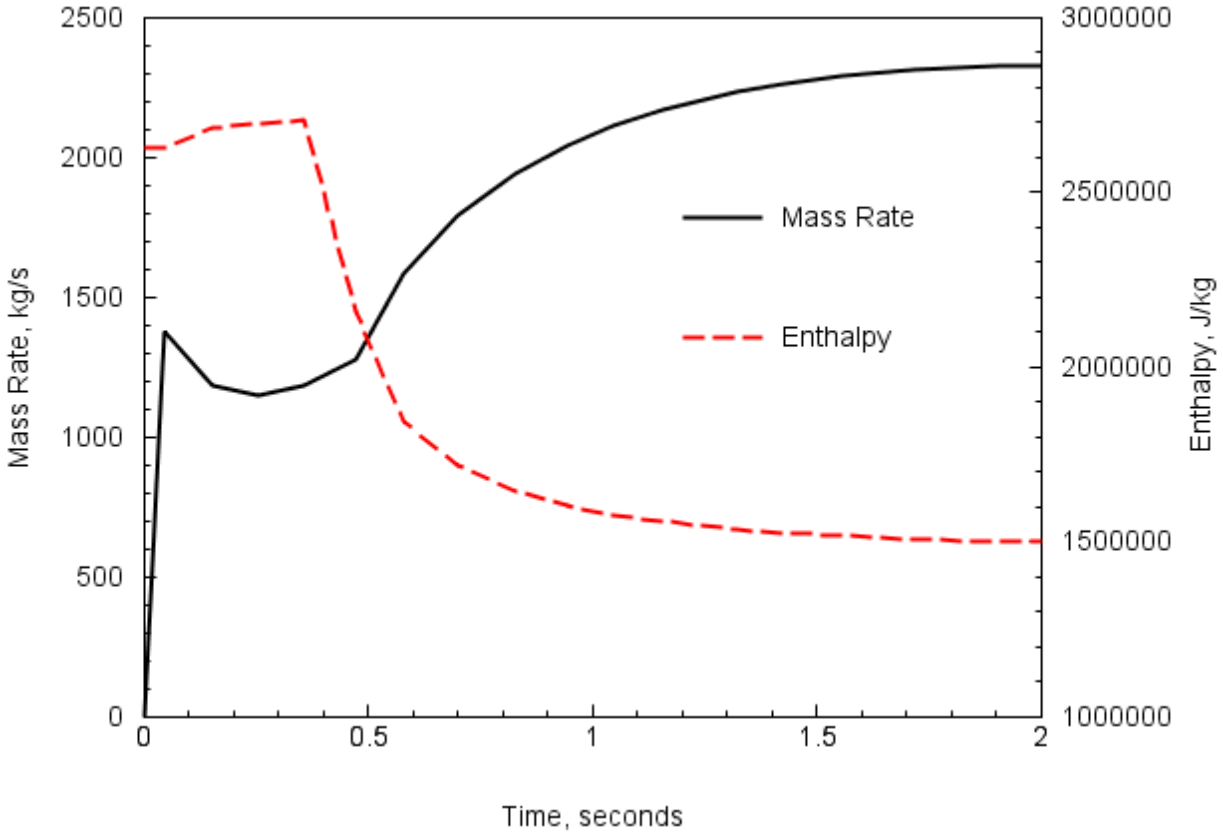

Figure B-5 Short-term steam injection mass and energy for HDR test T31.5.

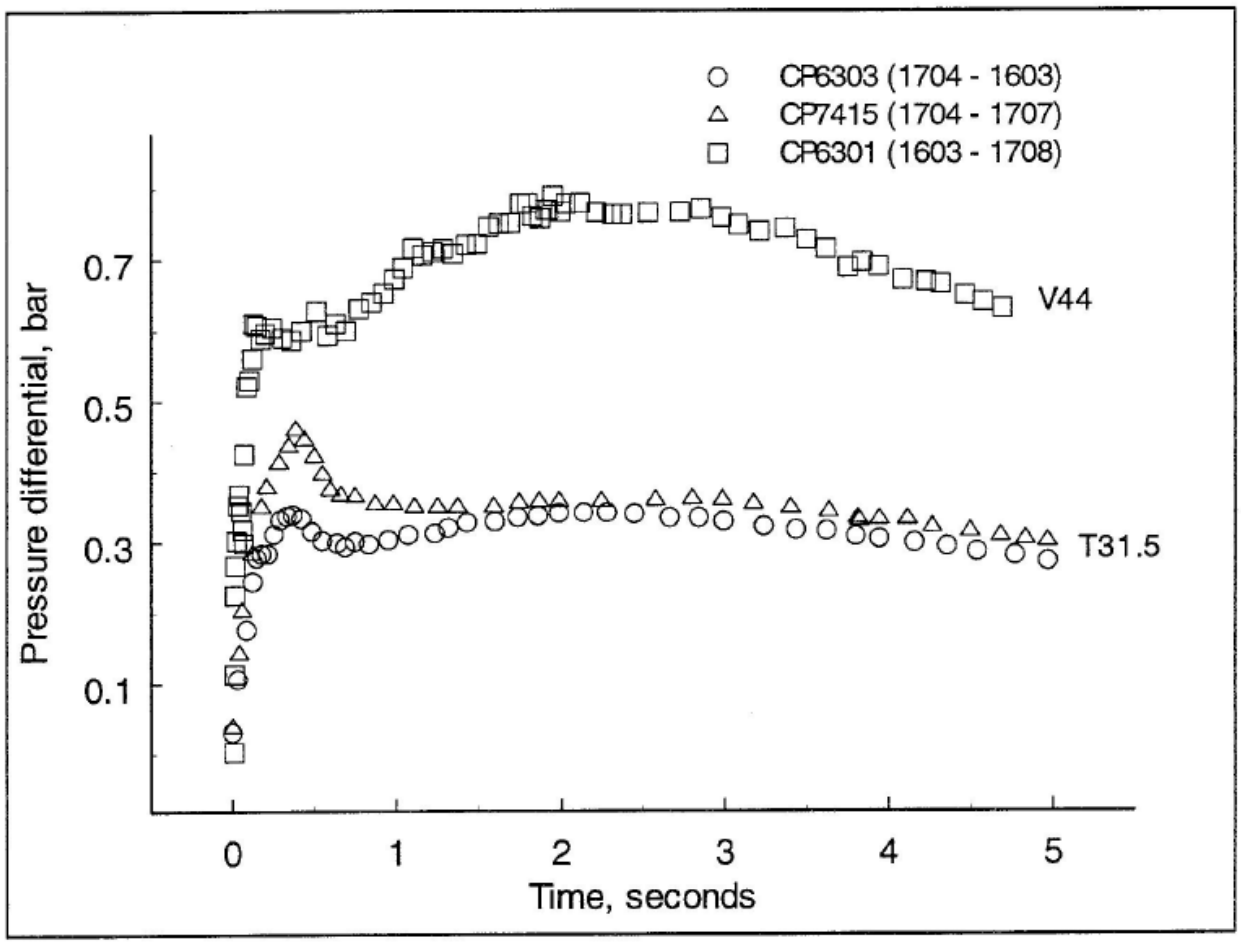

Figure B-6 **Measured pressure differentials for break room to adjoining rooms during HDR tests V44 and T31.5.**

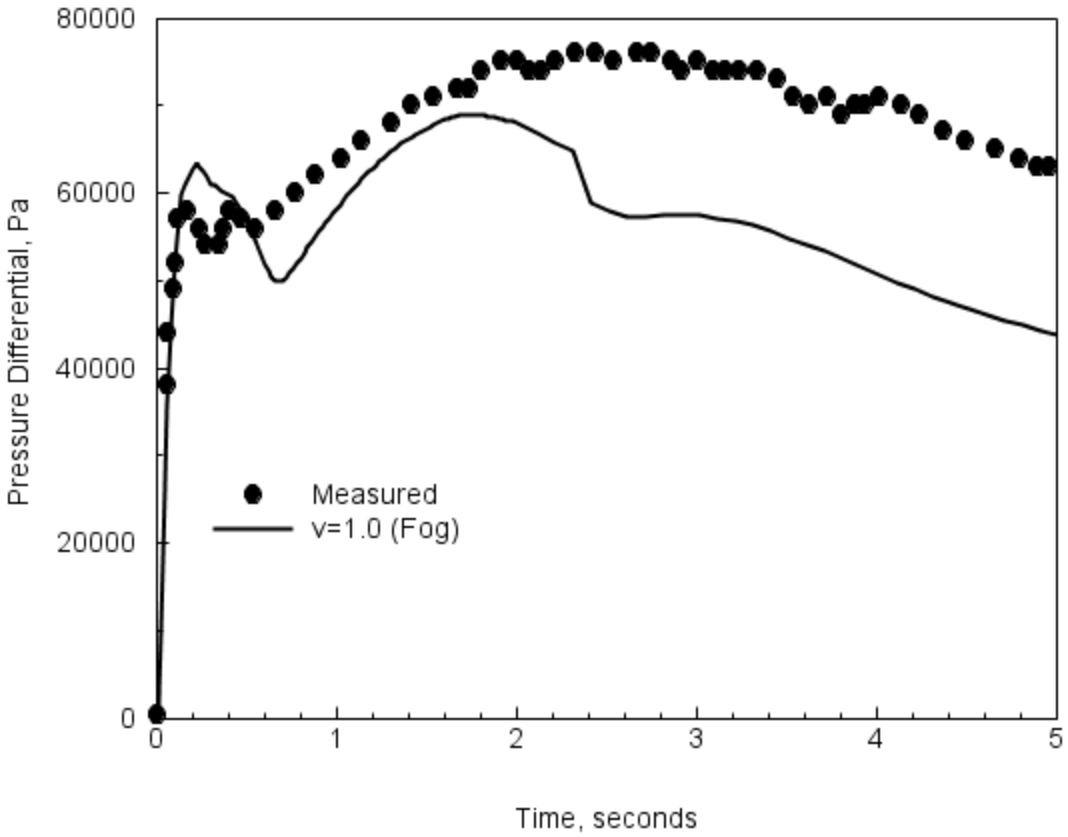

Figure B-7 **Comparison between measured and MELCOR reference calculation for break room 1603 to adjoining room 1708 differential pressure.**

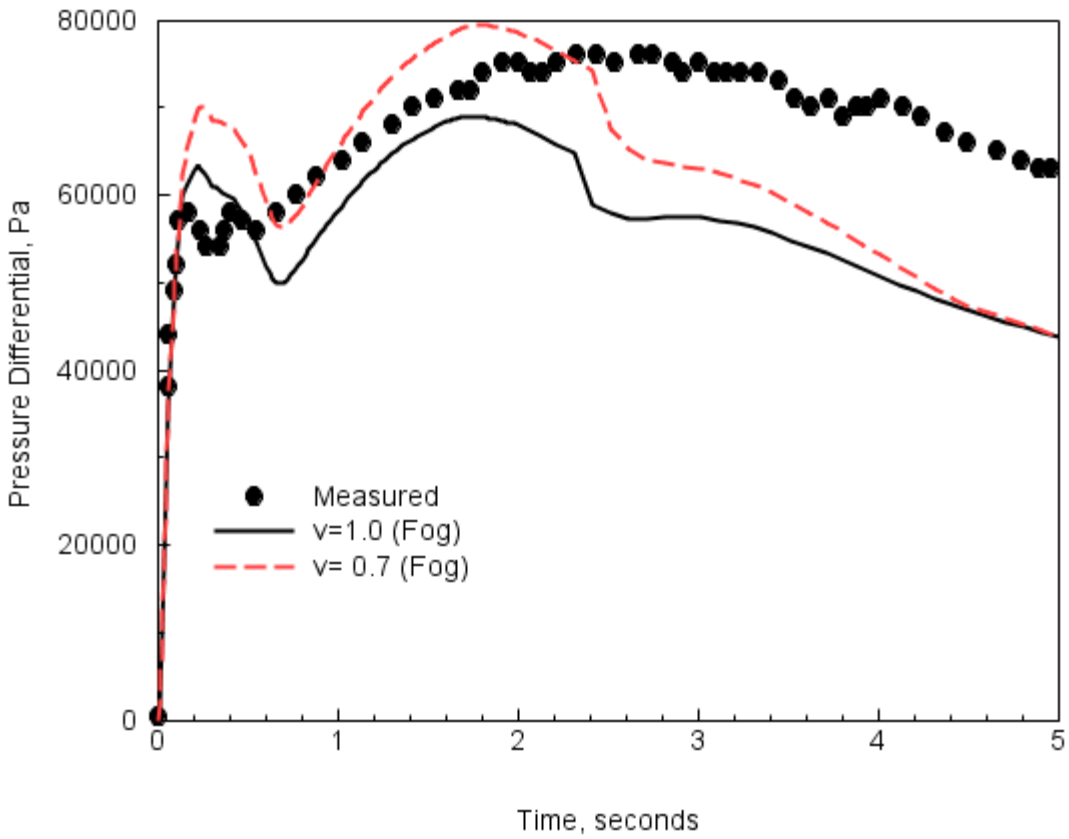

Figure B-8 **Comparison of measured and MELCOR calculated differential pressure for break room 1603 to adjoining room 1708 during the V44 test.**

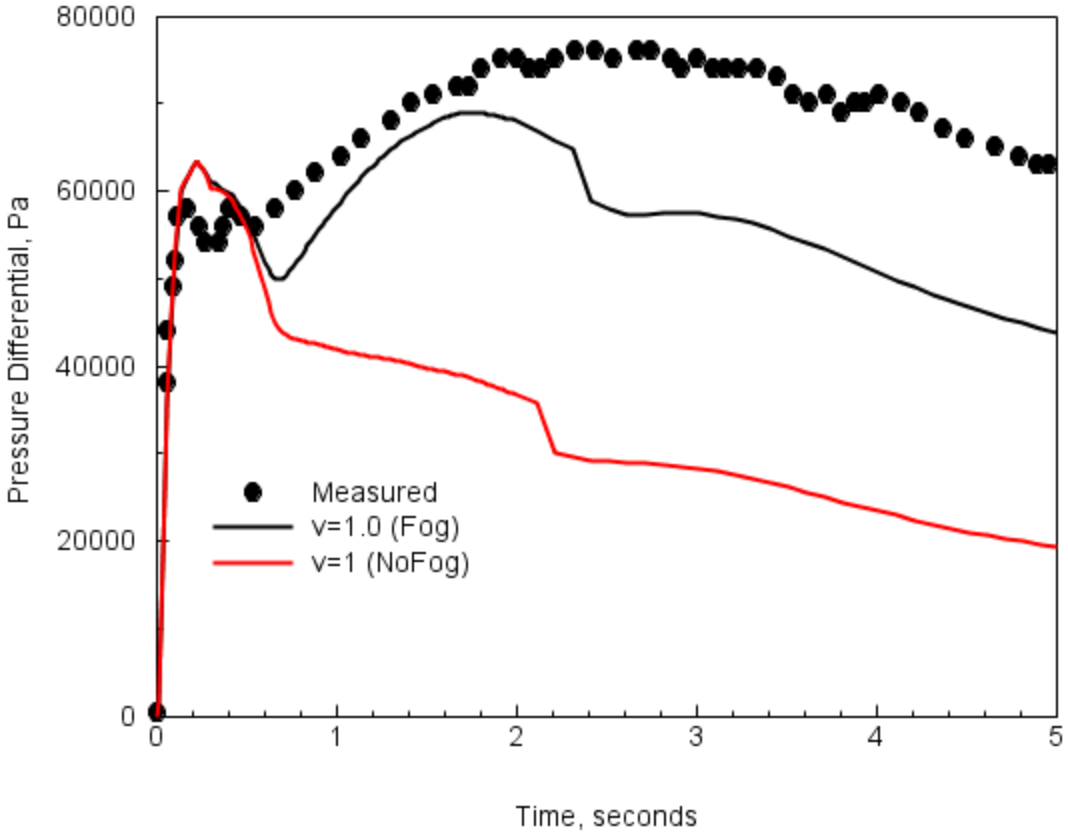

Figure B-9 **Comparison of measured and MELCOR calculated differential pressure for break room 1603 to adjoining room 1708 during the V44 test.**

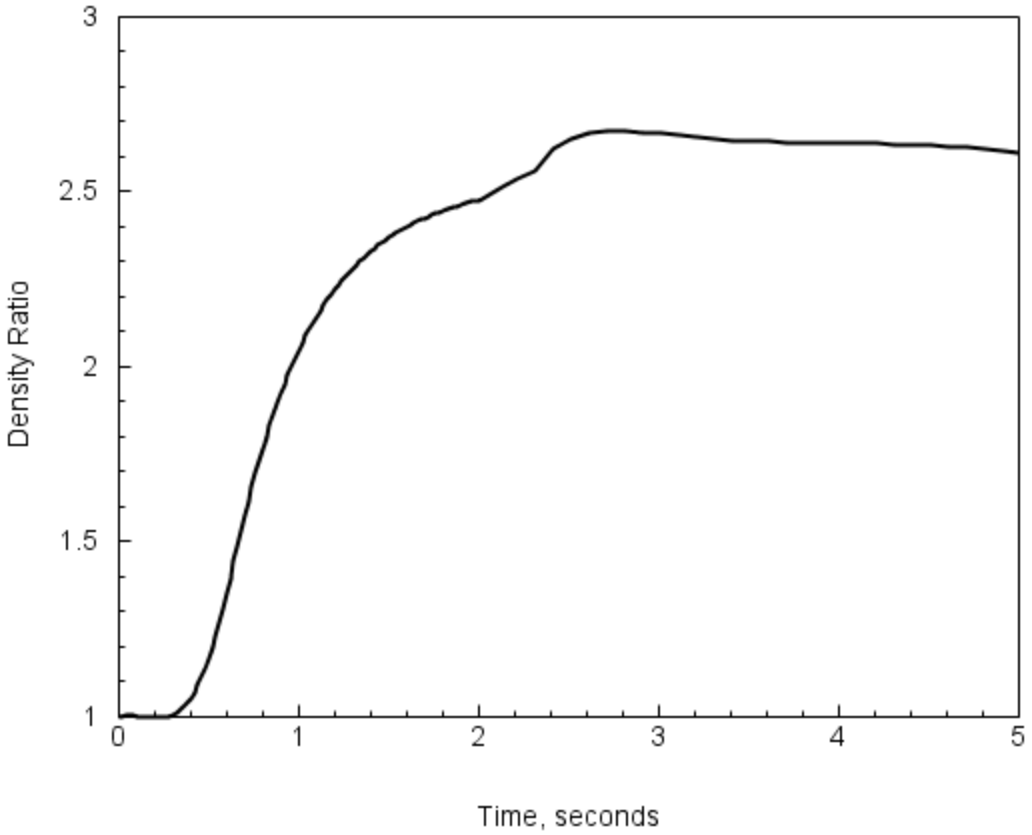

Figure B-11 **Plot of the MELCOR calculated atmospheric density ratio ρ_u/ρ_g in Break room 1603 for HDR test V44.**

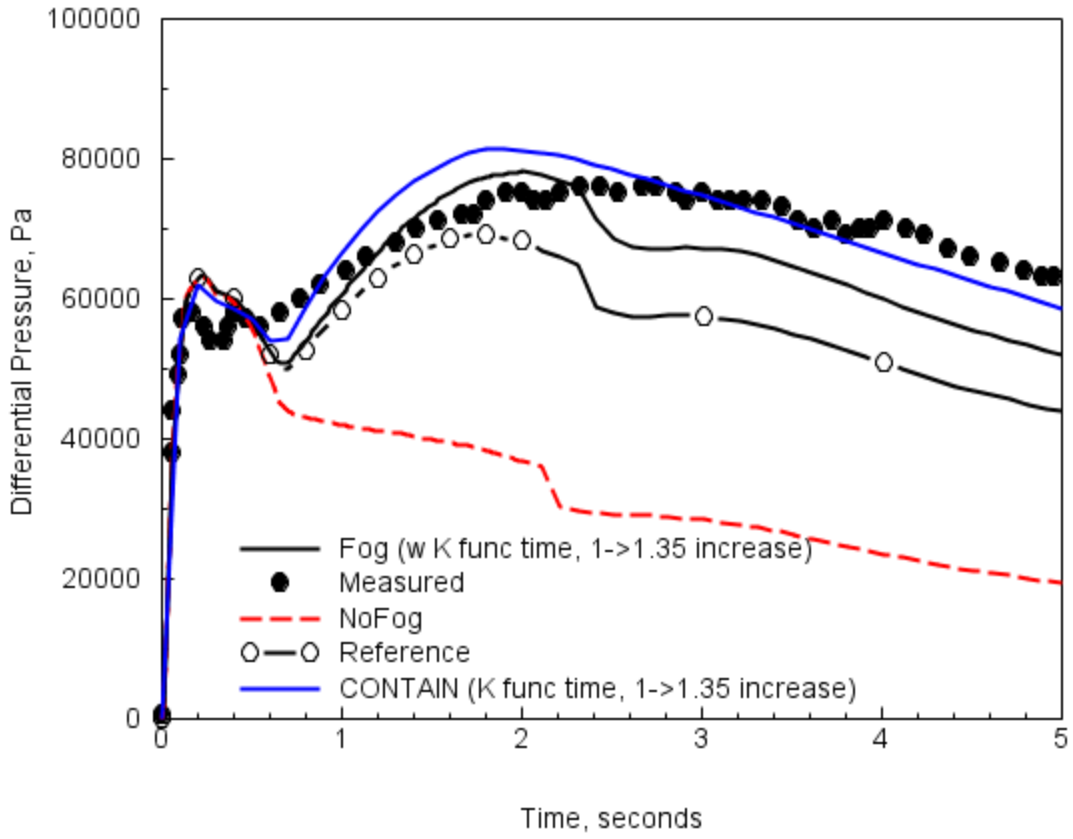

12

Figure B-12 **Comparison of measured and MELCOR calculated differential pressures for break room 1603 to adjoining room 1708 during the V44 test, showing sensitivity cases as well as the CONTAIN benchmark.**

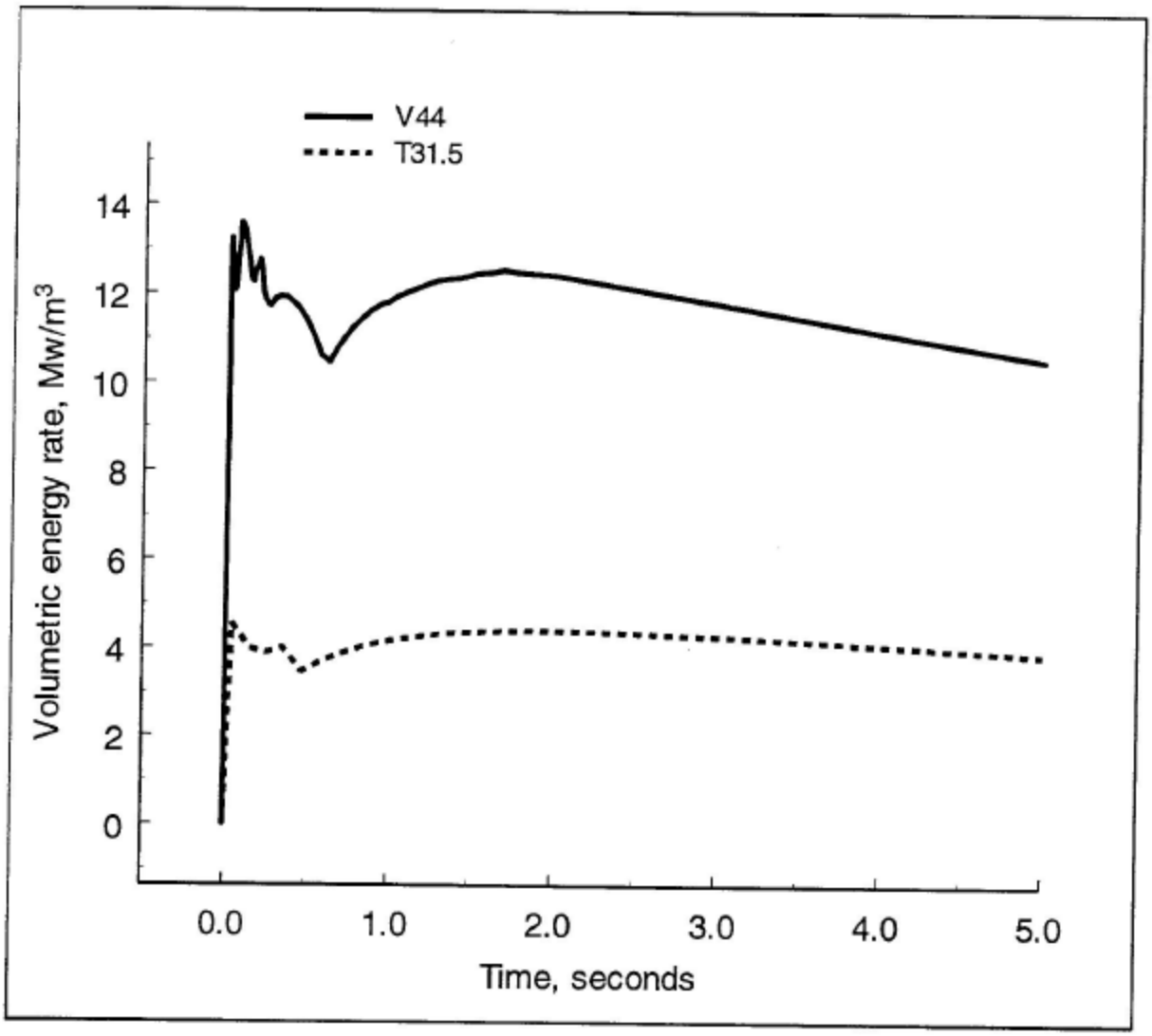

Figure B-13 **Injected energy density rate in the break rooms of HDR tests V44 and T31.5.**

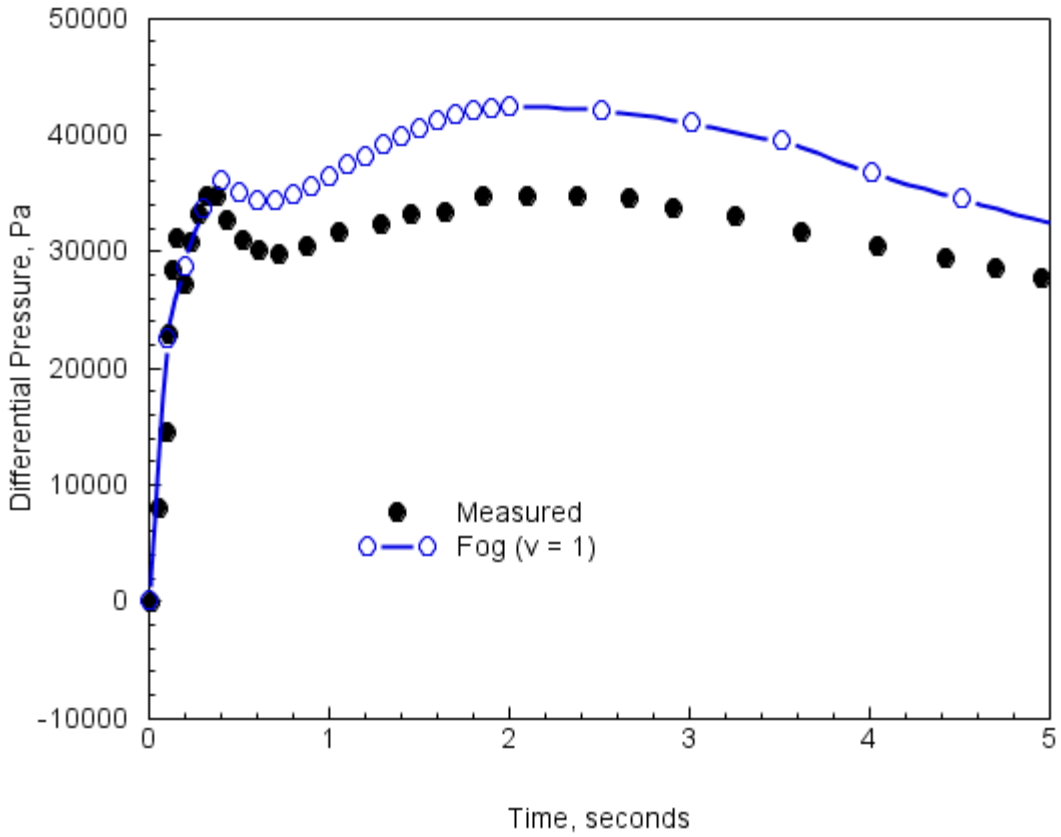

Figure B-14 **Comparison of the reference MELCOR differential pressure with measurement for pathway #176 (1704 to 1603) during the HDR T31.5 test. The "Fog" setting is for 100% entrainment of unflashed water, and the augmentation factor setting of unity reproduces the HFM without adjustment for two-phase flow.**

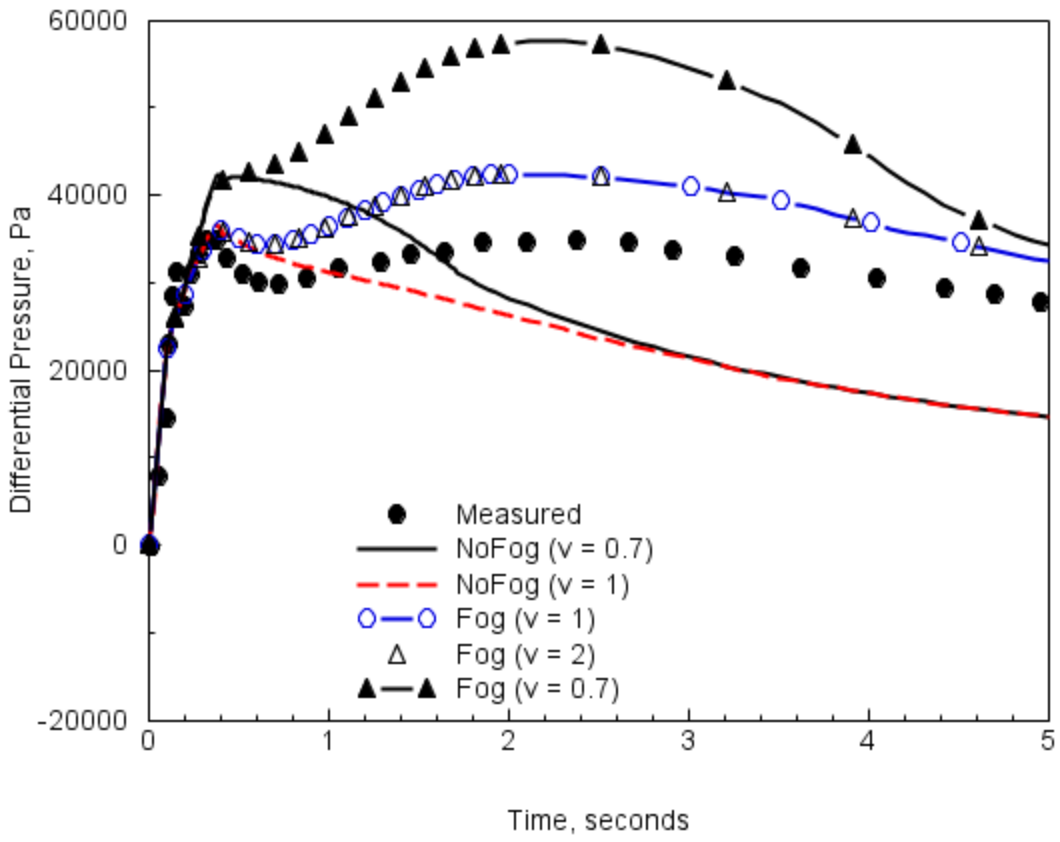

Figure B-15 **Comparison of the MELCOR differential pressure sensitivity calculations with measurement for pathway #176 (1704 to 1603) during the HDR T31.5 test.**

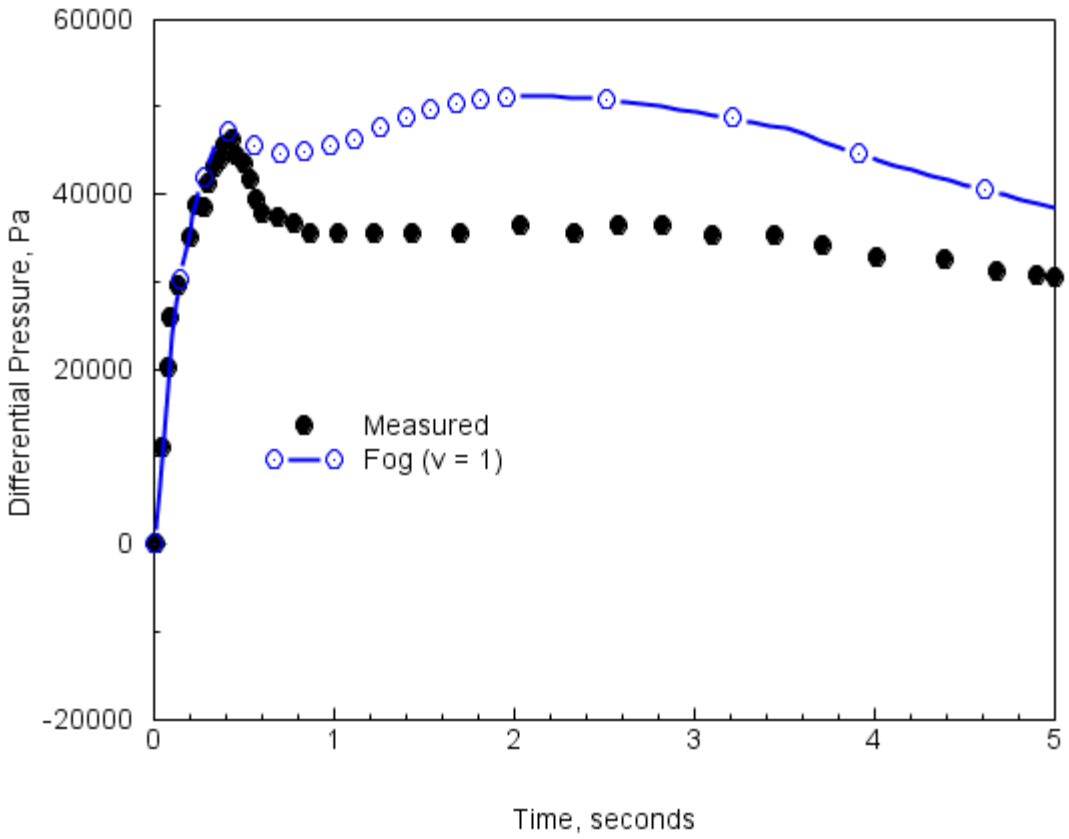

Figure B-16 **Comparison of the reference MELCOR differential pressure with measurement for pathway #92 (1704 to 1707) during the HDR T31.5 test. The "Fog" setting is for 100% entrainment of unflashed water, and the augmentation factor setting of unity reproduces the HFM without adjustment for two-phase flow.**

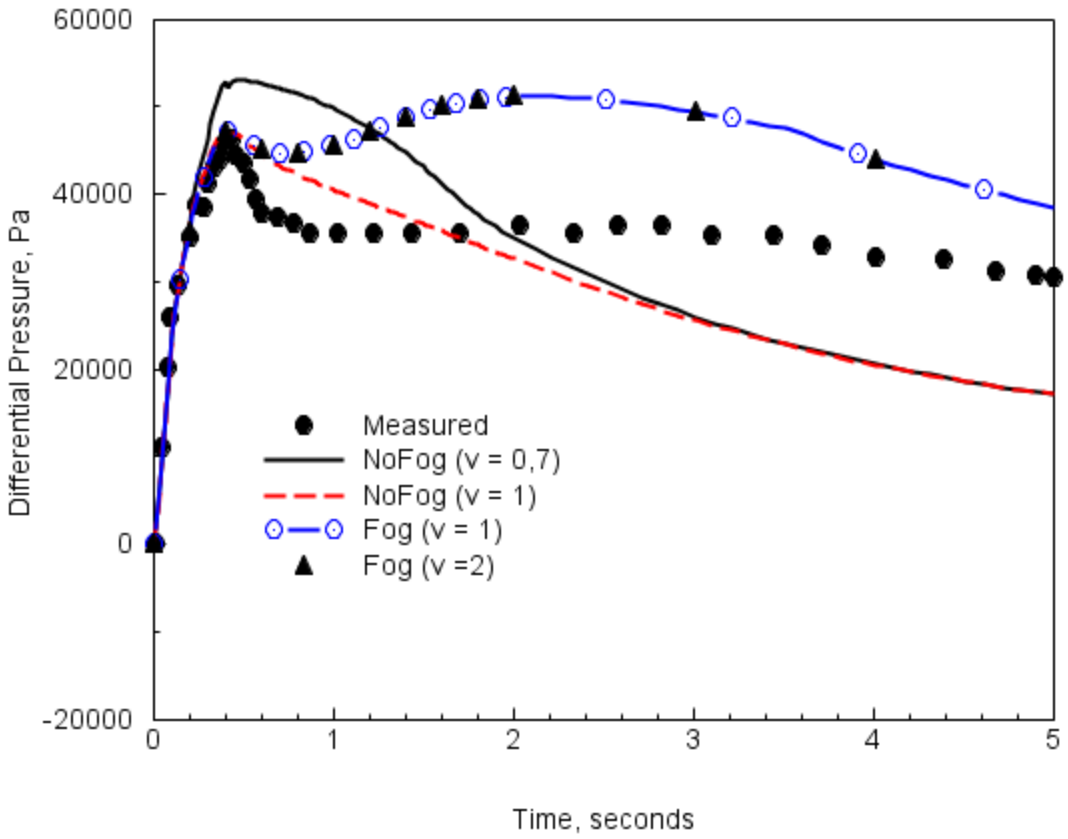

Figure B-17 **Comparison of the MELCOR differential pressure sensitivity calculations with measurement for pathway #92 (1704 to 1707) during the HDR T31.5 test.**

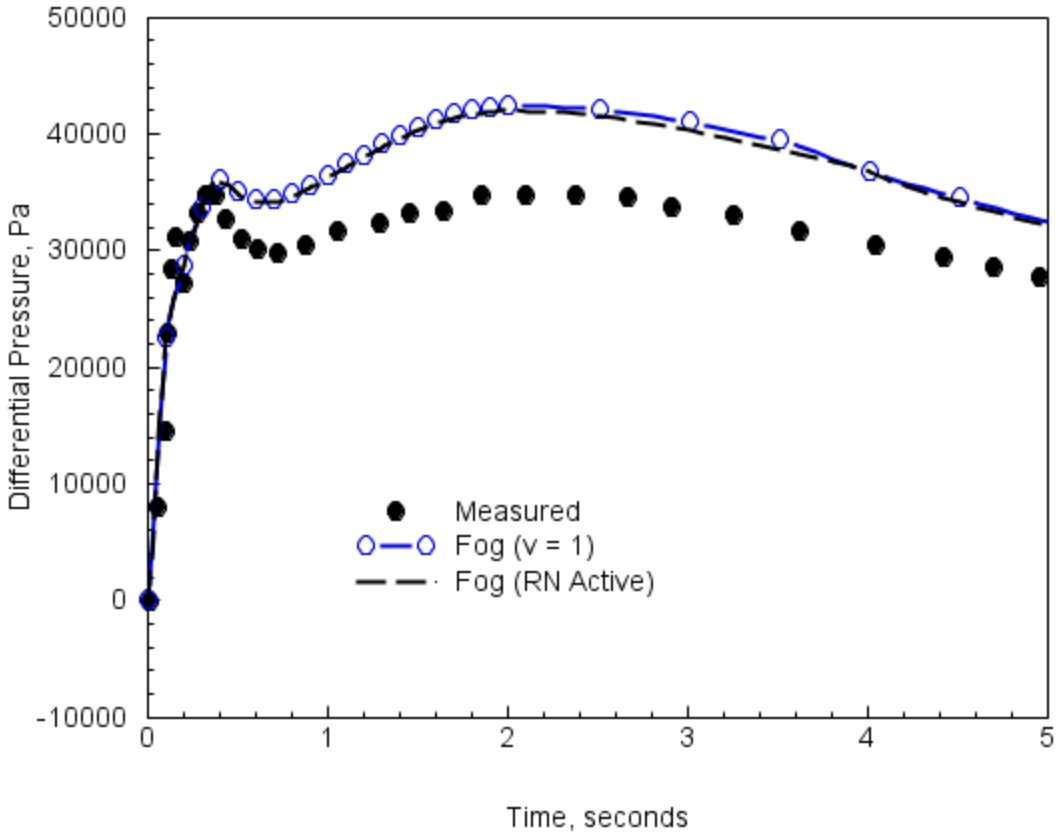

Figure B-18 **Comparison of the MELCOR differential pressure calculations (with and without fog modeling by the aerosol physics model) compared with measurement for pathway #176 (1704 to 1603) during the HDR T31.5 test.**

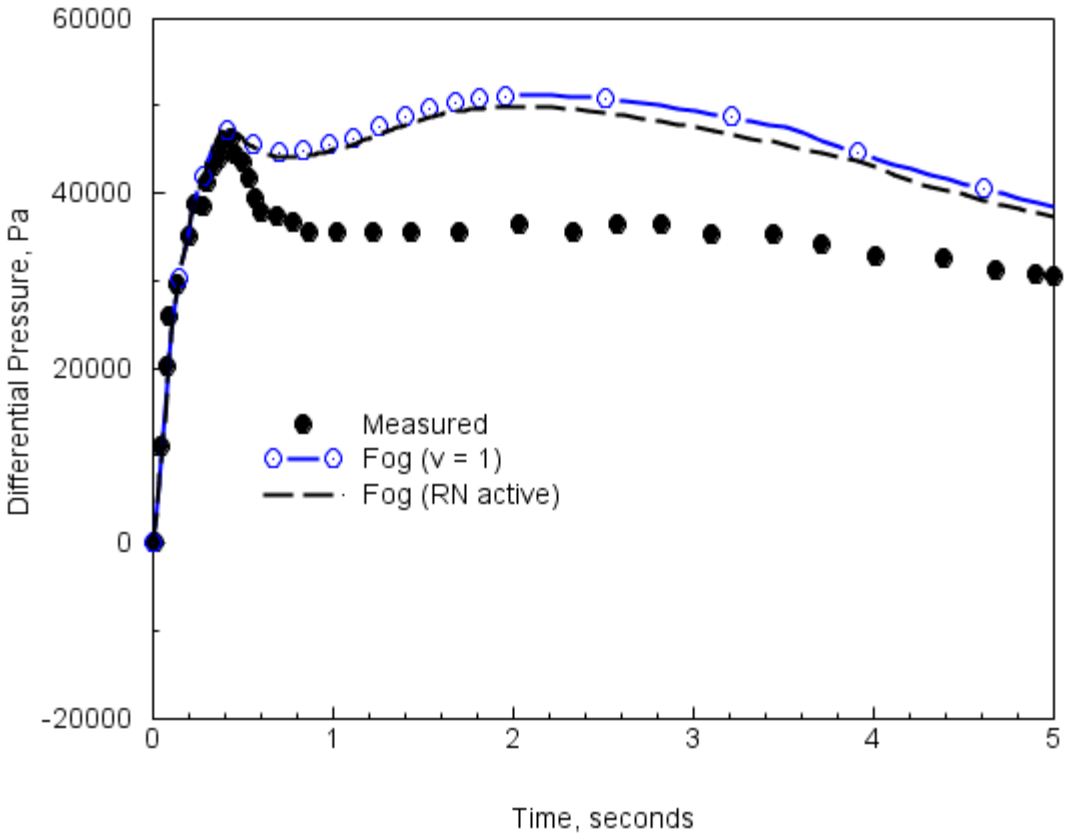

Figure B-19 **Comparison of the MELCOR differential pressure calculations (with and without fog modeling by the aerosol physics model) compared with measurement for pathway #92 (1704 to 1707) during the HDR T31.5 test.**

APPENDIX C. LISTING OF MELCOR INPUT DECKS

The supporting input files used to perform the reference analyses presented in this report have been moved to a supplemental document. Given the detailed information contained within the input files, it is unclear if all associated information has been released. Therefore, a supplemental document containing this information has been made accessible only to the U.S.NRC [Til18}.

DISTRIBUTION

1	MS0899	Technical Library	9536 (electronic copy)


Sandia National Laboratories